НАУЧНОМ ВЕЋУ
ИНСТИТУТА ЗА ФИЗИКУ
У БЕОГРАДУ

Предмет: Молба за покретање поступка за избор у звање виши научни сарадник

МОЛБА

Молим Научно веће Института за физику у Београду да у складу са Правилником о поступку, начину вредновања и квантитативном исказивању научноистраживачких резултата истраживача Министраства за просвету, науку и технолошки развој покрене поступак за мој избор у звање виши научни сарадник.

У прилогу достављам:

- Мишљење руководиоца са предлогом чланова комисије;
- Биографске податке;
- Преглед научне активности;
- Елементе за квалитативну оцену научног доприноса;
- Елементе за квантитативну оцену научног доприноса;
- Списак објављених научних радова и фотокопије радова објављених након претходног избора у звање;
- Податке о цитираности;
- Копију решења о претходном избору у звање;
- Додатне прилоге са доказима.

У Београду,

21.02.2022.

С поштовањем,

Ранковић Милош

Др Милош Ранковић

НАУЧНОМ ВЕЋУ

ИНСТИТУТА ЗА ФИЗИКУ

У БЕОГРАДУ

Предмет: Мишљење руководиоца за избор др Милоша Ранковића у звање виши научни сарадник

Др Милош Ранковић запослен је у Лабораторији за атомске сударне процесе Института за физику у Београду од 2013. године. на пројекту интегралних интердисциплинарних истраживања финансираним од Министарства просвете, науке и технолошког развоја: ОИ 171020 "Физика судара и фото процеса у атомским, (био) молекуларним и нанодимензионим системима". Био је ангажован на пословима експерименталних мерења диференцијалних пресека атома племенитих гасова и мањих молеукла, као и интеракције електрона са металним и изолаторским капиларама. Учествовао је на више пројеката на различитим експерименталним линијама синхротрона СОЛЕИЛ поред Париза у Француској, где је истраживао интереакције фотона и електрона са биомолекулима. Од 2017. године је запослен у лабораторији за Динамику Молекула и Кластера, J. Хејровски Институт за Физичку Хемију, при Чешкој академији науке и уметности, где је учествовао на више међународних пројеката претежно фокусираних на експерименталним истраживањима интеракције електрона са мањим молекулима.

С обзиром да испуњава све критеријуме прописане Правилником о поступку, начину вредновања и квантитативном исказивању научноистраживачких резултата истраживача Министарства просвете, науке и технолошког развоја, сагласан сам са покретањем поступка за избор др Милоша Ранковића у звање виши научни сарадник.

Предлажем да комисију за избор др Милоша Ранковића у звање виши научни сарадник чине:

1. др Ненад Симоновић, научни саветник, Институт за физику у Београду,
2. др Братислав Маринковић, научни саветник у пензији, Институт за физику у Београду и
3. проф. др Горан Попарић, редовни професор, Физички факултет, Универзитет у Београду

У Београду,

21.02.2022.

Руководилац лабораторије,

N. Simonović

Др Ненад Симоновић
научни саветник
Институт за физику у Београду

1. БИОГРАФСКИ ПОДАЦИ

Ранковић Милош је рођен у Београду 17.06.1986. године, општина Савски Венац, Република Србија. Основну школу и средњу електротехничку школу "Никола Тесла" је похађао у Београду. Основне академске студије на Физичком факултету, Универзитет у Београду, смер Примењена физика и информатика, уписао је 2005. године. У јулу 2012. године је дипломирао са просечном оценом 8.97 и оценом 10 на дипломском испиту са темом "Примена акустичких мерења у волуметријској анализи", под менторством др Зорана Николића. Добитник је награде *Проф. др Љубомир Ћирковић* за најбољи дипломски рад одбрањен на Физичком факултету исте године. У децембру 2012. године је уписао докторске студије на Физичком факултету, Универзитет у Београду. Од априла 2013. године је запослен у Институту за физику, Универзитет у Београду, Центар за физику атомских ударних процеса, као истраживач-приправник на пројекту ОИ 171020 "Физика судара и фото процеса у атомским, (био) молекуларним и нанодимензионим системима", који финансира Министарство просвете, науке и технолошког развоја Србије. На Физичком факултету, Универзитета у Београду, у септембру 2016. године одбранио је доктроску дисертацију под називом: Фотонска и електронска акциона спектроскопија трапираних биомолекуларних јона - Од излованих до наносолватисаних честица", под менторством др Александра Милосављевића. Убрзо затим успоставља међународну сарадњу и почев од августа 2017. године се прикључује групи за Динамику Молекула и Кластера, J. Хејровски институт за физичку хемију, Чешка академија науке и уметности у Прагу. Под руководством др Јураја Федора, наставља научноистраживачки рад у оквиру после докторских истраживања из области атомских и молекулских ударних процеса са електронима, где учествује на више међународних пројеката.

Решење о избору у звање истраживач сарадник је добио 17.06.2014. године, док је у звању научни сарадник од 27.09.2017. године.

Милош је аутор/коаутор укупно 19 радова у водећим међународним часописима (од чега 5 у категорији М21а, 8 у категорији М21, 2 у категорији М22 и 4 у категорији М23), више саопштења са међународних и националних конференција, укључујући и 7 предавања по позиву на међународним конференцијама.

OrcidID: 0000-0003-1317-0132

ResearcherID: F-6843-2016

2. ПРЕГЛЕД НАУЧНЕ АКТИВНОСТИ

Научна активност др Милоша Ранковића везана је за област атомске, молекулске и хемијске физике, пре свега за експериментална истраживања процеса који настају при сударима електрона са атомима и молекулима, као и интеракције фотона из синхротронског радијационог извора са различитим биолошки релевантним молекулима у гасној фази.

У току рада на докторској дисертацији Милош Ранковић је био ангажован на пројекту ОИ 171020 "*Физика судара и фото процеса у атомским, (био)молекуларним и нано системима*", финансираном од стране Министарство за просвету, науку и технолошки развој Републике Србије (интегрална и интердисциплинарна истраживања). Трајање пројекта: 2011-2019. Руководилац пројекта је био др Братислав Маринковић. Поред тога, с обзиром на показани таленат и мотивацију за експериментални рад, Милош Ранковић је учествовао и на другим истраживањима у Лабораторији за атомске сударне процесе, пре свега у развоју система за истраживање трансмисије електрона ниских енергија кроз проводне и изолаторске микрокапиларе, путем сарадње са колегама из Мађарске.

Такође, Милош је био ангажован на пројекту билатералне научне сарадње између Србије и Немачке „*Истраживање радијационог оштећења ДНК на молекуларном нивоу помоћу електронске и фотонске акционе спектроскопије*" (2014-2015) под руководством др Александра Милосављевића. Учествовао је и на више пројеката на синхротронском извору зрачења СОЛЕИЛ, под руководством др Александра Милосављевића у периоду (2012-2016):

- "Inner-shell spectroscopy of nanosolvated Supstance P peptide ions isolated in gas phase" (2016, main proposer A. Milosavljevic),
- "The interplay between protein folding and its electronic structure probed by soft X-ray absorption tandem mass action spectroscopy" (2015, main proposer A. Milosavljevic),
- "Inner-shell spectroscopy of nanosolvated protein ions isolated in gas phase" (2014, main proposer A. Milosavljevic),
- "Influence of nanosolvation onto the ionization energy of multiply charged full proteins isolated in the gas phase" (2014, main proposer A. Milosavljevic),
- "Nanosolvation-induced stabilization of biopolymers and fragile biomolecular complexes isolated in the gas phase probed by VUV photoactivation" (2013, main proposer A. Milosavljevic),
- "Inner-shell spectroscopy of protein ions isolated in gas phase: Near-edge X-ray ion yield spectra dependence on molecular charge state" (2013, main proposer A. Milosavljevic),
- "Photoionization of nanosolvated nucleotides and nucleoside triphosphates isolated in the gas phase" (2012, main proposer A. Milosavljevic)

Међународну сарадњу са Чешким колегама након одбрањене докторске дисертације, др Милош Ранковић је започео крајем 2017. године прикључењем групи за динамику молекула и кластера у „J. Хејровски" Институ за физичку хемију у лабораторији за електрон-молекулске сударе, под руководством др Михала Фарника, док је 2020. године руковођење групе преузео др Јурај Федор. Након претходног избора у звање, радом у лабораторији за

електрон-молекулске сударе у Прагу, кандидат је проширио своје експериментално искуство у техникама електронске спектроскопије и тиме фокусирао своју научну активност на фундаментално истраживање процеса резонаци у молекулима.

Напомена: радови означени звездицом (*) су публиковани након претходног избора у звање.

2.1 Интеракције електрона са површинама

Разумевање механизама који доводе до расејања електрона уназад при судару са чврстим површинама и објашњење тако добијених електронских спектара је релеватно за неке процесе из области физике чврстог стања, а потребно је у многим технолошким применама као што су карактеризација површина, дијагностика оштећења материјала и површинска модификација материјала. Додатно изучавањем интеракције наелектрисаних честица са чврстим површинама се може доћи до бољег фундаменталног разумевања процеса расејања.

Кандидатов допринос се садржао у модификацији постојеће експерименталне поставке у лабораторији за физику атомских сударних процеса која је омогућила истраживање интеракције различитих непроводних и проводних капилара са електронима, као и учествовању у прикупљању и обради података. Комбинован је теоријски приступ који су урадиле Мађарске колеге, са експерименталном техником укрштених млазева где су анализирани секундарни електрони расејани на платинумској капилари под различитим упадним угловима и енергијама. Добијено је добро подударање измереног и симулираног електронског спекра након расејања са капиларе. Резултати су показали присуство еластично и нееластично расејаних електрона чак и изван угла дефинисаним геометријском трансмисијом, што указује на ефекат вођења електрона кроз капилару путем вишеструке секундарне емисије са платинумске површине, као и нагомилавања наелектрисања на нечистоћама.

(M21) A. R. Milosavljević, **M. Lj. Ranković**, D. Borka, J. B. Maljković, R. J. Bereczky, B. P. Marinković and K. Tőkési,
“Study of electron transmission through a platinum tube“,
Nucl. Instr. Meth. **B** (2015).
DOI: 10.1016/j.nimb.2014.11.087

(M22)* J. B. Maljković, D. Borka, **M. Lj. Ranković**, B. P. Marinković, A. R. Milosavljević, C. Lemell, and K. Tőkési,
“Electron transmission through a steel capillary”,
Nucl. Instrum. Meth. B, **423**, 87–91 (2018).
DOI: 10.1016/j.nimb.2018.03.020

2.2 Интеракција фотона и електрона са биомолекулима

Велики допринос развоју модерне физике даје изучавање интеракција насталих при процесу судара електрона и фотона са различитим атомима и молекулима, са становшта разумевања многих процеса из области атомске и молекулске физике, физике атмосфере, биофизике, астрофизике и физике чврстог стања. Фундаментално изучавање елементарних процеса и

реакција иницираних сударом електрона са атомима и молекулима може довести до бољег разумевања механизама преко којих се објашњавају разни макроскопски феномени. Од посебног је интереса изучавање интеракције фотона добијених из синхронтронских извора са изолованим биомолекулима, као и утицај присуства водених молекула тј. наносолватације на утицај њихових фундаменталних физичко-хемијских особина, због уске везе са разумењем процеса радијационог оштећења на молекуларном нивоу.

Научна активност и допринос кандидата пре претходног избора у звање је била везана за истраживања процеса интеракције електрона и фотона са биомолекулима, као и утицаја наносолватације на особине биомолекула. У оквиру ове тематике, Милош Ранковић је превасходно радио паралелно на: а) дизајну и развоју извора електронског млаза, као вакуумског система, у циљу конструкције, тестирања и имплементирања система за истраживање судара електрона са биомолекулима заробљеним у јонској замци или доведеним у вакуум на други начин; б) мерењу и обради резултата експерименталног истраживања интеракције "VUV" и "X" фотона са биомолекулима (нуклеотиди, амино киселине, пептиди и протеини), као и наносолватисаним биомолекулима, изолованим у вакууму помоћу јонске замке.

У оквиру тематике а) кандидат је помоћу симулације кретања електрона под условима дефинисаним задатом геометријом електронске оптике, испитивао рад електронског топа, у континуалном и пулсном режиму. Добијени резултати су важни за конструкцију и имплементацију извора електронског млаза. Кандидат је затим извео експерименталну реализацију повезивања електронског топа и јонске замке, при чему су добијени први резулати електронски индуковане дисоцијације/јонизације пептида и протеина заробљених у линеарној квадруполној јонској замци. Овај експеримент представља веома важан доказ принципа да је могуће довести електроне средњих енергија (око 300 eV) у линеарну јонску замку са радиофреквентним електричним пољима. Показано је да пертурбација енергије и геометрије електронског млаза под таквим условина довољно мала и да је могуће разлучити електронску структуру протеина. Конкретно, разложен је абсорпциони пик који одговара електронској ексцитацији 1s електрона из најниже љуске угљениковог атома у вишу непопуњену везивну молекулску орбиталу π^* која одговара пептидној вези између угљеникових и азотових атома.

У оквиру тематике б) презентовани су резултати експерименталног истраживања фотонски индуковане дисоцијације пентапептида леуцин-енкефалин, у опсегу енергија 5-14 eV. У опсегу енергија до око 8 eV, испод енергије јонизације, дисоцијација је иницирана електронском побудом молекула чиме овакво истраживање пружа могућност детаљног испитивања електронске структуре пептида као и сусцептибилности биомолекула у односу на ултраљубичасто електромагнетно зрачење. Експеримент је остварен повезивањем линеарне јонске замке са синхротронским зрачењем и мерењем тандем масених спектара у функцији енергије фотона. Такође су презентовани резултати фотонски индуковане дисоцијације за исте енергије фотона, хидратисаног протонисаног нуклеотида аденозин монофосфата. У експерименту је показано да хидратисање поменутог нуклеотида чак и са једним молекулом воде доводи до значајног смањења инзензитета фрагментације поменутог нуклеотида. У експериментима интеракције фотона из опсега енергија благих X-зрака са заробљеним вишеструко протонисаним протеином убикјутин, је показано да

повећање стања наелектрисања протеина утиче на просторну уређеност (секундарну структуру која дефинише биолошку функцију - од компактних до издужених формација), што се може довести у везу са електронском структуром протеина. Најзад, експериментални резултати добијени интеракцијом електрона из тематике а) су упоређени са интеракцијама фотона из тематике б) за исти протеин убикјутин, при чему су добијена веома добра поклапања. Иако су процеси који иницирају Ожеов процес (избацивање валентног електрона, након ексцитације електрона из унутрашње К-љуске) различити за случај фотона (резонантни) и електрона (нерезонантни), показало се да се релаксациони канали у тандем масеним спектрима добро поклапају.

Након претходног избора у звање кандидат је наставио сарадњу са Француским колегама и у експериментима под руковођењем др Александра Милосављевића у радијационом синхротронском постројењу СОЛЕИЛ је наставио истраживања ефекта наносолватације на фундаменталне особине биомолекуларних јона изолованог и хидратисаног пептида у јонској замци, под дејством фотона из области меких "X" зрака. Коршћена је техника "NEXAFS" (*near edge soft X ray absorption fine structure*) спектроскопије, а резултати су показали значајно повећање фрагментисања испитиваног пептида након наносоватације са 11 молекула воде. Кандидатов допринос се садржао у припреми и извођењу експеримента, као и прикупљању и обради података из серије мерења где су изоловани и хидратисани прекурсори пептида подвргнути дејству фотона енергија из области које одговарају електронској ексцитацији кисеоникових атома.

Објављени радови и саопштења представљају значајан научни допринос у области истраживања интеракције електрона и фотона са биомолекулима. Од посебног значаја је испитивање дисоцијације јона пептида у вакууму услед електронске побуде у "VUV" области испод енергије јонизације, као и у области меких "X" зрака, што је значајно како са фундаменталног аспекта и разумевања физичко-хемијских особина биомолекула, тако и за истраживања радијационог оштећења на молекуларном нивоу.

(M21a) A. R. Milosavljević, C. Nicolas, **M. Lj. Ranković**, F. Canon, C. Miron and A. Giuliani,
"K-Shell Excitation and Ionization of a Gas-Phase Protein: Interplay Between Electronic Structure and Protein Folding",
J. Phys. Chem. Lett. **6**, 16 (2015), pp 3132–3138
DOI: 10.1021/acs.jpclett.5b01288

(M21a)* Aleksandar R. Milosavljević, Christophe Nicolas, **Miloš Lj. Ranković**, Francis Canon, Catalin Miron, and Alexandre Giuliani,
"Correction to "K-Shell Excitation and Ionization of a Gas-Phase Protein:
Interplay between Electronic Structure and Protein Folding",
J. Phys. Chem. Lett., **10**(23), 7397-7397 (2019).
DOI: 10.1021/acs.jpclett.9b03345

(M21a) Aleksandar R. Milosavljević, Viktor Z Cerovski, Francis Canon, **Miloš Lj. Ranković**, Nikola Škoro, Laurent Nahon, Alexandre Giuliani,
"Energy-Dependent UV Photodissociation of Gas-Phase Adenosine Monophosphate Nucleotide Ions: The Role of a Single Solvent Molecule",
J. Phys. Chem. Lett. **5**, 11 (2014), pp 1994–1999.
DOI: 10.1021/jz500696b

(M21)* Aleksandar R. Milosavljević, Kari Jänkälä, **Miloš Lj. Ranković**, Francis Canon, John Bozek, Christophe Nicolas and Alexandre Giuliani,
"Oxygen K-shell spectroscopy of isolated progressively solvated peptide",
Phys. Chem. Chem. Phys., **22**, 12909-12917 (2020).
DOI: 10.1039/D0CP00994F

(M21) **Miloš Lj. Ranković**, Alexandre Giuliani and Aleksandar R. Milosavljević,
"Electron impact action spectroscopy of mass/charge selected macromolecular ions: inner-shell excitation of ubiquitin protein",
Appl. Phys. Lett. **108**, 064101 (2016).
DOI: 10.1063/1.4941798

(M21) **M. Lj. Ranković**, F. Canon, L. Nahon, A. Giuliani, and A. R. Milosavljević,
"VUV action spectroscopy of protonated leucine-enkephalin peptide in the 6-14 eV range",
J. Chem. Phys. **143**, 244311 (2015).
DOI: 10.1063/1.4939080

(M23) **Miloš Lj. Ranković**, Alexandre Giuliani and Aleksandar R. Milosavljević,
"Design and performance of an instrument for electron impact tandem mass spectrometry and action spectroscopy of mass/charge selected macromolecular ions stored in RF ion trap",
Eur. Phys. J. D **70,** 6 (2016).
DOI: 10.1140/epjd/e2016-70108-7

(M23) A. R. Milosavljević, V. Z. Cerovski, **M. Lj. Ranković**, F. Canon, L. Nahon, and A. Giuliani,
"VUV photofragmentation of protonated leucine-enkephalin peptide dimer below ionization energy",
Eur. Phys. J. D **68**, 68 (2014).
DOI: 10.1140/epjd/e2014-40826-y

(M31) **M. Lj. Ranković**, F. Canon, L. Nahon, A. Giuliani and A. R. Milosavljević,
"Photoinduced fragmentation of gas-phase protonated leucine-enkephalin peptide in the VUV range",
Journal of Physics: Conference Series **635**, (2015) 012034
DOI: 10.1088/1742-6596/635/1/012034

2.3 Интеракција електрона са ДНК

Једна од најважнијих метода лечења разних врста канцера путем радио терапије подразумева коришћење високо енергијских честица попут фотона, електрона или јона. У претходним годинама је показано да су за радијационо оштећење на молекуларном нивоу највише одговорне ниско енергијске честице настале као последица јонизације медијума под дејством примарног високо енергијског зрачења. Међу овим честицама највећи допринос оштећењу дају ниско енергијски електрони испод 20eV. Као секундарни продукти произведени у највећем броју, могу се директно накачити на молекул ДНК или друге биомолекуле формирањем прелазних негативних јона, односно анјонских стања - резонанци. Најчешћи канали релаксације ових стања су дисоцијација молекула, а конкретно за молекул ДНК процес дисоцијативног електронског захвата "DEA" (*dissociative electron attachment*) може довести до једноструког или двоструког кидања ланца. Посебна пажња је усмерена на експерименталне технике које омогућавају да се огроман молекул ДНК уведе

у гасну фазу без оштећења, где се може испитивати под строго контролисаним експерименталним условима у вакууму. За побољшање технике радио терапије од великог је интереса пронаћи начин да се радијационо оштећење највише усмери само на оболеле ћелије, а да се при томе не изврши велики утицај на околно здраво ткиво. У ту сврху се користе посебни молекули који се називају радиосенситизери (*radiosensitizers*), чије присуство изазива повећање ефекта радијационог оштећења.

Из билатералне сарадње са колегама из Немачке, тематика истраживања је била испитивање интеракције ниско енергијских електрона са олигонуклеотидима посебно закачених на странице нано-димензионих троугластих структура састављених од једноструког ланца ДНК молекула. У оквиру ове тематике, кандидат је значајно допринео развоју, реализацији и оспособљавању експерименталне апаруре за потребе ових експеримената. Кандидат је дизајнирао и саставио специјалан окретни носач за узорке, у коме је додатно интегрисан Фарадејев кавез за мерење струје електрона, за потребе карактеризације електронског млаза. У овим експериментима су испитиване различите секвенце једноструког ланца ДНК молекула озрачивањем са нискоенергијским електронима, а затим су помоћу технике "AFM" (*atomic force microscopy*) пронађена и квантификована појединачна оштећења секвенци олигонуклеотида, где је кандидат дао значајан допринос у прикупљању и анализи великог броја АФМ снимака. Резултати су показали да се значајно повећање пресека тј. вероватноће за једноструко кидање ланца добија када се у олигонуклеотидску секвенцу уместо аденинске базе "A" убаци нуклеотид флударабин (*fludarabine*) "^{2F}A". Из ове сарадње је проистекао један рад у врхунском међународном часопису.

(M21a) Jenny Rackwitz, Janina Kopyra, Iwona Dabkowska,
Kenny Ebel, **Miloš Lj. Ranković**, Aleksandar R. Milosavljević and Ilko Bald,
"Sensitizing DNA towards low-energy electrons with 2-fluoroadenine",
Angew. Chem. Int. Ed. **55,** 35 (2016).
DOI: 10.1002/anie.201603464

(M23)* Jenny Rackwitz, **Miloš Lj. Ranković**, Aleksandar R. Milosavljević and Ilko Bald, "A novel setup for the determination of absolute cross sections for low-energy electron induced strand breaks in oligonucleotides – The effect of the radiosensitizer 5-fluorouracil",
Eur. Phys. J. D **71**, 32 (2017). [9pp]
DOI: 10.1140/epjd/e2016-70608-4

2.4 Интеракција електрона са молекулима

Елементарни процеси који учествују у формирању електронских резонанци имају фундаменталну улогу у многим областима науке и технологије, почев од астрофизике и биологије, па све до дистрибуције електричне енергије и технологије израде полупроводничких елемената. Под одређеним експерименталним условима, при сударима електрона са неутралним молекулима може доћи до формирања кратко-живећег привременог јона, тј. стања. Тај феномен се укратко назива резонанца и могуће га је истраживати применом технике електронске спектроскопије губитка енергије (EELS - *electron energy loss spectroscopy*), у којој се при задатој енергији упадних електрона мери енергија нееластично расејаних електрона са молекула мете. Разлика ових енергија, тј. енергијски губитак је у фундаменталној вези са резонацом и користи за детаљно

испитивање датог молекула. Постоје два типа електронских вибрационих резонанци код молекула. Код првог, енергијски губитак се тачно поклапа са енергијом потребном за ексцитацију кванта специфичног вибрационог мода датог молекула. У овом случају вишак енергије упадног елекрона одлази у виду спонтано избаченог елекрона. Код другог типа, енергија упадног електрона је насумично распоређена по свим могућим нуклеарним степенима слободе молекула, што називамо неспецифична или неодређена ексцитација. У том случају долази до термалне емисије електрона са малим енергијама, за велики опсег енергија упадних електрона. Недаванним развојем дво димензионалне "EELS" примећен је и трећи тип екситације код неких молекула, који се не може сврстати ни у једну од претходно дефинисаних типова. У овом случају могу се видети избачени електрони термалних енергија у великом опсегу упадних енергија електрона, али њихов спектар има карактер који одговара спецфичној ексцитацији.

У комбинацији са експерименталном техником "DEA" могуће је добити ширу слику о фундаменталним особинама молекула доведених у гасну фазу у погледу изучавања процеса електронских резонанци, које су битне за боље разумевање процеса из многих области науке и технологије. Допринос кандидата у овим експериментима је развој и унапређење електронике и аквизиционих програма који су довели ефикаснијој могућности прикупљања и анализе података из експерименталних мерења. Током рада у лабораторији за електрон-молекулске сударе у Прагу под руковођењем др Јураја Федора, кандидат је дао значајан допринос експерименталним мерењима и анализи резултата добијених истраживањем разних молекула, који су публиковани у врхунским међународним часописима. Кандидат је такође дизајнирао и конструисао нову експерименталну поставку за испитивање изолационих гасова који се користе у енергетици као замена за SF_6. У сарадњи са Чешким колегама, користећи ову експерименталну поставку у кобинацији са техником инфрацрвене спектроскопије, кандидат је урадио квалитативну и квантитативну анализу продуката добијених под дејством електричног пражњења. Резултати из ових експеримената су искоришћени за симулације електричних особина нових изолационих гасова при дизајну и конструкцији функционалног прототипа сигурносног прекидача (*switchgear*) кроз заједнички пројекат са међународном компанијом која се бави продајом производа из области енергетике "Eaton". Кандидат се тренутно бави развојем нове експерименталне поставке за проучавање интеракције електрона са биолошки релевантним молекулима расвореним у течностима који се директно уводе у гасну фазу путем коришћења технике течних микроскопских млазева. Потенцијал овог типа експеримената је могућност да се обезбеди проучавање фундаменталних особина молекула и биомолекула у експерименталним условима течне фазе где се присуство воденог окружења (природна средина свих биомолекула) не занемарује, као код сличних експеримената изведених у гасној фази.

(M21a)* Cate S. Anstöter, Golda Mensa-Bonsu, Pamir Nag, **Miloš Ranković**, Ragesh Kumar T. P., Anton N. Boichenko, Anastasia V. Bochenkova, Juraj Fedor, and Jan R. R. Verlet,
"Mode-Specific Vibrational Autodetachment Following Excitation of Electronic Resonances by Electrons and Photons",
Phys. Rev. Lett. **124**, 203401 (2020) [6pp].
DOI: 10.1103/PhysRevLett.124.203401

(M21)* Ragesh Kumar T. P., P. Nag, **M. Ranković**, R. Čurík, A. Knížek, S. Civiš, M. Ferus, J. Trnka, K. Houfek, M. Čížek, and J. Fedor,
"Electron-impact vibrational excitation of isocyanic acid HNCO",
Phys. Rev. A **102**, 062822 (2020) [6pp].
DOI: 10.1103/PhysRevA.102.062822

(M21)* M. Zawadzki, **M. Ranković**, J. Kočišek and J. Fedor,
"Dissociative electron attachment and anion-induced dimerization in pyruvic acid",
Phys. Chem. Chem. Phys., **20**, 6838-6844 (2018).
DOI: 10.1039/c7cp07472g

(M21)* **M. Ranković**, J. Chalabala, M. Zawadzki, J. Kočišek, P. Slavíček and J. Fedor
"Dissociative ionization dynamics of dielectric gas C_3F_7CN",
Phys. Chem. Chem. Phys., **21,** 16451-16458 (2019).
DOI: 10.1039/c9cp02188d

(M21)* **M. Ranković**, P. Nag, M. Zawadzki, L. Ballauf, J. Žabka, M. Polášek, J. Kočišek, and J. Fedor,
"Electron collisions with cyanoacetylene HC_3N: Vibrational excitation and dissociative electron attachment",
Phys. Rev. A **98**, 052708 (2018) [9pp].
DOI: 10.1103/PhysRevA.98.052708

(M22)* **M. Ranković**, Ragesh Kumar T P, P. Nag, J. Kočišek, and J. Fedor,
"Temporary anions of the dielectric gas C3F7CN and their decay channels",
J. Chem. Phys. **152**, 244304 (2020) [7pp].
DOI: 10.1063/5.0008897

(M23)* **Miloš Lj. Ranković**, Jelena B. Maljković, Károly Tökési and Bratislav P. Marinković,
"Elastic electron differential cross sections for argon atom in the intermediate energy range from 40 eV to 300 eV",
Eur. Phys. J.D **72**, 30 (2018). [9pp]
DOI: 10.1140/epjd/e2017-80677-4

3. ЕЛЕМЕНТИ ЗА КВАЛИТАТИВНУ ОЦЕНУ НАУЧНОГ ДОПРИНОСА

3.1. Квалитет научних резултата

3.1.1. *Научни ниво и значај научних резултата, утицај научних радова*

Милош Ранковић је у свом досадашњем научном раду објавио укупно 19 радова у међународним часописима са ISI листе, од чега 5 категорије М21а (изузетни међународни часописи), 8 категорије М21 (врхунски међународни часописи), 2 категорије М22 (истакнути међународни часописи) и 4 рада у категорији М23 (међународни часописи). Поред тога, објавио је 1 рад категорије М31 (предавање по позиву са међународног скупа штампано у целини), 7 категорије М32 (предавање по позиву са међународног скупа штампано у изводу), 18 категорије М34 (саопштење са међународног скупа штампано у изводу), 3 категорије М63 (саопштење са скупа националног значаја штампано у целини).

Кандидат је након претходног избора у звање научни сарадник објавио 11 радова у међународним часописима са ISI листе. Од тога, 2 категорије М21а (изузетни међународни часописи), 5 радова су категорије М21 (врхунски међународни часописи), 2 рада категорије М22 (истакнути међународни часописи) и 2 рада у категорији М23 (међународни часописи). Поред тога, објавио је 4 рада категорије М32 (предавање по позиву са међународног скупа штампано у изводу) и 7 радова категорије М34 (саопштење са међународног скупа штампано у изводу).

Пет најзначајнијих радова након претходног избора у звање:

1. Cate S. Anstöter, Golda Mensa-Bonsu, Pamir Nag, **Miloš Ranković**, Ragesh Kumar T. P., Anton N. Boichenko, Anastasia V. Bochenkova, Juraj Fedor, and Jan R. R. Verlet,
"Mode-Specific Vibrational Autodetachment Following Excitation of Electronic Resonances by Electrons and Photons",
Phys. Rev. Lett. **124**, 203401 (2020) [6pp].
DOI: 10.1103/PhysRevLett.124.203401
ИФ=9.227 (за 2018), $M_{норм}$=7.14, СНИП=2.362, цитата 15

2. Aleksandar R. Milosavljević, Kari Jänkälä, **Miloš Lj. Ranković**, Francis Canon, John Bozek, Christophe Nicolas and Alexandre Giuliani,
"Oxygen K-shell spectroscopy of isolated progressively solvated peptide",
Phys. Chem. Chem. Phys., **22**, 12909-12917 (2020).
DOI: 10.1039/D0CP00994F
ИФ=3.676 (за 2020), СНИП=0.962, цитата 2

3. M. Zawadzki, **M. Ranković**, J. Kočišek and J. Fedor,
"Dissociative electron attachment and anion-induced dimerization in pyruvic acid",
Phys. Chem. Chem. Phys., **20**, 6838-6844 (2018).
DOI: 10.1039/c7cp07472g
IF= 4.123 (za 2016), SNIP=0.994, цитата 18

4. **M. Ranković**, J. Chalabala, M. Zawadzki, J. Kočišek, P. Slavíček and J. Fedor
"Dissociative ionization dynamics of dielectric gas C_3F_7CN",
Phys. Chem. Chem. Phys., **21,** 16451-16458 (2019).
DOI: 10.1039/c9cp02188d
ИФ=3.906 (за 2017), СНИП=0.973, цитата 9

5. **M. Ranković**, Ragesh Kumar T P, P. Nag, J. Kočišek, and J. Fedor,
"Temporary anions of the dielectric gas C3F7CN and their decay channels",
J. Chem. Phys. **152**, 244304 (2020) [7pp].
DOI: 10.1063/5.0008897
ИФ=3.488 (за 2020), СНИП=0.961, цитата 2

У првом раду (*Phys. Rev. Lett.* **124**, 203401 (2020)), резултати су прикуљени у „J. Хејровски" Институту за физичку хемију у Лабораторији за електрон-молекулске сударе. Молекул

нитробензена је испитиван дводимензионалном спектроскопијом електронског губитка енергије ("EELS" - *electron energy loss spectroscopy*). Експеримент показује специјалан тип емисије електрона који не може бити објашњен преко постојећа два механизма вибрационе ексцитације, где се први тип назива специфична вибрациона ексцитација, а други неспецифична (неодређена) ексцитација. Ново-откривен тип ексцитације је сличан другом типу јер показује емисију термалних електрона карактеристичну за неспецифичну ексцитацију, али са битном разликом која указује на емисиону структуру, тј. селективност емисије. Комбиновањем експерименталног и теоријског приступа у раду је предложен механизам који објашњава овај нови тип емисије електрона. Везан је за присуство не-валентног диполно везаног стања (*non-valence dipole bound state*), који потиче од инфрацрвено активних вибрационих модова неутралног молекула нитробензена. Овај проналазак је веома важан за фундаментално разумевање процеса електронских резонанци које играју кључну улогу у многим областима као што су на пример астрофизика, биофизика, дистрибуција електричне енергије и производња полупроводника.

Резултати из другог рада (*Phys. Chem. Chem. Phys.,* **22**, 12909-12917 (2020)) су добијени из експеримената урађеним на синхротрону СОЛЕИЛ, крај Париза. Комбиновањем метода елекро-спреј јонизације и масене спектрометрије, огромни биомолекул - неуротрансмитер пептид СупстанцаП (*SubstanceP*) доведен је у гасну фазу. Помоћу нано електро-спреј технике изоловани су нанохидратисани биомолекуларни јони који су озрачени фотонима из области меких "X" зрака. Коришћена метода се назива "NEXAFS" (*Near Edge soft X-ray absorption fine structure*) спектроскопија и због своје селективности омогућава да се велика количина енергије депонује у дати биомолекуларни јон на тачно одређеним енергијама, које одговарају енергији специфичних атома из пептидних веза. У датом раду је конкретно испитивана К љуска кисеоникових атома и утицај свега неколико молекула воде на фундаменталне физичко-хемијске особине биомолекуларног јона овог нанхидратисаног пептида. Резултати показују апсорпциони врх који одговара прелазу O_{1s} у $\pi_{(amide)}^{*}$ код изолованог биомолекуларног јона. Додавањем 4 или 11 молекула воде, примећује се повећање интензитета овог апсорпционог врха услед доприноса додатних кисеоникових атома који припадају молекулима воде. У презентованим тандем масеним спектрима се види да је последица нанохидратисања повећање фрагментисања, односно разарања биомолекула кидањем пептидних веза. Ови резултати представљају један од првих експеримената који директно даје увид у процес радијационог оштећења на молекуларном нивоу.

Резултати из трећег рада (*Phys. Chem. Chem. Phys.,* **20**, 6838-6844 (2018)) су прикупљени у „J. Хејровски" Институ за физичку хемију у Лабораторији за електрон-молекулске сударе у Прагу. Експеримент је урађен комбиновањем резултата са две експерименталне поставке, при чему се обе базирају на трохоидном електронском монохроматору као извору електрона. Апаратура са "TOF" (*time of flight*) детектором у пулсном режиму коришћена је за мерење апсолутних вредности "DEA" (*dissociative electron attachment*) пресека, док је апаратура са квадрополним масеним филтром, због нешто боље енергијске резолуције у континуалном режиму рада, дала функционалну зависност пресека од енергије упадних

електрона. Испитиван је молекул пригрожђане киселине (*piruvic acid)*, који је као најмања аминокиселина релевантан за многе процесе у атмосферској хемији, астрохемији и биохемији, јер потиче од оксидације биогених и антропогених прекурсора. Анализа измерених пресека показује богату фрагментацију, при чему најдоминантнији канал дисоцијације одговара кидању "COOH" (карбоксилне) везе. У парцијалном пресеку за "OH^- " (јон хидроксилне групе) се истиче повећање интензитета око 6 eV, док је кидање хидроксилне везе узрок појављивања фрагмента $(M-H)^-$, што представља доминантни дисоцијациони канал релевантан за многе биолошке молекуле. Сви бендови примећени у "DEA" парцијалним пресецима фрагмената потичу од диполно омогућених резонанци типова σ^*, π^* и Фешбах. Резултати додатно показују фрагменте који не могу настати у "DEA" процесу појединачних молекула, што указује на присуство секундарних реакција између прелазних јона (резонатних стања) M^{*-}, односно димеризације пригрожђане киселине.

У четвртом раду (*Phys. Chem. Chem. Phys*., **21,** 16451-16458 (2019)) је испитиван обећавајући кандидат "C_3F_7CN" (флуоронитрил) који представља заменски изолациони гас за SF_6. Са развојем свести о глобалном загревању од велике је важности да се пронађу мање штетне алтернативе за SF_6, који има високог "GWP" (*global warming potential*) и употребу широм света у постројењима за дистрибуцију електричне енергије. Резултати су прикупљени коришћењем експерименталне поставке са трохоидалним монохроматором и "TOF" детектором у Лабораторији за електрон-молекулске сударе у Прагу. Измерен је апсолутни пресек за јонизацију овог молекула у области (0-100) eV. Пресек се користи као улазни параметар за симулацију електричних пражњења при дизајну високоенергетских сигурносних прекидача, за дистрибуцију електричне енергије. Поред тога овај молекул је интересантан и са фундаменталног становишта изучавања процес при електрон-молекулским сударима. Комбиновани теоријски и експериментални приступ показује да процес јонизације доводи до потпуне досицојације молекула, при чему је најдоминантнији релаксациони канал производња фрагмента CF_3^+. Теоријски прорачун показује да се иницијално формира јако велики број катјонских стања услед присуства непопуњених молекулских орбитала, а да се затим брзом интерном конверзијом услед великог броја степени слободе неутралног молекула, са ових стања систем релаксира на основно електронско стање катјона. Резултати такође показују да чак поред потпуне дисоцијације, овај гас је веома добар у прикупљању слободних електрона који настају у електронској лавини током пражњења, али и да се као последица реакција у пражњењу стварају штетни радикали као што је на пример C_3F_4N.

Пети рад (*J. Chem. Phys.* **152**, 244304 (2020)) је наставак серије истраживања изолационог гаса флуоронитрила, при чему су резултати такође прикупљени коришћењем комбинације експерименталних поставки у Прагу. Фокус истраживања је на динамици прелазних анјонских стања овог молекула, а примењена техника је вибрациона "EELS" (*electron energy loss spectroscopy*). Измерени електронски спектри показују ексцитацију великог броја

вибрационих стања, при чему доминантни модови одговарају степенима слободе вибрација “C-C” и “C-F” веза у датом молекулу. Услед директне диполне ексцитације долази до појачања вибрационе ексцитације и на енергијама упадних електрона око 0.58 eV и 1.18 eV долази до појаве вибрационих резонанци, док се на вишим енергијама појављују и широке σ^* резонанце. Поред њих, у спектру се види и статистичка емисија термалних електрона ниских енергија у великом опсегу упадних енергија електрона која одговара механизму неспецифичне вибрационе ексцитације. “DEA” процес има за последицу појаву неколико анјонских фрагмената, при чему је најдоминантнији $C_4F_7N^-$ који се види као врх у парцијалном пресеку при енергијама упадних електрона блиским нули, док се остали фрагменти виде на енергијама око 1eV. Приказани резултати дају детаљну слику динамике прелазних анјона која је веома важна за разумевање процеса електричних пражњења у овом гасу, а тиме и моделовању његових диелектричних особина.

Резултати до којих је кандидат дошао и који су представљени у радовима 1, 3, 4 и 5 представљају значајан научни допринос разумевању фундаменталне интеракције електрона са молекулима са становишта формирања резонанци, док су резултати представљени у раду 2 међу првим експериментима који доприносе бољем разумевању комплексног процеса радијационог оштећења.

3.1.2. *Позитивна цитираност научних радова*

Према Web of Science цитатној бази, научни радови др Милоша Ранковића цитирани су 163 пута, односно 149 пута без самоцитата (h-index=9).

3.1.3. *Параметри квалитета радова и часописа*

За процену квалитета часописа у којима су радови публиковани у наставку су приказане категорије часописа и њихов фактор утицаја, односно импакт фактор – ИФ (наведена је најбоља вредност из периода до две године уназад од када је рад објављен). Подвучени су фактори утицаја часописа у којима су објављени радови након претходног избора у звање.

Категорија М21а

1 рад у *Physical Review Letters* (ИФ 9.227)
1 рад у *Angewandte Chemie (International Edition)* (ИФ 11.709)
3 рада у *Journal of Physical Chemistry Letters* (ИФ 8.709, ИФ 8.539, ИФ 7.458)

Категорија М21

3 рада у *Physical Chemistry Chemical Physics* (ИФ 3.676, ИФ 3.906, ИФ 4.132)
2 рада у *Physical Review A* (ИФ 3.140, ИФ 2.925)
1 рад у *Applied Physics Letters* (ИФ 3.142)
1 рад у *Journal of Chemical Physics* (ИФ 2.894)
1 рад у *Nuclear Instruments and Methods in Physics Research. Section B: Beam Interactions with Materials and Atoms* (ИФ 1.389)

Категорија М22

1 рад у *Journal of Chemical Physics* (ИФ 3.448)
1 рад у *Nuclear Instruments and Methods in Physics Research. Section B: Beam Interactions with Materials and Atoms* (ИФ 1.323)

Категорија М23

4 рада у *The European Physical Journal D* (ИФ 1.393 два рада, ИФ 1.513, ИФ 1.208)

Укупан импакт-фактор радова др Милоша Ранковића износи 82.017, а фактор утицаја радова у периоду након избора у претходно звање је 43.303. Научни ниво и значај резултата је исказан кроз чињеницу да су радови публиковани у реномираним часописима који представљају референтне часописе у области атомске, молекулске и хемијске физике.

Додатни библиометријски показатељи према Упутству о начину писања извештаја о изборима у звања које је усвојио Матични научни одбор за физику приказани су у следећој табели:

	ИФ	М	СНИП
Укупно	43.303	76	11.865
Усредњено по чланку	3.936	6.909	1.078
Усредњено по аутору	6.917	12.195	1.921

3.1.4. *Степен самосталности и степен учешћа у реализацији радова у научним центрима у земљи и иностранству*

Др Милош Ранковић је током рада у Лабораторији за физику атомских сударних процеса у Институту за физику у Београду под руковођењем др Братислава Маринковића показао самосталност и изражену способност у практичном делу извођења експерименталних поставки, почев од дизајна, конструкције, изведбе и модификације делова апаратуре и електронике, а затим и симулација електронске оптике и модификације софтверских делова аквизиционих програма.

Током многобројних посета различитих млазних линија у синхронтроском радијационом постројењу СОЛЕИЛ у Француској, поред Париза под руковођењем др Александра Милосављевића, кандидат је дао значајан допринос састављању експерименталних поставки и прикупљању података, како обради тако и анализи велике количине резултата мерења, који су касније кроз сарадњу са француским колегама публиковани у неколико врхунских међународних часописа категорија М21а и М21. Током ове сарадње кандидат је проширио своје експериментално искуство у разним техникама. Најпре, електро спреј јонизације која служи за увођење великих макромолекула у гасну фазу, а затим и методама

масене акционе спектроскопије, где се тако добијени јони макромолекула доводе у интеракцију са фотонима или електронима из области "VUV" или благих "X" зрака (*soft X ray*), са циљем истраживања фундаменталних физичко-хемијских особина биолошки релевантних макромолекула.

Након завршеног доктората, кроз сарадњу са Чешким колегама у „J. Хејровски" Институту за физичку хемију, Одељење за динамику молекула и кластера, Лабораторија за истраживање електронских сударних процеса под руководством др Јураја Федора, започиње самосталан истраживачки рад и додатно проширење експерименталног искуства у техникама електронске спектроскопије методом губитка енергије (*EELS - electron energy loss*). Кандидат је значајно допринео унапређењу постојећих експерименталних поставки за мерења пресека електрон-молекулских процеса, као и дизајну и изградњи нових, који су омогућили нова истраживања везаних за испитивање заменских гасова за SF_6 (сумпорхексафлуорид). Током ове сарадње кроз више Чешких националних и међународних пројеката под руковођењем др Јураја Федора, произашла је већина радова кандидата, публикованих након претходног избора у звање у врхунским међународним часописима категорија М21а, М21 и М22 на којима је кандидат дао значајан допринос.

3.1.5. *Награде*

Милош Ранковић је добитник награде *Проф. др Љубомир Ћирковић* за најбољи дипломски рад одбрањен на Физичком факултету 2012. године.

3.1.6. Елементи применљивости научних резултата

Истраживања везана за ефекат вођења електрона кроз микро и макро капиларе доприносе бољем разумевању елементарних процеса на атомском нивоу који се могу довести у везу са применама у биомедицини, конкретно за развој тзв. електронског ножа, односно технике за увођење електрона у ћелије.

Истраживања интеракције фотона и електрона са биомолекулима, генерално доприноси бољем разумевању њихових фундаменталних физичко-хемијских особина, а тиме и њихове структуре која је уско везана за њихову биолошку функцију у ћелији. Заједно са разумевањем утицаја воде као растварача (стварно окружење биомолекула је већински водено) на фундаменталне особине биомолекула путем истраживања наносолватације, може се довести у везу са истраживањем радијационог оштећења живе материје, што је послењих година веома активна област. Боље разумевање елементарних процеса радијационог оштећења подстиче унапређењу ефикасности и проналажењу нових експерименталних техника са применама у радиотерапији различитих тешких болести.

Истраживања фундаменталних особина молекула путем сударних процеса при интеракцији са електронима, у виду квантификовања пресека за процесе еластичних и нееластичних расејања електрона на овим молекулима, омогућава добијање улазних параметара за нумеричко моделовање разних елементарних процеса, пре свега важних за разумевање атмосферских процеса који се доводе у везу са заштитом животне средине на Земљи. Додатно, резултати добијени у истраживањима електронских судара са молекулима из

приложених радова кандидата су релевантни са процесе астрохемије и биохемије.

Последњих година се интезивно ради на проналажењу заменскинх гасова за SF_6, који се користи широм света у готово свим постројењима за производњу и дистрибуцију електричне енергије унутар специјалних склопова (*switchgear*). Истраживања путем ударних процеса електрона са кандидатима заменских гасова као што су C_3F_7CN (*Novec4710*) доводе до бољег разумевања елементарних процеса који играју кључну улогу у електричном пражњењу у поменутом гасу. Добијени резултати имају директну примену у симулацијама које доприносе побољшању дизајна и конструкције постојеће опреме са далеко мањим штетним утицајем на животну средину, конкретно путем смањења доприноса ефекту глобалног загревања.

3.2. Ангажованост у формирању научних кадрова

Кандидат је учествовао у изради мастер радова:

- Јелене Вуковић, дипломираног физичара (Физички факултет Универзитета у Београду, 2018. године)
- Иве Бачић, дипломираног физичара (Физички факултет Универзитета у Београду, 2015. године)

Кандидат је учествовао у изради дипломског рада:

- Јелене Вуковић (Природно-математички факултет - студијски програм за физику, Универзитет у Бањој Луци, 2015. године)

3.3. Нормирање броја коауторских радова, патената и техничких решења

У периоду након претходног избора у звање да Милош Ранковић је објавио 11 радова, од којих се 8 рачунају са пуном тежином док је на 3 рада више од 7 аутора. Нормирање М бодова урађено је по правилнику, а остварен и нормиран број М поена приказан је у табели у делу **4. Елементи за квантитативну оцену научног доприноса кандидата**. Укупан број М поена је 85.5, нормираних поена има 77.5 што је изнад захтеваног броја бодова за избор у звање виши научни сарадник.

3.4. Руковођење пројектима, потпројектима и пројектним задацима

Кандидат је учествовао у следећим пројектима основних, интердисциплинарних и технолошких истраживања Министарства просвете, науке и технолошког развоја Републике Србије (наведени су само пројектни задаци којима се кандидат бавио након претходног избора у звање):

- (2011-2019) “Физика судара и фото процеса у атомским, (био) молекуларним и нанодимензионим системима”, (пројекат ОИ 171020)

Кандидат учествује у следећим пројектима основних, интердисциплинарних и технолошких истраживања Чешке Републике, под руковођењем др Јураја Федора:

- (2017-2019) Czech Science Foundation Project “Cross sections and dynamics of electron scattering on molecular systems”, (пројекат ЈФ1)

- (2017-2020) Technological Agency of the Czech Republic Project “SF6 replacement in high voltage switchgear”, (пројекат ЈФ2)
- (2020-2023) Czech Science Foundation Project “Dynamics of electron-induced nuclear motion in cold molecules“, (пројекат ЈФ3)
- (2020-2024) MŠMT InterCOST project “Electronic and nuclear dynamics in molecules initiated by electron impact“, (пројекат ЈФ4)
- (2021-2026) Czech Science Foundation EXPRO project ”Probing and transforming matter by electrons in liquid jets“, (пројекат ЈФ5)
- (2022-2024) Technological Agency of the Czech Republic Project “Streamers and flashover discharges on insulators in alternative gases to SF6”, (пројекат ЈФ6)

На пројекту ОИ 171020 „Физика судара и фото процеса у атомским, (био)молекуларним и нано системима”, у оквиру теме 2 интеракције са површинама на нанометарској скали (нанокапиларе, нанотачке) које воде фунционализацији материјала или модификацији нанофилмова, др Милош Ранковић руководио је задатком 2.1. Кандидат је за потребе овог задатка урадио модификацију постојеће експерименталне апаратуре тако што је дизајнирао и конструисао специјалан носач који је коришћен за причвршћење металних капилара различитих типова и величина. Тиме је омогућено експериментално испитивање трансмисије електрона разних енергија под различитим угловима кроз дате капиларе, што је кандидат затим извршио. Кандидат је такође урадио симулацију електронске оптике анализаторског дела апаратуре како би се проверио допринос непожељног ефекта вођења електрона са електричним пољима неопходних за рад анализатора. Научни резултати који су том приликом прикупљени, кроз сарадњу са колегама из Мађарске који су дали допринос теоретском делу испитивања су публиковани у раду категорије М21, а такође су и изложени на неколико међународних конференција у виду постер презентација.

На пројекту ЈФ1, др Милош Ранковић је обављао пројектни задатак мерења пресека за електрон-молекулске сударе, разних молекула релевантних за астрохемијске и биохемијске процесе. Резултати су публиковани у врхунским међународним часописима категорија М21 и изложени су на међународним конференцијама у виду постер излагања.

На пројекту ЈФ2, др Милош Ранковић је обављао следеће пројектне задатке:
(а) мерења пресека за електрон-молекулске сударе заменских изолационих гасова,
(b) дизајн и конструкцију експерименталне поставке за испитивање продуката након утицаја парцијалног пражњења (*partial discharge*) у изолационим гасовима,
(б) одређивање и квантификацију продуката добијених парцијалним пражњењима у изолационим гасовима. Резултати су публиковани у врхунским међународним часописима категорија М21 и изложени су на међународним конференцијама у виду предавања по позиву као и постер излагања.

На пројекту ЈФ3, др Милош Ранковић се бави пројектним задаком дизајна и унапређења електронике за нову експерименталну поставку за мерење електрон-молекулских судара.

На пројекту ЈФ4, др Милош Ранковић се бави пројектним задатком припреме предлога пројеката за синхронтронске мисије (*beamtime proposals*) за потребе истраживања електронски индуковане нуклеарне динамике у хладним молекулима.

На пројекту ЈФ5, др Милош Ранковић се бави следећим пројектним задацима:
(а) учешће у дизајну коморе за испитивање и спектроскопију изолационих гасова,
(б) "VUV" спектроскопија изолационих гасова у оквиру синхротронских мисија.

3.5. Активност у научним и научно-стручним друштвима

- Чланство у организационом одбору међународне конференције - 3rd *Int. Workshop on Dissociative Electron Attachment - DEA CLUB 2018, Prague, Czech Republic*.
- Чланство у организационом одбору међународне конференције: *XUV/X-ray light and fast ions for ultrafast chemistry expert meeting on biomolecules - XLIC 2015, Fruška Gora, Serbia.*
- Чланство у организационом одбору међународне конференције: *27th Summer School and International Symposium on the Physics of Ionized gases - SPIG 2014, Belgrade, Serbia.*

3.6. Утицај научних резултата

Утицајност научних радова кандидата је наведена у одељцима **3.1. Квалитет научних резултата**. Пун списак радова дат је у одељку 5, док су подаци о цитираности наведени након списка свих радова.

3.7. Конкретан допринос кандидата у реализацији радова у научним центрима у земљи и иностранству

За више детаља о доприносу кандидата у реализацији радова у научним центрима у земљи и ностранству погледати одељак ***3.1.1. Научни ниво и значај научних резултата, утицај научних радова*** и ***3.1.4. Степен самосталности и степен учешћа у реализацији радова у научним центрима у земљи и иностранству***.

3.8. Уводна предавања на конференцијама, друга предавања и активности

Предавања по позиву на конференцијама одржана у периоду након претходног избора у звање:

M. Ranković, C. S. Anstöter, G. Mensa-Bonsu, P. Nag, R. Kumar T. P., J. R. R. Verlet, and Juraj Fedor,
"Vibrational autodetachment following excitation of electronic resonances",
Proc. 32nd International Conference on Photonic, Electronic and Atomic Collisions - ICPEAC 2021, July 20 - 23, 2021, Progress Report, p.49.
https://www.icpeac2021.ca/

M. Ranković, R. Kumar T. P., P. Nag, J. Kočišek and J. Fedor,
"Electron Collisions with Dielectric Gases Considered as SF6 Replacement",
Proc. 30th Summer School and International Symposium on the Physics of Ionized Gases - SPIG 2020, August 24 – 28, 2020, Šabac, Serbia, Invited Lecture, p.24.

http://spig2020.ipb.ac.rs/

M. Lj. Ranković, A. R. Milosavljević, K. Jänkälä, F. Canon, J. Bozek, C. Nicolas and A. Giuliani,
"Oxygen K-shell spectroscopy of isolated bare and solvated peptide",
Proc. 29th Summer School and Int. Symp. on Physics of Ionized Gases – SPIG 2018, 29th august - 1st september 2018, Belgrade, Serbia, Progress report, p.9.
http://www.spig2018.ipb.ac.rs/

M. Lj. Ranković, F. Canon, L. Nahon, A. Giuliani and A. R. Milosavljević,
Photodissociation of hydrated peptide by synchrotron radiation in the VUV region,
Proc. 4th XLIC General Meeting, 14-16 march 2017, Prague, Czech Republic, Young Scientists Forum (Oral presentation and abstract), p.31.
http://www.jh-inst.cas.cz/xlic2017/home

Предавања по позиву на конференцијама одржана у периоду пре претходног избора у звање:
M. Lj. Ranković, A. Giuliani and A. R. Milosavljević,
"Electron impact action spectroscopy of mass/charge selected macromolecular ions",
Proc. 28th Summer School and Int. Symp. on Physics of Ionized Gases – SPIG 2016, 29th august - 1st september 2016, Belgrade, Serbia, Editors: Dragana Marić Aleksandar Milosavljević, Bratislav Obradović and Goran Poparić, Progress report, p.9.
http://www.spig2016.ipb.ac.rs/

Miloš Lj. Ranković, Alexandre Giuliani and Aleksandar R. Milosavljević,
"Design and performance of an instrument for gas phase electron spectroscopy of trapped molecular ions"
Proc.The 3rd CELINA Meeting, May 18-20, 2016, Kraków, Poland, Editors: Petra Swiderek and Janina Kopyra, Progress report, p.40.
http://celina.uni-bremen.de/celina/celina2016/

M. Lj. Ranković, F. Canon, L. Nahon, A. Giuliani and A. R. Milosavljević,
"Photodissociation of protonated Leucine-Enkephalin peptide in the VUV range",
Proc. XXIX ICPEAC15 International Conference on Photonic, Electronic and Atomic Collisions, 22 July - 28 July 2015, Spain, Toledo, Editors: F. Martín, G. García, L. Méndez, L. Argenti and A. Palacios, Special Report, p.105.
http://www.icpeac2015.com/

4. ЕЛЕМЕНТИ ЗА КВАНТИТАТИВНУ ОЦЕНУ НАУЧНОГ ДОПРИНОСА КАНДИДАТА

Остварени М-бодови кандидата у периоду након претходног избора у звање

Категорија	М бодова по раду	Број радова	Укупно М бодова	Нормирано М бодова
M21a	10	2	20	17.14
M21	8	5	40	35.11
M22	5	2	10	10
M23	3	2	6	6
M32	1.5	4	6	5.75
M34	0.5	7	3.5	3.5

Поређење оствареног броја М-бодова са минималним условима потребним за избор у звање виши научни сарадник:

Минималан број М бодова		Остварено	Остварено нормирано
Укупно	50	85.5	77.5
M10+M20+M31+M32+M33+M41+M42+M90	40	85.5	77.5
M11+M12+M21+M22+M23	30	76	68.25

5. СПИСАК ОБЈАВЉЕНИХ НАУЧНИХ РАДОВА

Радови у изузетним међународним часописима (М21а)

публиковани након претходног избора у звање

A1. Cate S. Anstöter, Golda Mensa-Bonsu, Pamir Nag, **Miloš Ranković**, Ragesh Kumar T. P., Anton N. Boichenko, Anastasia V. Bochenkova, Juraj Fedor, and Jan R. R. Verlet, "Mode-Specific Vibrational Autodetachment Following Excitation of Electronic Resonances by Electrons and Photons",
Phys. Rev. Lett. **124**, 203401 (2020) [6pp].
DOI: 10.1103/PhysRevLett.124.203401
IF= 9.227 (za 2018), M_{norm}=7.14, SNIP=2.362

A2. Aleksandar R. Milosavljević, Christophe Nicolas, **Miloš Lj. Ranković**, Francis Canon, Catalin Miron, and Alexandre Giuliani,
"Correction to "K-Shell Excitation and Ionization of a Gas-Phase Protein: Interplay between Electronic Structure and Protein Folding",
J. Phys. Chem. Lett., **10**(23), 7397-7397 (2019).
DOI: 10.1021/acs.jpclett.9b03345
IF= 8.709 (za 2017), SNIP=1.41

публиковани пре претходног избора у звање

A3. Jenny Rackwitz, Janina Kopyra, Iwona Dabkowska,
Kenny Ebel, **Miloš Lj. Ranković**, Aleksandar R. Milosavljević and Ilko Bald,
"Sensitizing DNA towards low-energy electrons with 2-fluoroadenine",
Angew. Chem. Int. Ed. **55,** 35 (2016).
DOI: 10.1002/anie.201603464
IF= 11.994 (za 2016)

A4. A. R. Milosavljević, C. Nicolas, **M. Lj. Ranković**, F. Canon, C. Miron and A. Giuliani, "K-Shell Excitation and Ionization of a Gas-Phase Protein: Interplay Between Electronic Structure and Protein Folding",
J. Phys. Chem. Lett. **6**, 16 (2015), pp 3132–3138
DOI: 10.1021/acs.jpclett.5b01288
IF= 8.539 (za 2015)

A5. Aleksandar R. Milosavljević, Viktor Z Cerovski, Francis Canon, **Miloš Lj. Ranković**, Nikola Škoro, Laurent Nahon, Alexandre Giuliani,

"Energy-Dependent UV Photodissociation of Gas-Phase Adenosine Monophosphate Nucleotide Ions: The Role of a Single Solvent Molecule",
J. Phys. Chem. Lett. **5**, 11 (2014), pp 1994–1999.
DOI: 10.1021/jz500696b
IF= 7.458 (za 2014)

Радови у врхунским међународним часописима (M21)

публиковани након претходног избора у звање

Б.1. Aleksandar R. Milosavljević, Kari Jänkälä, **Miloš Lj. Ranković**, Francis Canon, John Bozek, Christophe Nicolas and Alexandre Giuliani,
"Oxygen K-shell spectroscopy of isolated progressively solvated peptide",
Phys. Chem. Chem. Phys., **22**, 12909-12917 (2020).
DOI: 10.1039/D0CP00994F
IF= 3.676 (za 2020), SNIP=0.962

Б.2. Ragesh Kumar T. P., P. Nag, **M. Ranković**, R. Čurík, A. Knížek, S. Civiš, M. Ferus, J. Trnka, K. Houfek, M. Čížek, and J. Fedor,
"Electron-impact vibrational excitation of isocyanic acid HNCO",
Phys. Rev. A **102**, 062822 (2020) [6pp].
DOI: 10.1103/PhysRevA.102.062822
IF= 3.140 (za 2020), M_{norm}=4.44, SNIP=0.993

Б.3. **M. Ranković**, J. Chalabala, M. Zawadzki, J. Kočišek, P. Slavíček and J. Fedor
"Dissociative ionization dynamics of dielectric gas C_3F_7CN",
Phys. Chem. Chem. Phys., **21,** 16451-16458 (2019).
DOI: 10.1039/c9cp02188d
IF= 3.906 (za 2017), SNIP=0.973

Б.4. M. Zawadzki, **M. Ranković**, J. Kočišek and J. Fedor,
"Dissociative electron attachment and anion-induced dimerization in pyruvic acid",
Phys. Chem. Chem. Phys., **20**, 6838-6844 (2018).
DOI: 10.1039/c7cp07472g
IF= 4.123 (za 2016), SNIP=0.994

Б.5. **M. Ranković**, P. Nag, M. Zawadzki, L. Ballauf, J. Žabka, M. Polášek, J. Kočišek, and J. Fedor,
"Electron collisions with cyanoacetylene HC_3N: Vibrational excitation and dissociative electron attachment",

Phys. Rev. A **98**, 052708 (2018) [9pp].
DOI: 10.1103/PhysRevA.98.052708
IF= 2.925 (za 2017) M_{norm}=6.67, SNIP=0.989

публиковани пре претходног избора у звање

Б.6. **Miloš Lj. Ranković**, Alexandre Giuliani and Aleksandar R. Milosavljević,
"Electron impact action spectroscopy of mass/charge selected macromolecular ions: inner-shell excitation of ubiquitin protein",
Appl. Phys. Lett. **108**, 064101 (2016).
DOI: 10.1063/1.4941798
IF= 3.411 (za 2016)

Б.7. **M. Lj. Ranković**, F. Canon, L. Nahon, A. Giuliani, and A. R. Milosavljević,
"VUV action spectroscopy of protonated leucine-enkephalin peptide in the 6-14 eV range",
J. Chem. Phys. **143**, 244311 (2015).
DOI: 10.1063/1.4939080
IF= 3.122 (za 2013)

Б.8. A. R. Milosavljević, **M. Lj. Ranković**, D. Borka, J. B. Maljković, R. J. Bereczky, B. P. Marinković and K. Tőkési,
"Study of electron transmission through a platinum tube",
Nucl. Instr. Meth. **B** (2015).
DOI: 10.1016/j.nimb.2014.11.087
IF= 1.389 (za 2015)

Радови у међународним часописима (М22)

публиковани након претходног избора у звање

В.1. **M. Ranković**, Ragesh Kumar T P, P. Nag, J. Kočišek, and J. Fedor,
"Temporary anions of the dielectric gas C3F7CN and their decay channels",
J. Chem. Phys. **152**, 244304 (2020) [7pp].
DOI: 10.1063/5.0008897
IF= 3.488 (za 2020), SNIP=0.961

В.2. J. B. Maljković, D. Borka, **M. Lj. Ranković**, B. P. Marinković, A. R. Milosavljević, C. Lemell, and K. Tőkési,
"Electron transmission through a steel capillary",
Nucl. Instrum. Meth. B, **423**, 87–91 (2018).
DOI: 10.1016/j.nimb.2018.03.020
IF= 1.323 (za 2017), SNIP=0.797

Радови у међународним часописима (М23)

публиковани након претходног избора у звање

Г.1. **Miloš Lj. Ranković**, Jelena B. Maljković, Károly Tökési and Bratislav P. Marinković, "Elastic electron differential cross sections for argon atom in the intermediate energy range from 40 eV to 300 eV",
Eur. Phys. J.D **72**, 30 (2018). [9pp]
DOI: 10.1140/epjd/e2017-80677-4
IF= 1.393 (za 2017), SNIP=0.707

Г.2. Jenny Rackwitz, **Miloš Lj. Ranković**, Aleksandar R. Milosavljević and Ilko Bald, "A novel setup for the determination of absolute cross sections for low-energy electron induced strand breaks in oligonucleotides – The effect of the radiosensitizer 5-fluorouracil",
Eur. Phys. J. D **71**, 32 (2017). [9pp]
DOI: 10.1140/epjd/e2016-70608-4
IF= 1.393 (za 2017), SNIP=0.717

публиковани пре претходног избора у звање

Г.3. **Miloš Lj. Ranković**, Alexandre Giuliani and Aleksandar R. Milosavljević, "Design and performance of an instrument for electron impact tandem mass spectrometry and action spectroscopy of mass/charge selected macromolecular ions stored in RF ion trap",
Eur. Phys. J. D **70,** 6 (2016).
DOI: 10.1140/epjd/e2016-70108-7
IF= 1.288 (za 2016)

Г.4. A. R. Milosavljević, V. Z. Cerovski, **M. Lj. Ranković**, F. Canon, L. Nahon, and A. Giuliani,
"VUV photofragmentation of protonated leucine-enkephalin peptide dimer below ionization energy",
Eur. Phys. J. D **68**, 68 (2014).
DOI: 10.1140/epjd/e2014-40826-y
IF= 1.513 (za 2012)

Предавање по позиву са међународног скупа штампано у целини (неопходно позивно писмо) (М31)

публиковани пре претходног избора у звање

Д.1. **M. Lj. Ranković**, F. Canon, L. Nahon, A. Giuliani and A. R. Milosavljević, "Photoinduced fragmentation of gas-phase protonated leucine-enkephalin peptide in the VUV range", *Journal of Physics: Conference Series* **635**, (2015) 012034 DOI: 10.1088/1742-6596/635/1/012034

Предавање по позиву са међународног скупа штампано у изводу (М32)

публиковани након претходног избора у звање

Ђ.1. **M. Ranković**, C. S. Anstöter, G. Mensa-Bonsu, P. Nag, R. Kumar T. P., J. R. R. Verlet, and Juraj Fedor, "Vibrational autodetachment following excitation of electronic resonances", *Proc. 32nd International Conference on Photonic, Electronic and Atomic Collisions* - ICPEAC 2021, July 20 - 23, 2021, Progress Report, p.49. https://www.icpeac2021.ca/

Ђ.2. **M. Ranković**, R. Kumar T P, P. Nag, J. Kočišek and J. Fedor, "Electron Collisions with Dielectric Gases Considered as SF6 Replacement", *Proc. 30th Summer School and International Symposium on the Physics of Ionized Gases* - SPIG 2020, August 24 – 28, 2020, Šabac, Serbia, Invited Lecture, p.24. http://spig2020.ipb.ac.rs/

Ђ.3. **M. Lj. Ranković,** A. R. Milosavljević, K. Jänkälä, F. Canon, J. Bozek, C. Nicolas and A. Giuliani, "Oxygen K-shell spectroscopy of isolated bare and solvated peptide", *Proc. 29th Summer School and Int. Symp. on Physics of Ionized Gases* – SPIG 2018, 29th august - 1st september 2018, Belgrade, Serbia, Progress report, p.9. http://www.spig2018.ipb.ac.rs/

Ђ.4. **M. Lj. Ranković**, F. Canon, L. Nahon, A. Giuliani and A. R. Milosavljević, Photodissociation of hydrated peptide by synchrotron radiation in the VUV region, *Proc. 4th XLIC General Meeting*, 14-16 march 2017, Prague, Czech Republic, Young Scientists Forum (Oral presentation and abstract), p.31. http://www.jh-inst.cas.cz/xlic2017/home

публиковани пре претходног избора у звање

Ђ.5. **M. Lj. Ranković**, A. Giuliani and A. R. Milosavljević,

"Electron impact action spectroscopy of mass/charge selected macromolecular ions", *Proc. 28th Summer School and Int. Symp. on Physics of Ionized Gases* – SPIG 2016, 29th august - 1st september 2016, Belgrade, Serbia, Editors: Dragana Marić Aleksandar Milosavljević, Bratislav Obradović and Goran Poparić, Progress report, p.9. http://www.spig2016.ipb.ac.rs/

Ђ.6. **Miloš Lj. Ranković**, Alexandre Giuliani and Aleksandar R. Milosavljević, "Design and performance of an instrument for gas phase electron spectroscopy of trapped molecular ions" *Proc.The 3rd CELINA Meeting*, May 18-20, 2016, Kraków, Poland, Editors: Petra Swiderek and Janina Kopyra, Progress report, p.40. http://celina.uni-bremen.de/celina/celina2016/

Ђ.7. **M. Lj. Ranković**, F. Canon, L. Nahon, A. Giuliani and A. R. Milosavljević, "Photodissociation of protonated Leucine-Enkephalin peptide in the VUV range", *Proc. XXIX ICPEAC15 International Conference on Photonic, Electronic and Atomic Collisions*, 22 July - 28 July 2015, Spain, Toledo, Editors: F. Martín, G. García, L. Méndez, L. Argenti and A. Palacios, Special Report, p.105. http://www.icpeac2015.com/

Саопштења са међународних скупова штампана у изводу (М34)

публиковани након претходног избора у звање

E.1. **M. Ranković**, P. Nag, M. Zawadzki, M. Polášek, J. Žabka, J. Kočišek and J. Fedor, "Vibrational Excitation and Dissociative Electron Attachment Cross Sections in Cyanoacetylene HC3N", Proc. XX International Workshop on Low-Energy Positron and Positronium Physics, XXI International Symposium on Electron-Molecule Collisions and Swarms and V Workshop on Non-Equilibrium Processes – POSMOL2019, 18 - 20 July 2019 Belgrade, Serbia, Book of Abstracts, eds. D. Cassidy, M.J. Brunger, Z.Lj. Petrovic, S. Dujko, B.P. Marinkovic, D. Maric and S. Tošic (Serbian Academy of Sciences and Arts and Institute of Physics Belgrade, Serbia, 2019) Poster EMS 23 HOT TOPIC, p.105. http://posmol2019.ipb.ac.rs/

E.2. **M. Ranković**, J. Chalabala, M. Zawadzki, J. Kočišek, P. Slavíšek and J. Fedor, "Dissociative Ionization Dynamics of Dielectric gas C3F7CN",

Proc. XX International Workshop on Low-Energy Positron and Positronium Physics, XXI International Symposium on Electron-Molecule Collisions and Swarms and V Workshop on Non-Equilibrium Processes – POSMOL2019, 18 - 20 July 2019 Belgrade, Serbia, Book of Abstracts, eds. D. Cassidy, M.J. Brunger, Z.Lj. Petrovic, S. Dujko, B.P. Marinkovic, D. Maric and S. Tošic (Serbian Academy of Sciences and Arts and Institute of Physics Belgrade, Serbia, 2019) Poster EMS 46, p.128.
http://posmol2019.ipb.ac.rs/

E.3. **Ranković M**., Zawadski M., Kočišek J. and Fedor J.,
"Dissociative electron attachment and anion-induced dimerization in pyruvic acid",
Proc. 3rd Int. Workshop on Dissociative Electron Attachment, April 10.-13., 2018, Prague, Czech Republic, Book of Abstracts, Local organizers: Juraj Fedor, Jaroslav Kocišek, Miloš Rankovic, Pamir Nag, Dominika Kollárová (J. Heyrovský Institute of Physical Chemistry of the Czech Academy of Sciences, Prague, 2018) Posters, p.67.
http://www.jh-inst.cas.cz/~dea2018/index.html

E.4. P. Nag, **M. Ranković**, and J. Fedor,
"Vibrational and dissociative dynamics of resonant states in nitrobenzene",
Proc. 7th International Conference on Many Particle Spectroscopy of Atoms, Molecules, Clusters and Surfaces (MPS2018), 21-24 August 2018, Budapest, Hungary, Károly Tokési (Chair), Programme and Book of Abstracts, Editors: K. Tokési, B. Paripás, G. Pszota, Poster presentation P88, p.141.
http://www.mpsbudapest2018.com/

E.5. R. Milosavljević, K. Jânkâlâ, C. Nicolas, **M. Lj. Ranković**, F. Canon, J. Bozek, and A. Giuliani,
"Oxygen K-edge action spectroscopy of isolated nanosolvated Substance P: Resolving the excitation of the peptide and the attached water network",
4th XLIC General Meeting COST Action CM1204, 14-16 March 2017, Prague, Czech Republic, Book of Abstracts, Editors: Miroslav Polasek, Vera Krizova (J. Heyrovsky Institute of Physical Chemistry of the CAS, v.v.i., Prague, 2017) Poster presentation, p.81.
http://www.jh-inst.cas.cz/xlic2017/programme

E.6. B.P. Marinković, **M.Lj. Ranković**, J.B. Maljković, A.R. Milosavljević, D. Borka, C. Lemell, K. Tökesi,
"Electron transmission through steel capillary",

Proc. 7th Conference on Elementary Processes in Atomic Systems (CEPAS 2017), 3rd – 6th September 2017, Pruhonice, Czech Republic, Editors: M. Tarana, R. Curík (J. Heyrovský Institute of Physical Chemistry, Prague, 2017), Abstracts of Posters, p.47. https://www.jh-inst.cas.cz/cepas2017/

E.7. **M. Ranković**, A. Milosavljević, A. Giuliani,F. Canon and Laurent Nahon, "VUV action spectroscopy of protonated Tri-Alanine peptide", Proc. 7th Conference on Elementary Processes in Atomic Systems (CEPAS 2017), 3rd – 6th September 2017, Pruhonice, Czech Republic, Editors: M. Tarana, R. Curík (J. Heyrovský Institute of Physical Chemistry, Prague, 2017), Abstracts of Posters, p.55. https://www.jh-inst.cas.cz/cepas2017/

публиковани пре претходног избора у звање

E.8. A. R. Milosavljević, **M. Lj. Ranković**, D. Borka, J. Maljković, R. Bereczky, B. Marinković, K. Tőkési, "Study of electron transmission through a metallic capillary" XXIX International Conference on Photonic, Electronic, and Atomic Collisions (ICPEAC2015), 22–28 July 2015, Toledo, Spain, Abstracts, TU-106. *Journal of Physics: Conference Series* **635**, 062011 (2015). http://iopscience.iop.org/article/10.1088/1742-6596/635/6/062011/meta

E.9. J. Rackwitz, **M. Ranković**, A. Milosavljević, I. Bald, "Novel approaches to study low-energy electron-induced damage to DNA oligonucleotides" XXIX International Conference on Photonic, Electronic, and Atomic Collisions (ICPEAC2015), 22–28 July 2015, Toledo, Spain, Abstracts, TU-096. *Journal of Physics: Conference Series* **635**, 062001 (2015). http://iopscience.iop.org/article/10.1088/1742-6596/635/6/062001/meta

E.10. I. Bačić, **M. Lj. Ranković**, F. Canon, V. Cerovski, C. Nicolas, A. Giuliani and A. R. Milosavljević, "Gas-phase X-ray action spectroscopy of protonated nanosolvated substance P peptide around O K-edge", *Proc. WG2 Expert Meeting on Biomolecules, COST Action CM1204, XLIC - XUV/X-ray Light and fast Ions for ultrafast Chemistry*, April 27-30, 2015, Book of Abstracts, Eds. Paola Bolognesi and Aleksandar Milosavljević, Poster presentation P08, p.71. http://www.xlic-wg2-2015.ipb.ac.rs/

E.11. **M. Lj. Ranković**, V. Cerovski, F. Canon, L. Nahon, A. Giuliani and A. R. Milosavljević, "VUV action spectroscopy of bare and hydrated protonated leucine-enkephalin peptide", *Proc. WG2 Expert Meeting on Biomolecules, COST Action CM1204, XLIC - XUV/X-ray Light and fast Ions for ultrafast Chemistry*, April 27-30, 2015, Book of Abstracts, Eds. Paola Bolognesi and Aleksandar Milosavljević, Poster presentation P07, p.69. http://www.xlic-wg2-2015.ipb.ac.rs/

E.12. **M. Lj. Ranković**, J. Rackwitz, I. Bald and A. R. Milosavljević, "Optimization of a Low-Energy Electron Gun by Electron Ray-Tracing Simulations", *Proc. 27th Summer School and Int. Symp. on Physics of Ionized Gases* – SPIG 2014, 26th - 29th August 2014, Belgrade, Serbia, Contributed Papers & Abstracts of Invited Lectures, Topical Invited Lectures, Progress Reports and Workshop Lectures, Editors: Dragana Marić, Aleksandar R. Milosavljević and ZoranMijatović, (IOP Belgrade and SASA, Belgrade, Serbia), Poster Presentation 1.10, pp.58-61. http://www.spig2014.ipb.ac.rs/

E.13. A. R. Milosavljević, C. Nicolas, **M. Lj. Ranković**, F. Canon, C. Miron and A. Giuliani, "N K-Shell X-Ray Tandem Mass Spectrometry of Gas-Phase Ubiquitin Protein", *Proc. 27th Summer School and Int. Symp. on Physics of Ionized Gases* – SPIG 2014, 26th - 29th August 2014, Belgrade, Serbia, Contributed Papers & Abstracts of Invited Lectures, Topical Invited Lectures, Progress Reports and Workshop Lectures, Editors: Dragana Marić, Aleksandar R. Milosavljević and ZoranMijatović, (IOP Belgrade and SASA, Belgrade, Serbia), Poster Presentation 1.9, pp.54-57. http://www.spig2014.ipb.ac.rs/

E.14. A. R. Milosavljević, **M. Lj. Ranković**, J. B. Maljković, R. J. Bereczky, B. P. Marinković and K. Tökési, "Kinetic Energy Distribution of Electrons Scattered Inside a Platinum Tube at the Incident Energy of 200 eV", *Proc. 27th Summer School and Int. Symp. on Physics of Ionized Gases* – SPIG 2014, 26th - 29th August 2014, Belgrade, Serbia, Contributed Papers & Abstracts of Invited Lectures, Topical Invited Lectures, Progress Reports and Workshop Lectures), Editors: Dragana Marić, Aleksandar R. Milosavljević and ZoranMijatović, (IOP Belgrade and SASA, Belgrade, Serbia), Poster Presentation 2.11, pp.210-213. http://www.spig2014.ipb.ac.rs/

E.15. J. B. Maljković, **M. Lj. Ranković**, R. J. Bereczky, B. P. Marinković, K. Tőkési and A. R. Milosavljević,
"Electron transmission through a metallic capillary",
Proc. *26th International Conference on Atomic Collisions in Solids* (ICACS-26), 13th – 18th July 2014, Debrecen, Hungary, Book of Abstracts, Editor: Attila Csík, Poster presentation P23, p.59.
http://icacs26.atomki.mta.hu/

E.16. A. R. Milosavljević, J. B. Maljković, R. J. Bereczky, **M. Lj. Ranković**, B. P. Marinković and K. Tőkési,
"Transport of electrons through a long metallic microcapillary: characterization of the outgoing low-energy electron beam",
Proc. The First Annual Meeting of COST Action CM1301 (CELINA), 19th - 22nd March 2014, Erlangen, Germany, Book of Abstracts, Eds. Hubertus Marbach and Petra Swiderek, Poster presentation P22, p.47.

E.17. A. R. Milosavljević, F. Canon, V. Z. Cerovski, **M. Lj. Rankovic**, C. Nicolas, C. Miron, L. Nahon, and A. Giuliani,
"Photoionization of isolated charged proteins - the role of charge state and nanosolvation",
Proc. COST Action CM 1204 - Book of Abstract - lst Meeting of the XLIC Working Group 2, "REACTIVITY OF HIGHLY EXCITED AND HIGHLY CHARGED MOLECULES" 24th - 27th February, 2014, Port-en-Bassin-Huppain, France, Oral presentation, p.43.

E.18. A. R. Milosavlievć, F. Canon, V. Z. Cerovski, **M. Lj. Ranković**, L. Nahon, A. Giuliani,
"VUV photodissociation of bare and nanosolvated protonated nucleotide isolated in the gas phase",
Proc. 2nd NANO-IBCT Conference 2013 (Radiation Damage in Biomolecular Systems: Nanoscale Insights into Ion-Beam Cancer Therapy), Sopot, Poland 20-24 May, 2013.Book of Abstracts, Poster, p.91.

Саопштења са скупа националног значаја штампана у целини (М63)

публиковани пре претходног избора у звање

Ж.1. **M. Lj. Ranković**, M. Čelikić, A. R. Milosavljević,
"Optimization of electron gun in continuous and pulsed operation modes",
3rd National Conference on Electronic, Atomic, Molecular and Photonic Physics (CEAMPP2013) 25th August 2013, Belgrade, Serbia, Contributed Papers & Abstracts of Invited Lectures and Progress Reports, Contributed Papers pp.34-37.

Ж.2. **M. Lj. Ranković**, M. Čelikić and A. R. Milosavljević,
"Optimizacija rada elektronskog topa u opsegu energija 1-1000 eV",
XII Kongres fizičara Srbije, Zbornik radova – usmena predavanja, predavanja po sekcijama, usmena i poster saopštenja, 28. april - 2. maj 2013. Vrnjačka banja, Srbija, Urednici: J. Labat, N. Cvetanović i I. Dojčinović, Usmeno Poster u sekciji: 4. Atomska i molekulska fizika str. 312-315.

Ж.3. A. R. Milosavljević, **M. Lj. Ranković**, V. Z. Cerovski, F. Kanon, L. Nahon, A. Đulijani,
"Uticaj nanosolvatacije na stabilnost peptida izolovanog u gasnoj fazi",
XII Kongres fizičara Srbije, Zbornik radova – usmena predavanja, predavanja po sekcijama, usmena i poster saopštenja, 28. april - 2. maj 2013. Vrnjačka banja, Srbija, Urednici: J. Labat, N. Cvetanović i I. Dojčinović, Usmeno Poster u sekciji: 4. Atomska i molekulska fizika str. 304-307.

Одбрањена докторска дисертација (М70)

3.1. „Electron and photon action spectroscopy of trapped biomolecular ions - From isolated to nanosolvated species" *(„Електронска и фотонска акциона спектроскопија трапираних биомолекуларних јона - Од изолованих до наносолватисаних честица")*, Милош Ранковић, 2. септембар 2016. године, Физички факултет, Универзитет у Београду.

#ICPEAC2021

VIRTUAL

ICPEAC 2021

32nd International Conference on Photonic, Electronic and Atomic Collisions

July 20 - 23, 2021

www.icpeac2021.ca

Vibrational autodetachment following excitation of electronic resonances

M Ranković[1] *, C S Anstöter[2] , G Mensa-Bonsu[2], P Nag[1], R Kumar T P[1], J R R Verlet[2] and Juraj Fedor[1]

[1]J. Heyrovský Institute of Physical Chemistry, Czech Academy of Sciences, Prague, 18223, Czech Republic
[2]Department of Chemistry, Durham University, Durham, DH1 3LE, United Kingdom

Synopsis We probe the electron detachment from electronic resonances in nitrobenzene by 2D electron energy loss and 2D photoelectron spectroscopy.

Under certain conditions, a collision of electron with neutral molecule may lead to a formation of short-lived transient anion called resonance. Knowing the incident and measuring the outgoing electron energy one may study this resonance by means of electron energy loss (EEL) spectroscopy [1]. Generally, upon formation of such resonance two types of vibrational excitations can be distinguished. The first is when the electron energy loss coincides with the energy required for excitation of vibrational quanta of a specific vibrational mode. Here, exces energy is carried away by a spontaneusely ejected (autodetached) electron. The second type is unspecific, where the electron energy is randomly distributed among nuclear degrees of freedom. In this case, a statistical themal electron emission is observed.

A recent development of two-dimensional (2D) EEL spectroscopy [2] enabled a third type of excitation to be observed in a few molecules, which does not fit into any of the previous types. In this case, electrons are emitted with a very low constant energy over a wide range of incident electron energies, but the spectra have the vibrational structure. So far, there has been no explanation for it.

A similar effect has been observed by means of 2D anion photoelectron (PE) spectroscopy [3] were resonances are created by photoexcitation of the bound anions. It features a constant low energy PE spectrum with vibrational structure associated with nonvalence states [4].

In this talk, we will explore this effect in more details and our suggested mechanism [5] for electron emission involving a nonvalence dipole-bound state of nitrobenzene anion will be presented.

References

[1] M. Allan, *J. Electron Spectrosc. Relat. Phenom.* 48, 219 (1989).
[2] K. Regeta and M. Allan, *Phys. Rev. Lett.* **110**, 203201 (2013).
[3] C. S. Anstöter, J. N. Bull, and J. R. R. Verlet, *Int. Rev. Phys. Chem.* **35**, 509 (2016).
[4] J. N. Bull and J. R. R. Verlet, *Sci. Adv.* **3**, e1603106 (2017).
[5] C. S. Anstöter, *Phys. Rev. Lett.* **124**, 203401 (2020).

* E-mail: milos.rankovic@jh-inst.cas.cz

Subject **Invitation to give a talk at ViCPEAC 2021**

From Till Jahnke <jahnke@atom.uni-frankfurt.de>
To <milos.rankovic@jh-inst.cas.cz>
Cc Aumayr, Friedrich <aumayr@iap.tuwien.ac.at>, Sokell Emma <emma.sokell@ucd.ie>, Kirchner Tom <tomk@yorku.ca>
Date 2021-03-01 18:25

Dear Dr. Rankovic,

Due to the on-going pandemic, the 32nd International Conference on Photonic, Electronic and Atomic Collisions (ICPEAC) initially planned to take place this year in Ottawa, Canada, has been postponed to 2023.
In its place the ICPEAC General Committee decided to organize a fully virtual edition of ICPEAC this coming July. In addition, the General Committee voted to promote scientific exchange specifically for early career researchers.

The meeting has the same scientific scope and audience as previous ICPEACs and the process to select speakers was as rigorous and as highly competitive as for any other ICPEAC. Thus, it is our great pleasure to invite you, on behalf of the ICPEAC 2021 International Program Committee, to present a progress report on

Vibrational autodetachment following excitation of electronic resonances

at the XXXII International Conference on Photonic, Electronic and Atomic Collisions which will be held in virtual format (ViCPEAC 2021) from Tuesday 20th July to Friday 23rd July 2021.

The talk is scheduled for 25 minutes followed by 5 minutes of discussions.

We would be very pleased, if you could accept our invitation. Please let us know your (hopefully positive!) response by March 14, 2021. We look forward to welcoming you at our virtual venue (www.icpeac2021.ca) this coming summer 2021. Please do not hesitate to contact us in case you have any further questions.

Yours sincerely,

Till Jahnke
(Chair of the non-local Organizing Committee)

Friedrich Aumayr
(Chair of the ICPEAC Executive Committee)

--
Prof. Dr. Till Jahnke
European XFEL
Holzkoppel 4
D-22869 Schenefeld

Tel: +49 69 798 47025
Fax: +49 69 798 47100

jahnke@atom.uni-frankfurt.de
www.xfel.eu/facility/instruments/sqs
www.atom.uni-frankfurt.de

ПУБЛИКАЦИЈЕ АСТРОНОМСКЕ ОПСЕРВАТОРИЈЕ У БЕОГРАДУ
PUBLICATIONS OF THE ASTRONOMICAL OBSERVATORY OF BELGRADE
Св. 99 No. 99

30th Summer School and International Symposium on the Physics of Ionized Gases

Šabac, Serbia,
August 24 -28, 2020

CONTRIBUTED PAPERS

&

ABSTRACTS of INVITED LECTURES, TOPICAL INVITED LECTURES and PROGRESS REPORTS

Editors:
Luka Č. Popović, Duško Borka,
Dragana Ilić and Vladimir Srećković

БЕОГРАД
2020

PUBL. ASTRON. OBS. BELGRADE No. 99, 1 - 344 BELGRADE, AUGUST 2020

30th Summer School and International Symposium on the Physics of Ionized Gases

August 24 – 28, 2020, Šabac, Serbia

S P I G 2020

CONTRIBUTED PAPERS

&

ABSTRACTS OF INVITED LECTURES,
TOPICAL INVITED LECTURES AND
PROGRESS REPORTS

Editors

Luka Č. Popović, Duško Borka,
Dragana Ilić and Vladimir Srećković

Faculty of Mathematics
(Department of Astronomy)
Astronomical Observatory
of Belgrade

Institute of Physics,
University of Belgrade

Belgrade, 2020

SPIG 2020

SCIENTIFIC COMMITTEE

D. Borka (Co-chair), Serbia
L. Č. Popović (Co-chair), Serbia

R. White, Australia
J. Burgdörfer, Austria
J. Cvetić, Serbia
E. Danezis, Greece
Z. Donko, Hungary
V. Guerra, Portugal
D. Ilić, Serbia
M. Ivković, Serbia
I. Mančev, Serbia
D. Marić, Serbia
N. J. Mason, UK
A. Milosavljević, France
K. Mima, Japan
Z. Mišković, Canada
L. Nahon, France
B. Obradović, Serbia
G. Poparić, Serbia
P. Roncin, France
I. Savić, Serbia
Y. Serruys, France
N. Simonović, Serbia
M. Škorić, Japan
M. Trtica, Serbia
S. Tošić, Serbia

ADVISORY COMMITTEE

D. Belić
N. Bibić
M. S. Dimitrijević
S. Đurović
N. Konjević
M. M. Kuraica
J. Labat
G. Malović
B. P. Marinković
Z. Mijatović
M. Milosavljević
Z. Lj. Petrović
L. Č. Popović
J. Purić
B. Stanić

ORGANIZING COMMITTEE

D. Ilić (Co-chair)
V. Srećković (Co-chair)

J. Kovačević-Dojčinović (Co-secretary)
N. Cvetanović (Co-secretary)

J. Aleksić
A. Kovačević
S. Marčeta-Mandić
A. Nina
D. Onić
S. Simić
V. Zeković

ELECTRON COLLISIONS WITH DIELECTRIC GASES CONSIDERED AS SF_6 REPLACEMENT

M. RANKOVIĆ[1*], R. KUMAR T P[1], P. NAG[1], J. KOČIŠEK[1] and J. FEDOR[1]

[1]*J. Heyrovský Institute of Physical Chemistry, Czech Academy of Sciences, Dolejškova 3, 18223 Prague, Czech Republic*
E-mail [*]milos.rankovic@jh-inst.cas.cz

Abstract. During the past decades, sulfur hexafluride (SF_6) has been globally used as an insulating medium in high-voltage power distributing circuits such as switchgears. It has a very high dielectric strength and ability to recombine itself in reactions driven by electric discharge, but on the other hand, it also has an alarmingly high global warming potential (GWP of 23.5k). Given the rising ecological awareness, there are big efforts to find a suitable replacement gas which at the same time is environmentally friendly and has good dielectric properties, among other criteria. Several candidates have been suggested already, but so far, a little is known about their fundamental physical and chemical properties, namely electron collision processes which govern their behavior under electric discharge.

We probe these insulating gas candidates with electrons in vacuum under single collision conditions, on three elementary channels: (i) electron attachment, (ii) electron impact ionization and (iii) elastic and inelastic electron scattering. By combining results from three electron-molecule collision setups, we are able to quantify all three channels and provide corresponding absolute cross sections for each process. In this talk, some of the experimental results will be presented with focus on the dynamics of atomic nuclei during the scattering, especially in the bond-breaking channels like dissociative ionization (Ranković et al. 2019), dissociative electron attachment and dissociation into neutral fragments (Ranković et al. 2020).

References

Ranković, M., Chalabala, J., Zawadzki, M., Kočišek, J., Slavíček, P., and Fedor, J. : 2019*, Phys. Chem. Chem. Phys.,* **21***,* 16451.

Ranković, M., Kumar T P, R., Nag, P., Kočišek, J., and Fedor, J. : accepted in 2020*, J. Chem. Phys.*

30th Summer School and International Symposium on the Physics of Ionized Gases

Professor Miloš Ranković

Belgrade, December 2nd, 2019

Dear Professor Ranković,

On behalf of the Scientific and Organizing Committees, we have a pleasure to invite you to attend the *30th Summer School and International Symposium on the Physics of Ionized Gases* (SPIG 2020) and present a **Topical invited talk**.

The SPIG 2020 will be held from August 24th to 28th, 2020 in Šabac, Serbia. The details of the conference are available at official website: http://www.spig2020.ipb.ac.rs/ Please note that due to the limited conference budget, the SPIG2020 organizers will try to provide partial support to students and early stage researchers, as well as colleagues from economically less privileged countries. Thank you for your understanding and support.

We look forward to welcoming you to Belgrade.

Yours sincerely,

Luka Č. Popović
(Co-Chair of the Scientific Committee)

Dragana Ilić
(Co-Chair of the Loc. Org. Committee)

Duško Borka
(Co-Chair of the Scientific Committee)

Vladimir Srećković
(Co-Chair of the Loc. Org. Committee)

SPIG 2020 Organizer:
University of Belgrade, Faculty of Mathematics, Department of Astronomy

SPIG 2020 Co-organizers:
University of Belgrade, Institute of Physics
Astronomical Observatory of Belgrade

29th Summer School and International Symposium on the Physics of Ionized Gases

Aug. 28 - Sep. 1, 2018, Belgrade, Serbia

CONTRIBUTED PAPERS

&

ABSTRACTS OF INVITED LECTURES, TOPICAL INVITED LECTURES, PROGRESS REPORTS AND WORKSHOP LECTURES

Editors:
Goran Poparić, Bratislav Obradović,
Duško Borka and Milan Rajković

Vinča Institute of
Nuclear Sciences

Serbian Academy
of Sciences and Arts

29th Summer School and International Symposium on the Physics of Ionized Gases

S P I G 2018

CONTRIBUTED PAPERS

&

ABSTRACTS OF INVITED LECTURES,
TOPICAL INVITED LECTURES, PROGRESS REPORTS
AND WORKSHOP LECTURES

Editors

Goran Poparić, Bratislav Obradović,
Duško Borka and Milan Rajković

Vinča Institute of
Nuclear Sciences

Serbian Academy
of Sciences and Arts

Belgrade, 2018

CONTRIBUTED PAPERS & ABSTRACTS OF INVITED LECTURES, TOPICAL INVITED LECTURES, PROGRESS REPORTS AND WORKSHOP LECTURES

of the 29th Summer School and International Symposium on the Physics of Ionized Gases

August 28 – September 1, 2018, Belgrade, Serbia

Editors:
Goran Poparić, Bratislav Obradović,
Duško Borka and Milan Rajković

Publisher:
Vinča Institute of Nuclear Sciences,
University of Belgrade,
P.O. Box 522,
11001 Belgrade, Serbia

Computer processing:
Tatjana Milovanov

Printed by
Skripta Internacional, Mike Alasa 54, Beograd

Number of copies
200

ISBN 978-86-7306-146-7

OXYGEN K-SHELL SPECTROSCOPY OF ISOLATED BARE AND SOLVATED PEPTIDE

M. Lj. Ranković [1, 2], A. R. Milosavljević [3], K. Jänkälä [4], F. Canon [5], J. Bozek [3], C. Nicolas [3] and A. Giuliani [3, 6]

[1]*Institute of Physical Chemistry J. Heyrovsky, Czech academy of sciences, Dolejškova 3, 18223 Prague 8, Czech Republic*
[2]*Institute of Physics Belgrade, University of Belgrade, Pregrevica 118, 11080 Belgrade, Serbia*
[3]*SOLEIL, l'Orme des Merisiers, St Aubin, BP48, 91192 Gif sur Yvette Cedex, France*
[4]*Nano and Molecular Systems Research Unit, University of Oulu, P.O. Box 3000, 90014 Oulu, Finland*
[5]*INRA, UMR1324 Centre des Sciences du Goût et de l'Alimentation, F-21000 Dijon, France*
[6]*INRA, UAR1008, CEPIA, Rue de la Géraudière, BP 71627, 44316 Nantes, France*

The possibility to bring large macromolecules in the gas phase using the electrospray ionization technique along with mass spectrometry tools and synchrotron radiation sources, allows one to probe physicochemical properties of such systems. Since the complex interaction of natural surrounding water network plays a crucial role at molecular level [1], it is of great importance to study the hydration effects of peptides and proteins on both their electronic and spatial structure, in order to give more insights into radiation damage.
Recently, A. Milosavljević and coworkers demonstrated a pioneering studies of a protein in the gas phase, by coupling a VUV [2] and soft X-ray [3] synchrotron beamlines with the linear quadrupole ion trap mass spectrometer. In this talk, we will present the results from one of the following studies of hydrated SubstanceP peptide in the Oxygen K-shell energy region, performed at soft X-ray beamline PLEIADES of SOLEIL radiation facility near Paris, with focusing on the experimental techniques and details of the applied method.

Acknowledgements: This work was supported by ANR, France, under project ANR-08-BLAN-0065, MESTD of Republic of Serbia project #171020. We are grateful to SOLEIL general staff for running the beam smoothly.

REFERENCES

[1] O. Dopfer et al, *Chem. Rev*. **116**, 9 (2016).
[2] A. R. Milosavljević et al, *J. Synchrotron Radiat.* **19**, 2 (2012).
[3] A. R. Milosavljević et al, *J. Phys. Chem. Lett.* **16,** 6 (2015).

X-ray **I**nteraction with **Bi**omolecules in **G**as **P**hase (XiBiGP) workshop

Dr. Miloš Ranković
J. Heyrovský Institute of Physical Chemistry v.v.i.,
Academy of Sciences of the Czech Republic, Prague,
Czech Republic

Saint-Aubin, 22nd November 2017

Dear Dr. Ranković,

On behalf of the Scientific and Organizing Committees, we have the pleasure to invite you to attend the *29th Summer School and International Symposium on the Physics of Ionized Gases* (SPIG 2018) and present a **lecture** (30 min, including questions and discussions) at the *3rd Workshop on X-ray Interaction with Biomolecules in Gas Phase (XiBiGP)*.

The SPIG 2018 will be held from 28th August to 1nd September in Belgrade, Serbia. The XiBiGP workshop is scheduled for 28th of August. The details of the conference are available at www.spig2018.ipb.ac.rs. Unfortunately, due to the limited conference budget, the organizers cannot commit to any financial support.

We hope that you will be able to accept our invitation. Please let us know by the 8th of December 2017 and, if possible, send us the title of your lecture. Please note that your talk is foreseen for a session on Action spectroscopy of trapped macromolecular ions.

We look forward to welcoming you to Belgrade in 2018.

Yours sincerely,

Goran Poparić **Bratislav Obradović** **Duško Borka**

(Co-Chairs of the SPIG 2018 Scientific and Local Organizing Committees)

Aleksandar R. Milosavljević **Sanja Tošić**

(Co-Chairs of the **3rd XiBiGP** Workshop)

	Monday	*Tuesday*	*Wednesday*	*Thursday*
8:30 - 9:00		**Registration Opening 9:15**		
9:00 - 10:00		Invited 1 **Paul Scheier**	Invited 12 **Jens Biegert**	Invited 15 **Fernando Martín**
10:00 - 11:00		Invited 2 **Jana Roithová**	Invited 13 **Jason Greenwood**	Invited 16 **Piero Decleva**
11:00 - 12:00		**Coffee Break**	Invited 14 **Carlo Callegari**	Invited 17 **Armin Scrinzi**
12:00 - 13:00		Invited 3 **Bernard Piraux**	**Coffee Break**	**Coffee Break**
13:00 - 14:00		Invited 4 **Marcus Dahlström**	Young Scientist Forum Part I **Filippo Campi** **Milos Rankovic** **Kristina Isaković** **Gediminas Galinis** **Samuel Jenkins** **Carlos Marante**	Invited 18 **Raluca Cireasa**
14:00 - 15:00		Invited 5 **Alexander Blättermann**		Invited 19 **Yoni Toker**
15:00 - 16:00		**Lunch**	**Lunch (Conference Photo)**	Invited 20 **Tatiana Marchenko**
16:00 - 17:00		Invited 6 **Minna Patanen**		**Lunch**
17:00 - 18:00		Invited 7 **Michal Fárník**		Invited 21 **Christine Joblin**
18:00 - 19:00		Invited 8 **Patrick Rousseau**	Young Scientist Forum Part II **Linda Giacomozzi** **Alexander Galstyan** **Arkadiusz Mika** **Sylwia Stefanowska** **Marta Tarkanovskaja** **Alexander Kaiser**	Invited 22 **Christian Alcaraz**
19:00 - 20:00		**Coffee Break**		Invited 23 **Henning Schmidt**
		Invited 9 **Ines Corral**		**Concluding remarks**
	Registration	Invited 10 **Ágnes Vibók**		
		Invited 11 **Cristina Sanz-Sanz**	**Coffee Break**	
		Poster Session I **MC Meeting**	**Poster Session II**	
		Dinner	**Conference Dinner**	**Dinner**

PRAGUE 2017

4th XLIC GENERAL MEETING

XLIC
XUV/X-ray light and fast ions for ultrafast chemistry

cost
EUROPEAN COOPERATION IN SCIENCE & TECHNOLOGY

COST is supported by the EU Framework Programme Horizon 2020

4th XLIC General Meeting
COST Action CM1204

14 - 16 March 2017

Prague, Czech Republic

BOOK OF ABSTRACTS

The Czech Academy of Sciences

ÚFCH JH

4th XLIC GENERAL MEETING

COST Action CM1204

14 – 16 March 2017

Prague, Czech Republic

BOOK OF ABSTRACTS

4th XLIC GENERAL MEETING

14 – 16 March 2017

Organised by: J. Heyrovský Intitute of Physical Chemistry of the CAS, v.v.i.
Dolejškova 2155/3
182 23 Prague 8

Venue

The Conference will be hosted by Hotel Pyramida (Bělohorská 24, 169 01 Prague 6). The hotel is located near the Prague Castle, which is only one tram stop away, and other touristic attractions as well, e.g. Strahov Monastery, Petřín Hill, the Lesser Town of Prague, etc.

Publisher: J. Heyrovský Intitute of Physical Chemistry of the CAS, v.v.i.
Editors: Miroslav Polášek, Věra Křížová
Printed by: 24print s.r.o. division iDigitisk, Bořivojova 818/99,130 00 Praha 3
ISBN: 978-80-87351-41-3

Photodissociation of hydrated peptide by synchrotron radiation in the VUV region

M. Lj. Ranković[1*], F. Canon[2], L. Nahon[3], A. Giuliani[3,4] and A. R. Milosavljević[1,3]

[1]*Institute of Physics Belgrade, University of Belgrade, Pregrevica 118, 11080 Belgrade, Serbia.*
[2]*INRA, UMR1324 Centre des Sciences du Goût et de l'Alimentation, F-21000 Dijon, France.*
[3]*SOLEIL, l'Orme des Merisiers, St Aubin, BP48, 91192 Gif sur Yvette Cedex, France.*
[4]*INRA, UAR1008, CEPIA, Rue de la Géraudière, BP 71627, 44316 Nantes, France.*
[*]*Corresponding author:* mrankovic@ipb.ac.rs

Development of electrospray ionization along with already established synchrotron radiation and mass spectrometry techniques, made the studies of interaction of large biomolecules with energetic photons in the gas phase easily accessible. Combination of these techniques gave rise to action spectroscopy[1], a very powerful method, that can give more insights into fundamental physical and chemical properties of biologically relevant macromolecules such as nucleotides, amino acids, peptides[2] or proteins[3]. It is also very important to investigate the influence of the water surroundings or solvation effects on fundamental properties of these biomolecules in order to get more realistic picture of the radiation damage at molecular level.

We present the action spectroscopy results of protonated and hydrated Leucin-Enkephalin peptide, performed by coupling the VUV synchrotron radiation beamline (DESIRS, synchrotron SOLEIL) with the ion trap mass spectrometer. Results suggest that hydration with only three water molecules may have significant influence on the fragmentation pattern of this peptide, Figure 1.

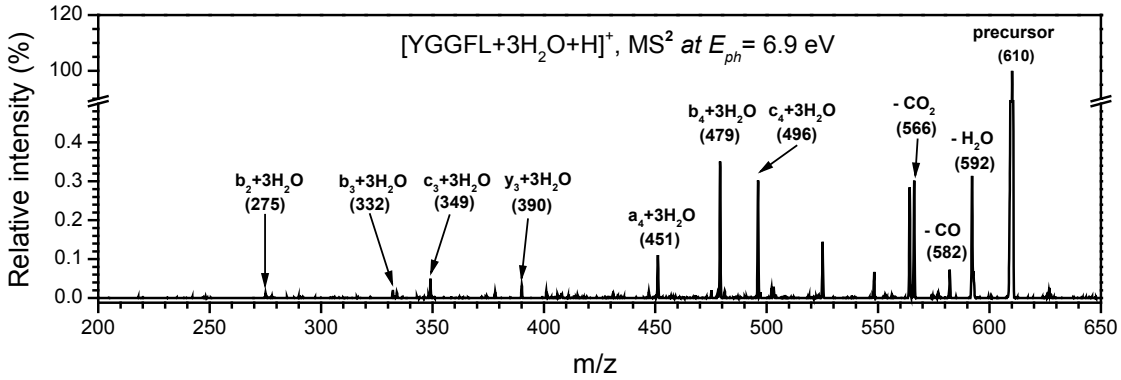

Figure 1. Tandem mass spectra (MS^2) recorded for Leucin-Enkephalin (YGGFL) peptide hydrated with three water molecules, obtained at photon energy of 6.9 eV.

Acknowledgments: This work was supported by the French ANR (Project ANR-08-BLAN-0065), the "Pavle Savic" bilateral scientific project between Serbia and France (N27482TE) and the COST Action MP1002 (Nano-IBCT). M. Lj. R. and A. R. M. acknowledge support by the MESTD of Republic Serbia, project #171020. We are grateful to SOLEIL staff for smooth beamtimes under projects 20110324 and 20130388.

References

[1] A. Giuliani et al, *Mass Spectrom. Rev.* 2014, **33**, 424-441.
[2] A. R. Milosavljević et al, *Angew. Chem.-Int. Edit.* 2013, **52**, 7286-7290.
[3] A. Giuliani et al, *Angew. Chem.-Int. Edit.* 2012, **51**, 9552-9556.

Oxygen K-edge action spectroscopy of isolated nanosolvated Substance P: Resolving the excitation of the peptide and the attached water network

A. R. Milosavljević[1]*, K. Jänkälä[2], C. Nicolas[1], M. Lj. Ranković[3], F. Canon[4], J. Bozek[1], and A. Giuliani[1,5]

[1]*SOLEIL, l'Orme des Merisiers, St. Aubin, BP48, 91192 Gif sur Yvette Cedex, France*
[2]*Centre for Molecular Materials Research, University of Oulu, P.O. Box 3000, 90014 Oulu, Finland*
[3]*Institute of Physics Belgrade, University of Belgrade, Pregrevica 118, 11080 Belgrade, Serbia*
[4]*Centre des Sciences du Goût et de l'Alimentation, CNRS, INRA, Université de Bourgogne Franche-Comté, F-21000 Dijon, France*
[5]*INRA, UAR1008, CEPIA, Rue de la Géraudière, BP 71627, 44316 Nantes, France*

[*]*Corresponding author:* milosavljevic@synchrotron-soleil.fr

The study of isolated biomolecules solvated on an atomic level is important to understand the hydrogen bonding network of water molecules and their interaction with the biomolecule that overall defines its structure and functionality [1]. Here we report preliminary results of a pioneering study of inner-shell excitation of an isolated nanosolvated peptide.

We have performed O K-edge inner-shell action spectroscopy of both bare and hydrated Substance P peptide ions isolated in the gas phase, by coupling a commercial linear quadrupole ion trap mass spectrometer (LTQ XL) to the PLEIADES soft X-ray beamline at the SOLEIL synchrotron, as previously described [2,3]. For the first time, we recorded O K-edge ion yield spectra for isolated doubly charged Substance P peptide, as well as for the same system hydrated with 11 water molecules. The present results suggest that processes upon excitation of the peptide and the attached water cluster could be resolved. We are presently performing high-level DFT calculations in order to understand the structure and the excitation processes of the solvated peptide.

Acknowledgments: Supported by ANR-08-BLAN-0065, MESTD Republic of Serbia (#171020) and COST action "XUV/X-ray light and fast ions for ultrafast chemistry − XLIC". The SOLEIL synchrotron is acknowledged for providing beamtime under Project 20160335.

References

[1] N. S. Nagornova, T. R. Rizzo, O. V. Boyarkin, *Science,* 2012, **336**, 320.
[2] A. R. Milosavljević, F. Canon, C. Nicolas, C. Miron, L. Nahon, and A. Giuliani, *J. Phys. Chem. Letters*, 2012, **3**, 1191.
[3] A. R. Milosavljević, C. Nicolas, M. Lj. Ranković, F. Canon, C. Miron and A. Giuliani, *J. Phys. Chem. Letters*, 2015, **6**, 3132.

Subject **invitation - 3rd Young Scientist Forum of the XLIC COST Action**

From Alicja DOMARACKA <domaracka@ganil.fr>

To Milos Rankovic <mrankovic@ipb.ac.rs>

Cc Miroslav Polášek <miroslav.polasek@jh-inst.cas.cz>

Date 2016-12-07 14:21

Dear Milos Rankovic,

The 4th General Meeting of the XLIC COST Action will take place from 14th to 16th March 2017 in Prague, Czech Republic. It will include the 3rd Young Scientist Forum -- a special half-day section with talks given by PhD students and young post-docs.

It is a pleasure for us to invite you to give a talk during special section dedicated for young scientist. We invite you to present results of your STSM financed by the XLIC COST Action or/and of your PhD thesis/ post-doc. The format of the talk is 15 minutes and 5 minutes of discussion.

Could you inform us before 22nd December 2016 if you can accept the invitation?

If so, please send us a tentative title and an abstract of your talk.

You can find more information about XLIC COST Action at www.xlic.eu and information about the meeting at http://www.jh-inst.cas.cz/xlic2017. The meeting will have no registration fees for participants and COST Action will cover the travel, meals and accommodation expenses of invited speakers.

Best regards,

Alicja Domaracka (XLIC-Young Scientists Coordinator)

and

Miroslav Polášek (Local Chair of the meeting)

XX International Workshop on
Low-Energy Positron and Positronium Physics

XXI International Symposium on
Electron-Molecule Collisions and Swarms

V Workshop on Non-Equilibrium Processes

18-21 July 2019, Belgrade, Serbia

POSMOL 2019

BOOK OF ABSTRACTS

XX Међународна радионица о физици
ниско енергијских позитрона и позитронијума

XXI Међународни симпозијум о
електрон-молекулским сударима и појевима

V Радионица о неравнотежним процесима

Serbian Academy of Sciences and Arts

UNIVERSITY OF BELGRADE
INSTITUTE OF PHYSICS | BELGRADE

Panacomp
Wonderland Travel
Lufthansa City Center

XX International Workshop on
Low-Energy Positron and Positronium Physics

XXI International Symposium on
Electron-Molecule Collisions and Swarms

V Workshop on Non-Equilibrium Processes

POSMOL 2019

BOOK OF ABSTRACTS

Editors

David Cassidy, Michael J. Brunger,
Zoran Lj. Petrović, Saša Dujko, Bratislav P. Marinković,
Dragana Marić and Sanja Tošić

Serbian Academy
of Sciences and Arts

Institute of Physics Belgrade
University of Belgrade

Belgrade, 2019

BOOK OF ABSTRACTS of the

XX International Workshop on Low-Energy Positron and Positronium Physics

XXI International Symposium on Electron-Molecule Collisions and Swarms

V Workshop on Non-Equilibrium Processes

18-21 July 2019, Belgrade, Serbia

Editors:

David Cassidy, Michael J. Brunger,
Zoran Lj. Petrović, Saša Dujko, Bratislav P. Marinković,
Dragana Marić and Sanja Tošić

Publishers:

Serbian Academy of Sciences and Arts
Kneza Mihaila 35
11000 Belgrade, Serbia

Institute of Physics Belgrade
Pregrevica 118, P. O. Box 68
11080 Belgrade, Serbia

Computer processing:

Dragana Marić and Sanja Tošić

Printed by

Serbian Academy of Sciences and Arts
Belgrade

Number of copies

250

ISBN 978-86-7025-819-8

Dissociative Ionization Dynamics of Dielectric gas C_3F_7CN

M. Ranković[1], J. Chalabala[2], M. Zawadzki[1,3], J. Kočišek[1], P. Slavíček[1,2] and J. Fedor[1]
[1] J. Heyrovský Institute of Physical Chemistry, Czech Academy of Sciences, Dolejškova 3, 18223 Prague, Czech Republic
[2] Department of Physical Chemistry, University of Chemistry and Technology, Technická 5, 166 28 Prague, Czech Republic
[3] Department of Atomic, Molecular, and Optical Physics, Faculty of Applied Physics
[4] Mathematics, Gdańsk University of Technology, ul. G. Narutowicza 11/12, 80-233 Gdańsk, Poland
milos.rankovic@jh-inst.cas.cz

Due to a very high global warming potential (GWP) of 23500, a widely used insulation gas SF_6 will no longer be applicable in high-voltage equipment, such as switchgears and other high power energy distributing circuits. A big effort has been invested in finding a suitable alternative that is environmentally friendly and has good dielectric strength. One of very promising candidates that meets those criteria is heptafluoroisobutyronitrile (C_3F_7CN). While a few companies are already supplying their switchgear products with this insulating gas, the majority of equipment around the world is still using SF_6.

The electron collisions are elementary mechanism which governs the discharge chemistry and physics in an insulating medium under high-voltage switching conditions. In order to better understand discharge reactions in this gas, it is important to know its fundamental physical properties. Being quite a new replacement gas in the industry, C_3F_7CN is not well studied and there is a lack of cross sections data in the literature. Apart from one experimental study done by Li et al [1], there are only a few theoretical studies, where Xiong et al. [2] reported calculated cross sections.

In this work, we present the experimental absolute partial ionization cross sections in the range (0-100) eV and electron impact ionization mass spectra of C_3F_7CN [3]. A reflectron time-of-flight (RTOF) experimental setup was used to record the mass spectra. Second experimental setup based on trochoidal electron monochromator and equipped with time of flight ion detection was originally designed for dissociative electron attachment experiments. We modified it in order to be able to measure absolute total ionization cross sections. We show that ionization proceeds mainly through one dominant channel leading to a complete dissociation of molecule. Our computational non-adiabatic treatment is able to reproduce experimental findings with a good agreement.

References

[1] Y. Li, X. Zhang, S. Xiao, Q. Chen, J. Tang, D. Chen and D. Wang, *Ind. Eng. Chem. Res.*, **57**, (2018), 5173–5182.
[2] J. Xiong, X. Li, J. Wu, X. Guo and H. Zhao, *J. Phys. D*, **50**, (2017), 445206.
[3] M. Ranković, J. Chalabala, M. Zawadzki, J. Kočišek, P. Slavíček and J. Fedor, accepted in *Phys. Chem. Chem. Phys* (2019).

Vibrational Excitation and Dissociative Electron Attachment Cross Sections in Cyanoacetylene HC_3N

M. Ranković[1], P. Nag[1], M. Zawadzki[1,2], M. Polášek[1], J. Žabka[1], J. Kočišek[1], J. Fedor[1]
[1]J. Heyrovský Institute of Physical Chemistry, Academy of Sciences of the Czech Republic, Dolejškova 3, 182 23 Prague, Czech Republic
[2]Atomic Physics Division, Department of Atomic, Molecular and Optical Physics, Faculty of Applied Physics and Mathematics, Gdansk University of Technology, ul. Gabriela Narutowicza 11/12, 80-233 Gdansk, Poland
juraj.fedor@jh-inst.cas.cz

Cyanoacetylene, HC_3N, has been attracting attention due to its abundance in a number of extraterrestrial environments, such as molecular clouds or Titan's atmoshere. It is believed, that the chemical transormation in such environments is to a large degree driven by an electron impact. At the same time, there is very little data on the electron collisions with HC_3N available, we are aware only of one experimental quantitative DEA study. [1]

We have used three electron collision setups: an electrostatic spectrometer with hemispherical analyzers, quantitative DEA spectrometer with time-of-flight analyzer, and high-resolution DEA spectrometer with quadrupole analyzer. With the first one, we probed the elastic and vibrationally inelastic cross sections at 135º scattering angle, combining the two later ones, we determined the partial DEA cross sections.

The vibrational excitation cross sections reveal presence of four shape resonances. The first one gives rise to a pronounced boomerang structure which overlaps with the threshold peak originating from the electron-dipole excitation, and thus creates and interesting patterm. This resonance is visible in all the vibrations. The other resonances are much more selective, especially the two σ^* states are prominent only in the excitation of the CH and CN stretch modes. The DEA cross sections are in an excellent qualitative agreement with the data of Gilmore and Field [1], however, the present absolute data are approximately by a factor of two lower. The comparison with the vibrational excitation data allows for assignment of the DEA bands.

References

[1] T. D. Gilmore, T. A. Field, *J. Phys. B*, **48**, (2015), 035201.
[2] M. Ranković et al., *Phys. Rev. A*, **98**, (2018), 052708.

MPS '18
Budapest

INTERNATIONAL CONFERENCE ON MANY PARTICLE SPECTROSCOPY OF ATOMS, MOLECULES, CLUSTERS AND SURFACES

BUDAPEST, HUNGARY
21-24 AUGUST 2018

PROGRAMME AND BOOK OF ABSTRACTS

International Conference on Many Particle Spectroscopy of Atoms, Molecules, Clusters and Surfaces

Budapest, Hungary

21-24 August 2018

MPS '18

Budapest

Programme
and
Book of Abstracts

Local Organizing Committee

Károly Tőkési (Chair)
Arnold Farkas
Henrik Haspel
Zoltán Kónya
Béla Paripás
Gábor Pszota

Web address: mpsbudapest2018.com **E-mail**: mpsbudapest2018@gmail.com

Damir Nag

Vibrational and dissociative dynamics of resonant states in nitrobenzene

P. Nag[1], M. Ranković[1,2], J. Fedor[1]

[1], *J. Heyrovský Institute of Physical Chemistry, Dolejškova 2155/3, Prague 8, Czech Republic*
[2]*Laboratory for atomic collision processes, University of Belgrade, Pregrevica 118, 11080 Belgrade, Serbia*
Corresponding author: pamir.nag@jh-inst.cas.cz

A standard tool for probing the dynamics of nuclear motion is by time-resolved ultrafast spectroscopy. We use a different approach by forming a resonance (temporary negative ion) in an electron-molecule collision and utilizing the fact that the competition between the electron detachment and molecular dissociation is happening on a femto- to picosecond timescale.

We have measured the 2-dimensional electron impact spectroscopy [1] to understand the vibrational excitation of nitrobenzene ($C_6H_5NO_2$) via different temporary negative ion (TNI) states. The energy loss spectra in between 0-1.5 eV recorded for 0.6 eV constant residual energy is shown in Figure 1.

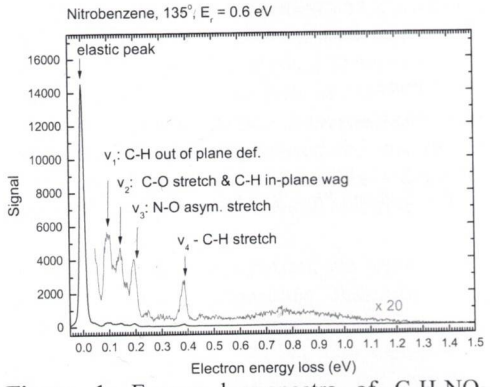

Figure 1. Energy loss-spectra of $C_6H_5NO_2$ recorded at 135° for constant residual energy of 0.6 eV

In electron impact vibrational excitation, the incoming electron resonantly captured by the molecule, forming a TNI state. The TNI ejects the electron and decays into ground and different vibrationally excited states. The cross-section of the scattered electrons with a fixed energy loss for different incident electron energies is shown in figure 2. We also have measured the absolute cross-section of all the fragments formed due to dissociative electron attachment to nitro-benzene [2]. In the presentation we will discuss the results in detail.

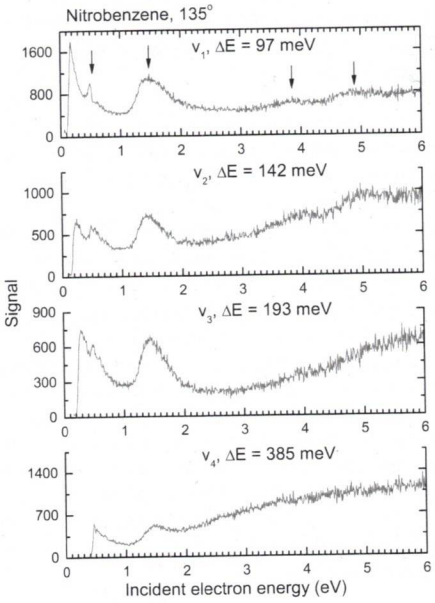

Figure 2. Vibrational excitation of nitrobenzene via different resonant states.

References

[1] K. Regeta, M. Allan, *Phys. Rev. Lett.* **(2013)** 110, 203201.

[2] A Pelc, P.Scheier, T. D. Märk , Vacuum, (2007) 81, 1180

CEPAS 2017

7th Conference on Elementary Processes in Atomic Systems

3rd – 6th September 2017

Průhonice, Czech Republic

PRAGUE CEPAS 2017

Local organizing comitee:

Václav Alt
Martin Čížek
Roman Čurík
Karel Houfek
Dávid Hvizdoš
Michal Tarana
Petra Votavová

International scientific committee:

Friedrich Aumayr, Austria
Joachim Burgdorfer, Austria
Robert DuBois, United States
Gustavo Garcia Gomez-Tejedor, Spain
Jiří Horáček, Czech Republic
Bratislav P. Marinkoviá, Serbia
Nigel J. Mason, United Kingdom
Ladislau Nagy, Romania
Zoran Lj. Petrović, Serbia
Otto B. Shpenik, Ukraine
Andrey Solovyov, Germany
Viorica Stancalie, Romania
John A. Tanis, United States
Károly Tőkesi, Hungary
Mariusz Zubek, Poland

Editors: Michal Tarana, Roman Čurík

First published: September 2017

Published by:

J. Heyrovský Institute of Physical Chemistry, v.v.i.
Academy of Sciences of the Czech Republic
Dolejškova 3, 18223 Prague 8
Czech Republic

ISBN 978-80-87351-46-8

Electron transmission through steel capillary

B.P. Marinković[1], M.Lj. Ranković[1], J.B. Maljković[1], A.R. Milosavljević[2], D. Borka[3], C. Lemell[4], K. Tökesi[5]

[1]*Institute of Physics Belgrade, University of Belgrade, Pregrevica 118, 11080 Belgrade, Serbia*

[2]*PLÉIADES beamline, Synchrotron SOLEIL, L'orme des Merisiers, Saint-Aubin - BP48, 91192 GIF-sur-YVETTE CEDEX, France*

[3]*Atomic Physics Laboratory, Vinča Institute of Nuclear Sciences, University of Belgrade, Belgrade, Serbia*

[4]*Institute for Theoretical Physics, Vienna University of Technology, Vienna, Austria*

[5]*Institute for Nuclear Research, Hungarian Academy of Sciences (ATOMKI), Debrecen, Hungary and ELI-ALPS, ELI-HU Non-profit Kft., Szeged, Hungary*

The transmission of low-energy electrons through platinum [1, 2] and steel capillaries have been investigated both experimentally and theoretically. The length of the present steel capillary was $L = 19.50$ mm while the inner diameter was $d = 0.90$ mm. Kinetic energy distribution of electrons transmitted through steel capillary was recorded at two tilt angles (the angle between the incident electron beam and the capillary axis) of 2.64° and 4.0°, respectively. The experimental results were obtained by an electron spectrometer which consists of an electron gun, a double cylindrical mirror energy analyzer (DCMA) and a channeltron detector.

Electron transmission is modelled by a classical trajectory Monte Carlo simulation taking both elastic and inelastic scattering events of primary electrons colliding with the inner wall of the capillary and transport of secondary electrons into account.

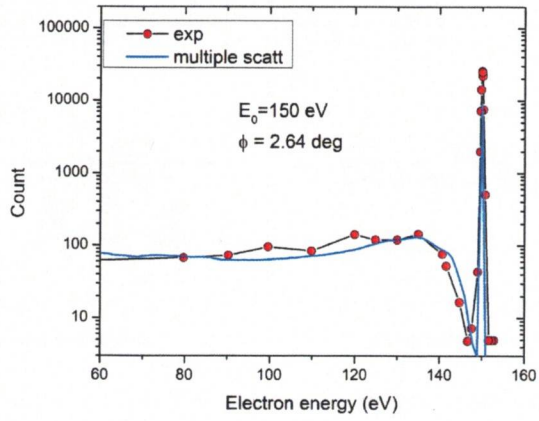

Figure 1: Energy spectra of electrons transmitted through a steel capillary.

Figure 1 shows energy spectra of 150 eV electrons passing through the steel capillary at 2.64° tilt angle. We found excellent agreement between our simulated electron-energy spectra with experimental data.

[1] A.R. Milosavljević *et al.*. Nucl. Instr. Meth. Phys. Res. B **354** (2015) 86.

[2] D. Borka *et al.*, Nucl. Instr. Meth. Phys. Res. B, in press (2017), http://dx.doi.org/10.1016/j.nimb.2017.02.024

VUV action spectroscopy of protonated Tri-Alanine peptide

M. Ranković[1], A. Milosavljević[2], A. Giuliani[3],F. Canon[4] and Laurent Nahon[2]

[1]*Institute of Physics Belgrade, Pregrevica 118, 11080 Belgrade, Serbia*

[2]*SOLEIL, l'Orme des Merisiers BP48, 91192, Paris, France*

[3]*INRA, Rue de la Géraudiére BP 71627, 44316, Nantes, France*

[4]*CNRS, Boulevard Jeanne d'Arc 9E, F-21000, Dijon, France*

The studies of interaction of energetic photons with big macromolecules such as amino acids, peptides and proteins in the gas phase have become accessible in recent years with developments of electrospray (ESI) and mass spectrometry techniques. A wide photon energy range and high flux provided by synchrotron radiation sources in combination with these techniques gives one a very powerful tool [1] for closer investigation of radiation damage at molecular level.

We present the photodisociation results of protonated small peptide Tri-Alanine obtained at VUV beamline DESIRS of synchrotron SOLEIL near Paris, France. The experiment was performed by coupling the beamline with quadrupole ion trap mass spectrometer [2]. Electrosprayed cation precursor $[AAA+H]^+$ was selected in the ion trap and subjected to VUV photons of (6.7-9.7) eV energy range.

The backbone fragments corresponding to the peptide bond scision are visible, although neutral losses dominate the mass spectrum Fig 1. Weak energy band at about 7 eV was observed for some backbone ion yields. Moreover, ion yields from almost all fragments show strong increase after 9 eV, suggesting another energy band. For small peptides, these bands might be traced to $\pi\pi^*$ transitions as previously observed [3].

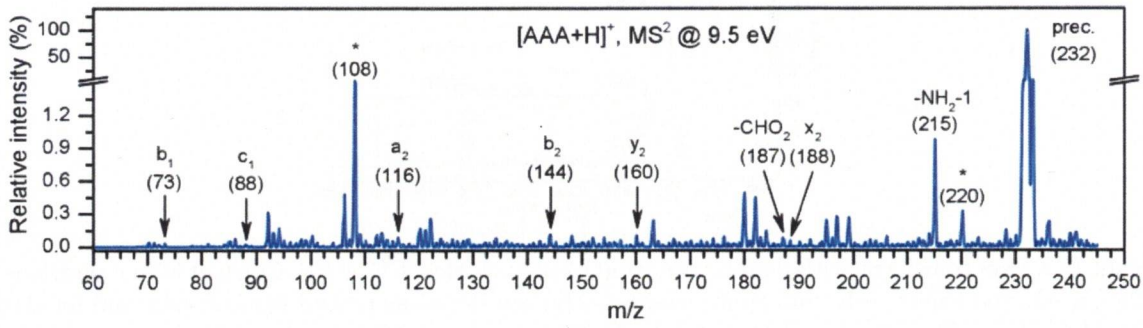

Figure 1: Tandem mass spectrum of protonated AAA peptide recorded at 9.5 eV.

Acknowledgements. This work was supported by the French ANR (project no. ANR-08-BLAN-0065), the "Pavle Savic" bilateral scientific project between Serbia and France (No. 27482TE) and the COST Action MP1002 (Nano-IBCT). A.R.M. and M.Lj.R., acknowledge support by the Ministry of Education, Science and Technological Development of the Republic of Serbia under project 171020. We are grateful to the SOLEIL general staff for providing beamtime under project no. 20120874 and 20130388.

[1] A. Giuliani *et al.*, Mass Spectrom. Rev. **33** (2014) 424.
[2] A.R. Milosavljević *et al.*, Angew. Chem.-Int. Edit. **52** (2013) 7286.
[3] M. Lj. Ranković *et al.*, J. Chem. Phys. **143** (2015) 244311, 1-8.

3rd International Workshop on Dissociative Electron Attachment

Book of Abstracts

Villa Lanna, Prague, April 10-13, 2018

3rd International Workshop on Dissociative Electron Attachment

In honor of

E. Krishnakumar

for his outstanding contribution to the field of dissociative electron attachment.

April 10.-13., 2018

Villa Lanna, Prague, Czech Republic

Local organizers:

Juraj Fedor, Jaroslav Kočišek, Miloš Ranković, Pamir Nag, Dominika Kollárová

J. Heyrovský Institute of Physical Chemistry of the Czech Academy of Sciences

Supported by The Sir John Mason Academic Trust

DISSOCIATIVE ELECTRON ATTACHMENT AND ANION-INDUCED DIMERIZATION IN PYRUVIC ACID

Ranković M.[1,2], Zawadski M.[3], Kočišek J.[1] and Fedor J.[1]

[1]*Department for dynamics of molecules and clusters, Czech academy of sciences, Dolejškova 3, 18223 Prague 8, Czech Republic*
[2]*Laboratory for atomic collision processes, University of Belgrade, Pregrevica 118, 11080 Belgrade, Serbia*
[3] *Department of atomic, molecular and optical physics, Gdańsk University of Technology, ul. Gabriela Narutowicza 11/12, 80-233 Gdańsk, Poland*
milos.rankovic@jh-inst.cas.cz

Pyruvic acid (CH_3–CO–COOH) is the simplest α-keto acid and it is a relevant molecule for processes involving atmospheric chemistry, biochemistry and astrochemistry. Photo-oxidation of biogenic and anthropogenic precursors like isoprene emitted from trees leads to a formation of pyruvic acid in the atmosphere. In living cells, pyruvic acid is a product of glycolysis and can serve as a precursor for important species in Kerbs cycle where energy stored from fat, proteins and carbohydrates is released. Moreover, it has been suggested as a prebiotic molecule since it can be synthesized from H_2O and CO_2 in conditions of high pressures and temperatures. Such conditions are present in carbonaceous meteorites [1] where pyruvic acid has been previously observed.

We report experimental results of dissociative electron attachment (DEA) to pyruvic acid [2] in the low energy range. The data set is obtained from experiments performed on two setups equipped with trochoidal electron monohromators, recently transferred to Prague from Fribourg in Switzerland. One setup is coupled with time of flight (TOF) spectrometer providing the absolute measurements. The other setup with higher energy resolution is coupled to a quadrupole mass filter (QMS). The latter provides relative ion yields that are brought to an absolute scale by using data from the TOF setup. A rich fragmentation pattern is observed were many channels show distinct features corresponding to Feshbah resonances. Here, we present the absolute partial cross sections for all visible dissociation channels in pyruvic acid. The one observed at mass-to-charge ratio 87, originating from the cleavage of hydroxyl bond is displayed in Figure 3. Furthermore, some fragments do not originate from the DEA of a single pyruvic acid molecule, instead they are a result of secondary reactions with transient negative ion $M^{\#-}$. Such reactions most probably proceed via a fast proton transfer from neutral pyruvic acid to the anion that forms a vibrationally hot dimer complex and induces the fragmentation.

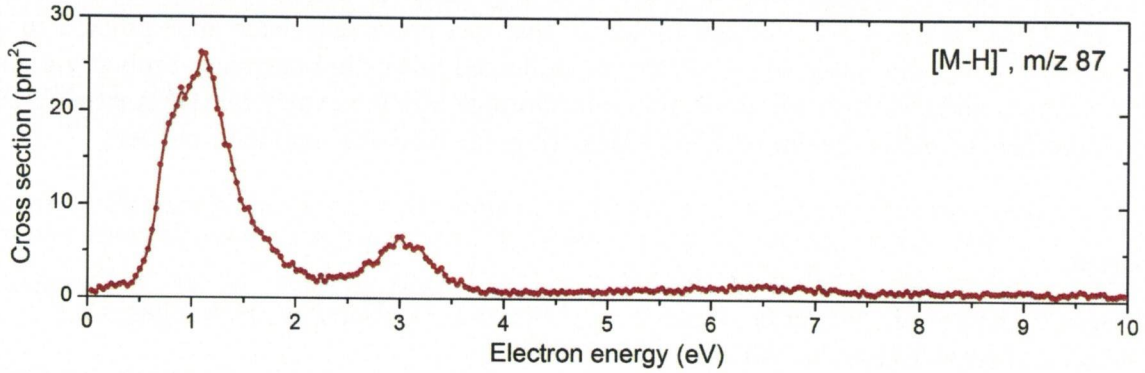

Figure 3 – Partial cross section of dehydrogenated Pyruvic acid as a function of incident electron energy.

References:

[1] Cooper, G.; *Proc. Natl. Acad. Sci. U. S. A.*, 108, 14015-14020, 2011

[2] Zawadzki, M.; *Phys.Chem.Chem.Phys.* 20, 6838, 2018

Photoinduced fragmentation of gas-phase protonated leucine- enkephalin peptide in the VUV range

2015 J. Phys.: Conf. Ser. 635 012034

(http://iopscience.iop.org/1742-6596/635/1/012034)

Journal of Physics: Conference Series **635** (2015) 012034 doi:10.1088/1742-6596/635/1/012034

Photoinduced fragmentation of gas-phase protonated leucine-enkephalin peptide in the VUV range

M Lj Ranković[1*], F Canon[2], L Nahon[3], A Giuliani[3,4] and A R Milosavljević[1,5]
[1] Institute of Physics Belgrade, University of Belgrade, Pregrevica 118, 11080 Belgrade, Serbia
[2] INRA, UMR1324 Centre des Sciences du Goût et de l'Alimentation, F-21000 Dijon, France
[3] SOLEIL, L'Orme des Merisiers, St Aubin, BP48, 91192 Gif sur Yvette Cedex, France
[4] INRA, UAR1008, CEPIA, Rue de la Géraudière, BP 71627, 44316 Nantes, France
[5] Radiation Laboratory, University of Notre Dame, Notre Dame, Indiana 46556, USA

E-mail: mrankovic@ipb.ac.rs

Abstract. In this article we report new results for action spectroscopy of protonated peptide Leucine enkephalin (YGGFL). By coupling a linear ion trap mass spectrometer with a vacuum ultraviolet (VUV) synchrotron radiation beamline, we investigate photofragmentation pattern of this peptide, through the analysis of tandem mass spectra recorded over a range of VUV photon energies, below and above the ionization energy. The obtained fragmentation patterns are discussed and compared to previous results.

1. Introduction

Development of electrospray ionization (ESI) [1], along with the advances in mass spectrometry techniques in recent years, has allowed manipulation of large bio-molecular ionic species in the gas phase. Therefore, fundamental properties of peptides, proteins, and nucleic acids such as ionization energies, bond energies and electronic energy levels could be investigated through action spectroscopy methods. In the present work ESI technique is used to produce intact biomolecular ionic species in the gas phase, from liquid solutions of these molecules. Tandem mass spectrometry by using VUV as an activation method was employed to investigate targets of interest.

Leucine enkephalin (Leu-enk) peptide is formed from five amino acids joined through peptide bonds, with the sequence tyrosine-glycine-glycine-phenylalanine-leucine (or YGGFL, in one letter coding). Leu-enk is an ideal candidate to study because it is small enough to be easily manageable with mass spectrometry techniques and to allow clear analysis of fragmentation products, while still being big enough to represent peptides. Usually the site of protonation is at N-terminus of the first amino acid - tyrosine, although other protonation sites were reported in the literature, as a consequence of proton mobility (see [2] and references therein). A standard nomenclature of the backbone fragments is based on where the positive charge (proton) stays upon bond scission and which particular bond is cleaved. If the proton stays at C-terminal, fragments a, b, c are formed, while fragments x, y, z originate from the N-terminal. Numbers in the subscripts of the fragment letters indicate the number of amino acid residues left in the particular fragment. Cleavage of the peptide C-N bonds is the origin of b and y fragment ions. Figure 1 displays a schematic structure of the Leu-enk peptide and denotation of some backbone fragments relevant for the present work.

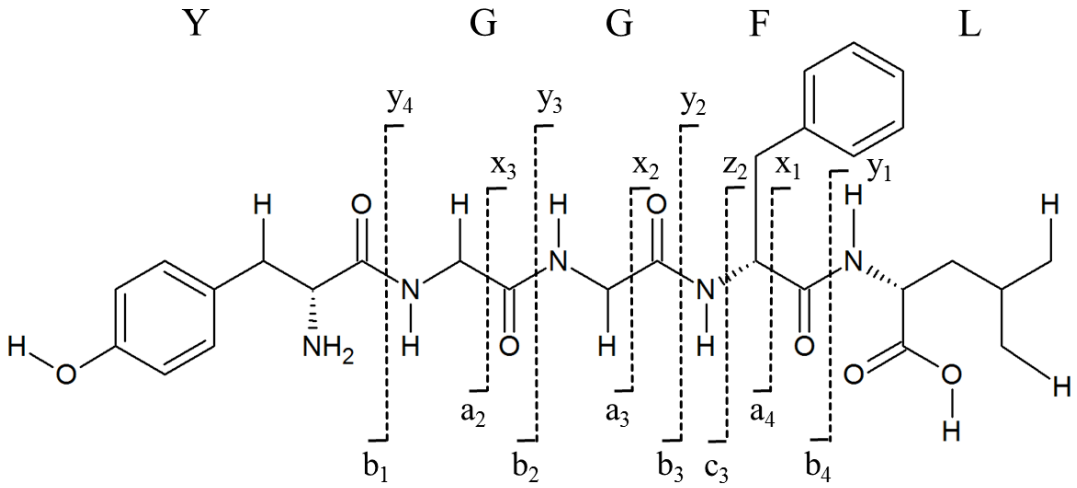

Figure 1. Schematic structure of Leucine enkephalin peptide with denoted fragments (dashed lines) and constituent amino acids (in one letter code).

Leu-enk has been probed with a vast number of different techniques, covering fragmentation pattern information and fragment yields. The reported results include collision induced dissociation (CID) [3], surface induced dissociation (SID) [4], blackbody infrared radiative dissociation (BIRD) [5] and laser-induced dissociation (LID) [6]. Each of these methods produces different conditions which favor certain decomposition pathways governed by certain fragmentation mechanisms. An extensive study of fragmentation schemes has been reported for protonated Leu-enk in the experiment involving multiple-resonance CID, by V. Rakov *et al*. in [3]. One of the reasons Leu-enk is used as a standard peptide is because it is very useful for testing and tuning new experimental setups, since it has been found that abundance ratios of some fragment ions can indicate an amount of internal energy deposited in the precursor ions [7]. Therefore, experimental parameters of a setup are adjusted in such a way that various ratios of Leu-enk's fragment intensities are kept constant. On the other hand, ratios of a_4/b_4 and b_3/y_2 can indicate at least qualitatively the degree of excitation of the precursor ions.

Amino acids and peptides strongly absorb VUV light [8]. Therefore an investigation of VUV interaction with peptides is of great interest. The only VUV light source with high enough brilliance and flexibility to continuously change the photon energy over a wide range is the synchrotron radiation source. A comprehensive study of VUV-induced fragmentation of protonated Leu-enk was reported by S. Bari *et al* in [9]. In the present work, we extend this investigation by means of mass resolution, the number of assigned ionic fragments and the photon energy range. The obtained results are also compared with existing data.

2. Experiment

Mass spectra in this article were obtained using the experimental setup located at the synchrotron SOLEIL near Paris, France. A commercial mass spectrometer Thermo Phiningan LTQ XL (LTQ) equipped with ESI was connected to the synchrotron VUV beamline DESIRS [10], with custom made turbo differential vacuum manifold [11-13]. Leu-enk ions produced by ESI were isolated in a linear quadrupole ion trap and subjected to VUV photons. After well-defined time of irradiation (500 ms in the present experiment) at particular photon energy, tandem mass spectra (MS^2) were recorded.

The LTQ mass spectrometer was connected to the synchrotron beamline from the back side of the LTQ. A dedicated vacuum manifold has been made to accommodate the pressure difference between

the LTQ and the beamline. One side of the vacuum manifold was fixed to the beamline where the pressure is in the order of 10^{-8} mbar, while the other side was connected via flexible bellow to the back plate window of the mass spectrometer. The pressure of the Helium buffer gas inside the ion trap of LTQ is of the order of 10^{-3} mbar while the pressure in the spectrometer is of the order of 10^{-5} mbar. During the operation and photon irradiation, the pressure inside the vacuum manifold was in the order of 10^{-6} mbar. A home-made rotating mechanical shutter driven by an electric motor was built and positioned in front of the photon beam inside the vacuum manifold. Cooling of the electric motor in the vacuum was established through heat conduction through a massive copper heat sink (holder) tightly surrounding the motor [14]. Alignment of the photon beam with respect to the ion trap's axis was achieved by using a custom supporting frame, mounted under the LTQ. It has several degrees of freedom, both translational and rotational, which allow for a fine alignment of the ion trap position with respect to the incident photon beam. An optimal alignment provides the highest overlap between cylindrical ion trapping region and the photon beam and is essential for the experiment.

Leu-enk was provided from Sigma-Aldrich as a powder and it was diluted with water/acetonitrile 75:25% v/v solution to the final concentration of 10 μM. The ESI source is positioned on the front side of LTQ. The ions formed by ESI source from the solution are guided by a system of ion lenses and stored in the ion trap. Parameters of ESI were optimized to obtain highest possible abundance of protonated Leu-enk cations $[YGGFL+H]^+$. A typically recorded mass spectrum (MS^1) produced by ESI is displayed in figure 2.

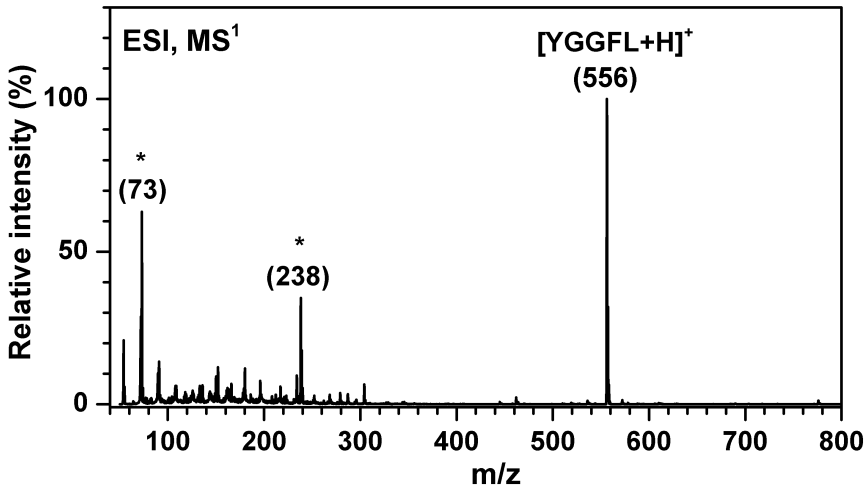

Figure 2. The mass spectrum of electro-sprayed Leu-enk ions from water/acetonitrile 75/25% solution with 10 μM concentration of peptide molecules. The peak in the spectrum at m/z 556 corresponds to the protonated Leu-enk cation $[YGGFL+H]^+$, while two peaks denoted with a star originate from pollutions.

The precursor ions of interest, in this case $[YGGFL+H]^+$, were selected and isolated in the ion trap, by means of ejecting all other ions. When enough precursor ions are accumulated in the ion trap or when a time limit for ion accumulation is reached, the mechanical shutter opens and the monochromatic VUV photon beam of defined energy irradiates the precursor ions. Synchrotron beamline DESIRS [10] is equipped with a gas filter cutting off higher order harmonics, which can create an additional signal originating from higher photon energies. If filled with Krypton, the gas filter cuts off all photon energies above 14 eV. Additionally, a MgF_2 glass filter is inserted as the part of the vacuum manifold assembly, to cut off the higher harmonics over 10.6 eV. The photon beam produced by the beamline undulator is monochromatized by using a normal incidence monochromator, resulting in final energy resolution of around 10 meV in the present case.

3. Results and discussion

J. Sztáray *et al*. in [15] performed a review of the studies about Leu-enk energetics and reaction pathways, so we will focus here only on the discussion of the most prominent fragments prevailing under our experimental conditions. Figure 3 displays the tandem mass spectra obtained for protonated Leu-enk precursor ions $[YGGFL+H]^+$ after activation with synchrotron VUV photons at three different energies. The mass spectra have been normalized to show the precursor ions $[YGGFL+H]^+$ at m/z 556 with 100 % relative intensity.

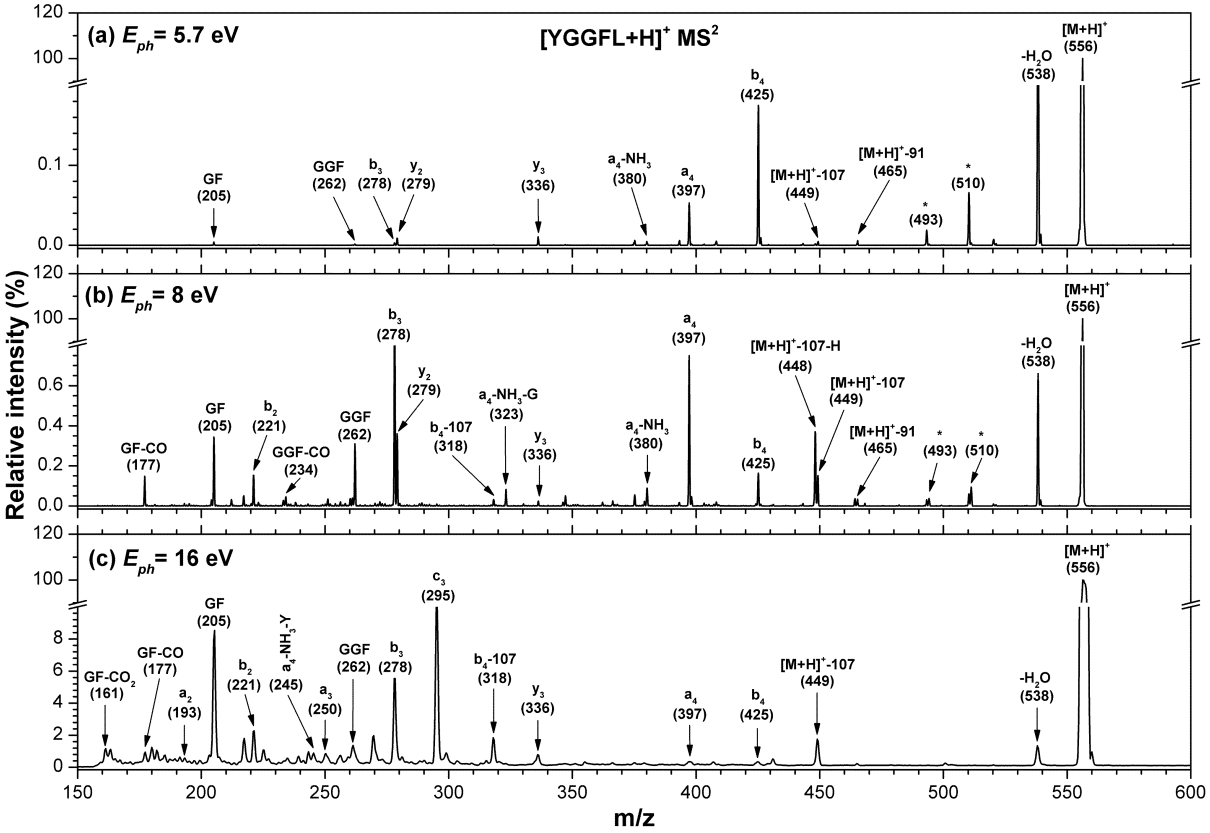

Figure 3. Tandem mass spectrum of protonated Leucine enkephalin precursor ions after irradiation with photons of a) 5.7 eV b) 8 eV and c) 16 eV.

Fragmentation patterns in our spectra are in good agreement with the ones reported in [9], which is expected considering the similar experimental conditions: VUV synchrotron photon activation of trapped ions. The lack of x and z and low abundant y-sequence ions in our spectra confirm that N-terminal ions are favoured. The ionization energy (IE) of protonated Leu-enk was determined by DFT calculations to be 8.87 eV [16]. The radical cation is not observed in our spectra and it is likely that it is not stable and fragments readily after its formation, as it has been proposed by Bari *et al*. [9]. For sub-ionisation energies absorption of photons by precursor ions leaves them in an excited electronic state. This energy may be redistributed internally via intramolecular vibrational processes, causing the weak peptide C-N bonds to break first, forming the backbone ions b and y. According to the fragmentation scheme proposed in [3], the major reaction pathway is following: YGFFL-b_4-a_4-b_3-b_2-a_2-Y. All these ions are present in our mass spectra, except Y (136), due to the mass cut off at m/z 150. Backbone ion b_4 (m/z 425) needs the lowest photon energy to form and it shows up as the strongest fragment at 5.7 eV in our mass spectrum. This ion is formed directly from dissociation of the precursor ions. The fragment at m/z 538 corresponds to the loss of a water molecule from the

precursor ions. Its intensity is highest among all fragments in the lowest energy region but falls quickly with the increase of the photon energy. Note that this fragment has not been discussed in the previous work by Bari et al. [9]. Following figure 1, after CO loss, b_4 forms into the fragment ion a_4 (m/z 397). Ion a_4 dissociates with the neutral loss of NH_3 into fragment at m/z 380. After Glycine residue loss (-57) near ionization energy, this ion is observed at a_4-NH_3-G (m/z 323). It is also reported and discussed in detail by a group of Glish, as a rearrangement fragment FYG (m/z 323) [17]. The intensity of the ion a_4 exceeds the b_4 intensity and peaks at around 7 eV, where it is the most prominent fragment in the mass spectrum. This energy corresponds to the peak of the absorption band coming from the π-π^* peptide transition. Fragment b_3 (m/z 278) is the next in line to show up as a dominant fragment with further increase of the photon energy. Ion b_3 is formed from a_4 ion while further dissociation of b_3 forms b_2 (m/z 221). C-terminal ion y_2 (m/z 279) has a higher intensity than b_3 (278) in the low energy region. With the increase of photon energy, the internal energy of the precursor ions rises, resulting in the drop of the intensity of y_2 ions compared to the intensity of b_3 ions, similarly as for b_4 and a_4 ions, respectively. The peak designated at m/z 449 corresponds to the tyrosine side chain loss of the precursor ions while the loss of the phenylalanine side chain is responsible for a small peak at m/z 465. H loss from 449 leads to a fragment designated at m/z 448. Loss of tyrosine side chain is also noticed from backbone fragment b_4, so fragment b_4-107 (318) is observed. As the photon activation energy goes over the IE of Leu-enk (8.87 eV) more reaction channels become open. New reaction channels above the IE lead to internal fragments GGF (m/z 262) and GF (m/z 205). These fragments are also present in the sub ionization energies, but with very small abundances. Suffering the CO loss, these ions form GGF-CO (m/z 234) and GF-CO (m/z 177). In the second channel with another CO_2 loss from GF, fragments at m/z 161 are created. Above the IE internal fragments dominate over the backbone by more than a factor of 10. At 16 eV, the most prominent fragments are c_3 (m/z 295) and GF (m/z 205). Mass-to-charge ratio of doubly ionized precursor ions $[Leu\text{-}enk+H]^{2+}$ is the same as for b_3 ion at m/z 278. According to [9], it is possible that small abundance of doubly ionized precursor ions contributes to the intensity of the m/z 278 peak. Internal C-terminal fragment a_3 (m/z 250) is formed upon CO loss from b_3 ion and along with ion a_2 (m/z 193) shows up at energies above 14 eV. Both backbone and internal fragment ions peak at around 20 eV with a very broad peak, which is also reported in [9]. At 24 eV being the final energy point in our scans, all fragments are in a decline with GF (205), b_2 (221), b_3 (278) and c_3 (295) dominating the spectra at around 1% of the precursor ion intensity.

4. Conclusions

A linear quadrupole ion trap mass spectrometer was coupled to a synchrotron beamline to study the VUV photo-induced dissociation of gas-phase protonated Leu-enk cations. The present experiment extends previous studies by means of high spectral purity of the photon beam, increased sensitivity and mass resolution (in the case of VUV/ion trap results) and increased energy range. Presented mass spectra are in good agreement with the existing fragmentation data in the literature. The fragmentation of the Leu-enk peptide shows a clear and interesting energy dependence that can be related to electronic excitation processes, which will be investigated in more details in future papers.

5. Acknowledgments

This work was supported by the French ANR (Project ANR-08-BLAN-0065), the “Pavle Savic” bilateral scientific project between Serbia and France (N27482TE) and the COST Action MP1002 (Nano-IBCT). Milosavljević A R and Ranković M Lj acknowledge support by the Ministry of education, science and technological development of Republic or Serbia under the Project 171020. We are grateful to the SOLEIL synchrotron general staff for providing the beamtime under the Projects 20110324 and 20130388.

6. References

[1] Yamashita M, Fenn J B 1984 *J Phys Chem* **88** (20) 4451-4459
[2] Polfer N C, Oomens J, Suhai S, Paizs B 2007 *J Am Chem Soc* **129** 5887-5897
[3] Rakov V S, Borisov O V, Whitehouse C M 2004 *J Am Soc Mass Spectrom* **15** 1794–1809
[4] Laskin J 2006 *J Phys Chem* A **110** 8554
[5] Schnier P, Price W, Strittmatter E and Williams E 1997 *J Am Soc Mass Spectrom* **8** 771
[6] Tabarin T, Antoine R, Broyer M and Dugourd P 2005 *Rapid Commun Mass Spectrom* **19** 2883
[7] Alexander A J, Boyd R K 1989 *Int J Mass Spectrom Ion Processes* **90** 211-240
[8] Kobayashi K, Kasamatsu T, Kaneko T, Koike J, Oshima T, Saito T, Yamamoto T and Yanagawa H 1995 *Adv Space Res* **16** 21
[9] Bari S, Gonzalez M O, Reitsma G, Werner J, Schippers S, Hoekstra R and Schlatholter T 2011 *J Chem Phys* **134** 024314
[10] Nahon L, Oliveira N, Garcia G, Gil J F, Pilette B, Marcouille O, Lagarde B and Polack F 2012 *J Synchrotron Radiat* **19** 508-520
[11] Milosavljević A R, Nicolas C, Lemaire J, Déhon C, Thissen R., Bizau J M, Réfrégiers M, Nahon L and Giuliani A 2011 *Phys Chem Chem Phys* **13** 15432
[12] Milosavljević A R, Canon F, Nicolas C, Miron C, Nahon L and Giuliani A 2012 *J Phys Chem Lett* **3** 119
[13] Milosavljević A R, Nicolas C, Gil J F, Canon F, Réfrégiers M, Nahon L and Giuliani A 2012 *J Synchrotron Radiat* **19** 174
[14] Milosavljević A R, Nicolas C, Gil J F, Réfrégiers M, Nahon L and Giuliani 2012 *Nucl Instrum Methods Phys Res B* **279** 34-36
[15] Sztáray J, Memboeuf A, Drahos L and Vékey K 2010 *Mass Spectrom Rev* **30** 298
[16] Frisch M J, Trucks G W and Schlegel H B 2004, Gaussian 03, Revision C.02 (Gaussian Inc. Wallingford CT)
[17] Vachet R W, Bishop B M, Erickson B W and Glish G L 1997 *J Am Chem Soc* **119** 5481-5488

BACK TO SEARCH RESULTS

Citation Report

DOI: 10.1103/PhysRevLett.124.203401 (DOI) or DOI: 10.1021/acs.jpclett.9b03345 (DOI) or DOI: 10.1002/anie.201603464 (...

Analyze Results | Create Alert

Export Full Report

Publications

19
Total

From 1900 to 2022

Citing Articles

134 Analyze
Total

123 Analyze
Without self-citations

Times Cited

163
Total

8.58
Average per item

149
Without self-citations

H-Index

9

Times Cited and Publications Over Time

DOWNLOAD

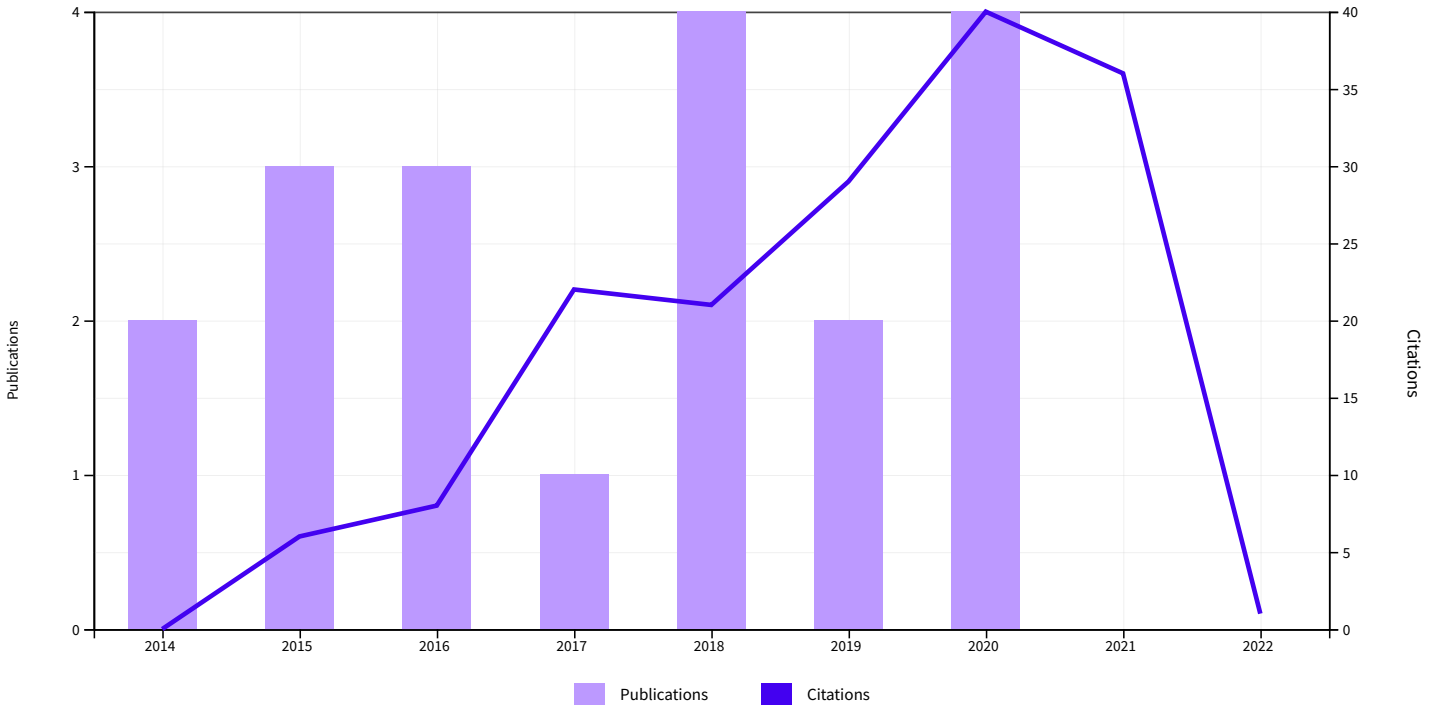

19 Publications

Sort by: Citations: highest first

1 of 1

		Citations						
		Back				Forward	Average per year	Total
		2018	2019	2020	2021	2022		
	Total	21	29	40	36	1	20.38	163
1	Sensitizing DNA Towards Low-Energy Electrons with 2-Fluoroadenine Rackwitz, J; Kopyra, J; (...); Bald, I Aug 22 2016 | ANGEWANDTE CHEMIE-INTERNATIONAL EDITION 55 (35) , pp.10248-10252	8	9	4	4	0	4.86	34
2	Dissociative electron attachment and anion-induced dimerization in pyruvic acid Zawadzki, M; Rankovic, M; (...); Fedor, J Mar 14 2018 | PHYSICAL CHEMISTRY CHEMICAL PHYSICS 20 (10) , pp.6838-6844	4	6	5	3	0	3.6	18
3	A novel setup for the determination of absolute cross sections for low-energy electron induced strand breaks in oligonucleotides - The effect of the radiosensitizer 5-fluorouracil Rackwitz, J; Rankovic, ML; (...); Bald, I	3	6	2	2	0	2.67	16

36

	Feb 14 2017 | EUROPEAN PHYSICAL JOURNAL D 71 (2)							
4	Mode-Specific Vibrational Autodetachment Following Excitation of Electronic Resonances by Electrons and Photons Anstoter, CS; Mensa-Bonsu, G; (...); Verlet, JRR May 19 2020 | PHYSICAL REVIEW LETTERS 124 (20)	0	0	9	6	0	5	15
5	K-Shell Excitation and Ionization of a Gas-Phase Protein: Interplay between Electronic Structure and Protein Folding Milosavljevic, AR; Nicolas, C; (...); Giuliani, A Aug 20 2015 | JOURNAL OF PHYSICAL CHEMISTRY LETTERS 6 (16) , pp.3132-3138	3	1	2	3	0	1.88	15
6	Electron collisions with cyanoacetylene HC3N: Vibrational excitation and dissociative electron attachment Rankovic, M; Nag, P; (...); Fedor, J Nov 29 2018 | PHYSICAL REVIEW A 98 (5)	0	2	7	2	0	2.2	11
7	VUV action spectroscopy of protonated leucine-enkephalin peptide in the 6-14 eV range Rankovic, ML; Canon, F; (...); Milosavljevic, AR Dec 28 2015 | JOURNAL OF CHEMICAL PHYSICS 143 (24)	1	0	1	4	0	1.25	10
8	Energy-Dependent UV Photodissociation of Gas-Phase Adenosine Monophosphate Nucleotide Ions: The Role of a Single Solvent Molecule Milosavljevic, AR; Cerovski, VZ; (...); Giuliani, A Jun 5 2014 | JOURNAL OF PHYSICAL CHEMISTRY LETTERS 5 (11) , pp.1994-1999	0	1	1	1	0	1.11	10
9	Dissociative ionization dynamics of dielectric gas C3F7CN Rankovic, M; Chalabala, J; (...); Fedor, J Aug 14 2019 | PHYSICAL CHEMISTRY CHEMICAL PHYSICS 21 (30) , pp.16451-16458	0	1	7	1	0	2.25	9
10	Elastic electron differential cross sections for argon atom in the intermediate energy range from 40 eV to 300 eV Rankovic, ML; Maljkovic, JB; (...); Marinkovic, BP Feb 2018 | EUROPEAN PHYSICAL JOURNAL D 72 (2)	0	1	2	2	1	1.2	6
11	Study of electron transmission through a platinum tube Milosavljevic, AR; Rankovic, ML; (...); Tokesi, K Jul 1 2015 | NUCLEAR INSTRUMENTS & METHODS IN PHYSICS RESEARCH SECTION B-BEAM INTERACTIONS WITH MATERIALS AND ATOMS 354 , pp.86-89	2	0	0	0	0	0.63	5
12	VUV photofragmentation of protonated leucine-enkephalin peptide dimer below ionization energy Milosavljevic, AR; Cerovski, VZ; (...); Giuliani, A Mar 25 2014 | EUROPEAN PHYSICAL JOURNAL D 68 (3)	0	1	0	2	0	0.56	5
13	Temporary anions of the dielectric gas C3F7CN and their decay channels Rankovic, M; Kumar, TPR; (...); Fedor, J Jun 28 2020 | JOURNAL OF CHEMICAL PHYSICS 152 (24)	0	0	0	2	0	0.67	2
14	Oxygen K-shell spectroscopy of isolated progressively solvated peptide Milosavljevic, AR; Jankala, K; (...); Giuliani, A Jun 21 2020 | PHYSICAL CHEMISTRY CHEMICAL PHYSICS 22 (23) , pp.12909-12917	0	0	0	2	0	0.67	2
15	Electron impact action spectroscopy of mass/charge selected macromolecular ions: Inner-shell excitation of ubiquitin protein Rankovic, ML; Giuliani, A and Milosavljevic, AR Feb 8 2016 | APPLIED PHYSICS LETTERS 108 (6)	0	0	0	0	0	0.29	2
16	Electron-impact vibrational excitation of isocyanic acid HNCO Kumar, TPR; Nag, P; (...); Fedor, J Dec 24 2020 | PHYSICAL REVIEW A 102 (6)	0	0	0	1	0	0.33	1
17	Electron transmission through a steel capillary Maljkovic, JB; Borka, D; (...); Tokesi, K May 15 2018 | NUCLEAR INSTRUMENTS & METHODS IN PHYSICS RESEARCH SECTION B-BEAM INTERACTIONS WITH MATERIALS AND ATOMS 423 , pp.87-91	0	1	0	0	0	0.2	1
18	Design and performance of an instrument for electron impact tandem mass spectrometry and action spectroscopy of mass/charge selected macromolecular ions stored in RF ion trap Rankovic, ML; Giuliani, A and Milosavljevic, AR Jun 2 2016 | EUROPEAN PHYSICAL JOURNAL D 70 (6)	0	0	0	1	0	0.14	1

⊖ 19	K-Shell Excitation and Ionization of a Gas-Phase Protein: Interplay between Electronic Structure and Protein Folding (vol 6, pg 3132, 2015) Milosavljevic, AR; Nicolas, C; (...); Giuliani, A Dec 5 2019 | JOURNAL OF PHYSICAL CHEMISTRY LETTERS 10 (23) , pp.7397-7397	0	0	0	0	0	0	0

Citation Report Publications Table

Република Србија
МИНИСТАРСТВО ПРОСВЕТЕ,
НАУКЕ И ТЕХНОЛОШКОГ РАЗВОЈА
Комисија за стицање научних звања

Број: 660-01-00001/640
27.09.2017. године
Б е о г р а д

На основу члана 22. став 2. члана 70. став 4. Закона о научноистраживачкој делатности ("Службени гласник Републике Србије", број 110/05, 50/06 – исправка, 18/10 и 112/15), члана 3. ст. 1. и 3. и члана 40. Правилника о поступку, начину вредновања и квантитативном исказивању научноистраживачких резултата истраживача ("Службени гласник Републике Србије", број 24/16, 21/17 и 38/17) и захтева који је поднео

Институт за физику у Београду

Комисија за стицање научних звања на седници одржаној 27.09.2017. године, донела је

ОДЛУКУ
О СТИЦАЊУ НАУЧНОГ ЗВАЊА

Др Милош Ранковић
стиче научно звање
Научни сарадник

у области природно-математичких наука - физика

О Б Р А З Л О Ж Е Њ Е

Институт за физику у Београду

утврдио је предлог број 1933/1 од 15.11.2016. године на седници Научног већа Института и поднео захтев Комисији за стицање научних звања број 1980/1 од 24.11.2016. године за доношење одлуке о испуњености услова за стицање научног звања ***Научни сарадник***.

Комисија за стицање научних звања је по претходно прибављеном позитивном мишљењу Матичног научног одбора за физику на седници одржаној 27.09.2017. године разматрала захтев и утврдила да именовани испуњава услове из члана 70. став 4. Закона о научноистраживачкој делатности ("Службени гласник Републике Србије", број 110/05, 50/06 – исправка,18/10 и 112/15), члана 3. ст. 1. и 3. и члана 40. Правилника о поступку, начину вредновања и квантитативном исказивању научноистраживачких резултата истраживача ("Службени гласник Републике Србије", број 24/16, 21/17 и 38/17) за стицање научног звања ***Научни сарадник***, па је одлучила као у изреци ове одлуке.

Доношењем ове одлуке именовани стиче сва права која му на основу ње по закону припадају.

Одлуку доставити подносиоцу захтева, именованом и архиви Министарства просвете, науке и технолошког развоја у Београду.

ПРЕДСЕДНИК КОМИСИЈЕ

Др Станислава Стошић-Грујичић,
научни саветник

МИНИСТАР

Младен Шарчевић

The Czech Academy of Sciences
J. Heyrovský Institute of Physical Chemistry, v. v. i.
Dolejškova 3, 182 23 Prague 8, Czech Republic
Phone: (+420) 28658 3014, (+420) 26605 2011
Fax: (+420) 28658 2307, e-mail: director@jh-inst.cas.cz

Mr. Miloš Ranković, Ph.D.
Palmira Toljatija 48/02
Belgrade
Serbia

18. 5. 2017
Ref No UFCHJH-436/ODP/2017

Dear colleague,

I have the pleasure in informing you that with regard to the evaluation of the competition of 17 May 2017 I am prepared to engage you in the staff of the Institute. Details of your contract please specify with Dr. Juraj Fedor.

Yours sincerely,

Prof. Martin Hof, Dr. rer. nat., DSc.
Director of the Institute

J.Heyrovský Institute of Physical Chemistry

Czech Academy of Sciences
J. Heyrovský Institute of Physical Chemistry, v. v. i.
Dolejškova 2155/3, 182 23 Prague 8, Czech Republic
VAT Nr. CZ61388955

Dr. Juraj Fedor
Tel: +420 2 6605 3636
Email: juraj.fedor@jh-inst.cas.cz
http://www.jh-inst.cas.cz/dynamics

February 15, 2022

Participation of Dr. Miloš Ranković on research projects in 2017-2022

This is to confirm that Dr. Miloš Ranković participated in the following research projects where I was the principal investigator:

08/2017 – 08/2018: Czech Science Foundation Project *'Cross sections and dynamics of electron scattering on molecular systems'*
Employment: 1.0 FTE
Role in the project: Measurements of cross sections for electron-molecule collisions

09/2018 – 10/2020: Technological Agency of the Czech Republic Project *'SF_6 replacement in high voltage switchgear'*
Employment: 1.0 FTE
Role in the project: (i) Measurement of cross sections for electron collisions with novel dielectric gases, (ii) Design and construction of the apparatus for determining decomposition products of partial discharges, (iii) Determining decomposition products of dielectric gases in partial discharges

11/2020 – now: Czech Science Foundation Project *'Dynamics of electron-induced nuclear motion in cold molecules'*
Employment: 0.8 FTE
Role in the project: Design of the electronics for a new apparatus measuring electron-molecule collisions

11/2020 – now: MŠMT InterCOST project *'Electronic and nuclear dynamics in molecules initiated by electron impact'*
Employment: 0.1 FTE
Role in the project: Preparation of missions to synchrotron light sources.

01/2022 – now: Technological Agency of the Czech Republic Project *'Streamers and surface flashover discharges on insulators in alternative gases to SF_6'*
Employment: 0.1 FTE
Role in the project: (i) Participation on the design of discharge cells for spectroscopy of dielectric gases, (ii) VUV spectroscopy of dielectric gases.

Best regards,

Juraj Fedor
Head of the Department of Molecular and Cluster Dynamics

Универзитет у Крагујевцу
ПРИРОДНО-МАТЕМАТИЧКИ ФАКУЛТЕТ
Радоја Домановића 12, 34000 Крагујевац, Србија

University of Kragujevac
FACULTY OF SCIENCE
Radoja Domanovića 12, 34000 Kragujevac, Serbia

KRAGUJEVAC JOURNAL OF SCIENCE

На лични захтев др Милоша Ранковића, истраживача сарадника на Институту за физику Београд, Универзитет у Београду, часопис KRAGUJEVAC JOURNAL OF SCIENCE издаје следећу

П О Т В Р Д У

др Милош Ранковића је на молбе уредника часописа KRAGUJEVAC JOURNAL OF SCIENCE, који издаје Природно-математички факултет Универзитета у Крагујевцу, а Матични одбор за физику категорише као М51, **рецензирао следеће радове** (сређено по годиштима публиковања):

2019 (Vol. 41)

VISUALIZATION OF THE IONIZATION YIELDS MODEL OF THE NOBLE ATOMS IN AN ELLIPTICALLY POLARIZED LASER FIELD BY USING SYMBOLIC PROGRAMMING LANGUAGE
Аутори: Христина С. Делибашић, Иван Д. Петровић и Виолета М. Петровић
Рад је на страницама 25-36, односно адреси
https://www.pmf.kg.ac.rs/KJS/images/volumes/vpl41/kjs41delibasic25.pdf

2020 (Vol. 42)

NUMERICAL INVESTIGATION OF THE PLASMA FORMATION IN AIR GENERATED BY 355 nm Nd: YAG LASER PULSES
Аутори: Христина С. Делибашић, Константинос Калерис, Виолета М. Петровић и Иван Д. Петровић
Рад је на страницама 19-28, односно адреси
https://www.pmf.kg.ac.rs/KJS/images/volumes/vpl42/kjs42delibasic19.pdf

2021 (Vol. 43)

THE EFFECT OF MAGNETIC FIELD ON THE TUNNELING YIELD OF AMMONIA MOLECULES
Аутори: Виолета М. Петровић, Христина С. Делибашић и Иван Д. Петровић
Рад је на страницама 5-14, односно адреси
https://www.pmf.kg.ac.rs/KJS/images/volumes/vpl43/kjs43petrovic5.pdf

У Крагујевцу, 07.02.2022.

Технички уредник часописа

Др Ивана Радојевић, доцент
e-mail ivana.radojevic@pmf.kg.ac.rs
Tel. 034-300-240, lok. 273

Годишњи извештај о раду на пројекту у 2019. години

Име: Братислав
Презиме: Маринковић
Број телефона: 316-0882
E-mail адреса: bratislav.marinkovic@ipb.ac.rs
Радна организација: 200024-Универзитет у Београду, Институт за физику
Град: Belgrade
Број поште: 11080

Страна 1 - Општи подаци

Програм ОСНОВНА ИСТРАЖИВАЊА
Област Физика
Број пројекта 171020
Назив Пројекта Физика судара и фотопроцеса у атомским, (био)молекулским и нанодимензионим системима
Тип пројекта Б-Експериментални

Страна 2 - Опис истраживања

Циљеви истраживања (према достављеном плану истраживања) остварени у 2019. години имајући у виду значај, квалитет и ниво остварених резултата. ТЕМА 1. ИНТЕРАКЦИЈЕ ЕЛЕКТРОНА, ЈОНА И ФОТОНА СА АТОМИМА И (БИО)МОЛЕКУЛИМА (КОНСТИТУЕНТИМА ИЛИ АНАЛОГОНИМА ДНК МОЛЕКУЛА) РАДИ БОЉЕГ РАЗУМЕВАЊА ПРОЦЕСА РАДИЈАЦИОНОГ ОШТЕЋЕЊА. Задатак 1.1 а) На апаратури OHRHA (Omicron High Resolution Hemispherical Analyser) измерени су спектри избачених електрона аутојонизационих стања и Coster-Kronig прелаза у атому Ar, а публиковани у међународном часопису [P18. Energy analysis of ejected electrons in the region of the Ar L1-⁻L2,3M Coster-Kronig transitions (25-56 eV) induced by electron impact, J. Electron Spectrosc. 237, 146898 (2019) 6pp]. б) На апаратури ESMA завршена су и публикована мерења диференцијалних пресека за еластично расејање електрона при упадним енергијама електрона од 10-100 eV на атому Zn [P12. Experimental and theoretical cross sections for elastic electron scattering from zin, Phys. Rev. A 99, 062702 (2019) 10pp]. Задатак 1.2 (руководилац задатка др Јелена Маљковић): а) Извршена су мерења еластичног расејања електрона на молекулу три-етил-фосфату. Резултати су обрађени и публиковани [P03. Elastic electron scattering cross sections for triethyl phosphate molecule at intermediate electron energies from 50 to 250 eV, Eur. Phys. J.D 73, 27 (2019) 5pp]. б) Прелиминарна мерења еластичног расејања електрона на молекулу метана су представљена на престижним међународним конференецијама ECAMP13 и XXXI ICPEAC [CI08. Integral cross sections for elastic electron scattering by methane molecule; CI01. Elastic electron scattering from methane molecule in the energy range from 50-300 eV] в) У оквиру пост доктората у сарадњи са колегама из Прага обављен је рад о дисоцијативној јонизацији молекула флуоронитрила [O02 Phys. Chem. Chem. Phys. 21(30) 16451-16458 (2019)]. Задатак 1.3 Изучавана је теорија судара тешких честица: а) Публикован је рад у коме је примењена динамичка адијабатска теорија судара у опису атома водоника у s-стању [P05. Classical representation for hydrogen atom in s-states, Quantum Stud.: Math. Found. 6(2) 225-233 (2019)]. б) (руководилац задатка др Ненад Милојевић): Истраживан је парцијални и укупни пресек за захват електрона из K-љуске вишеелектронских мета од стране потпуно огољених пројектила. Написан је и публикован прегледни рад на ову тему у реномираном часопису. [P15. State-selective and total cross sections for electron capture from the K-shell of multi-electron atoms by fully stripped projectiles. At. Data Nucl. Data Tables, (2019) 18pp]. ТЕМА 2. ИНТЕРАКЦИЈЕ СА ПОВРШИНАМА НА НАНОМЕТАРСКОЈ СКАЛИ (НАНОКАПИЛАРЕ, НАНОТАЧКЕ) КОЈЕ ВОДЕ ФУНЦИОНАЛИЗАЦИЈИ МАТЕРИЈАЛА ИЛИ МОДИФИКАЦИЈИ НАНОФИЛМОВА. Задатак 2.1: (руководилац задатка др Милош Ранковић): Завршена тематика. Задатак 2.2 а) (руководилац задатка др Маја Рабасовић): Извршена су мерења оптичких особина прашкастих нано материјала (Sr_2CeO_4:Eu; $GdVO_4$:Sm; $Gd_2Zr_2O_7$:Eu; $CaWO_4$:Nd),као и апконверзионог материјала(Gd_2O_3:Er,Yb). Могућности примене материјала YVO_4:Eu^{3+} за мерења промене температуре су публиковани [P22. J. Phys. D: Appl. Phys. 53, 015106, 10pp, online 1st Oct. 2019]. Резултати анализе и карактеризације материјала CdSe/ZnS-PMMA публиковани су у радову [P17. Optical properties $CaWO_4$:Nd^{3+}/PMMA composite layered structures, Opt. Mater. 96, 109361 (2019) 8pp]. Оптичке особине материјала $CaWO_4$:Nd су представљене у раду [P11. Optical properties and fluorescence of quantum dots CdSe/ZnS-PMMA composite films with interface modifications, Opt. Mater. 92, 405-410 (2019)]. б) Настављено је изучавање ласерски индукованог пробоја и посматрани различити временски размаци узорковања [P01. Laser-Induced Plasma Measurements Using Nd:YAG Laser and Streak Camera: Timing Considerations, Atoms, 7(1), 6 (2019) 12pp]. в) Испитивана је локализација електрона у двоелектронским квантним тацкама у зависности од јачине спољашњег магнетног поља и веза са квантном преплетеношћу најнижих стања и публикован је рад. [P19. Effect of the magnetic field on electron density distributions in two-electron quantum dots. J. Phys. A. Math. Theo. 52, 435303 (2019) 21pp]. 2.3 Настављена је обрада резултата TiO_2 мемристора добијених FEBID техником. ТЕМА 3. ФОТОПРОЦЕСИ ВЕЗАНИ ЗА ИНТЕРАКЦИЈЕ ЛАСЕРСКОГ И СИНХРОТРОНСКОГ ЗРАЧЕЊА СА АТОМИМА, ЈОНИМА И (БИО)МОЛЕКУЛИМА. Задатак 3.1 а) Интеракција ласерског зрачења са биомолекулима (руководилац задатка др Маја Рабасовић): Настављено је изучавање временски разложених луминесцентних спектара алкалоида биљке руса [CI10. Nonlinear microscopy and time resolved fluorescence spectroscopy of Chelidonium majus L. Proc. PHOTONICA2019]. б) Интеракција синхротронског зрачења са (био)молекулима (руководилац задатка др Сања Тошић): Проучавани су могући механизми фрагментације молекула као директне последице апсорпције X зрачења помоћу подесивог синхротронског зрачења у комбинацији са различитим експерименталним техникама (PES, XPS, NEXAFS, PEPICO, PIPICO, масена спектрометрија) на различитим молекулима: i) нитроимидазолима [P10. Radiation Damage Mechanisms of Chemotherapeutically Active Nitroimidazole Derived Compounds, Front. Chem. 7, 329 (2019) 14pp: P06. Core shell investigation of 2-nitroimidazole, Front. Chem. 7, 151 (2019) 13pp]; ii) Титанијум-изо-пропоксид (органометалик, прекурсор за хемијску депозицију и ФЕБИД технику високе резолуције која омогућава стварање и уређивање наноструктурних материјала) [CI13. Photo-induced fragmentation of the titanium (IV) iso-propoxide molecule, VEIT 2019: CI12. Inner-shell spectroscopy of titanium (IV) iso-propoxide, PHOTONICA2019]. Ова истраживања су представљена и на уводном предавању у оквиру прве европске радионице корисника синхротрона одржане у Београду ESUO Organization [IT02. Core Shell Investigation and Radiation Damage Mechanisms of Nitroimidazole Compounds studies at the Gasphase Beamline @ Elettra, Photonica 2019 and 1st ESUO Regional Meeting, Belgrade, 28.08.2019] Задатак 3.2 (руководилац задатка др Предраг Коларж): Истражена ефективна доза озрачености појединих делова Балкана [O01. Effective Doses Estimated from the Results of Direct Radon and Thoron Progeny Sensors (DRPS/DTPS), Exposed in Selected Regions of Balkans, Radiation

UNIVERSITY OF BELGRADE
FACULTY OF PHYSICS

INNER-SHELL ACTION SPECTROSCOPY OF TRAPPED SUPSTANCE P PEPTIDE IONS AND THEIR NANOSOLVATED COMPLEXES

Iva Bačić, 7047/2014

Master Thesis
Belgrade, 2015

Acknowledgements

Firstly, I would like to express my sincere gratitude to my advisor dr. Aleksandar R. Milosavljević, who provided me an opportunity to participate in this work, and guided me through the whole course of this research with excellent help and great patience in correcting my writing. I would also like to thank my co-supervisor dr. Bratislav Marinković, for his assistance in the writing of this paper, along with dr. Aleksandar R. Milosavljević. My sincere thanks also go to mr. Miloš Ranković for great help in performing the experiment and processing the data, and dr. Alex Giulliani and dr. Cristophe Nicolas, with whom I worked during the experiment at the research facility SOLEIL for admitting me to their team and advising me during the beamtime. I am also grateful to dr. Viktor Cerovski for his help during the measurements and to the general SOLEIL staff for running the overall facility. Besides those who directly participated in the making of this work, I would like to thank the rest of my thesis committee: dr. Jelena Maljković, prof. dr. Goran Poparić, and prof. dr. Dragoljub Belić for their critical reading of the thesis and useful suggestion. Finally, I also thank dr. Sanja Tošić for useful advises and help with preparing the thesis.

This work was performed under the project 20140023 “Inner-shell spectroscopy of nanosolvated protein ions isolated in gas phase” at the SOLEIL synchrotron radiation facility and also supported by the Ministry of Education, Science and Technological Development, Serbia, under the project numbers 171020. The experimental setup has been developed with the support from the Agence Nationale de la Recherche Scientifique, France, under the project number ANR-08-BLAN-0065.

УНИВЕРЗИТЕТ У БЕОГРАДУ

ФИЗИЧКИ ФАКУЛТЕТ

Јелена Вуковић

Апсолутни диференцијални пресеци за еластично расејање електрона на молекулу триетил фосфата

Мастер рад

Београд, 2018.

Резултати приказани у овом мастер раду добијени су у Лабораторији за атомске сударне процесе, Института за физику у Земуну. Радом на експерименту и на изради рада је руководила др Јелена Маљковић и овом приликом се много захваљујем Јелени на великој помоћи и подршци.

Захваљујем се и др Братиславу Маринковићу, директору Лабораторије за атомске сударне процесе, на указаном поверењу.

Захваљујем се и члановима комисије за преглед и оцену мастер рада, др Драгољубу Белићу, др Горану Попарићу и др Бранку Предојевићу.

Такође се захваљујем др Karoly Tókési на урађеном теоријском прорачуну пресека.

Захваљујем се и др Милошу Ранковићу на великој помоћи и сугестијама у експерименталном раду.

Захваљујем се пуно својим родитељима, сестри, пријатељима и Гогију.

У Београду, 2018. гор.

UNIVERZITET U BANJOJ LUCI
PRIRODNO – MATEMATIČKI FAKULTET
STUDIJSKI PROGRAM ZA FIZIKU

DIPLOMSKI RAD

Apsolutni diferencijalni presjeci za elastično rasijanje elektrona na atomu argona

Mentor:
prof. dr Branko Predojević

Student:
Jelena Vuković, 23/10

BANJA LUKA, 2015.

Ovaj diplomski rad urađen je u Laboratoriji za fiziku atomskih sudara, Instituta za fiziku u Zemunu, Beograd. Ovom prilikom se zahvaljujem dr Aleksandru Milosavljeviću koji mi je omogućio rad u Laboratoriji i na konsultacijama tokom izrade diplomskog rada.

Zahvaljujem se svome mentoru prof. dr Branku Predojeviću za pomoć, savjete i sugestije prilikom pisanja rada.

Takođe se zahvaljujem dr Jeleni Maljković i mr Milošu Rankoviću na velikoj pomoći u eksperimentalnom radu.

Zahvaljujem se puno roditeljima i sestri na podršci, pomoći i strpljenju.

U Banjoj Luci, 2015. godine

Eur. Phys. J. D (2017) 71: 32
DOI: 10.1140/epjd/e2016-70608-4

THE EUROPEAN PHYSICAL JOURNAL D

Regular Article

A novel setup for the determination of absolute cross sections for low-energy electron induced strand breaks in oligonucleotides – The effect of the radiosensitizer 5-fluorouracil*

Jenny Rackwitz[1], Miloš Lj. Ranković[2], Aleksandar R. Milosavljević[2,3], and Ilko Bald[1,4,a]

[1] Institute of Chemistry – Physical Chemistry, University of Potsdam, Karl-Liebknecht-Str. 24-25, 14476 Potsdam, Germany
[2] SOLEIL, l'Orme des Merisiers, St. Aubin, BP 48, 91192 Gif-sur-Yvette Cedex, France
[3] Institute of Physics Belgrade, University of Belgrade, Pregrevica 118, 11080 Belgrade, Serbia
[4] Department 1 – Analytical Chemistry and Reference Materials, BAM Federal Institute of Materials Research and Testing, Richard-Willstätter Str. 11, 12489 Berlin, Germany

Received 30 September 2016 / Received in final form 20 December 2016
Published online 14 February 2017 –

Abstract. Low-energy electrons (LEEs) play an important role in DNA radiation damage. Here we present a method to quantify LEE induced strand breakage in well-defined oligonucleotide single strands in terms of absolute cross sections. An LEE irradiation setup covering electron energies <500 eV is constructed and optimized to irradiate DNA origami triangles carrying well-defined oligonucleotide target strands. Measurements are presented for 10.0 and 5.5 eV for different oligonucleotide targets. The determination of absolute strand break cross sections is performed by atomic force microscopy analysis. An accurate fluence determination ensures small margins of error of the determined absolute single strand break cross sections σ_{SSB}. In this way, the influence of sequence modification with the radiosensitive 5-Fluorouracil (^{5F}U) is studied using an absolute and relative data analysis. We demonstrate an increase in the strand break yields of ^{5F}U containing oligonucleotides by a factor of 1.5 to 1.6 compared with non-modified oligonucleotide sequences when irradiated with 10 eV electrons.

1 Introduction

In cancer treatment by high energy radiation the simulation of dose distributions in patients is required to optimize the irradiation modalities [1]. These simulations must be based on the underlying fundamental physical processes in the interaction of high energy quanta with biological material [2]. This requires an accurate quantification of DNA radiation damage in terms of absolute cross sections for specific processes such as radiation induced DNA single and double strand breaks (SSBs and DSBs, respectively). Along the ionization track of high energy radiation secondary particles such as low-energy electrons (LEEs) and hydroxyl radicals are generated in copious amounts [3,4]. LEEs having an energy of roughly below 12 eV are able to induce DNA strand breaks by dissociative electron attachment (DEA) [5,6]. The electron then occupies a formerly unoccupied molecular orbital (MO) generating a transient negative ion (TNI), which is unstable towards autodetachment and dissociation [6]. Bond cleavage by DEA proceeds with high efficiency, i.e. high cross sections and often with pronounced site selectivity [7–9]. On the one hand research performed in the last couple of years on small model compounds focused on the question of where the excess charge is initially located and which specific bond cleavages finally lead to base losses and strand breaks [10,11]. In the condensed phase LEE induced strand breaks have mainly been studied using plasmid DNA. Since the early experiments by Boudaiffa et al. [5] in 2000 the LEE induced SSBs and DSBs have been studied by different groups, however, resulting in slightly different resonance profiles [12,13]. Effective cross sections for SSBs and DSBs have been determined by Boudaiffa et al. at electron energies of 10–50 eV [14] and by Panajotovic et al. in the energy regime 0.1–4.7 eV [15]. The determination of *absolute* strand break cross sections requires more sophisticated models such as the molecular survival model [16]. In general the determination of strand breaks induced by low-energy radiation in plasmid DNA is error-prone since the results depend on DNA film thickness and morphology, which is strongly influenced by experimental parameters [17–19]. Another draw-back of using plasmid DNA is the limited possibility to study the influence of DNA sequence and secondary structure on the strand breakage. Several novel experimental strategies have been proposed to study LEE

* Contribution to the Topical Issue "Low-Energy Interactions related to Atmospheric and Extreme Conditions", edited by S. Ptasinska, M. Smialek-Telega, A. Milosavljevic, B. Sivaraman.

[a] e-mail: bald@uni-potsdam.de

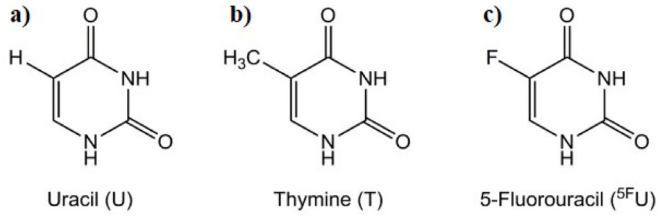

Fig. 1. Chemical structures of (a) the RNA nucleobase uracil; (b) the DNA nucleobase thymine and c) the radiosensitizer 5-fluorouracil (^{5F}U).

induced DNA damage in oligonucleotides including analysis by HPLC [20], surface-enhanced Raman scattering (SERS) [21,22], and the application of DNA microarrays and fluorescence spectroscopy as a read-out [23,24]. However, in all these approaches the quantification of DNA damage is limited to relative values. Recently, oligonucleotide target structures have been arranged on DNA origami nanostructures, which are analyzed by atomic force microscopy (AFM) after exposure to LEEs [25–27] or VUV photons [28]. The advantage of this method is that absolute strand break cross sections are readily accessible and that multiple sequences can be studied in a single irradiation experiment [27]. Furthermore, the target sequences can be freely chosen and even their secondary structure can be controlled in some way [29,30]. The control over the sequence enables the study of the modification of LEE induced strand break cross sections by radiosensitizers used in cancer radiation therapy [31,32].

In the present work we describe in detail the experimental setup used for LEE irradiation of oligonucleotides arranged on DNA origami substrates. We explore how absolute strand break cross sections can be determined using a reference sequence placed on the DNA origami substrate. Additionally, we study the effect of fluorinated nucleobase analogues on the strand break cross section after 10 eV electron irradiation. In particular, we focus on the radiosensitizer 5-fluorouracil (^{5F}U), which is a fluorinated derivative of uracil (U) and thymine (T) (Fig. 1). LEE induced reactions in ^{5F}U have been previously studied both in the gas phase [33,34] and in the condensed phase [35]. However, no strand break cross sections have been reported up to now. Finally, we compare the absolute strand break cross sections found for ^{5F}U containing oligonucleotides with those determined for 2-fluoroadenine (^{2F}A) containing oligonucleotides, which have recently been shown to effectively enhance the strand break cross sections upon LEE irradiation [32].

2 Experimental setup

2.1 The general setup of the electron irradiator

The LEE irradiator is shown in Figure 2 and consists of a high-vacuum chamber housing an electron gun and a sample holder. A DN100 six-way cross with CF flanges is the central element of the high-vacuum chamber. The

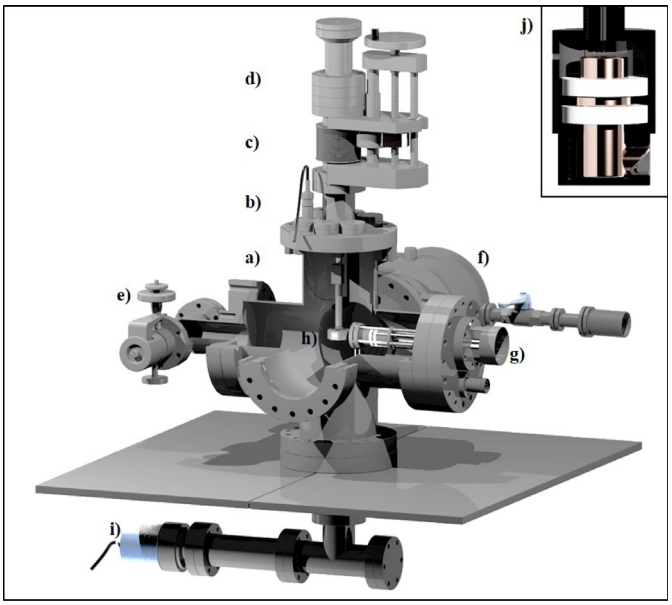

Fig. 2. 3D model of the setup with (a) the six-way cross, (b) the BNC feed through, (c) the z-translator, (d) the rotor, (e) the valve, (f) the turbomolecular pump, (g) the electron gun, (h) the sample stage, (i) the pressure gauge, and (j) the additional Faraday cup containing sample stage for beam characterization.

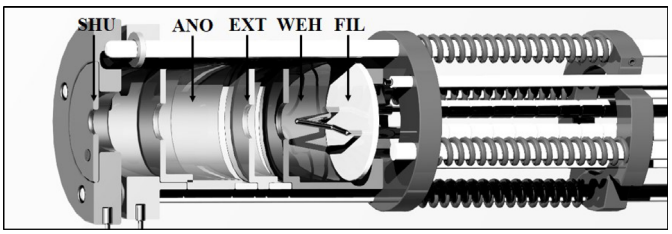

Fig. 3. 3D model of the electron gun with the filament FIL, the Wehnelt cylinder WEH, the electrostatic lens EXT between two ceramics, the modified electrostatic lens ANO, the ceramic spacer and the additionally implemented electrostatic lens SHU.

vacuum is generated by a turbomolecular pump (*Agilent* TwissTorr 304 FS) backed by a dual stage rotary vane pump (*Agilent* DS 102), resulting in a base pressure of 1.0×10^{-8} mbar. A full range combined pirani and inverted magnetron pressure gauge (*Agilent* FRG-700 CF35) measures the pressure inside the vacuum chamber and is attached at a remote position with respect to the electron gun to prevent the magnetic field disturbing the LEE beam. The electron gun (*Omnivac* FS100) is aligned horizontally at the six-way cross. A detailed illustration of the electron gun is shown in Figure 3. Thermal electrons are emitted from a tungsten hairpin filament (FIL) and collected by a Wehnelt cylinder (WEH). An aperture (EXT) in front of the Wehnelt cylinder extracts the electrons and accelerates them toward the sample. In order to defocus the beam, a low potential of around 1 V is applied to the next aperture (ANO). With decreasing kinetic energy the electrons are less focused. In result, fewer electrons reach

the sample and to keep the current at the sample constant, the voltage at ANO needs to be reduced. An additional aperture (SHU) is positioned in front of the electron flood gun serving as a shutter switching the electron beam on and off. If SHU is grounded, the electrons will pass the 4 mm diameter hole in the aperture. If a voltage of −14 V is applied, the beam will be totally defocused and no electrons will reach the sample.

The custom built sample stage is aligned vertically to the electron gun. It consists of an eight sided sample holder which is insulated from the chamber with a ceramic. The Si/SiO_2 substrates have a maximum size of 12×12 mm^2 and are fixed with conductive copper tape. The sample holder is electrically connected via a copper sliding contact (DN16 ring) and a BNC feed through with the picoamperemeter (*Keithley* 6485E). The electron current is measured in real-time during irradiation. The stage is positioned vertically with a z-translator over 50 mm travel distance and can be rotated by 360°.

For an accurate beam profile determination another sample stage was constructed. This stage is grounded on the outside along with the samples and contains an isolated faraday cup, held in position by two Teflon rings (Fig. 2j). An 8 mm diameter hole in the aluminum housing in front of the faraday cup allows to collect the complete electron beam. To determine the beam profile, a cover with a central hole of 1 mm diameter is attached to the sample stage. Since the sample stage is grounded, no real-time measurements during irradiation can be done in this configuration. Therefore, this stage is used only for beam characterization while the insulated stage is used for sample irradiation itself, since the electron current is in general not constant during irradiations.

A UHV dosage valve with gas inlet and sapphire seal (*Vacom* 11LVM-4016CF-MS-S) is used for slow venting to avoid decomposition of the DNA origami structures. It is connected to the main chamber by a DN40 T-flange, resulting in two 90° angles to create turbulences to avoid a pressure front hitting the sample surface. Additionally, the sample stage is moved up to the highest position during venting to take the sample out of the direct airflow.

2.2 Characterization of the electron beam

During the LEE irradiation of the DNA origami samples only a small electron current has been used to minimize sample charging [13]. At the same time the beam needs to be slightly defocused to increase the homogenously irradiated area. The following settings have been used: $I(\mathrm{FIL}) = 2.1$ A, $U(\mathrm{EXT}) = 65$ V and $U(\mathrm{ANO}) = 1.5$ V for 10 eV electron energy to defocus the electron beam.

Charging of the native SiO_2 layer on the silicon surface during the electron irradiation may result in an additional repulsive potential, slowing the approaching electrons down. To determine the surface charging, the origin of the electron energy scale and the electron energy distribution, the electron current has been recorded as a function of applied voltage around the current onset. Below 2.0 V no electrons passed the silicon surface, which defines the origin of the electron energy scale. The energy distribution can be obtained from the full width at half maximum (FWHM) of the gauss fit of the first derivative of the measured current, which is 1.2 ± 0.1 eV for the current setup.

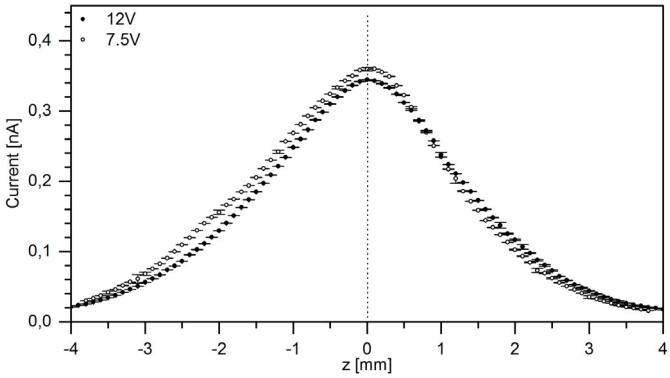

Fig. 4. Beam profile of two measurements with 12 V (•) and 7.5 V (◦) ENG.

In order to accurately determine the strand break cross section the fluence needs to be determined at the position on the sample, on which AFM measurements are performed. The faraday cup has been used to determine the beam profile by moving it vertically through the beam at defined height increments of 0.2 mm. At each height position the current was measured and averaged over 15 s. The average and error of each current measurement was plotted as a function of the z coordinate to visualize the beam profile (Fig. 4). Here, $z = 0$ mm corresponds to a height position in which the faraday cup aperture is aligned with the axis of the electron gun. To account for aging of the filament, the beam profile was determined periodically.

2.3 Determination of the fluence

The fluence F is defined as the ratio of the total number of electrons N_e and the area of irradiation A (Eq. (1)). The number of electrons N_e is given by the time of irradiation t and the current I measured at the sample provided that no electrons are reflected from the surface

$$F = \frac{N_e}{A} = \frac{tI}{Ae}. \tag{1}$$

In real-time measurements during irradiation, the total current at the sample is measured. Thus, the area of irradiation A corresponds to the total area irradiated by the beam. According to the beam profile measurements the width of the beam profile is between 7 and 8 mm. Due to the Gaussian shape of the beam, more electrons reach the sample at the central region than at the outer regions. Therefore, if the fluence F is calculated with the total current I_{total} and the total area A_{total}, an average value for F results. The surface analysis is done using AFM images of 4×4 μm^2 size. Thus, even with several AFM images, only a small fraction out of the total irradiated area A_{total} can be analyzed in these single molecule studies.

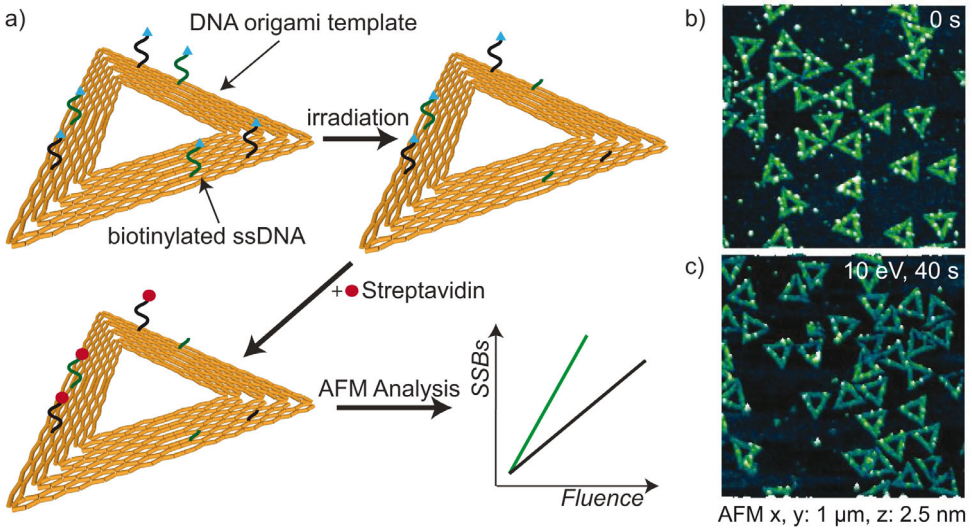

Fig. 5. (a) Scheme of the DNA origami structure and the experimental procedure. The DNA origami triangle consists of three trapezoids. On each trapezoid two different target sequences (one in the center (green) and one on the side (black)) are immobilized carrying a biotin (Bt) modification at its end. After irradiation some of the target sequences are broken due to LEE induced strand breakage. The samples are then incubated with streptavidin (SAv), which binds to the Bt modification of intact strands. The SAv can be easily identified in AFM images enabling the quantification of LEE induced strand breakage. (b) AFM image of a non-irradiated control sample. (c) AFM image of a sample irradiated with 10 eV electrons for 40 s.

Table 1. List of all modified sequences used during the experiments (Bt – biotin).

Protruding oligonucleotide sequence	Position on the DNA origami triangle (nomenclature according to Ref. [37])
5'-Bt-d(TT(ATA)$_3$TT)-3'	t7s8/18/28g
5'-Bt-d(TT(A^{5F}UA)$_3$TT)-3'	t1s8/18/28i
5'-Bt-d(TT(^{2F}AT^{2F}A)$_3$TT)-3'	t1s8/18/28i
5'-Bt-d(TT(^{5F}UT^{5F}U)$_3$TT)-3'	t-5s8/18/28g

Thus, it is necessary to precisely determine the fluence at the position of the AFM image within the beam profile. For this, the irradiated area is divided into constant sub areas A_i, for which the partial current I_i arriving on this area is determined [36]. The area A_i is small enough to assume that the fluence is homogeneous on A_i. The current I_i is determined from the beam profile using the Faraday cup as described above. By scanning the electron beam profile with the Faraday cup, a current percentage $I_{\%}$ has been determined for each sub area A_i: $I_{\%} = I_i/I_{total}$. The AFM measurements are performed in the center of the electron beam within a sub area corresponding to a circle with a diameter of 1.0 mm, for which the current percentage is $I_{\%} = 5.95\%$. This method allows for the direct calculation of the fluence at a certain sample subarea A_i from measured current values along the z-axis. Thus, no further theoretical models or fits are required.

The experiments were done with very short irradiation times of below 2 min, thus the beam profile can be assumed to be constant over this short time. With an electron gun warm-up period of exactly 30 min, the determined beam profile can be used for $I_{\%}$ calculation of the sub areas on the samples irradiated with identical conditions.

2.4 Preparation and irradiation of DNA origami structures

The DNA origami triangles are assembled according to the original protocol by Rothemund [37]. The circular single stranded genome m13mp18 with 7249 nucleotides is used as the scaffold. The viral strand is folded into the triangle pattern by a set of designed artificial staple strands. As shown in Figure 5 the triangle is formed from three trapezoids. The staple strands can be extended with a protruding DNA strand sequence representing the target sequence. Table 1 contains all protruding DNA strand sequences used in the experiments of this work. Since the DNA origami triangle has a symmetric geometry, the three trapezoids cannot be distinguished in the AFM images. On one trapezoid two protruding strands are attached. One strand is positioned in the center and one in the corner of the trapezoid, with a distance of 30 nm between both. The distance between these positions is sufficient to reliably distinguish both streptavidin (SAv) molecules at the end of the protruding strands in the AFM images. The asymmetric pattern is identical for all three trapezoids.

The modified target strands (Tab. 1) and unmodified staple strands are combined to a mixture containing

0.15 μL of each strand. Additionally, 5 μL of the viral DNA strand m13mp18 (100 nM in 10 mM Tris and 1 mM EDTA), 10 μL buffer (10 × TAE with 200 mM $MgCl_2$), and 41.65 μL deionized water are added to the solution. For annealing the prepared solution is heated up to 80 °C and cooled down stepwise over 2 h to 4 °C. Subsequently, the annealed DNA origami triangle solution is spin filtered two times with 300 μL 1 × TAE buffer containing 20 mM $MgCl_2$ with 6000 rpm for 5 minutes using 100 kDa molecular cutoff centrifugal filters (*Millipore*). The DNA origami containing filtrate is isolated and stored at 4 °C.

The silicon wafers are cut into 8 × 8 mm^2 pieces, marked with a central cross and cleaned with air plasma for 5 min, directly before DNA origami immobilization on the surface. From the freshly prepared DNA origami solution one drop of 0.8 μL is placed directly at the cross marker. To prevent drying effects, instantly afterwards 15 μL of 10 × TAE buffer with 200 mM $MgCl_2$ is added. The sample is incubated for 1 h at room temperature in an incubation chamber containing water to maintain high humidity to prevent drying. Subsequently, the sample is cleaned once with 1 mL of 1:1 deionized water/ethanol, and instantly placed in 10 mL ethanol for 1 h. Afterwards, the sample is dried with air and mounted on the sample stage for irradiation. The UHV chamber is evacuated slowly down to 10^{-3} mbar, before the turbomolecular pump is started. At a base pressure below 1.0×10^{-7} mbar the electron gun is switched on and warmed up for 30 min with 2.1 A filament current. Subsequently, the sample stage is positioned in the electron beam and the samples are irradiated for several seconds. Afterwards, the sample stage is lifted up, and the electron gun is switched off and cooled down for 1 h. The UHV chamber is vented slowly to atmospheric pressure using the dosage valve. The irradiated samples are removed from the sample stage and incubated with a 50 nM solution of SAv in 1 × TAE buffer with 20 mM $MgCl_2$. After 2 min of incubation the sample is rinsed with 0.5 mL 1:1 water/ethanol and dried with air.

2.5 AFM analysis

AFM imaging is performed with an *Agilent* 5500 instrument and Tap150-Al-G cantilevers by *Budget Sensors*. Using the top-view camera of the AFM, the images are taken at (300 ± 100) μm from the center of the marker, to coincide with the central circular area of 1 mm diameter, for which the fluence is calculated. At least one AFM image is taken in each quadrant separated by the cross marker with 4×4 μm image size, usually containing between 1000 and 2000 DNA origami structures.

Within each AFM image, all intact DNA origami triangles are analyzed. The number of intact strands is counted, corresponding to their position on the DNA origami. If all protruding strands are intact, three SAv molecules at the corners of the triangle and three SAv molecules at the central positions of the DNA origami trapezoids are visible. In case that one or more single strand breaks occur, the protruding strand is no longer labelled with biotin (Bt) and thus, no SAv can bind at the protruding strand. In result, the number of target strands on top of the origami will decrease. The number of strand breaks (N_{SB}) is calculated as

$$N_{SB} = \left(1 - \frac{\sum N_{SAv}}{3\ N_{Origami}}\right) \times 100 \tag{2}$$

with N_{SAv} being the number of still intact strands and $N_{Origami}$ being the number of analyzed DNA origami. N_{SB} is then plotted as a function of the fluence F.

3 Results and discussion

The absolute cross sections for strand breakage of oligonucleotides σ_{SSB} can be determined using two different methods. Initial values of σ_{SSB} need to be determined by recording the fluence dependence of strand breaks. In the following, this is referred to as the absolute method. By using an oligonucleotide sequence with known value of σ_{SSB} this sequence can be used as a reference, and the strand break cross section for another sequence can be determined relative to it. In the following, this is referred to as the relative method.

3.1 Absolute method

In the absolute method two different sequences are positioned on one DNA origami design. From AFM analysis, the number of strand breaks N_{SB} is determined as a function of fluence F:

$$N_{SB} = \sigma_{SSB} F + N_{SB0} \tag{3}$$

with N_{SB0} being the number of strand breaks without irradiation. For low fluences, the dose response curve is linear [5]. Thus, the absolute strand break cross section can be obtained from the instrumental weighted linear fit to the data. The resulting strand break cross section σ_{SSB} is then obtained from:

$$\sigma_{SSB} = (N_{SB} - N_{SB0})/F. \tag{4}$$

In a single irradiation experiment the strand break cross sections of at least two different sequences is obtained. A fluence dependency needs to be recorded, thus at least two different sample series are irradiated under identical conditions to prove repeatability. The total amount of samples irradiated with different fluence values has been at least ten samples to improve the accuracy of the determined absolute strand break cross sections. To reduce the number of irradiated samples, the relative method is applied by using one target sequence as a reference.

3.2 Relative method

The relative method allows to reduce the amount of samples which need to be irradiated to determine the strand

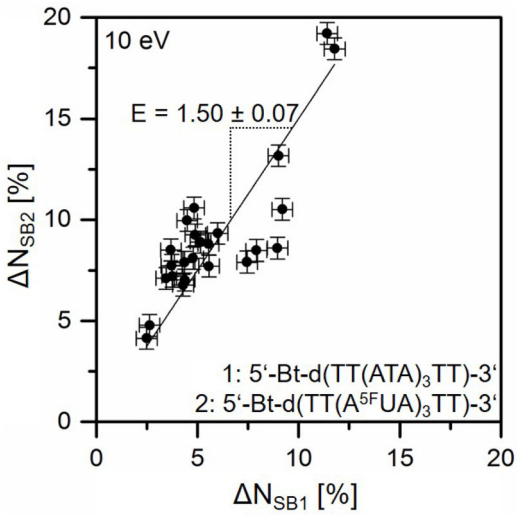

Fig. 6. Graphical correlation of the LEE induced strand breakage at 10 eV between the known 5'-Bt-d(TT(ATA)$_3$TT)-3' sequence and the unknown 5'-Bt-d(TT(A^{5F}UA)$_3$TT)-3' sequence, to determine the ratio E from the slope of the linear fit.

break cross section for a given sequence. A sequence with known σ_{SSB} at a certain energy is used as an internal reference. In combination with the reference sequence, the strand break cross section for an unknown sequence is determined. Both sequences are placed on one DNA origami and thus irradiated under identical conditions. The fluence F is therefore identical for both sequences:

$$(N_{SB} - N_{SB0})/\sigma_{SSB} = F = (N_{SB,ref} - N_{SB0,ref})/\sigma_{SSB,ref}. \quad (5)$$

The unknown strand break cross section σ_{SSB} can then be calculated based on the reference strand break cross section $\sigma_{SSB,ref}$:

$$\sigma_{SSB} = \sigma_{SSB,ref}\,(N_{SB} - N_{SB0})\,/\,(N_{SB,ref} - N_{SB0,ref}) = \sigma_{SSB,ref} E \quad (6)$$

with

$$E = (N_{SB} - N_{SB0})\,/\,(N_{SB,ref} - N_{SB0,ref}) = \Delta N_{SB}/\Delta N_{SB,ref}. \quad (7)$$

The value E is obtained as the slope of the plot of ΔN_{SB} against $\Delta N_{SB,ref}$ (Fig. 6). For this method, rather few samples are needed. To ensure reproducibility, at least three samples are irradiated. This method is independent of the fluence, as long as all irradiations are performed in the linear response regime. Thus, all samples have been irradiated with rather short times at low current. At very short irradiation times, the N_{SB} is very similar to N_{SB0}, resulting in stronger variations for E. Over all experiments, the error of E is quite small. Yet this error is added to the error of the reference strand break cross section $\sigma_{SSB,ref}$. Thus, it is useful to apply the absolute method to determine absolute strand break cross sections with an error around 10%. Then, the less time consuming relative method can be used for further strand break cross section determination for a variety of sequences.

The margin of error of the absolute strand break cross section is higher when the relative method is used, since the error of the reference sequence is taken into account as well. Yet compared to the error of the strand break cross sections obtained with the absolute method, the additional error through the relative method is rather small. This indicates that the error of the strand break cross section using the absolute method arises from fluence variations. These variations can occur through an off-center irradiation position and AFM images taken at different distances from the center of irradiation.

3.3 Biotin label for oligonucleotide visualization

Since in the above described experiments Bt is irradiated just like the oligonucleotide sequences, its stability towards 10 eV electrons over the analyzed fluence range needs to be confirmed. Therefore, only the Bt label was attached to the sequences 5'-Bt-t-1s4i-3', -t-1s14i and -t-1s24i on the DNA origami triangle and analyzed with the absolute method. With an obtained damage cross section of $(0.26 \pm 0.92) \times 10^{-15}$ cm^2 Bt remains stable with no detectable fragmentation at 10 eV up to a fluence of at least 10^{13} cm^{-2}.

3.4 Strand breaks in modified oligonucleotides

Previously, we have studied the radiosensitizing effect of ^{2F}A [32]. In the present work we have determined the absolute cross sections for single strand breakage upon irradiation with 10 eV electrons for oligonucleotides containing the radiosensitizer ^{5F}U using the relative method and reference sequences that have been analyzed previously using the absolute method [32].

The sequence 5'-Bt-d(TT(A^{5F}UA)$_3$TT)-3' has been irradiated together with the T containing 5'-Bt-d(TT(ATA)$_3$TT)-3' sequence with 10 eV electrons. The ratio E between the sequence containing ^{5F}U and the known reference sequence has been obtained from all ΔN_{SB} values as $E = 1.50 \pm 0.07$ (Fig. 6). This ratio was then multiplied with the absolute strand break cross section of the 5'-Bt-d(TT(ATA)$_3$TT)-3' sequence of $(0.80 \pm 0.12) \times 10^{-14}$ cm^2 [32], resulting in a strand break cross section of $(1.20 \pm 0.20) \times 10^{-14}$ cm^2 for the 5'-Bt-d(TT(A^{5F}UA)$_3$TT)-3' sequence.

To compare the radiosensitizing effect of both ^{5F}U and ^{2F}A, the nucleotide sequence of 5'-Bt-d(TT(^{2F}AT^{2F}A)$_3$TT)-3' at the center positions of the DNA origami triangle was combined with the ^{5F}U containing sequence 5'-Bt-d(TT(^{5F}UT^{5F}U)$_3$TT)-3' at the corner positions. In both sequences the amount of F containing nucleobases is identical with each modified nucleobase being flanked by T. The experiment yields a ratio $E = 0.98 \pm 0.03$, resulting in an absolute strand

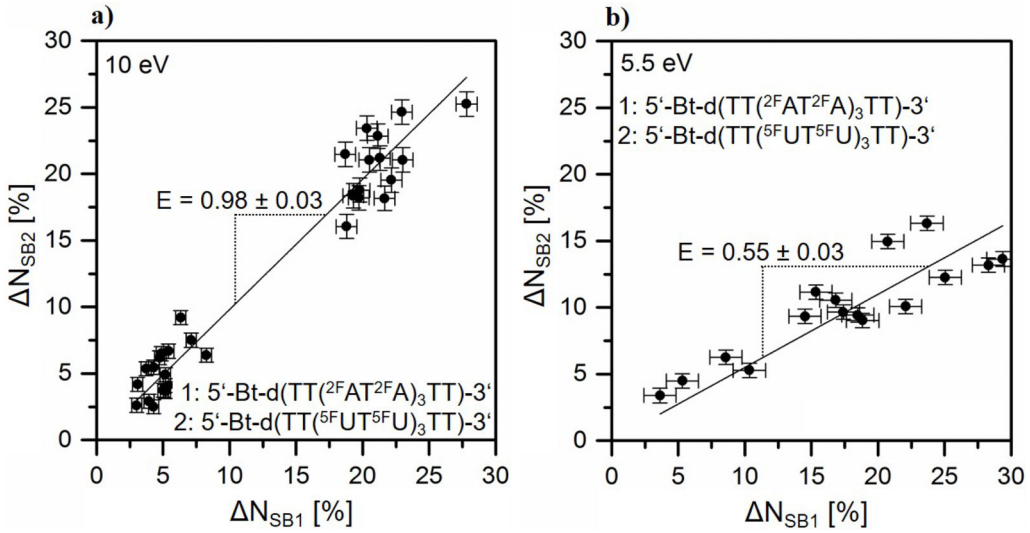

Fig. 7. Correlation between ΔN_{SB} values of the sequences 5'-Bt-d(TT(^{5F}UT^{5F}U)$_3$TT)-3' and 5'-Bt-d(TT(^{2F}AT^{2F}A)$_3$TT)-3' (a) at 10 eV and (b) at 5.5 eV. The x-axis corresponds to the reference sequences. The ratios E have been obtained from the slopes of the linear fits.

Table 2. Overview of the absolute strand break cross sections σ_{SSB} of the ^{2F}A and ^{5F}U containing oligonucleotides at 10 eV and 5.5 eV (results from Ref. [32] included).

5'-Bt-d(TTXTT)-3'	σ_{SSB} (at 10 eV)	σ_{SSB} (at 5.5 eV)
X = (ATA)$_3$	$(0.80 \pm 0.12) \times 10^{-14}$ cm^2	$(1.36 \pm 0.02) \times 10^{-14}$ cm^2
X = (^{2F}AT^{2F}A)$_3$	$(1.34 \pm 0.22) \times 10^{-14}$ cm^2	$(2.12 \pm 0.09) \times 10^{-14}$ cm^2
X = (^{5F}UT^{5F}U)$_3$	$(1.31 \pm 0.25) \times 10^{-14}$ cm^2	$(1.17 \pm 0.11) \times 10^{-14}$ cm^2
X = (A^{5F}UA)$_3$	$(1.20 \pm 0.20) \times 10^{-14}$ cm^2	
X = T$_8$	$(0.79 \pm 0.07) \times 10^{-14}$ cm^2	

break cross section of $(1.31 \pm 0.25) \times 10^{-14}$ cm^2 for 5'-Bt-d(TT(^{5F}UT^{5F}U)$_3$TT)-3', based on the strand break cross section for 5'-Bt-d(TT(^{2F}AT^{2F}A)$_3$TT)-3' of $(1.34 \pm 0.22) \times 10^{-14}$ cm^2 (Fig. 7a) [32].

The same DNA origami design with oligonucleotides containing ^{5F}U and ^{2F}A was also irradiated with 5.5 eV electrons, and analyzed with the relative method (Fig. 7b). Based on the strand break cross section for 5'-Bt-d(TT(^{2F}AT^{2F}A)$_3$TT)-3' of $(2.12 \pm 0.09) \times 10^{-14}$ cm^2 and a ratio $E = 0.55 \pm 0.03$ the absolute strand break cross section for 5'-Bt-d(TT(^{5F}UT^{5F}U)$_3$TT)-3' was determined to be $(1.17 \pm 0.11) \times 10^{-14}$ cm^2 (Fig. 7b).

All the obtained values of σ_{SSB} are summarized in Table 2 and compared in Figure 8. At 10 eV the absolute strand break cross section for 5'-Bt-d(TT(A^{5F}UA)$_3$TT)-3' is $(1.20 \pm 0.20) \times 10^{-14}$ cm^2 and thus only slightly below the strand break cross section for 5'-Bt-d(TT(^{5F}UT^{5F}U)$_3$TT)-3', which is $(1.31 \pm 0.25) \times 10^{-14}$ cm^2. Both strand break cross sections are identical within the margin of error. Thus, the sensitivity towards electrons of 10 eV energy is independent of the amount of ^{5F}U in the oligonucleotide and the neighboring nucleobases A or T in the oligonucleotide sequence. The latter observation is also supported by the comparison of 5'-Bt-d(TT(ATA)$_3$TT)-3' and 5'-Bt-d(T)$_{12}$-3' [32]. Within the margin of error, both sequences have identical strand break cross sections of (0.80 ± 0.12) and $(0.79 \pm 0.07) \times 10^{-14}$ cm^2, respectively. However, both aspects, the neighboring nucleobase A or T and the amount of ^{5F}U in the sequence (either 3 or 6 times), can have an opposite influence on the sensitivity of the sequence,

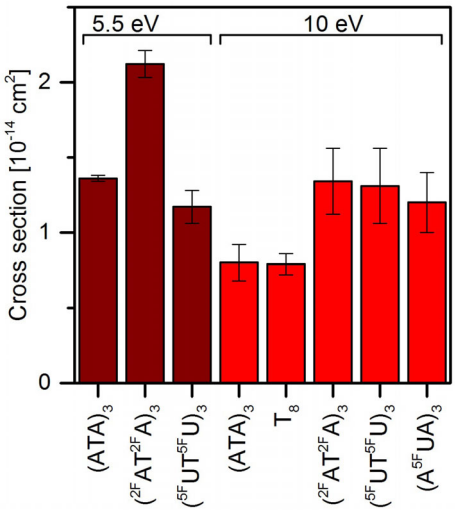

Fig. 8. Comparison of all obtained absolute strand break cross sections for the oligonucleotides 5'-Bt-d(TTXTT)-3', with X = (ATA)$_3$, T$_8$, (^{2F}AT^{2F}A)$_3$, (^{5F}UT^{5F}U)$_3$ and (A^{5F}UA)$_3$ at 5.5 eV and 10 eV.

resulting in an identical strand break cross section for both sequences 5'-Bt-d(TT(A^{5F}UA)$_3$TT)-3' and 5'-Bt-d(TT(^{5F}UT^{5F}U)$_3$TT)-3'. Although it is rather unlikely that these two very different aspects influence the strand break cross section with similar intensity in opposite directions, it is not utterly out of question.

At 10 eV, both sequences containing ^{5F}U showed an enhancement factor of 1.5 ± 0.1 and 1.6 ± 0.5, compared to 5'-Bt-d(TT(ATA)$_3$TT)-3'. Thus, both have similar sensitivities towards 10 eV electrons also compared to the ^{2F}A containing nucleotide. Therefore, it can be concluded, that the fluorination at the nucleobase is more important for the sensitivity than the type of the nucleobase itself. This is rather surprising since the fragmentation of the pyrimidine base ^{2F}A in DEA gas phase experiments is quite different from that of the purine base ^{5F}U [33,34]. In addition, none of them show relevant resonances around 10 eV. Yet both *F* containing nucleobases showed significant SSB enhancement in oligonucleotides. The higher electronegativity of *F* compared to H might draw electron density from the nucleobase, improving the antenna effect for the electrons and leading to DNA backbone decomposition by electron delocalization.

Comparing energies of 5.5 eV and 10 eV, no change in the strand break cross section of 5'-Bt-d(TT(^{5F}UT^{5F}U)$_3$TT)-3' is observed. The ratio of the respective strand break cross sections was calculated to be 0.9 ± 0.2. Thus, although significant resonances were observed for gas phase ^{5F}U around 5 eV and none at 10 eV [33,38], these fragmentations do not lead to an increase in strand breaks. This is in contrast to the ^{2F}A containing nucleotide, in which an increase of 1.6 ± 0.3 was obtained also at 5.5 eV [32].

4 Conclusion

We have assembled a LEE irradiation setup dedicated for the irradiation of oligonucleotides attached to DNA origami substrates. The setup and the experimental procedure are described in detail. A particular focus is put on an accurate determination of the fluence, which is critical for the quantification of DNA strand breaks. By AFM analysis of the irradiated samples the absolute cross sections for strand breakage (σ_{SSB}) can be determined for specific oligonucleotide sequences. We have compared different ^{5F}U containing oligonucleotides with their non-fluorinated analogues and with sequences containing ^{2F}A using two different electron energies (5.5 eV and 10 eV). The absolute strand break cross sections determined here are summarized in Figure 7. We find identical σ_{SSB} values (within the error bars) at 10 eV for the non-fluorinated sequences 5'-Bt-d(TT(ATA)$_3$TT)-3' and 5'-Bt-dT$_{12}$-3'. Compared to these sequences all fluorinated single strands show a similar enhancement of σ_{SSB} of 1.5–1.6 at 10 eV. The amount of ^{5F}U appears to have no significant influence on the strand break cross section, as similar values are obtained for the oligonucleotide containing three or six ^{5F}U molecules, respectively. At 5.5 eV the situation is slightly different compared to 10 eV: Both, 5'-Bt-d(TT(ATA)$_3$TT)-3' and 5'-Bt-d(TT(^{2F}AT^{2F}A)$_3$TT)-3' have clearly higher strand break cross sections at 5.5 eV than at 10 eV, whereas 5'-Bt-d(TT(^{5F}UT^{5F}U)$_3$TT)-3' shows even slightly lower values for σ_{SSB} at 5.5 eV than at 10 eV. This implicates that ^{2F}A should be a more effective radiosensitizer than ^{5F}U (which is routinely used in tumor radiation therapy) because ^{2F}A is more reactive towards LEEs within a wider range of electron energies.

This research was supported by the Federal Institute of Materials Research and Testing (BAM), a Marie-Curie FP7 Integration Grant within the 7th European Union Framework Programme, by the Deutsche Forschungsgemeinschaft (DFG) and the University of Potsdam. We acknowledge a bilateral grant between Serbia and Germany through the German Academic Exchange Service (DAAD, project No. 57055766) supported by the German Federal Ministry of Education and Research. M.Lj.R. and A.R.M. acknowledge support by the MESTD of Republic of Serbia under Project No. #171020.

References

1. D.W.O. Rogers, Phys. Med. Biol. **51**, R287 (2006)
2. L.H. Toburen, Int. J. Radiat. Biol. **88**, 2 (2012)
3. S.M. Pimblott, J.A. LaVerne, Radiat. Res. **150**, 159 (1998)
4. I. Baccarelli, I. Bald, F.A. Gianturco, E. Illenberger, J. Kopyra, Phys. Rep. **508**, 1 (2011)
5. B. Boudaiffa, P. Cloutier, D. Hunting, M.A. Huels, L. Sanche, Science **287**, 1658 (2000)
6. I. Bald, J. Langer, P. Tegeder, O. Ingólfsson, Int. J. Mass Spectrom. **277**, 4 (2008)
7. I. Bald, I. Dabkowska, E. Illenberger, O. Ingólfsson, Phys. Chem. Chem. Phys. **9**, 2983 (2007)
8. I. Bald, J. Kopyra, E. Illenberger, Angew. Chem. Int. Ed. **45**, 4851 (2006)
9. S. Ptasinska, S. Denifl, P. Scheier, E. Illenberger, T.D. Märk, Angew. Chem. Int. Ed. **44**, 6941 (2005)
10. I. Bald, I. Dabkowska, E. Illenberger, Angew. Chem. Int. Ed. **47**, 8518 (2008)
11. S. Ptasinska, S. Denifl, S. Gohlke, P. Scheier, E. Illenberger, T.D. Märk, Angew. Chem. Int. Ed. **45**, 1893 (2006)
12. Y. Chen, A. Aleksandrov, T.M. Orlando, Int. J. Mass Spectrom. **277**, 314 (2008)
13. S.V.K. Kumar, T. Pota, D. Peri, A.D. Dongre, B.J. Rao, J. Chem. Phys. **137**, 45101 (2012)
14. B. Boudaiffa, P. Cloutier, D. Hunting, M.A. Huels, L. Sanche, Radiat. Res. **157**, 227 (2002)
15. R. Panajotovic, F. Martin, P. Cloutier, D. Hunting L. Sanche, Radiat. Res. **165**, 452 (2006)
16. M. Rezaee, P. Cloutier, A.D. Bass, M. Michaud, D.J. Hunting, L. Sanche, Phys. Rev. E **86**, 31913 (2012)
17. M.A. Smiałek, S.A. Moore, N.J. Mason, D.E.G. Shuker, Radiat. Res. **172**, 529 (2009)
18. M.A. Smiałek, R. Balog, N.C. Jones, D. Field, N.J. Mason, Eur. Phys. J. D **60**, 31 (2010)
19. M.A. Smiałek, N.C. Jones, R. Balog, N.J. Mason, D. Field, Eur. Phys. J. D **62**, 197 (2011)

20. Z. Li, P. Cloutier, L. Sanche, J.R. Wagner, J. Am. Chem. Soc. **132**, 5422 (2010)
21. A.N. Sidorov, T.M. Orlando, J. Phys. Chem. Lett. **4**, 2328 (2013)
22. R. Schürmann, I. Bald, J. Phys. Chem. C **120**, 3001 (2016)
23. T. Solomun, C. Hultschig, E. Illenberger, Eur. Phys. J. D **35**, 437 (2005)
24. T. Solomun, H. Seitz, H. Sturm, J. Phys. Chem. B **113**, 11557 (2009)
25. A. Keller, I. Bald, A. Rotaru, E. Cauët, K.V. Gothelf, F. Besenbacher, ACS Nano **6**, 4392 (2012)
26. A. Keller, J. Kopyra, K.V. Gothelf, I. Bald, New J. Phys. **15**, 83045 (2013)
27. A. Keller, J. Rackwitz, E. Cauët, J. Liévin, T. Körzdörfer, A. Rotaru, K.V. Gothelf, F. Besenbacher, I. Bald, Sci. Rep. **4**, 7391 (2014)
28. S. Vogel, J. Rackwitz, R. Schürman, J. Prinz, A.R. Milosavljević, M. Réfrégiers, A. Giuliani, I. Bald, J. Phys. Chem. Lett. **6**, 4589 (2015)
29. I. Bald, A. Keller, Molecules **19**, 13803 (2014)
30. L. Olejko, P.J. Cywinski, I. Bald, Angew. Chem. Int. Ed. **54**, 673 (2015)
31. J. Kopyra, A. Keller, I. Bald, RSC Adv. **4**, 6825 (2014)
32. J. Rackwitz, J. Kopyra, I. Dąbkowska, K. Ebel, M.Lj. Ranković, A.R. Milosavljević, I. Bald, Angew. Chem. Int. Ed. Engl. **55**, 10248 (2016)
33. H. Abdoul-Carime, M.A. Huels, E. Illenberger, L. Sanche, Int. J. Mass Spectrom. **228**, 703 (2003)
34. R. Abouaf, H. Dunet, Eur. Phys. J. D **35**, 405 (2005)
35. P.-C. Dugal, H. Abdoul-Carime, L. Sanche, J. Phys. Chem. B **104**, 5610 (2000)
36. J. Rackwitz, *A novel approach to study low-energy electron-induced damage to DNA oligonucleotides. Influence of DNA sequence, topology and nucleobase modification* (Dissertation, University of Potsdam, 2016)
37. P.W.K. Rothemund, Nature **440**, 297 (2006)
38. G. Hanel, B. Gstir, S. Denifl, P. Scheier, M. Probst, B. Farizon, M. Farizon, E. Illenberger, T.D. Märk, Phys. Rev. Lett. **90**, 188104 (2003)

Nuclear Inst, and Methods in Physics Research B 423 (2018) 87–91

Contents lists available at ScienceDirect

Nuclear Inst. and Methods in Physics Research B

journal homepage: www.elsevier.com/locate/nimb

Electron transmission through a steel capillary

J.B. Maljković[a], D. Borka[b], M. Lj. Ranković[a], B.P. Marinković[a,*], A.R. Milosavljević[c], C. Lemell[d], K. Tőkési[e]

[a] Institute of Physics Belgrade, University of Belgrade, Pregrevica 118, 11080 Belgrade, Serbia
[b] Atomic Physics Laboratory (040), Vinča Institute of Nuclear Sciences, University of Belgrade, P.O. Box 522, 11001 Belgrade, Serbia
[c] Synchrotron SOLEIL, L'orme des Merisiers, Saint-Aubin – BP48, 91192 GIF-sur-Yvette Cedex, France
[d] Institute for Theoretical Physics, Vienna University of Technology, Wiedner Hauptstraße 8-10, A-1040 Vienna, Austria
[e] Institute for Nuclear Research, Hungarian Academy of Sciences (ATOMKI), H-4026 Debrecen, 4026 Debrecen Bem tër 18/c, Hungary

ARTICLE INFO

Keywords:
Electron scattering from surfaces
Capillary transmission
Metallic capillary
Energy loss

ABSTRACT

The transmission of low-energy electrons through a macroscopic steel capillary has been investigated both experimentally and theoretically. The length of the steel capillary was $L = 19.5$ mm and the inner diameter was $d = 0.9$ mm. The kinetic energy distribution of electrons transmitted through the steel capillary was recorded for a tilt angle of $\psi = 2.6°$ of the incident electron beam with respect to the capillary axis. Accompanying simulations based on classical transport theory reproduce the experimental data to a high degree of agreement. Transmission for other tilt angles has also been simulated to investigate the influence of the tilt angle on the guiding efficiency.

1. Introduction

The understanding and interpretation of electron spectra backscattered from solid surfaces is important for many technical applications, e.g., for surface characterization and diagnostics to assess material damage and surface modification [1–4]. Additionally, analysis of particles scattered off solid surfaces allows for studying the scattering process itself.

With the advent of capillary targets [5,6] the change of the internal state of the (ionic) projectiles due to the close interaction with the inner capillary wall have become topics of research, since 2002 the redirection of charged particles by nanocapillary targets (see [7,8] and references therein) was investigated in detail.

In our experiment we study electrons escaping macroscopic metallic capillaries after (multiple) impact on the inner wall of the target. Deflection of incident electrons along the capillary axis is accompanied by both elastic and inelastic scattering events and the production of secondary electrons with considerable energy loss of the projectile [9–12]. Clearly, an experimental distinction between transmitted primary particles and secondary electrons generated in inelastic scattering events remains impossible and requires extensive simulations of the transmission process [13–15].

In this work we study the transmission of 150 eV electrons through a macroscopic steel capillary and model the experiment based on classical transport theory [16–19]. The theoretical spectra are presented in the energy range between 60 eV and 150 eV. For smaller electron energies calculated cross sections become unreliable.

2. Experiment

The experiment was performed on the electron spectrometer UGRA (Institute of Physics Belgrade) which has been modified to allow for mounting of a capillary target [12] instead of a gas needle. The experimental set-up is shown in Fig. 1.

The system consists of a rotatable electron gun, steel capillary, 4-electrode lens, double cylindrical mirror energy analyzer (DCMA), 3-electrode lens, channeltron as a detector and a Faraday cup for obtaining the incident electron beam profile. All components are electrically shielded and enclosed in a vacuum chamber which is magnetically shielded with two layers of μ metal. The working pressure in the experimental chamber during the measurements was about 7×10^{-7} mbar. The electron energy resolution of the system is about 0.7 eV at full width half maximum. The electron gun produces a well collimated electron beam which is directed on the capillary target.

To align the experimental components and to measure the electron beam profile, a Faraday cup was mounted on $X-Y$ manipulator as indicated in Fig. 2. After optimizing and focusing the electron optics for 150 eV energy, the electron beam profile was measured by recording the current in the Faraday cup as a function of the rotation angle $\Theta_{relative}$ within the range of about ± 4° relative to the Faraday cup axis. The

* Corresponding author.
E-mail address: bratislav.marinkovic@ipb.ac.rs (B.P. Marinković).

https://doi.org/10.1016/j.nimb.2018.03.020
Received 14 December 2017; Received in revised form 15 February 2018; Accepted 15 March 2018
0168-583X/

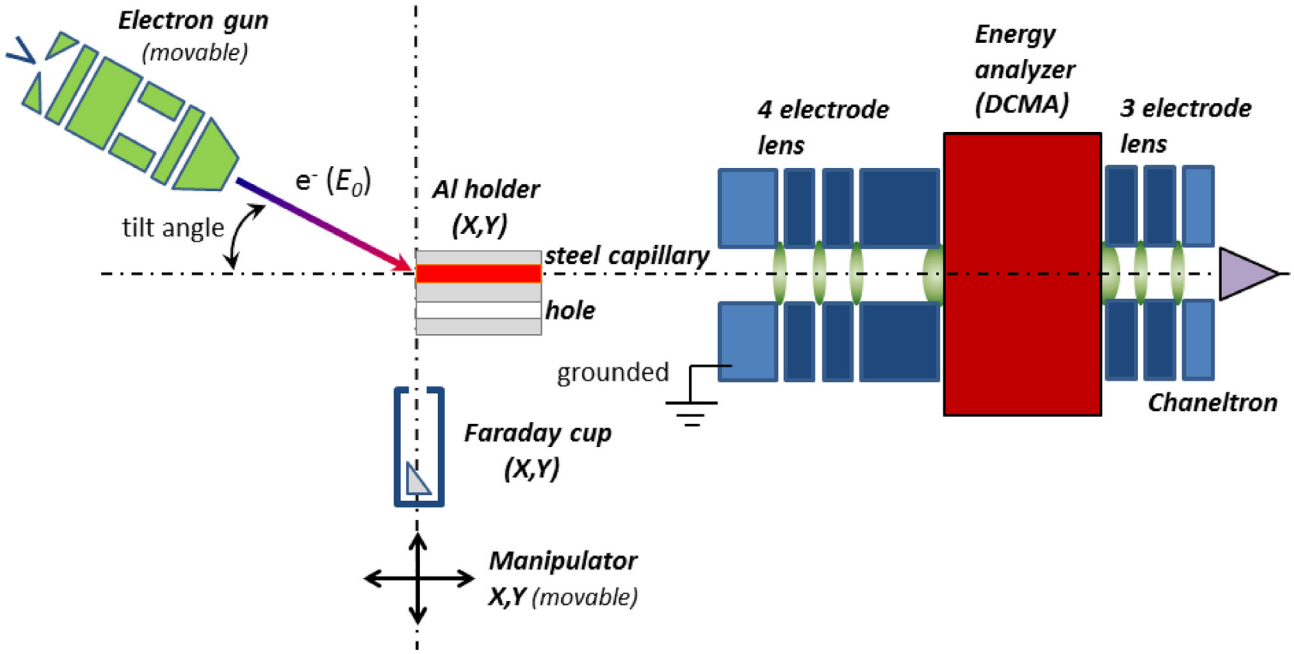

Fig. 1. The experimental set-up UGRA with the movable electron gun, stainless steel capillary, manipulator and double cylindrical mirror energy analyzer with a detector. The analyzer optics and detector are fixed in place. The $X-Y$ manipulator is used to mount either a Faraday cup prior to experiment or an aluminum target holder with the capillary during the experiment.

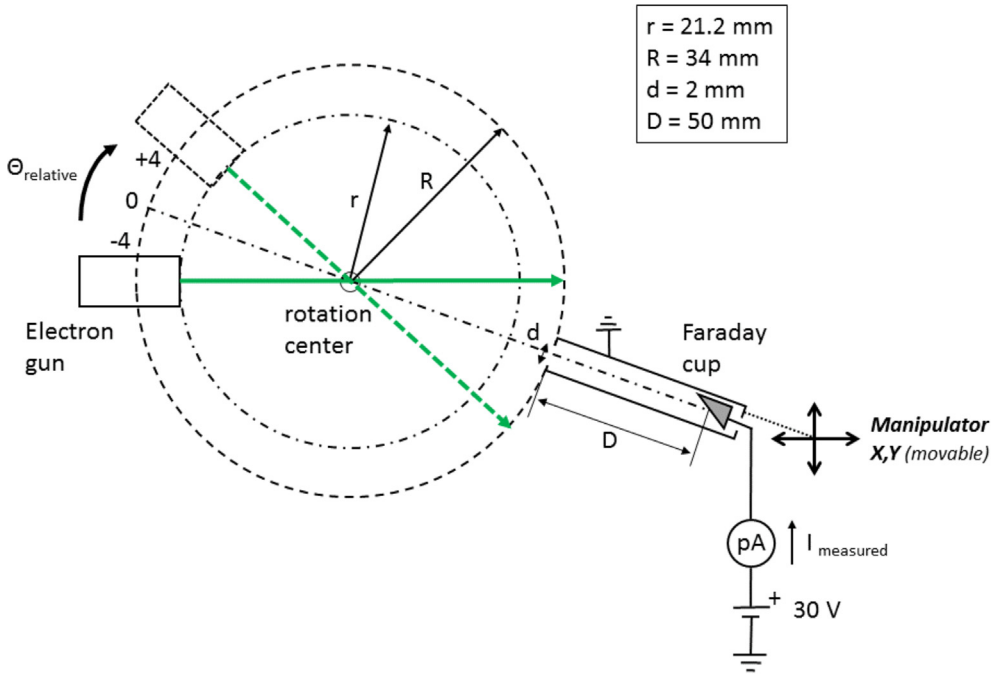

Fig. 2. Schematic representation of setup for measuring the electron beam profile.

Faraday cup was set at a distance of 55 mm from the last electrode of the electron gun.

In order to estimate electron beam width and divergence, a SIMION simulation [20] with the real experimental electrode geometry was performed. In this simulation, starting conditions of electron trajectories were characterized by two parameters, the electron beam width w and the angular divergence da. Initial conditions were uniformly distributed within w and da. The transmission function $T(w,da)$ was simulated for different combinations of w and da until the best agreement between experimental result and simulated data was achieved (Fig. 3). From the comparison we estimated the beam divergence to be 0.3° and a beam diameter of 0.82 mm at the exit of the electron gun.

For the experiment the Faraday cup was replaced by a steel capillary with a diameter of 0.9 mm and a length of 19.5 mm. It has an aspect ratio of 21.7 or, equivalently, a geometric opening angle of 2.6°. The vertical distance between the capillary and a hole was 5.8 mm, while distance between the capillary entrance and last electron gun lens was about 25 mm. The capillary position was adjusted to align with the incident electron beam and the energy analyzer axis. The tilt angle between the incident electron beam and the capillary axis is adjusted by rotating the electron gun with the capillary and analyzer remaining fixed.

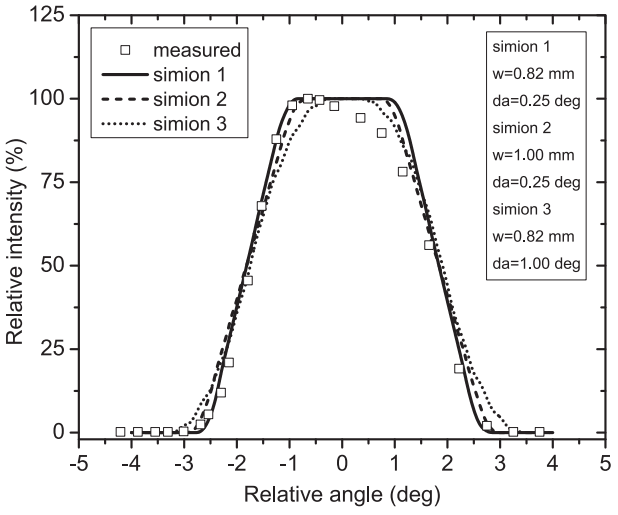

Fig. 3. Measured and simulated electron beam profiles. Symbols: measured profile, lines: SIMION simulations with different parameters; solid line – $w = 0.82$ mm, $da = 0.25°$, dash line – $w = 1.0$ mm, $da = 0.25°$, dot line - $w = 0.82$ mm, $da = 1.0°$.

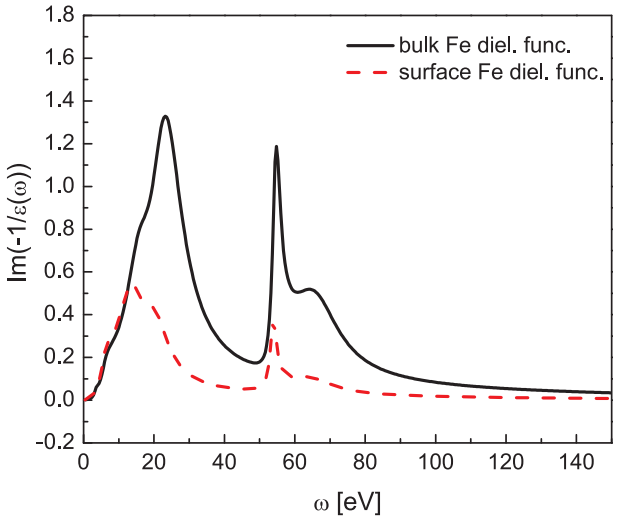

Fig. 4. Bulk (thick solid black line) and surface (thin dashed red line) dielectric functions of Fe [37]. (For interpretation of the references to colour in this figure legend, the reader is referred to the web version of this article.)

The system allows for measurements of the transmitted electron current as a function of both the tilt angle and the kinetic energy of electrons escaping the capillary [12]. The electrons transmitted through the steel capillary were energy analyzed by the DCMA operating in constant pass energy mode with counts recorded as a function of a retarding potential. As the transmission of the 4-electrode lens depends on the retarding potential energy distributions of transmitted electrons were corrected according to the transmission function obtained by SIMION. An optimal system alignment was verified by measuring the total transmitted electron current at the inner cylinder of the DCMA.

3. Theory

In our simulation stainless steel is approximated with iron by neglecting any admixtures (Cr, O, C) of unknown quantity. Both elastic and inelastic collisions in Fe are taken into account. Energy dependent cross sections for elastic scattering off Fe atoms modeled with muffin-tin potential were calculated using non-relativistic Schrödinger partial wave analysis [21].

For the description of inelastic scattering cross sections we rely on the dielectric response formalism [22]. Accordingly, the momentum- and energy-loss dependent dielectric function $\epsilon(q,\omega)$ can be approximated by extrapolation of optical data $\mathrm{Im}[-\epsilon\ (q = 0,\omega)^{-1}]$ into the $q-\omega$ plane [23–27]. Then, the bulk and surface energy loss functions are given by $\mathrm{Im}[-\epsilon\ (q,\omega)^{-1}]$ and $\mathrm{Im}[-\{\epsilon(q,\omega) + 1\}^{-1}]$, respectively [28,29]. The dielectric response of an electron gas has been extensively studied mainly by using the Lindhard type dielectric function [30–35]. The analytical expression given by the Lindhard [36] dielectric function provides a convenient framework for the dielectric properties of Fe. Here, surface and bulk dielectric functions were obtained following Werner et al. [37,38] (see Fig. 4).

Within the capillary electrons follow straight line trajectories. Upon impact on the inner wall of the capillary projectiles undergo a sequence of stochastic scattering events determined by the elastic and inelastic mean free paths. If an electron eventually reescapes from the inner capillary surface the next impact point on the opposite side of the capillary or its escape point from the capillary is calculated. In case of an inelastic scattering event a secondary electron is created with a kinetic energy equal to the energy lost by the primary particle. The initial direction of the secondary electron is chosen randomly from 4π. If its initial kinetic energy is larger than 60 eV its trajectory is subsequently followed as well.

4. Results and discussion

In our experiment we selected the smallest angle for which all projectiles have to interact with the inner wall of the capillary, i.e., an angle slightly larger than the geometric opening angle of the capillary. With the linear dimensions of our target capillary (diameter $d = 0.9$ mm, length $L = 19.5$ mm) the tilt angle in the experiment was set to $\psi = 2.6°$. Geometrically, the dominant fraction of electrons are expected to hit the inner surface of the capillary only once. Assuming specular reflection conditions and accounting for a beam divergence of 0.3° more than 75% are expected to undergo only one impact event, another ~ 20% two impact events (Fig. 5).

From the general shape of the surface and bulk dielectric loss functions (rather broad and featureless functions, Fig. 4) and the small number of impact events we expect the energy distribution of

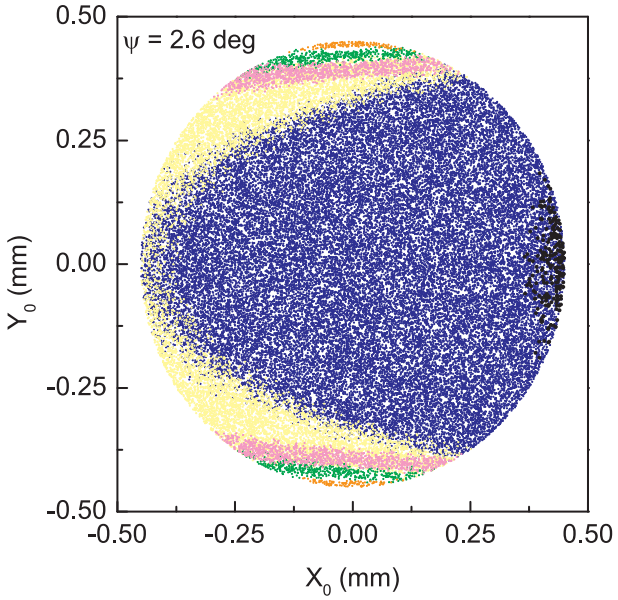

Fig. 5. Trajectories starting from randomly selected positions on the entrance plane under an incidence angle of 2.6 ± 0.3° with respect to the capillary axis are calculated assuming specular reflection upon impact on the inner capillary wall. The number of scattering events is shown in color (0: black 1: blue, 2: yellow, 3: green 4: pink, >4: orange). (For interpretation of the references to colour in this figure legend, the reader is referred to the web version of this article.)

transmitted electrons to resemble the usual energy distributions after backscattering from plane solid surfaces: a sharp elastic peak together with a broad distribution of projectiles having lost a considerable fraction of their initial energy. Towards smaller energies the admixture of secondary electrons increases. Fig. 6 shows our experimental results for 150 eV electrons incident on a steel capillary under an incidence angle of 2.6° (symbols). In general, for small incidence angles one would expect the surface excitations to dominate inelastic scattering events and cause smaller energy loss. Here, however, a clear distinction between surface and bulk losses is not visible presumably due to the surface roughness of the inner wall of the capillary target accompanied by deep penetration into the target under an effectively larger incidence angle. Phonon excitations with energy losses less than about 0.1 eV will only appear as a slight broadening of the elastic peak but have not been analyzed in our experiment. The dominant loss peaks with maxima around 20 and 60 eV are the material characteristic energy losses of electrons in inelastic scattering events containing collective excitations (or plasmons) and single electron excitations. Due to the large number of d electrons in Fe the plasmon peak ($\hbar\omega_{pl} \approx 15.3$ eV) is submerged in the broad distribution around 20 eV (shoulder on the low-energy side of the distribution) and, consequently, cannot be singled out in the electron-energy spectrum as a solitary feature.

To identify surface- or bulk-loss channels we have performed simulations allowing only for surface excitations (thin blue line in Fig. 6) and also for bulk excitations only (thick red line in Fig. 6). Neither simulation run succeeds in perfectly reproducing the experimental results. It can, however, be clearly seen that surface excitation contributions are only responsible for a small fraction of inelastic energy losses. As stated above, this points to a large surface roughness shifting the weight from surface to bulk losses. Additionally, only a minority of electrons leave the surface under the angle of incidence as assumed in the specular reflection model. Therefore, trajectories with more than one impact on the surface will feature on average a larger effective impact angle. This becomes evident when comparing Fig. 5 with Fig. 7 which shows again the starting points of trajectories on the entrance plane.

The dominant fraction of transmitted electrons is still scattered only once but a more realistic description of the electron-wall interaction removes the boundaries between regions with different number of impact events due to an effective randomization of the exit angle from the

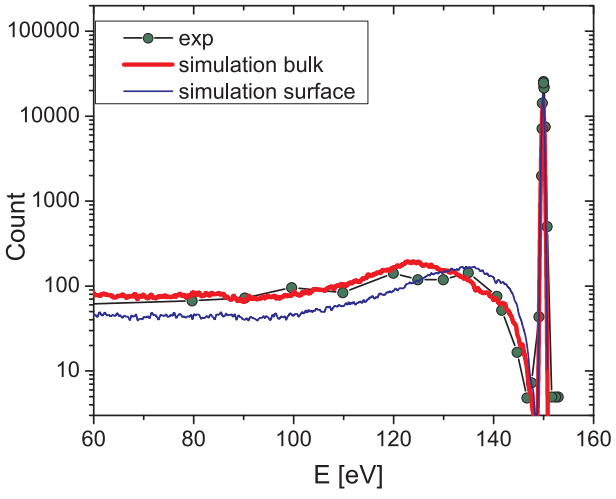

Fig. 6. Comparison between the experimentally obtained kinetic energy spectrum and calculated spectra of electrons escaping the steel tube, for an incident electron energy of 150 eV and electron beam incident angle $\psi = 2.6°$. The simulated spectra have been obtained using the bulk dielectric function (thick red line) and the surface dielectric function (thin blue line) of iron. Experimental data are presented by green circles. (For interpretation of the references to colour in this figure legend, the reader is referred to the web version of this article.)

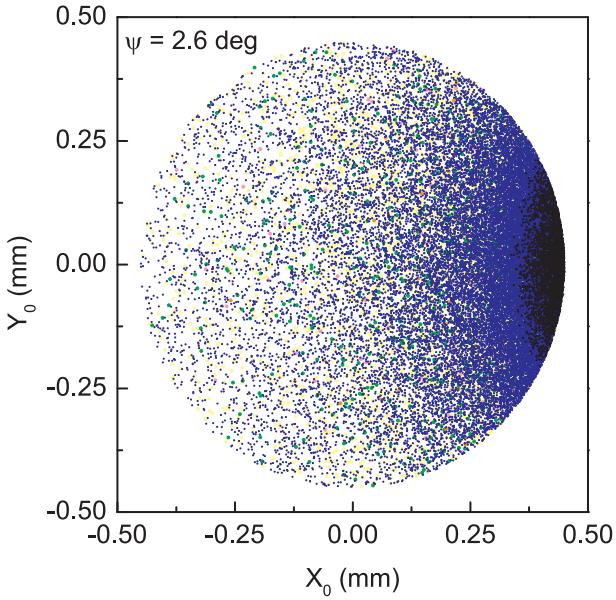

Fig. 7. Same as Fig. 5 but from results of the full simulation for an incidence angle of $\psi = 2.6 \pm 0.3°$. (0: black 1: blue, 2: yellow, 3: green 4: pink, > 4: orange). (For interpretation of the references to colour in this figure legend, the reader is referred to the web version of this article.)

inner capillary wall. This is also related to the neglected reflection at the collective potential of surface atoms [13] active at flat parts of the inner target wall for very grazing incidence angles. Both, the height of the elastic scattering peak in our simulation and the inelastic part of the spectrum is modeled very well.

Increasing the tilt angle in the simulations we have calculated the reduction of the transmission ratio of the capillary, i.e., number of electrons (including secondaries) divided by the number of trajectories started on the entrance plane of the capillary (Fig. 8). The energy and incidence angle of simulated electrons were randomly picked from Gaussian distributions with $E_0 = 150$ eV, $\sigma_E = 0.5$ eV and $\sigma_\psi = 0.3°$, respectively. Only electrons with kinetic energy larger than 50 eV were considered.

Two angular ranges can be discerned: as electrons hitting the surface have only a small probability to re-escape the surface the transmission ratio is for incidence angles smaller than the geometric angle

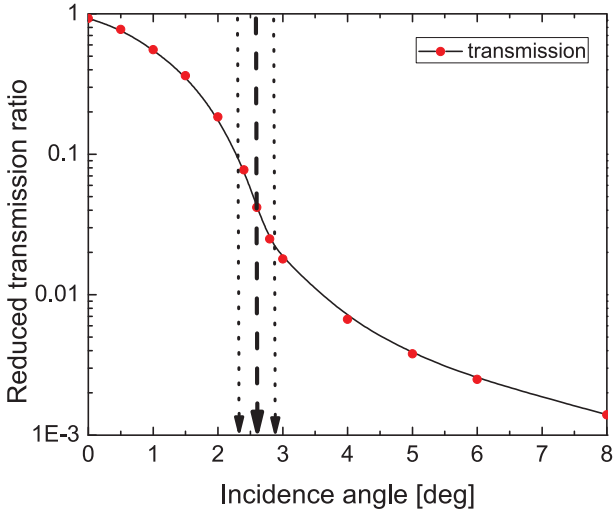

Fig. 8. Reduced transmission ratio as a function of incidence angle. The geometric opening angle is indicated by the dashed line, the beam divergence by the area between the dotted lines. Even at large incidence angles a considerable fraction of electrons are transmitted through the capillary.

dominated by transmission without interaction with the capillary wall. In contrast, for larger angles ($\psi \gtrsim 3°$) every projectiles hits the surface at least once thereby considerably reducing the transmission probability. Note, however, that even at larger angles electrons may still be transmitted at the original energy of 150 eV. In our simulation from $\psi = 2.6°$ to $\psi = 5°$ the total transmission probability is reduced by almost an order of magnitude (not considering the increasing intensity of low-energy electrons not included in our simulation).

5. Conclusion

We have presented a joint experimental and theoretical investigation of electrons transmission through a steel capillary with 150 eV primary incident electron energy at $\psi = 2.6°$ which is tilt angle of the capillary. The electron beam divergence was 0.3°. Theoretical spectra were obtained in the energy range between 60 and 150 eV. In the simulation both elastic and inelastic scattering of primary electrons colliding with the inner capillary surface as well as secondary electron emission from the capillary wall were taken into account.

From a comparison of experimental and simulated energy spectra we conclude that the inner wall of our capillary target was very rough suppressing to a large extend specular reflection and interaction with surface loss channels. Instead, best agreement between experiment and theory was found considering only bulk excitations in the simulation of inelastic scattering processes.

Furthermore, we have calculated the transmission ratio of electrons with energies ranging from 60 to 150 eV and found a slowly decreasing transmission function outside the geometric transmission range ($\psi \gtrsim 3°$). While in specular reflection approximation projectiles would have to undergo a large number of impact events for large ψ a realistic description of the surface interaction leads to a randomization of the scattering angle and, consequently, an increased number of trajectories having suffered only few impacts.

Acknowledgments

The work was supported by the Ministry of education, science and technological development of Republic of Serbia under the grants OI 171020 and III 45005. D.B. and C.L. acknowledge support by the bilateral Austrian-Serbian project “Interaction of charged particles with capillaries” number 451-03-01039/2015–09/25, K.T. and C.L. by the *Stiftung Aktion Österreich-Ungarn* under Project No. 96öu9. K.T. acknowledges support by the National Research, Development and Innovation Office (NKFIH) Grant KH 126886. D.B. and K.T. acknowledge support by the European COST Actions CA15107 (MultiComp) and MP1306 (EUSpec).

References

[1] T.L. Ferrell, P.M. Echenique, Phys. Rev. Lett. 55 (1985) 1526.
[2] H. Cohen, T. Maniv, R. Tenne, Y. Rosenfeld Hacohen, O. Stephan, C. Colliex, Phys. Rev. Lett. 80 (1998) 782.
[3] F.J. Garcia de Abajo, Rev. Mod. Phys. 82 (2010) 209.
[4] W.S.M. Werner, M. Novák, F. Salvat-Pujol, J. Zemek, P. Jiricek, Phys. Rev. Lett. 110 (2013) 086110.
[5] Y. Yamazaki, S. Ninomiya, F. Koike, H. Masuda, T. Azuma, K.-I. Komaki, K. Kuroki, M. Sekiguchi, J. Phys. Soc. Jpn. 65 (1996) 1199.
[6] S. Ninomiya, Y. Yamazaki, F. Koike, H. Masuda, T. Azuma, K. Komaki, K. Kuroki, M. Sekiguchi, Phys. Rev. Lett. 78 (1997) 4557.
[7] C. Lemell, J. Burgdörfer, F. Aumayr, Prog. Surf. Sci. 88 (2013) 237.
[8] N. Stolterfoht, Y. Yamazaki, Phys. Rep. 629 (2016) 1.
[9] A.R. Milosavljević, Gy. Víkor, Z.D. Pešić, P. Kolarž, D. Šević, B.P. Marinković, S. Mátéfi-Tempfli, M. Mátéfi-Tempfli, L. Piraux, Phys. Rev. A 75 (2007) 030901(R).
[10] S. Das, B.S. Dassanayake, M. Winkworth, J.L. Baran, N. Stolterfoht, J.A. Tanis, Phys. Rev. A 76 (2007) 042716.
[11] B.S. Dassanayake, R.J. Bereczky, S. Das, A. Ayyad, K. Tőkési, J.A. Tanis, Phys. Rev. A 83 (2011) 012707.
[12] A.R. Milosavljević, M. Lj, D. Ranković, J.B. Borka, R.J. Maljković, B.P. Bereczky, K. Tőkési Marinković, Nucl. Instrum. Methods Phys. Res. B 354 (2015) 86.
[13] K. Schiessl, K. Tőkési, B. Solleder, C. Lemell, J. Burgdörfer, Phys. Rev. Lett. 102 (2009) 163201.
[14] D. Borka, K. Tőkési, Nucl. Instrum. Methods Phys. Res. B 354 (2015) 112.
[15] D. Borka, V. Borka Jovanović, C. Lemell, K. Tőkési, Nucl. Instrum. Methods Phys. Res. B 406 (2017) 413.
[16] Z.-J. Ding, R. Shimizu, Surf. Sci. 222 (1989) 313.
[17] R. Shimizu, Y. Kataoka, T. Ikuta, T. Koshikawa, H. Hasimoto, J. Phys. D: Appl. Phys. 9 (1976) 101.
[18] K. Tőkési, D. Varga, L. Kövér, T. Mukoyama, J. Electron Spectrosc. Relat. Phenom. 76 (1995) 427.
[19] K. Tőkési, L. Wirtz, C. Lemell, J. Burgdörfer, Phys. Rev. A 64 (2001) 042902.
[20] D.J. Manura, D.A. Dahl, SIMION Version 8.0, User Manual, Scientific Instruments Services Inc, 2007.
[21] F. Salvat, R. Mayol, Comput. Phys. Commun. 74 (1993) 358.
[22] D. Pines, Elementary Excitations in Solids, Benjamin, New York, 1964, p. 127.
[23] H. Ritchie, Phys. Rev. 106 (5) (1957) 874.
[24] H. Ritchie, A.L. Marusak, Surf. Sci. 4 (1966) 234.
[25] A.G. Eguiluz, D.A. Campbell, Phys. Rev. B 31 (1985) 7572.
[26] J.L. Gervasoni, F. Yubero, Nucl. Instrum. Methods Phys. Res. B 182 (2001) 96.
[27] F. Salvat-Pujol, W.S.M. Werner, Surf. Interface Anal. 45 (2013) 873.
[28] C.J. Powell, Surf. Sci. 44 (1974) 29.
[29] D.R. Penn, Phys. Rev. B 35 (1987) 482.
[30] J.J. Quinn, Phys. Rev. 126 (1962) 1453.
[31] A.L. Fetter, J.D. Walecka, Quantum Theory of Many-Particle Systems, McGraw-Hill, New York, 1971, p. 40.
[32] J.C. Ashley, et al., Surf. Sci. 81 (1979) 409.
[33] C.J. Tung, R.H. Ritchie, Phys. Rev. B 16 (1977) 4302.
[34] H. Raether, Excitation of Plasmons and Interband Transitions by Electrons, Springer, Berlin, 1980 ch. 7.
[35] K. Sturm, Adv. Phys. 31 (1982) 1.
[36] J. Lindhard, K. Dan, Vidensk. Selsk. Mat. Fys. Medd. 28 (1954) 1.
[37] W.S.M. Werner, K. Glantschnig, C. Ambrosch-Draxl, J. Phys. Chem. Ref. Data 38 (4) (2009) 1.
[38] Private comunications with W.S.M. Werner.

EPJ D

Recognized by European Physical Society

Atomic, Molecular, Optical and Plasma Physics

Eur. Phys. J. D (2018) 72: 30 DOI: 10.1140/epjd/e2017-80677-4

Elastic electron differential cross sections for argon atom in the intermediate energy range from 40 eV to 300 eV

Miloš Lj. Ranković, Jelena B. Maljković, Károly Tökési, and Bratislav P. Marinković

edp sciences

Società Italiana di Fisica

Springer

Eur. Phys. J. D (2018) 72: 30
https://doi.org/10.1140/epjd/e2017-80677-4

THE EUROPEAN PHYSICAL JOURNAL D

Regular Article

Elastic electron differential cross sections for argon atom in the intermediate energy range from 40 eV to 300 eV[⋆,⋆⋆]

Miloš Lj. Ranković[1], Jelena B. Maljković[1], Károly Tökési[2,3], and Bratislav P. Marinković[1,a]

[1] Institute of Physics Belgrade, University of Belgrade, Pregrevica 118, 11080 Belgrade, Serbia
[2] Institute for Nuclear Research, Hungarian Academy of Sciences (ATOMKI), Debrecen, Hungary
[3] ELI-ALPS, ELI-HU Non-profit Kft., Szeged, Hungary

Received 25 October 2017 / Received in final form 29 November 2017
Published online 6 February 2018 –

Abstract. Measurements and calculations for electron elastic differential cross sections (DCS) of argon atom in the energy range from 40 to 300 eV are presented. DCS have been measured in the crossed beam arrangement of the electron spectrometer with an energy resolution of 0.5 eV and angular resolution of 1.5° in the range of scattering angles from 20° to 126°. Both angular behaviour and energy dependence of DCS are obtained in a separate sets of experiments, while the absolute scale is achieved via relative flow method, using helium as a reference gas. All data is corrected for the energy transmission function, changes of primary electron beam current and target pressure, and effective path length (volume correction). DCSs are calculated in relativistic framework by expressing the Mott's cross sections in partial wave expansion. Our results are compared with other available data.

1 Introduction

Electron elastic differential cross sections (DCS) of argon atom have been investigated thoroughly in the past by many experimental groups and different theoretical approaches but they still need further analysis and improvements. There are numerous reasons for this study: (i) DCS is still one of the stringiest test for electron–atom interaction that is energy (E_o) and angle (θ) dependent and where different theoretical approximations work adequately only in a certain (E_o, θ) domain. DCS is one of the variables in the "perfect scattering experiment" which has to be determined in absolute values in order to reproduce all complex scattering amplitudes [1]; (ii) Argon atom is often used as a model for both experimental (easy to handle, inexpensive in high purity) and theoretical (closed shell, many electron system) studies. Recently, Bartschat et al. [2] used an argon atom to make an overview on quantum-mechanical approaches for generating the electron–atom cross sections and to perform uncertainty estimates; (iii) atomic argon is an important model for the numerous calculation codes, now available, which use either quantum chemistry codes [3] or through other codes, like relativistic Dirac partial-wave analysis, incorporated into databases [4]; an important model for all being argon atom; (iv) there is a need for accurate cross sections for argon atom in experiments that use relative flow method (RFM) to determine absolute values of DCS for more complex molecules [5]. One of the key requirements in RFM is to provide similar flowing conditions (special distributions) of the measured and reference gas. This is easier to achieve if the masses of gases are similar, hence Ar or N_2 gases are preferentially used as references rather than helium which has the best known literature values for DCSs; and (v) the authors want to extend previous DCS measurements on Ar (listed in Tab. 1 among the other e/Ar data).

The first measurements of the differential electron elastic scattering by argon atom include those performed in 1931 by Bullard and Massey [6] and by Arnot [7] where the angular distributions were obtained in the ranges 4–40 eV, 15°–125° and 42–780 eV, 20°–120°, respectively. A comprehensive review of later experimental and theoretical results on electron/Ar cross sections up to 1995 was given by Zecca et al. [8] and results up to 2002 were compiled by Raju [9]. A critical data evaluation and consistency of electron scattering by argon was made in 2008 by Gargioni and Grosswendt [10]. A comparison of sets of cross sections for electron scattering from ground-state Ar in the energy range from thermal to about 1 keV with the overview of cross sections maintained by LXCAT database is given in [11]. The most recent results are presented in Table 1. The present experiment covers the electron impact energy range from 40 eV to 300 eV and the scattering angles from 25° up to 126°, while calculations are performed in broader range of impact energies and for the full range of scattering angles.

[⋆] Contribution to the Topical Issue "Physics of Ionized Gases (SPIG 2016)", edited by Goran Poparic, Bratislav Obradovic, Dragana Maric and Aleksandar Milosavljevic.
[⋆⋆] Supplementary material in the form of one pdf file from the Journal web page at https://doi.org/10.1140/epjd/e2017-80677-4.
[a] e-mail: bratislav.marinkovic@ipb.ac.rs

Table 1. The latest experimental and theoretical work on DCS for elastic cross section for argon atom covering impact energy range from 40 to 300 eV.

Author	Type of experiment/ theoretical approach	Energy range (eV)	Angular range (°)
Paikeday and Alexander [12]	Model potential	20–500	0–180
Kelemen [13]	Optical potential	0.5–500	Spin polarisation 0–180
Blanco and García [14]	Quasifree nonempirical model	40–10 000	0–180
Blanco and García [15]	Quasifree nonempirical model	40–800	0–180
Salvat [16]	Optical-model potential	100–3000	0–180
Milosavljević et al. [17]	Crossed beams/ relativistic ab initio	40–150	40–126
Yousif Al-Mulla [18]	Local density approximations	10–100	0–180
Jablonski et al. [19]	Thomas–Fermi–Dirac/ Dirac–Hartree–Fock potential	50–3000	0–180
Adibzadeh and Theodosiou [20]	Relativistic/nonrelativistic phase shifts	5–1000	0–180
Hargreaves et al. [21]	Crossed beams (SSRDM)	20–50	20–135
McEachran and Stauffer [22]	Ab initio optical potential	40–100	0–180
Bote et al. [23]	Optical-model potential	10–3000	0–180

2 Experimental method and theoretical approach

2.1 Experimental set-up

The home-made experimental setup is based on a crossed-beam technique comprising of an electron gun, a single capillary gas needle and a detection system with single channel electron multiplayer detector (channeltron). Detailed description of the original setup is given in [24,25], while construction of a gas line used for relative flow technique, design and programming of digital acquisition system are detailed in [5]. Briefly, electrons are produced from an indirectly heated thoriated tungsten hairpin filament (diameter 0.2 mm). Emitted electrons are then doubly focused by a 9 electrode system of the electron gun, including two axis deflector electrodes. The energy resolution of electrons at the exit of the electron gun is limited by a thermal distribution of emitted electrons to about 0.5 eV as there is no monochromaticity. The electron gun is mounted on a turntable and can be rotated in the plane of scattering from $-40°$ to $126°$ around the fixed detection system. The angular resolution is estimated to about $\pm 1.5°$, while the zero angle uncertainty is better than $\pm 0.25°$ regarding the alignment and center precision of the entire system. The distance from the last electrode of the electron gun to the scattering centre (gas needle) is 30 mm, while the interaction volume is about 3 mm above the gas needle. The aspect ratio of the effusive beam capillary is 0.0125 with a length of 40 mm. The detection system consist of four electrode lens at the entrance of a double cylindrical mirror analyser (DCMA), three electrode lens at its exit and PHOTONIS X810BL channeltron enclosed in a shielded case. The first electrode of a four electrode lens is positioned 25 mm from the gas needle. Its function is to focus the scattered electrons and to apply the retarding potential such that electrons always have a fixed energy when entering DCMA. Therefore, DCMA is operated in a constant pass energy mode with an energy resolution down to about 0.4 eV.

2.2 Measurement procedure

DCS data as function of scattering angle, DCS (θ), is obtained by measuring the signal and background for each angle point. The signal measurement is performed first and is followed by background measurement, which involves the introduction of a target gas into the chamber from the side leak, whilst the signal is measured for target gas diverted through the gas needle. These two measurements were performed at least three times for each electron energy of interest. Subtracting the background from signal yields three corrected measurements which were weighted and averaged. For each electron energy, the analyser was set to allow the electrons corresponding to the elastic peak to pass through. Accordingly, the electron gun and two lenses before and after the analyser were readjusted for optimal signal and to compensate for the transmission functions.

DCS data as a function of electron energy, DCS (E_o), is obtained by fixing the angle and measuring the count for each energy point for at least three times. Prior to this measurement, the electron current in a Faraday cup as a function of electron energy was recorded, even though the electron gun was refocused. The transmission of the analyser system as a function of electron energy has been obtained from a simulation in SIMION8 [26], where optimal lens potentials were determined. These potentials were then used for the measurements and the obtained data was normalized to the simulated transmission. Additional normalization was performed to compensate for the small change in the gas needle pressure over time and measured electron current.

The relative flow measurements were taken for the needle pressure of about 0.373 mbar for Argon (target gas) and about 0.133 mbar for Helium (buffer gas). The ultimate base pressure in the experiment was about 5×10^{-7} mbar, while working pressure when both gasses were introduced in the chamber was in the order of 5×10^{-6} mbar. Each relative flow measurement was performed two times and the average values were taken for the normalization to absolute scale.

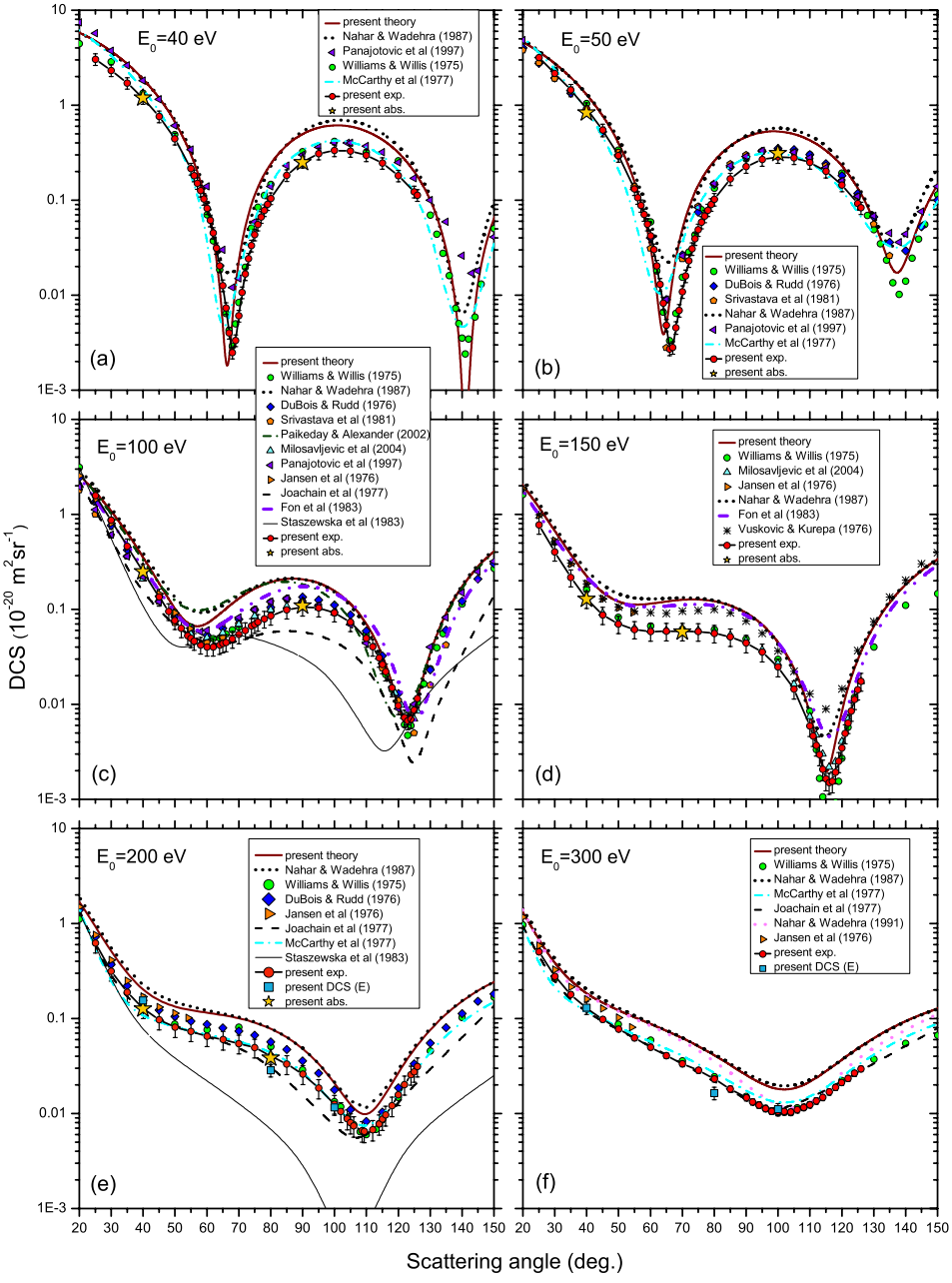

Fig. 1. Angular behaviour of differential cross section for elastic scattering of electrons on argon. The present experimental and theoretical data are compared with the selected set of previous results. The data symbols used correspond to: (red circles), present experiment; (yellow stars), present absolute data from relative flow; (dark cyan squares), present DCS (E); (dark red full line), present theory; (green circles), Williams and Willis [30]; (orange right triangles), Jansen et al. [31]; (asterisk); Vušković and Kurepa [32]; (blue diamond), DuBois and Rudd [33]; (dashed line), Joachain et al. [34]; (cyan dash dot line), McCarthy et al. [35]; (orange pentagons), Srivastava et al. [36]; (violet dash dot line), Fon et al. [37]; (thin line), Staszewska et al. [38]; (dotted line), Nahar and Wadehra [39]; (magenta short dash line), Nahar and Wadehra [42]; (violet left triangle), Panajotović et al. [44]; (olive dash dot line), Paikeday and Alexander [12]; (cyan up triangles), Milosavljević et al. [17].

2.3 Normalization and experimental uncertainties

The relative DCS data is made absolute by using the relative flow technique with Helium as a reference gas. Data for Helium was taken from Register et al. [27] and both DCS (θ) and DCS (E_o) were measured at least three times and the weighted average as well as weighted uncertainties were calculated. To this statistical uncertainty, the instrumental uncertainties (effective path length correction, uncertainty in energy and angular scale) and the uncertainty from a normalization originating from the relative flow measurements and Helium data, specified by the authors, was added. The total uncertainties vary with impact electron energy and span from 14% at the lowest up to 22% for the highest impact energy.

Table 2. Experimental and theoretical DCS for elastic cross section for argon atom used for a comparison with present results.

Author	Type of experiment/ theoretical approach	Energy range (eV)	Angular range (°)
Williams and Willis [30]	Modulated crossed beam	20–400	20–150
Jansen et al. [31]	Gas cell	100–3000	5–55
Vušković and Kurepa [32]	Gas cell	60–150	5–150
DuBois and Rudd [33]	Gas cell	20–800	2–150
Joachain et al. [34]	Optical potential	100–800	
McCarthy et al. [35]	Optical potential	20–3000	
Srivastava et al. [36]	Crossed beams (RFM/He)	3–100	20–135
Fon et al. [37]	R-matrix	3–150	
Staszewska et al. [38]	Quasifree-scattering model/ optical-model potential (SEPa)	30–3000	
Nahar and Wadehra [39]	Model potential	3–300	
Salvat et al. [40]	Semiphenomenological approach	100–5000	
Bartschat et al. [41]	Optical potential method	15–100	
Nahar and Wadehra [42]	Relativistic Dirac equation	3–300	
Cvejanović and Crowe [43]	Crossed beams	20.4–110	40–120
Panajotović et al. [44]	Crossed beams	10.3–100.3	20–150

RFM/gas – relative flow method with gas used as a reference; SEP – static, exchange, polarisation, absorption potential.

2.4 Calculations

The partial expansion method was used to describe the differential and total cross sections for elastic scattering. The relativistic differential cross section per unit solid angle is given by sum of squares of the direct $f(\theta)$ and spin-flip $g(\theta)$ scattering amplitudes:

$$\frac{d\sigma_e}{d\theta} = |f(\theta)|^2 + |g(\theta)|^2, \quad (1)$$

where θ denotes the scattering angle $f(\theta) = \sum_{l=0}^{\infty} F_l P_l(\cos(\theta))$, $g(\theta) = \sum_{l=0}^{\infty} G_l P_l^1(\cos(\theta))$, $P_l(\cos(\theta))$ are the Legendre polynomials, $P_l^1(\cos(\theta))$ are the associated Legendre functions. F_l and G_l can be calculated as follows:

$$F_l = \frac{1}{2ik}\left\{(l+1)\left[\exp\left(2i\delta_{l+}\right) - 1\right] + l\left[\exp\left(-2i\delta_{l-}\right) - 1\right]\right\}$$

$$G_l = \frac{1}{2ik}\left[\exp\left(2i\delta_{l-}\right) - \exp\left(-2i\delta_{l+}\right)\right],$$

where δ_{l+}, δ_{l-} are the phase shift of the order l, and k is the momentum of the projectile electron. Details of the calculations can be found in reference [29]. The total elastic cross section, σT, can be obtained after integration over the all possible scattering angles as:

$$\sigma_T = 2\pi \int_0^{\pi} \frac{d\sigma_e(E_o, \theta)}{d\Omega} \sin\theta \, d\theta. \quad (2)$$

3 Results and discussion

3.1 Angular behaviour of differential cross sections, DCS (θ)

Differential cross sections for electron elastic scattering by argon atom, DCS (θ), at impact energies of 40, 50, 100, 150, 200 and 300 eV are shown in Figure 1. The present experimental results are obtained from three separate sets of measurements: the direct angular distribution measurements over whole accessible angular range; data points at fixed angles derived from relative flow measurements with helium as a reference gas; and the direct measurements of energy dependence at fixed scattering angle. The first and third sets give the relative values, while the second set gives the absolute values. Relative sets are made absolute by fitting the curves to absolute data points by the least squares method. Present experimental and theoretical DCS are compared with other data listed in Table 2. Experimental values of DCS are tabulated in Table 3 with the quoted level of uncertainties.

The differential cross section at 40 eV exhibits two pronounced minima, at 68° and 142°. The excellent agreement between present measurements and former absolute measurements of Williams and Willis [30] is found. The value of the DCS at the first minimum is $(2.50 \pm 0.15) \times 10^{-23}$ m^2/sr and is as low as reported in [30]. The position of the minimum also agrees with the measurements of Panajotović et al. [44], but their minimum is less pronounced. The difference could be due to the proximity of the critical point in argon (around 41.30 ± 0.02 eV; $68.5° \pm 0.3°$ [44]), although even at the critical point, their minimal value is only $(6.1 \pm 1.3) \times 10^{-23}$ m^2/sr. This can indicate the importance of subtraction of the residual background gas obtained by diverting gas through a side leak, as explained in Section 2.2.

The present calculations have the best agreement with the calculations of Bartschat et al. [41] in both absolute values and positions and depth of minima. Calculated DCS first minimum is almost of the same absolute value, just shifted to lower scattering angle of 66.4° compared to the present measurements. The calculated values at smaller scattering angles are higher than the experimental results but agree with previous measurements in [44]. The

Table 3. Experimental DCS for elastic cross section for argon in units of 10^{-20} m^2/sr with the relative uncertainties indicated for each impact energy.

Angle (°)	10^{-20} $m^2\,sr^{-1}$					
	40 eV	50 eV	100 eV	150 eV	200 eV	300 eV
25	3.051	3.172	1.57	0.7762	0.6212	0.504
30	2.328	2.17	0.869	0.4039	0.316	0.277
35	1.711	1.442	0.461	0.2168	0.1888	0.1794
40	1.185	0.919	0.248	0.1289	0.1273	0.128
45	0.762	0.5475	0.135	0.0872	0.0972	0.098
48			0.0952			
50	0.444	0.2956	0.0765	0.07	0.081	0.0776
52			0.063			
54			0.053			
55	0.215	0.1314	0.0495	0.0615	0.073	0.0625
56	0.182	0.1067	0.0462			
57	0.151	0.0878				
58	0.126	0.0705	0.0422			
59	0.103	0.0558				
60	0.0820	0.0421	0.0401	0.0585	0.0649	0.0501
61	0.0612	0.0301				
62	0.0452	0.0202	0.0402			
63	0.0313	0.0130				
64	0.0204	0.0083	0.042			
65	0.0126	0.0048	0.0436	0.0588	0.0599	0.0406
66	0.0073	0.0027	0.0449			
67	0.004	0.0028				
68	0.0025	0.0046	0.0489			
69	0.0034	0.0069				
70	0.0061	0.0109	0.0543	0.0588	0.0545	0.0334
71	0.0107	0.0159				
72	0.0166	0.0231	0.0601			
73	0.0242	0.0309				
74	0.0332	0.0393	0.0666			
75	0.0435	0.0488	0.0699	0.0583	0.0495	0.0285
76	0.0554	0.0586	0.0733			
77	0.0663	0.0682				
78	0.0782	0.0788	0.0792			
79	0.0908	0.0902				
80	0.105	0.1024	0.0855	0.0559	0.0404	0.0231
85	0.183	0.1672	0.0989	0.0515	0.0332	0.0181
90	0.253	0.2265	0.1059	0.0442	0.026	0.0146
92						0.0133
94						0.0123
95	0.309	0.2674	0.1036	0.0355	0.0186	
96						0.0113
98						0.0106
100	0.334	0.2863	0.092	0.0247	0.0126	0.0105
102					0.0105	0.0105
104					0.0088	0.0103
105	0.3295	0.2792	0.073	0.0145	0.008	
106					0.0074	0.011
108					0.0066	0.0116
110	0.297	0.249	0.0497	0.0059	0.0065	0.0124
111				0.0047		
112			0.0403	0.0037	0.0068	0.0136
113				0.003		
114			0.0308	0.0021	0.0078	0.0147
115	0.246	0.2018	0.0263	0.0016	0.0087	
116			0.0221	0.0015	0.0097	0.0168
117				0.0016		
118			0.015	0.0019	0.0121	0.0189
119				0.0025		

(continued...)

Table 3. *(continued...)*

Angle (°)	10^{-20} m^2 sr^{-1}					
	40 eV	50 eV	100 eV	150 eV	200 eV	300 eV
120	0.181	0.1446	0.0097	0.0035	0.0157	0.0212
121				0.005		
122			0.0073	0.0064	0.0202	0.0234
123			0.0067	0.0085		
124			0.007	0.0113	0.0257	0.0265
125	0.123	0.0927	0.0087	0.0142	0.0275	
126	0.113	0.083	0.0115	0.0175	0.0313	0.0295
Relative uncertainty (%)	14	15	20	20	21	22

local maximum around 100° is larger than other experimental values and calculations of McCarthy et al. [35] but it is close to the values of Nahar and Wadehra [39]. The second minimum is found at 141° and is much deeper than both calculated [35] and measured [30,44] values.

The present experimental DCS at 50 eV agrees perfectly with previous measurements [30,33,36,44] in the whole angular range. The position and the value of the first minimum at 67° is the same as in [30,36]. The second minimum is beyond the angular range of the present experiment. The calculated DCS at 50 eV matches the experimental values at smaller scattering angles but has the minimum at 64.1°. Again at local maximum, the DCS is larger and has the same value as in [39]. The positions of both minima are close to other calculations [35,39] but with smaller values.

There are many experiments and theories for 100 eV impact energy. All experiments have an excellent agreement, at local maximum of 90° with discrepancy within ±15%. The present calculated values agree with other calculations [12,37,39] except when compared to calculations by Joachain et al. [34] whose values are smaller in the whole angular range. The values of the calculations of [34] agree very well with the present measurements at the position of the first minimum. The present calculated values in the range of the second minimum strongly agree with the previously measured values in our laboratory by Milosavljević et al. [24].

There are two sets of previously measured data for 150 eV: Jansen et al. [31]; Vušković and Kurepa [32]; and Milosavljević et al. [24]; Williams and Willis [30]. The main distinction is in the values of the plateau at around 70° where the DCS has a flexing point (the first minimum became very shallow at this energy) and the DCS values of the first group are larger for 60% than the vales of the second group. Interestingly, the present calculated values and those in [39] are even larger (factor 2.14) and they better match the experiments of the first group [31,32] while the present experiment favors the second group of results [24,30]. At this impact energy the second minimum is within the accessible range of the present experiment and its position at 116° agrees well with [24,30] – the present calculation gives the position of 115.1°. Also, the values of present measurement and calculation agree very well – in contrast with previous calculations [37,39] where the shallower minimum was obtained.

At 200 eV, the shapes and the values of all experiments and calculations, except for calculations by Staszewska et al. [38] and Salvat et al. [40], are virtually the same and all DCSs lay within ±40% band around mean value. For both impact energies of 200 eV and 300 eV, the present calculations agree excellently with calculations of [39] in the full angular range, but they exceed the experimental values. Inclusion of imaginary part in the Dirac potential brought the calculations at 300 eV in [42] in agreement with experimental values in the region of the minimum when compared to the previous nonrelativistic calculations of the same authors [39]. Still, these relativistic calculations are much higher than experiments at middle angles (50°–80°) where they agree with the present calculations based on the Mott's cross sections.

3.2 Energy dependence of differential cross sections, DCS (E_o)

Differential cross sections dependence on the impact energy, DCS (E_o), at fixed scattering angles of 40°, 80° and 100° are presented in Figures 2a–2c, respectively. Two sets of present experimental points are shown: the direct energy scans corrected for the analyser transmission and primary beam current and the single data points of relative flow measurements where absolute scale was established by helium data comparison [27]. Present experimental data are compared with other direct energy scan measurements of Cvejanović and Crowe [43]. The excellent agreement is found for all three scattering angles at the overlapping energies (40–100 eV). It is worth noting that the absolute scale of these two measurements have been established in different way, in [43] data have been normalized to previous absolute data of Srivastava et al. [36] while the present data were normalized on reference helium gas data obtained in a separate set of present measurements.

Present calculations generally give larger cross sections than experimental measurements, particularly at 100° and energies above 100 eV. This could be due to the sensitivity of DCS (E_o) at this angle because of the proximity of the

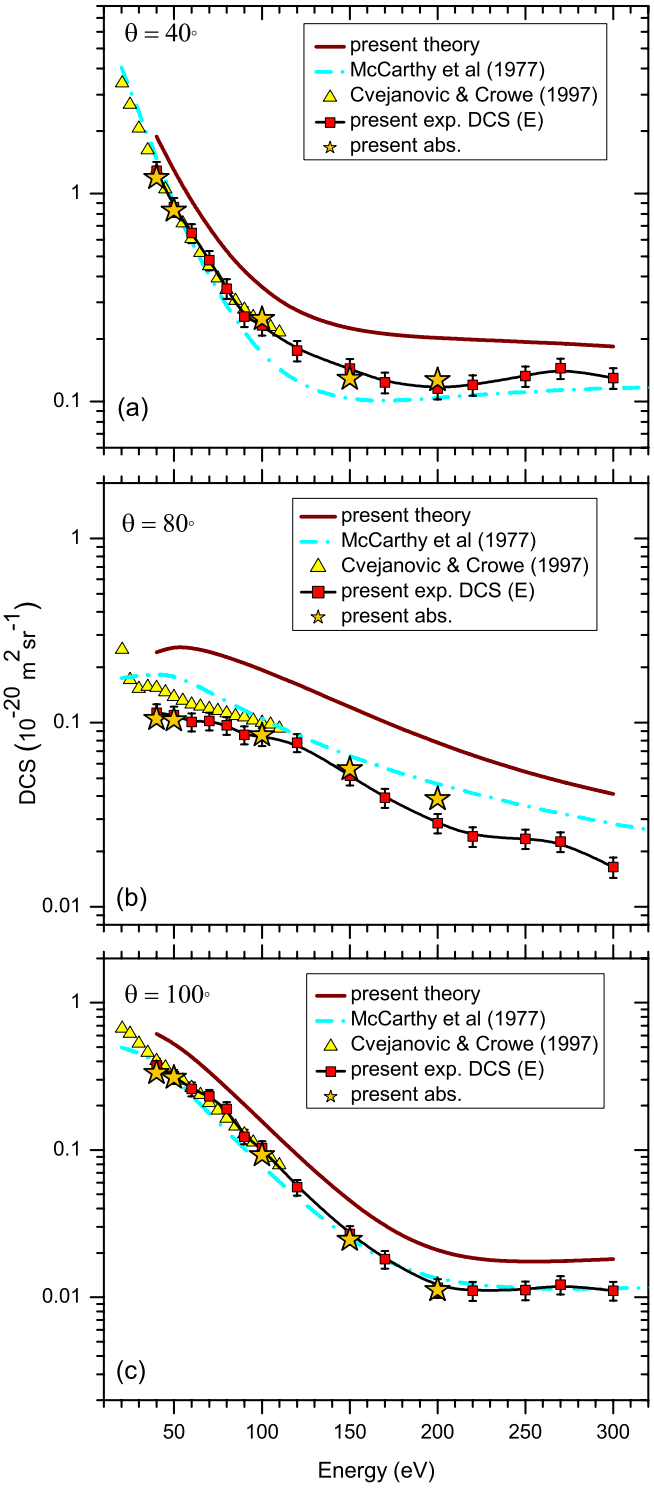

Fig. 2. Comparison of the present energy dependence of the differential cross section for elastic scattering of electrons on argon at a scattering angles of: (a) 40°; (b) 80° and (c) 100° with previous experimental and theoretical results. Error bars corresponding to the quoted uncertainties are presented on present data points. The data symbols used correspond to: (red squares), present experiment DCS (E); (yellow stars), present absolute data from relative flow; (dark red full line), present theory; (cyan dash dot line), McCarthy et al. [35]; (yellow up triangles), Cvejanović and Crowe [43].

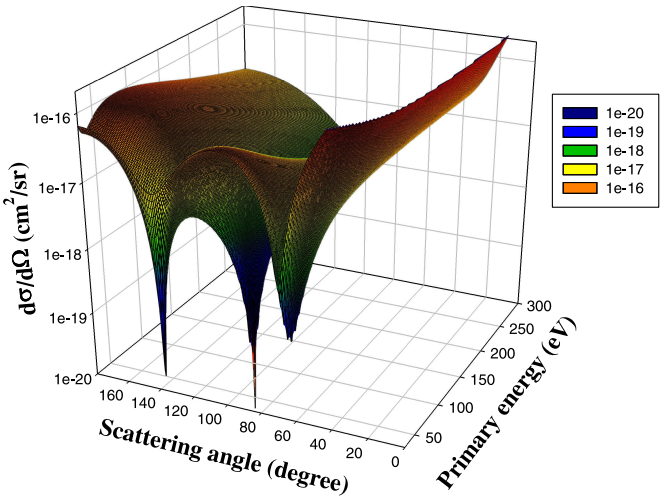

Fig. 3. Calculated differential cross section surface for electron elastic scattering by argon in the energy range from 40 to 300 eV. The full data set is given in the Supplementary material.

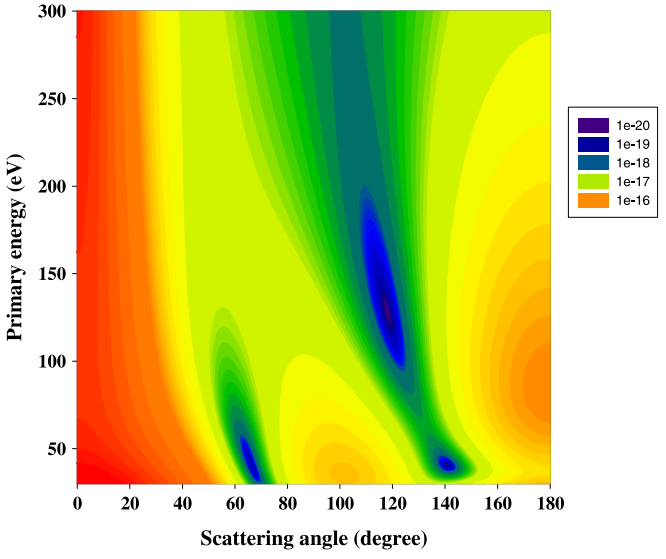

Fig. 4. Projection of 3D surface of elastic DCS for argon on the plane scattering angle – primary electron energy.

minimum point. The calculations of McCarthy et al. [35] agree better with the present measurements.

3.3 Differential cross section surface, DCS (E_o,θ), minima positions and critical points

It has been previously pointed out by Milosavljević et al. [25] that is of great importance to perform measurements of differential cross sections as independent energy and angular scans. This results in the whole DCS (E_o,θ) surface being crossed-checked so that experimental errors could be avoided. These errors include energy transmissions of electron gun and analyser as well as misalignment

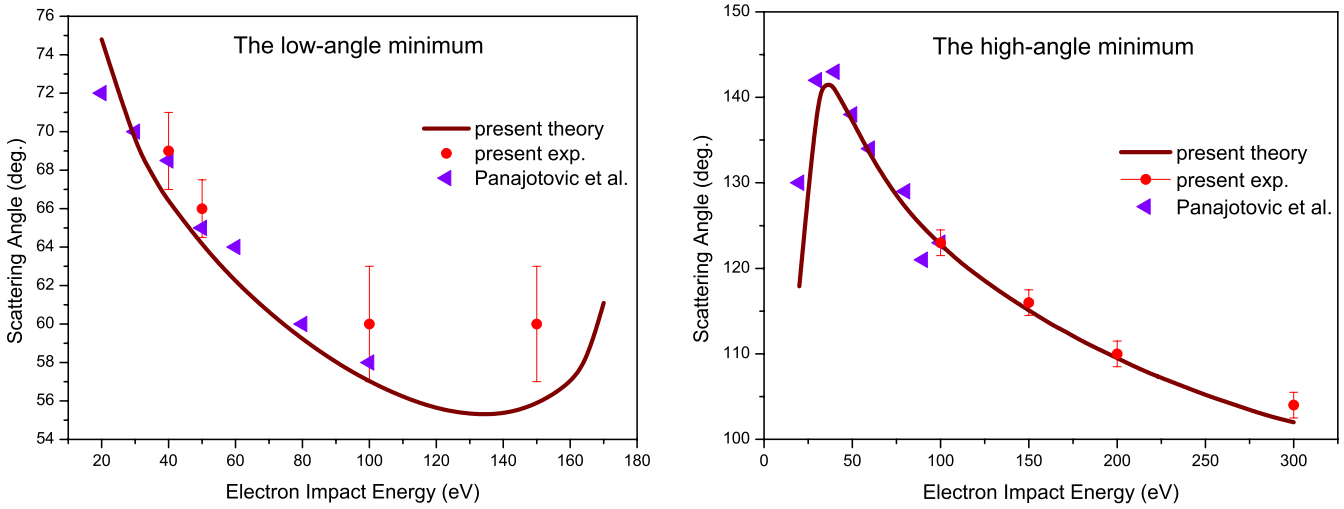

Fig. 5. Positions of low-angle and high-angle minima versus electron impact energy. The data symbols used correspond to: (red circles), present experiment; (dark red full line), present theory; (violet left triangle), Panajotović et al. [44].

of three axis, the primary beam axis, the target beam axis and the analyser axis.

In order to obtain the full 3D plot of the differential cross section surface it is necessary to calculate or measure differential cross sections on a rather dense grid, hence the present calculations being performed in angular steps of 0.1° and energy steps of 0.1 eV. The obtained surface is presented in Figure 3.

In the energy range from 30 to 300 eV differential cross sections show three critical points – places in 3D surface where DCS reach a minimum. The determination of these points is important as the critical minima represent a sensitive test of the interplay between direct and exchange potentials in electron interaction with the target atom. In the vicinity of critical minima the scattered electrons exhibit the largest change of the polarisation. Finding the pairs of incident energy and scattering angle where DCS minima attain their smallest values is a tedious task in experimental study and in the same time represents a crucial test of applied approximations in calculations. A detailed analysis of critical points in argon has been done by Lukas [45] and more recently by Sienkiewicz et al. [46] using ab initio relativistic calculations. Experimental values found in [44] are (37.30 ± 0.02 eV, $143.5° \pm 0.3°$) and at (41.30 ± 0.02 eV, $68.5° \pm 0.3°$) and the third minimum in [24] to be at (129.4 ± 0.5 eV, $119.4° \pm 0.5°$). The present calculations also reveal the positions of three critical points clearly shown in Figure 4. Positions of critical minima in the present calculations are found to be: (41 eV, 141°), (41 eV, 66°) and (128 eV, 118°). It could be compared with the previous calculations in [46] (39.3 eV, 68.0°), (39.5 eV, 141.0°) and with calculations presented in [24] (118.0 eV, 118.9°).

The positions of low-angle and high-angle minima could also be traced with the change of impact electron energy. The calculated values for the first and the second minimum with experimental points at fixed energies are shown in Figures 5a and 5b, respectively.

4 Conclusions

Absolute measured and calculated differential cross sections for electron elastic scattering by argon atom are presented. Measurements have been taken in the energy range from 40 eV to 300 eV and for scattering angles from 25° to 126°, with smaller steps around minima positions. Calculations were performed using relativistic expression of a partial wave expansion method for electron–atom scattering using the Mott's cross sections. Calculations have been performed in the energy range from 30 eV and for the full range of scattering angles, with the dense grid around critical points and positions of minima. The achieved agreement with other experiments and calculations is moderate and depends on impact energy and angular range. This indicates that advances in both experimental methods and applied theoretical approximations are required, despite the topic having been studied for a long time. It should not be forgotten that the differential cross sections and their absolute values are the crucial quantities in our quantum mechanical description of electron–atom interactions. We have achieved one of the goals, i.e. to provide a consistent set of data in this energy range that can be used in further experiments with other more complex targets, like biomolecules. All presented data, will be also maintained in the Belgrade electron/atom (molecule) database (BEAMDB) (http://servo.aob.rs/emol) [47].

We acknowledge the contribution of Drs. I. Čadež, S. Mandžukov and A.R. Milosavljević to the setting of the electron spectrometer UGRA at the Laboratory for Atomic Collision Processes, IPB. We are thankful to Dr. Andrew Cheesman for the critical reading of the manuscript. This work has been supported by the MESTD of the Republic of Serbia Grant #OI 171020. BPM acknowledges the grant of VAMDC consortium under open call 2016-1, project funded under the "Combination of Collaborative Projects and Coordination and

Support Actions" Funding Scheme of The Seventh Framework Program.

Author contribution statement

MLjR and JBM performed the experimental measurements, TK made all calculations, BPM, MLjR and TK wrote the manuscript. All authors discussed the results and commented on the manuscript.

References

1. N. Andersen, J.W. Gallagher, I.V. Hertel, Phys. Rep. **165**, 1 (1988)
2. K. Bartschat, J. Tennyson, O. Zatsarinny, Plasma Process. Polym. **14**, 1600093 (2017)
3. J. Tennyson, S. Rahimi, C. Hill, L. Tse, A. Vibhakar, D. Akello-Egwel, D.B. Brown, A. Dzarasova, J.R. Hamilton, D. Jaksch, S. Mohr, K. Wren-Little, J. Bruckmeier, A. Agarwal, K. Bartschat, A. Bogaerts, J.-P. Booth, M.J. Goeckner, K. Hassouni, Y. Itikawa, B.J. Braams, E. Krishnakumar, A. Laricchiuta, N.J. Mason, S. Pandey, Z.Lj. Petrović, Y.-K. Pu, A. Ranjan, S. Rauf, J. Schulze, M.M. Turner, P. Ventzek, J.C. Whitehead, J.-S. Yoon, Plasma Sour. Sci. Technol. **26**, 055014 (2017)
4. F. Salvat, A. Jablonski, C.J. Powell, A.Y. Lee, NIST Electron Elastic-Scattering Cross-Section Database Version 4.0, NIST Standard Reference Database Number 64, National Institute of Standards and Technology, Gaithersburg, MD, 20899 (2016), https://srdata.nist.gov/srd64/ (retrieved 7/07/2017)
5. J.B. Maljković, A.R. Milosavljević, F. Blanco, D. Šević, G. García, B.P. Marinković, Phys. Rev. A **79**, 052706 (2009)
6. E.C. Bullard, H.S.W. Massey, Proc. R. Soc. A **130**, 579 (1931)
7. F.L. Arnot, Proc. R. Soc. A **133**, 615 (1931)
8. A. Zecca, G.P. Karwasz, R.S. Brusa, R. Nuovo Cimento **19**, 1 (1996)
9. G.G. Raju, IEEE Trans. Dielectr. Electr. Insul. **11**, 649 (2004)
10. E. Gargioni, B. Grosswendt, Rev. Mod. Phys. **80**, 451 (2008)
11. L.C. Pitchford, L.L. Alves, K. Bartschat, S.F. Biagi, M.C. Bordage, A.V. Phelps, C.M. Ferreira, G.J.M. Hagelaar, W.L. Morgan, S. Pancheshnyi, J. Phys. B **46**, 33009 (2013)
12. J.M. Paikeday, J. Alexander, Int. J. Quant. Chem. **90**, 778 (2002)
13. V. Kelemen, Z. Techn. Phys. **72**, 13 (2002)
14. F. Blanco, G. García, Phys. Lett. A **295**, 178 (2002)
15. F. Blanco, G. García, Phys. Rev. A **67**, 022701 (2003)
16. F. Salvat, Phys. Rev. A **68**, 012708 (2003)
17. A.R. Milosavljević, S. Telega, D. Šević, J.E. Sienkiewicz, B.P. Marinković, Rad. Phys. Chem. **70**, 669 (2004)
18. S.Y. Yousif Al-Mulla, J. Phys. B **37**, 305 (2004)
19. A. Jablonski, F. Salvat, C.J. Powell, J. Electron Spectr. Rel. Phenom. **137–140**, 299 (2004)
20. M. Adibzadeh, C.E. Theodosiou, At. Data Nucl. Data Tabl. **91**, 8 (2005)
21. L.R. Hargreaves, J.R. Francis-Staite, T.M. Maddern, M.J. Brunger, S.J. Buckman, Meas. Sci. Technol. **18**, 2783 (2007)
22. R.P. McEachran, A.D. Stauffer, J. Phys. B **42**, 075202 (2009)
23. D. Bote, F. Salvat, A. Jablonski, C.J. Powell, J. Electron. Spectrosc. Relat. Phenom. **175**, 41 (2009)
24. A.R. Milosavljević, S. Telega, D. Šević, J.E. Sienkiewicz, B.P. Marinković, Eur. Phys. J. D. **29**, 329 (2004)
25. A.R. Milosavljević, S. Madžunkov, D. Šević, I. Čadež, B.P. Marinković, J. Phys. B **39**, 609 (2006)
26. SIMION8 http://simion.com/
27. D.F. Register, S. Trajmar, S.K. Srivastava, Phys. Rev. A **21**, 1134 (1980)
28. R.T. Brinkmann, S. Trajmar, J. Phys. E **14**, 245 (1981)
29. F. Salvat, R. Mayol, Comput. Phys. Commun. **74**, 358 (1993)
30. J.F. Williams, B.A. Willis, J. Phys. B **8**, 1670 (1975)
31. R.H.J. Jansen, F.J. de Heer, H.J. Luyken, B. van Wingerden, H.J. Blaauw, J. Phys. B **9**, 185 (1976)
32. L. Vušković, M.V. Kurepa, J. Phys. B **9**, 837 (1976)
33. R.D. DuBois, M.E. Rudd, J. Phys. B **9**, 2657 (1976)
34. C.J. Joachain, R. Vanderpoorten, K.H. Winters, F.W. Byron Jr, J. Phys. B **10**, 227 (1977)
35. I.E. McCarthy, C.J. Noble, B.A. Phillips, A.D. Turnbull, Phys Rev A **15**, 2173 (1977)
36. S.K. Srivastava, H. Tanaka, A. Chutjian, S. Trajmar, Phys. Rev. A **23**, 2156 (1981)
37. W.C. Fon, K.A. Berrington, P.G. Burke, A. Hibbert, J. Phys. B **16**, 307 (1983)
38. G. Staszewska, D.W. Schwenke, D.G. Truhlar, Int. J. Quant. Chem. **17**, 163 (1983)
39. S.N. Nahar, J.M. Wadehra, Phys. Rev. A **35**, 2051 (1987)
40. F. Salvat, R. Mayol, J.D. Martinez, J. Phys. B **20**, 6597 (1987)
41. K. Bartschat, R.P. McEachran, A.D. Stauffer, J. Phys. B **21**, 2789 (1988)
42. S.N. Nahar, J.M. Wadehra, Phys. Rev. A **43**, 1275 (1991)
43. D. Cvejanović, A. Crowe, J. Phys. B **30**, 2873 (1997)
44. R. Panajotović, D.M. Filipović, B.P. Marinković, V. Pejèev, M. Kurepa, L. Vušković, J. Phys. B **30**, 5875 (1997)
45. C.B. Lukas, J. Phys. B **12**, 1549 (1979)
46. J.E. Sienkiewicz, S. Telega, P. Syty, S. Fritzsche, Rad. Phys. Chem. **68**, 285 (2003)
47. B.P. Marinković, D. Jevremović, V.A. Srećković, V. Vujèić, Lj.M. Ignjatović, M.S. Dimitrijević, N.J. Mason, Eur. Phys. J. D **71**, 158 (2017)

Electron collisions with cyanoacetylene HC_3N: Vibrational excitation and dissociative electron attachment

M. Ranković,[1] P. Nag,[1] M. Zawadzki,[1,2] L. Ballauf,[3] J. Žabka,[1] M. Polášek,[1] J. Kočišek,[1] and J. Fedor[1,*]

[1]*J. Heyrovský Institute of Physical Chemistry, Czech Academy of Sciences, Dolejškova 3, 18223 Prague, Czech Republic*

[2]*Department of Atomic, Molecular, and Optical Physics, Faculty of Applied Physics and Mathematics, Gdańsk University of Technology, ul. G. Narutowicza 11/12, 80-233 Gdańsk, Poland*

[3]*Institute of Ion Physics and Applied Physics, University of Innsbruck, Technikerstrasse 25, A-6020 Innsbruck, Austria*

(Received 29 September 2018; published 29 November 2018)

We experimentally probe electron collisions with HC_3N in the energy range from 0 to 10 eV with the focus on vibrational excitation and dissociative electron attachment. The vibrational excitation cross sections show a number of resonances which are mode specific: the two dominant π^* resonances are visible in the excitation of all the vibrational modes; however, broad σ^* resonances are visible only in certain bond-stretching vibrational modes. The lower π^* resonance shows a pronounced boomerang structure. Since it overlaps with the threshold peak originating from a long-range electron-molecule interaction, the interference pattern is rather unusual. Somewhat surprisingly, the boomerang structure is visible also in the elastic scattering cross section. The dissociative electron attachment cross sections agree qualitatively with the data of Gilmore and Field [J. Phys. B **48**, 035201 (2015)]; however, approximately a factor of two difference is found in the absolute values.

DOI: 10.1103/PhysRevA.98.052708

I. INTRODUCTION

Cyanoacetylene, HC_3N, has been attracting attention due to its abundance in a number of extraterrestrial environments. Among these are interstellar clouds [1], circumstellar envelopes [2], comets [3], and the atmosphere of Saturn's moon Titan [4,5]. The particular interest in the electron collisions with this molecule stems primarily from two sources. The first is the presence of the carbon-chain molecular anions such as C_8H^-, C_6H^-, C_4H^-, and C_3N^- in the interstellar medium [6–8]. The second is the 2007 observation of the Cassini mission [5] that the upper atmosphere of Titan contains anions with mass/charge ratio of up to $\approx$10 000. Extensive investigations have shown that depending on the altitude, the dominant anion species in Titan's atmosphere are either CN^- and C_3N^-, or C_nH^-, with $n = 2, 4, 6$ [9].

The dissociative electron attachment (DEA) to neutral polyynes (HC_nH or HC_nN) as a possible dominant source of these anions was ruled out early. The DEA studies on C_2H_2 [10], C_4H_2 [11], and HC_3N [12] have shown that while the cross sections are considerably high, the fragmentation channels are endothermic. The energetic thresholds for the production of fragment anions lie in all these cases above 1 eV, and are thus inaccessible for thermal electrons. Nonetheless, the formation of transient anions—resonances—leads not only to DEA but, due to competing electron autodetachment channels, also to vibrational excitation of the molecules. This influences both the vibrational energy distribution of the gas and the electron energy distribution function in the above-mentioned astrochemical environments.

The only electron collision experiments with HC_3N to our knowledge are the early positive and negative ionization studies of Dibeler [13] and Harland [14] and the DEA experiments of the Field group at Queen's University Belfast [12,15]. The latter group has initially reported a yield of individual fragment ions [12] and later recalibrated these yields using signals from background water vapor to determine the absolute partial cross section values [15]. Theoretically, the resonances in cyanoacetylene were explored by Sommerfeld and Knecht [16] with the complex absorbing potential approach, by Sebastianelli and Gianturco [17] with the single-center expansion scattering calculations, and by Kaur *et al.* [18] by *R*-matrix theory. Orel and Chourou [19] performed multidimensional nuclear dynamics calculations on the resonant states of HC_3N.

In the present paper we probe the resonant states in cyanoacetylene by means of electron energy loss spectroscopy. We report the absolute differential elastic and vibrationally inelastic cross sections at 135° scattering angle. These measurements bring detailed information about the resonant electronic states and the dynamics of the nuclear motion on their potential energy surfaces. The observed selectivity in the excitation of certain vibrational modes facilitates the assignment of the involved resonances. We also report direct absolute measurement of the DEA cross section.

II. EXPERIMENT

Three electron-collision setups were used for the present experiments, recently transferred to Prague from the University of Fribourg.

The electron scattering experiments were performed on the electrostatic spectrometer with a hemispherical electron

*juraj.fedor@jh-inst.cas.cz

monochromator and analyzer [20,21]. The electrons scattered on the effusive beam of the pure sample gas were analyzed at the fixed scattering angle of 135°. The energy of the incident beam was calibrated on the 19.365 eV 2^2S resonance in helium. Electron-energy resolution was 17 meV. The absolute elastic scattering cross section was calibrated against the one of helium using a relative flow method. The detailed error budget of the cross section calibration is presented in Ref. [22]. The uncertainty of the elastic cross section is ±15%. The vibrationally inelastic cross sections are normalized with respect to the elastic peak. Since the individual vibrational modes are not fully resolved, the individual vibrational excitation cross sections are much less precise and should be considered as indicative values, which describe the intensity of the inelastic signal at a given energy loss.

The absolute dissociative electron attachment cross sections were measured on the absolute DEA spectrometer with a time-of-flight mass analyzer [10,11]. A pulsed magnetically collimated electron beam, produced in a trochoidal electron monochromator, crosses a collision cell filled with a stagnant gas and the anions produced are extracted towards a short (15 cm) time-of-flight mass analyzer placed perpendicularly to the electron beam. For the cross section calibration, we have used the 4.4 eV band in the O^- production from CO_2 with the energy-integrated cross section of 13.3 eV pm^2. The same band is used for the electron energy scale calibration and for the determination of the electron beam resolution which was ≈ 250 meV. The uncertainty of the absolute DEA calibration is ±20% which includes both the systematic and statistical errors.

The shape of the DEA bands was additionally measured on the DEA spectrometer with a trochoidal monochromator and quadrupole mass filter [23–25]. Here, a continuous electron beam crosses the effusive molecular beam and the yield of a certain anion mass chosen by the quadrupole is monitored. Due to absence of pulsing, this spectrometer has a better electron energy resolution of approximately 100 meV. The final DEA cross sections are thus obtained by scaling the high-resolution DEA yields from the quadrupole setup to the absolute values from the time-of-flight setup using the invariance of the energy-integrated cross sections [26,27].

The HC_3N sample was synthesized by the dehydration of the propiolamide, prepared by the reaction of methylpropiolate and ammonia, the method introduced by Miller and Lemmon [28]. During the measurements, the sample (confined in a lecture bottle) was kept at a temperature of 7 °C.

III. RESULTS AND DISCUSSION

A. Electronic structure and resonances

All three scattering processes probed in this work are strongly influenced by the formation of resonances—temporary anion states—in the electron molecule collision. We thus first review the available information on these states, which will facilitate the interpretation of the results and further discussion.

Since the resonant states are embedded in continuum, their proper characterization requires advanced scattering calculations or modifications of the traditional quantum chemistry approaches. However, a useful insight can be gained from the basic electronic structure of the target molecule and the use of scaling formulas. In a simplified picture a shape resonance can be imagined as trapping of the incident electron in an unoccupied molecular orbital of the target molecule. Cyanoacetylene is a linear polyyne with two triple bonds. The lowest four unoccupied orbitals, shown in Table I, have antibonding character along some or all bonds. For the purpose of this paper we denote them π_1^*, π_2^* and σ_1^*, σ_2^*. Chen and Gallup [29] developed an empirical scaling based on the Koopmans theorem, relating the orbital energies (E_{MO}) and the corresponding resonance energies [$E_{\text{res}} = (E_{MO} - 2.33\ \text{eV})/1.31$]. Values obtained using this formula are listed

TABLE I. Unoccupied molecular orbitals of neutral HC_3N and corresponding resonance energies formed by capture of an electron into the orbital (in eV).

Symmetry	MO isosurface	Present scaling	CAP [16]	Scattering calc. [17]	*R* matrix [18]
π_1^*	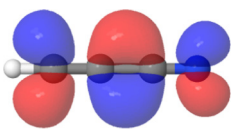	0.48	0.7	1.94	1.51
σ_1^*	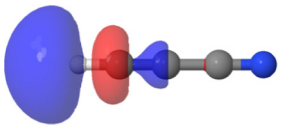	3.09			
π_2^*	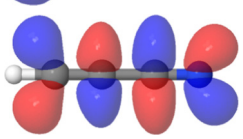	5.50	6.2	8.19	
σ_2^*	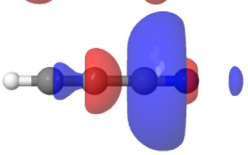	5.39		9.24	8.0

in Table I in the "present scaling" column. It should be noted that the sensitivity of such estimate of E_{res} to the choice of basis set and the scaling formula have been explored by Field and co-workers [12,30].

The resulting resonant energies can be considered only as indications; however, as can be seen in Table I they agree surprisingly well with the advanced theoretical approaches. The complex absorbing potential (CAP) method of Sommerfeld and Knecht predicted the π_1^* resonance at 0.7 eV (width 0.15 eV) and the π_2^* resonance at 6.2 eV (width 1.1 eV). The scattering calculations of Sebastianelli and Gianturco localized the π^* resonances at somewhat higher energies of 1.94 eV (width 0.15 eV) and 8.19 eV (width 0.76 eV) and the σ_2^* resonance at 9.23 eV (width 1.16 eV). The *R*-matrix calculations of Kaur *et al.* identified the π_1^* at 1.51 eV and σ_2^* at 8 eV. An alternative scaling formula developed recently by Field and co-workers especially for π^* states in conjugated systems predicts the two resonances at 0.5 and 5.1 eV.

Two notes should be added at this point. First, the figures in Table I are the isosurfaces of the molecular orbitals, i.e., unoccupied one-electron states. Sebastianelli and Gianturco [17] provided the graphical representations of the true one-electron scattering wave functions and they are very similar (basically indistinguishable by eye) to the present isosurfaces. This adds credit to the simplified picture of the temporary orbital occupation by the incoming electron. The nodal planes and electron densities of the unoccupied orbitals will be useful in interpreting the selectivity of vibrational excitation. The second note concerns the σ^* states. The corresponding resonances are expected to be very broad: their coupling with the barrierless *s*-wave autodetachment channel leads to their extremely short lifetimes. The fixed-nuclei scattering calculations, which localize the resonances from the variation of the eigenphase sum, have thus often difficulties in finding such broad resonances [31]: the eigenphase variation can be so weak that it is difficult to distinguish from the background scattering. This might be the case of the σ_1^* resonance, lying between the two π^* resonances, which was not reported in any of the scattering calculations. However, as will be shown below, this state is manifested in the vibrational excitation cross section of the C−H stretching mode.

B. Elastic scattering

Figure 1 shows the differential elastic electron scattering cross section at 135° scattering angle. The cross section sharply peaks towards 0 eV electron energy. This is caused by the dipole moment of HC_3N which is 3.72 D [32]. The elastic scattering cross sections in polar targets always reach high values, and in some cases even diverge, at very low energies [33]. It should be noted that the true height of the low-energy spike is of course not accessible by a cross beam experiment such as the present one, since the monochromator and the analyzer cannot reliably produce/analyze the electrons below some 30 meV kinetic energy.

Two interesting features can be observed in the cross section at higher energies. One is the shallow minimum around 5 eV. As shown in the next section, a broad π_2^* resonance dominates this region and the minimum is an imprint of this resonance in the elastic cross section. Since its formation leads

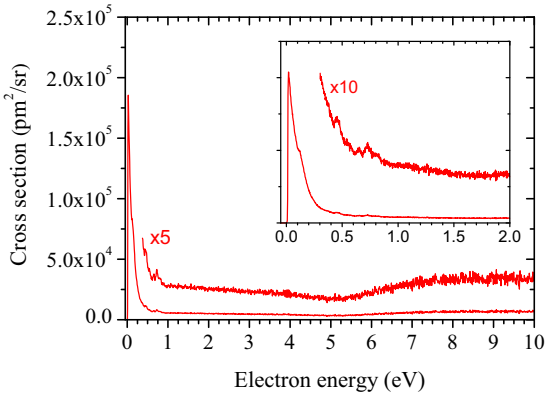

FIG. 1. Cross section for the elastic scattering on HC_3N at 135°. The inset shows horizontally magnified electron energy scale.

to increase in all vibrational excitation channels, the drop in the elastic channel is caused by the conservation of the probability flux. The second interesting feature in the elastic cross section is the oscillatory structure between 0.4 and 0.8 eV. It is clearly connected with the threshold peaks and the π_1^* resonance in the vibrational excitation cross sections in this energy range discussed below. Sebastianelli and Gianturco [17] and Kaur *et al.* [18] have seen the influence of the resonances in the elastic scattering (in computed integral cross sections). However, since these were fixed-nuclei calculations, which do not reflect the probability flux towards the nuclear motion, the resonances were manifested as peaks in the cross sections, not as the dips observed here.

C. Vibrational excitation

Figure 2 shows electron energy loss spectra recorded at two different electron incident energies. The energy loss spectra reflect which vibrational modes are excited upon the electron impact and their relative population with respect to the elastically scattered electrons with zero energy loss. The spectroscopic experimental vibrational energies from Ref. [34] are shown in Table II.

All three bending modes are excited to a certain extent. The softest vibration, the CCN bend (26 meV excitation energy), is visible as a shoulder of the elastic peak at both impact energies. The CCC bending vibration (62 meV) is not visible at 0.8 eV but present at 5.5 eV impact energy. The most prominent bending vibration is the CCH bend with an excitation energy of 82 meV, with at least one overtone excited at both incident energies (the possible $v = 2$ overtone peak overlaps with the C≡C stretching mode). The excitation of the stretching modes also shows certain selectivity: at both incident energies, the C−C stretch is excited only weakly and the other vibrations have varying strength. At 0.8 eV, the C≡N stretch (282 meV) progression dominates the spectrum, while at 5.5 eV the C−H stretch becomes the dominant stretching mode. An interesting peak occurs at 492 meV (unassigned in the figure), which has to originate from a combination vibration of C−H stretch and CCH bend ($\nu_1 + \nu_5$).

Figure 3 shows the excitation curves of the individual vibrations. Here, the energy difference between the monochromator and analyzer is kept constant and both are being

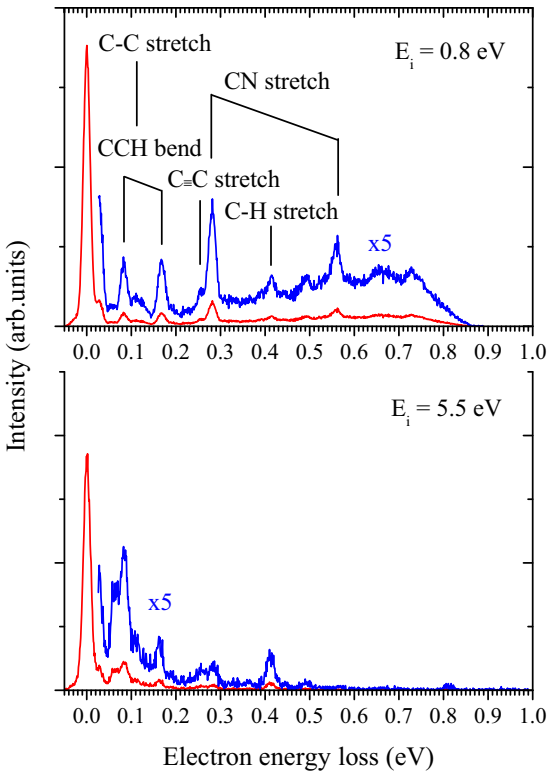

FIG. 2. Electron energy loss spectra of HC_3N at 135° recorded at incident energies of 0.8 eV (top panel) and 5.5 eV (bottom panel).

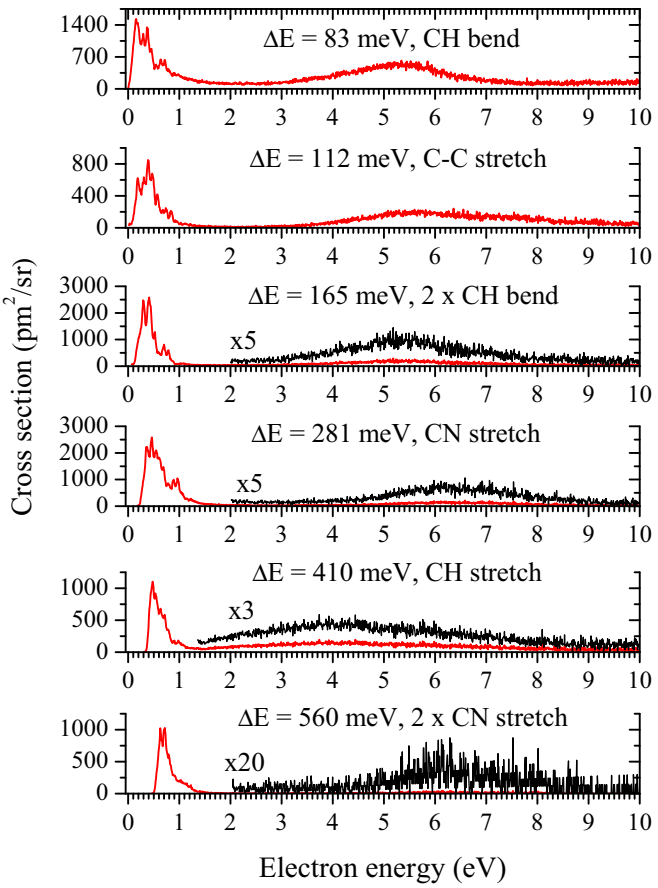

FIG. 3. The vibrational excitation cross sections for individual vibrations in HC_3N as functions of incident electron energy.

scanned. Such excitation curves are a sensitive probe for the formation of resonances: if a temporary anion is formed at a certain incident electron energy, the probability of energy transfer to nuclear motion (= vibrational excitation) strongly increases. The observed bands can be divided into two groups, the narrow ones at low energies, approximately below 1 eV, and much broader bands at higher energies, above 2 eV. The low-energy part of the spectra is separately shown in Fig. 4 and in the form of a two-dimensional spectrum in Fig. 5. The high-energy part (with the reduced number of channels) is shown rescaled in Fig. 6.

Let us first focus on the high-energy part. The dominant contribution to the excitation of all vibrations seems to originate from the formation of π_2^* resonance; however, clear differences in the excitation of individual modes are demonstrated in Fig. 6. Since the two σ^* resonances are dissociative along the molecular axis and will probably excite the bending vibrations only negligibly, we presume that the "true" shape of the π_2^* resonance is demonstrated by the CCH bend excitation curve (top panel of Fig. 6). This places the center of the π_2^* resonance at 5.3 eV.

TABLE II. Experimental vibrational frequencies of HC_3N from Ref. [34].

Type	Label	Energy (meV)
CCN bend	ν_7	28
CCC bend	ν_6	62
CCH bend	ν_5	82
C−C stretch	ν_4	109
C≡C stretch	ν_3	257
C≡N stretch	ν_2	282
C−H stretch	ν_1	412

The C−H stretch vibration has the maximum clearly shifted to lower energies. The σ_1^* orbital (Table I) has the largest coefficient on the corresponding carbon and hydrogen atoms and an antibonding character along this bond. We conclude that the C−H stretch vibration is the only one that is influenced by the formation of the broad σ_1^* resonance with the center around 4 eV.

The C≡N vibration excitation curve is shifted to higher energies when compared to the CCH bend. This is caused by the formation of the σ_2^* resonance with a strong antibonding character across the C≡N bond. This resonance is also visible in the excitation of the C−C stretch mode as the right shoulder superimposed on the dominant π_2^* resonance.

We now turn to the low-energy part of the vibrational excitation spectra shown in detail in Figs. 4 and 5. The excitation curves have peculiar shapes. This is caused by an interplay of two effects. The first one is related to the strong dipole moment of cyanoacetylene (3.72 D) which is expected to lead to threshold peaks in the vibrational excitation cross sections. Such peaks, first observed in hydrogen halides [35], are common in all polar molecules. The second effect is the formation of the π_1^* resonance around 0.5 eV. The small width

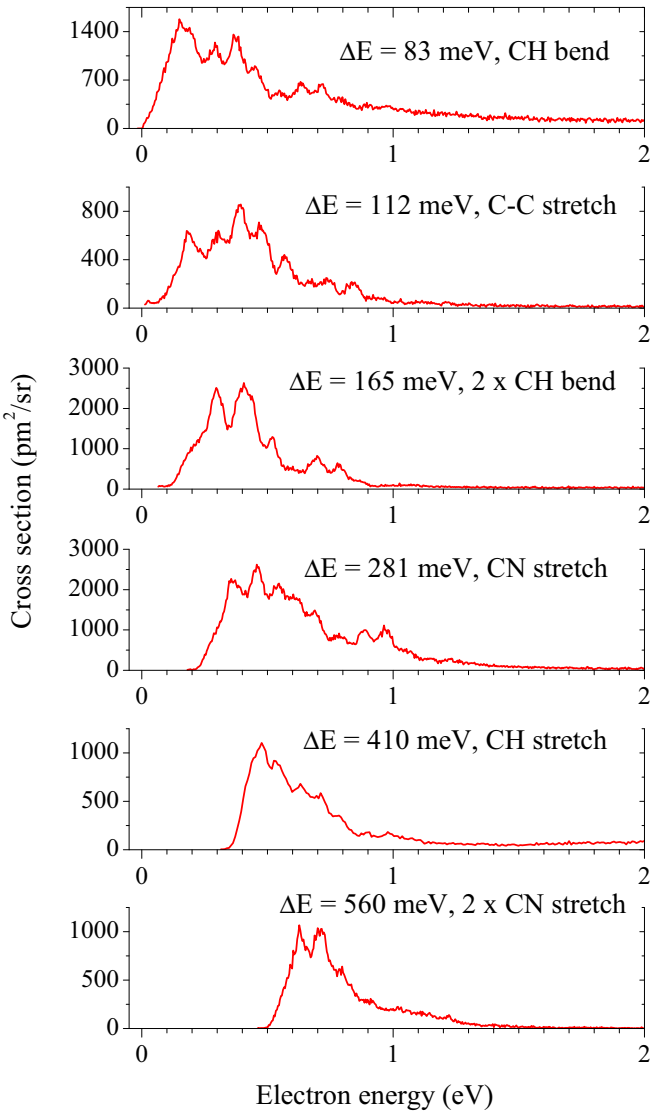

FIG. 4. The vibrational excitation cross sections for individual vibrations in HC_3N as functions of incident electron energy with the low-energy horizontal scale expanded.

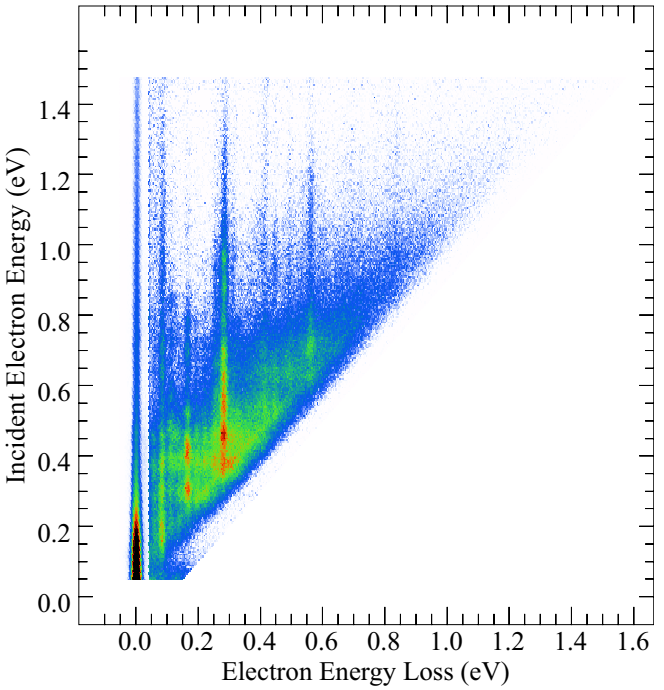

FIG. 5. Two-dimensional electron energy loss spectrum of HC_3N. The intensity of the elastic peak (energy loss = 0 eV) is reduced by a factor of 20 with respect to the rest of the spectrum.

of the resonance leads to a pronounced boomerang structure, visible in all vibrational modes. The boomerang structure originates from the vibrational motion of the nuclear wave packet on the anion potential energy surface. Due to the long lifetime of the resonant state, the nuclei will undergo several vibrations prior to the electron detachment. The oscillatory structure originates from the interference of the outgoing and returning nuclear wave packet [36]. It is commonly manifested as a structure on top of a vibrational excitation band. The present accidental overlap of the π^* resonance and the threshold peak causes the rather exotic accumulation of the boomerang structure on the falling edge of the peak.

The present data enable us to judge the accuracy of different methods used to calculate the resonant energies in Table I. So far, the only experimental data on these states have come from the DEA spectroscopy [12]. These are, however, influenced by energetic threshold cutoffs, or by the formation of core-excited resonances. The present data enable an unambiguous determination of the position of the π_2^* resonance at 5.3 eV. This compares surprisingly favorably with the value obtained from the scaling formula (5.5 eV) and reasonably well with the CAP value of 6.2 eV. The single-center expansion scattering calculation [17] overestimates the position of this resonance by almost 3 eV (8.18 eV). For the π_1^* resonance, the determination of the experimental center is complicated due to overlap with the threshold peak; however, judging from the boomerang structure in the C−C stretch and C−H bend excitations (Fig. 4), the center can be placed to 0.5 eV. Again, the CAP method predicts this resonance better than the two scattering calculations (0.7 eV vs 1.94 and 1.51 eV). These two also overestimate the energy of the σ_2^* resonance, which has the experimental center between 6 and 7 eV, judging from the C − N stretch excitation curve in Fig. 6.

A further insight into the low-energy part can be gained from the two-dimensional spectrum in Fig. 5. The 2D electron energy loss spectrum [37] is a collection of many energy loss spectra recorded at various incident energies. It provides a complete picture of the vibrational nuclear dynamics. A horizontal cut through such spectrum corresponds to an energy loss spectrum, such as shown in Fig. 2, and a vertical cut corresponds to an excitation curve of a given energy loss, such as shown in Fig. 4. The diagonal line $E_i = \Delta E$ is the threshold line, corresponding to the outgoing electrons with zero kinetic energies.

The 2D spectrum agrees fully with the individual vibrational cross sections. Additionally, it reveals one more feature: approximately above 0.2 eV incident electron energy, the electrons along the diagonal ($\Delta E = E_i$) form a weak continuous stripe instead of appearing only at the sharp energies of individual vibrations. These electrons are ejected with residual

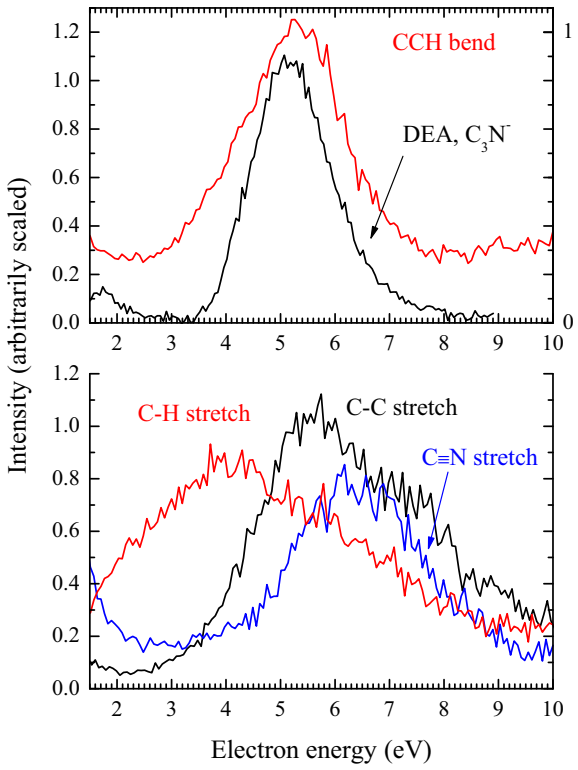

FIG. 6. High-energy part of the individual vibrational excitation cross sections and DEA C_3N^- ion yield. The raw data from Fig. 3 are reduced multiple times (neighboring channels are averaged). For the sake of this comparison, the data are arbitrarily scaled.

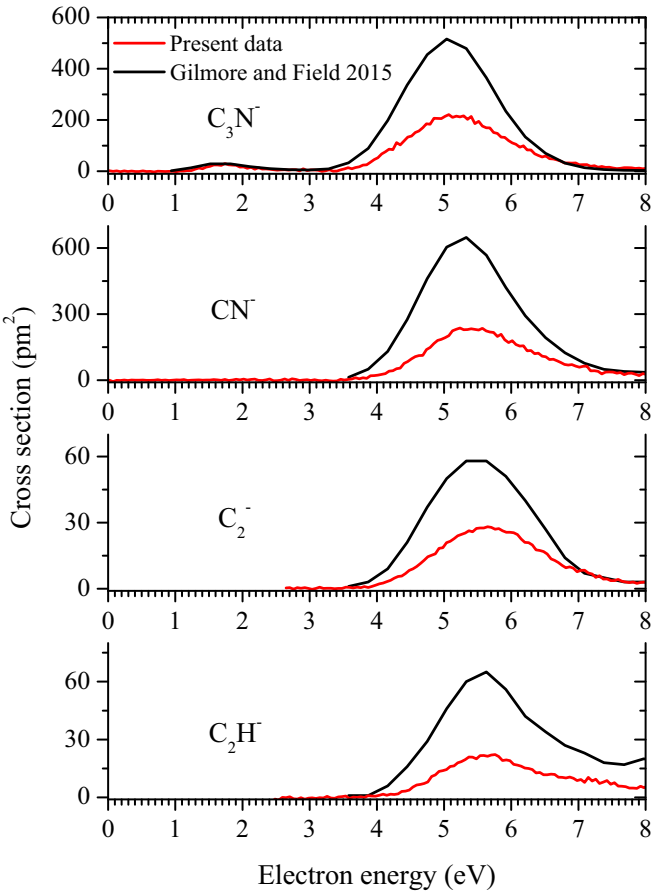

FIG. 7. Partial DEA cross sections for the production of all anionic fragments from HC_3N. Red lines: Present data, black lines: Gilmore and Field [15].

energies close to zero, independently of their incident energy. Note that the analyzer has a low transmission of electrons with residual energies below some 30 meV to 50 meV; hence the threshold signal appears somewhat higher than $E_r = 0$ eV. It is also visible as the high background signal in the energy loss spectrum in the upper panel of Fig. 2.

These threshold electrons can be interpreted using the potential energy surfaces of Sommerfeld and Knecht [16]. According to their calculations, cyanoacetylene possesses a valence-bound anion; however, its equilibrium geometry is far from the neutral one. It has a trans-bent zigzag structure, however, with an adiabatic electron affinity close to zero. Apart from this, HC_3N supports a dipole-bound state with the potential energy curve lying several meV below the neutral one; its equilibrium geometry thus corresponds to the neutral's linear structure. The linear transit between the two anion states (valence- and dipole-bound) shows a barrier of approximately 0.2 eV. The origin of the slow electrons is thus the following: if an electron with the incident energy $E_i > 0.2$ eV is captured in the low-lying π^* resonance, the nuclear framework starts to move towards the geometry of the valence-bound anion, distorting the linear structure towards the trans-cis bent one. As soon as the geometry gets to the point where the anion surface lies below that of the neutral, the electron detachment is suppressed: it is energetically impossible for the electron to detach. However, the excess energy is stored in the nuclear degrees of freedom and efficiently randomizes over the vibrational degrees of freedom. The motion on the electronically bound part of the potential surface is statistical, so the nuclei may again get to the configuration, where the valence anion energy lies above that of the neutral. At this crossing point of the neutral and the anion surface the electron is unbound again and can detach. A number of previous examples [38–40] shows that such electrons detach basically as soon as they can and are thus emitted with close-to-zero residual energies.

D. Dissociative electron attachment

Figure 7 shows the absolute cross section for the production of individual fragment anions from HC_3N. The recent data of Gilmore and Field [15] are shown for comparison. The two data sets show an excellent agreement concerning the shapes of the individual DEA bands. However, there is a consistent quantitative disagreement. We will use the energy-integrated cross section σ_I (invariant of the beam resolution) for the discussion. On the main DEA band, spanning between 3 and 8 eV, the ratio of our σ_I for the C_3N^- production (411 eV pm^2) to that of Gilmore and Field is 0.47. This disagreement is more or less consistent for all four fragments. The present branching ratios between the fragments C_3N^- : C_2^- : C_2H^- : CN^- are 1:0.14:0.12:0.95. The branching ratios of Gilmore and Field are 1:0.13:0.15:1.33; they thus agree very well, apart from the CN^- which had higher abundance in the measurements of Ref. [15]. At this point, it

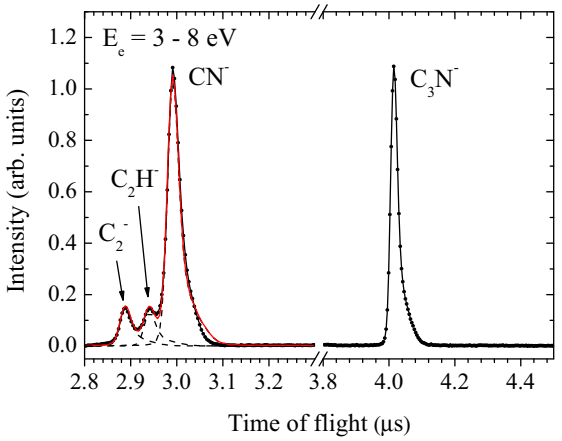

FIG. 8. Cumulative negative ion time-of-flight spectrum in the energy range 3 to 8 eV. Lines with points: Experimental data; dashed lines: fitted contributions from the peaks with mass-to-charge ratios 24, 25, and 26; red line: sum of the individual contributions.

should be noted that our time-of-flight analyzer does not fully resolve the three fragments with mass-to-charge ratios 24, 25, and 26. When designed [10], the resolution was compromised by the fact that the setup is quantitative. There are for example no grids separating the two acceleration regions. This on one hand distorts the Wiley-McLaren type time focusing; on the other hand it means undisturbed transmission of extracted anions. Still, as is illustrated in Fig. 8, the mass resolution is high enough to determine the branching ratios between the three fragments reliably. The spectrum is cumulative [41,42]; it has been obtained as a sum of the mass spectra in the energy range 3 to 8 eV. The dashed lines show the individual contributions of the three close-lying fragments and the full red line shows their sum.

Somewhat surprisingly, the quantitative level of agreement between the present data and those of Gilmore and Field is better for the first DEA band in the C_3N^- production, shown magnified in Fig. 9. The ratio of the energy-integrated cross sections of this band is 0.68.

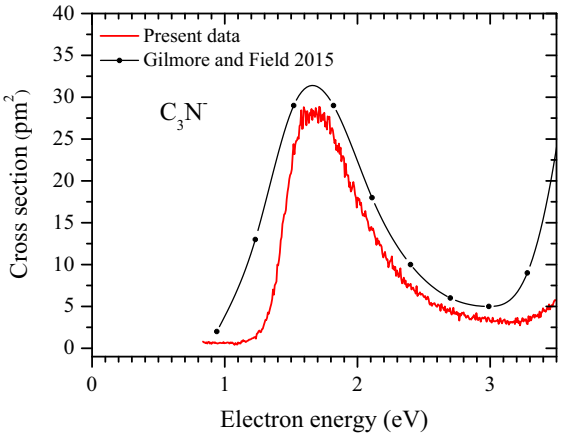

FIG. 9. Low-energy DEA band for the C_3N^- fragment. Red line: Present data, black points: Gilmore and Field [15].

The probable origin of the quantitative discrepancy is the different calibration methods used to obtain the absolute values. Gilmore and Field used the O^- signal from the background water vapor for the cross calibration. The ratio of the HC_3N/H_2O number densities was obtained from the recorded ion yields of the positive ions and their calculated absolute cross sections in the BEB formalism. Considering this rather indirect approach, the present agreement of the absolute cross section within a factor of two can be actually viewed as very good. Both experiments have quoted uncertainty of ±20 and the difference between the absolute values is only slightly larger than the combined error limits. Due to more direct calibration procedure, the present values might be considered to be more reliable.

The comparison with the vibrational excitation cross sections brings new light on the DEA mechanism. As seen in Fig. 6, the band at 5.5 eV is very similar to the CCH bend excitation cross section, which suggests that the DEA is mediated by the formation of the π_2^* resonance. Graupner *et al.* [12] did the same assignment; however, since their reference center of the π_2^* resonance was that calculated by Sommerfeld and Knecht [16] at 6.2 eV, they had to argue with a survival probability shift in order to explain the different DEA peak position. The current comparison in Fig. 6 shows that the DEA band actually overlaps with the π_2^* resonance very well.

Still, there is one aspect which invokes caution with this assignment, and that is the large width of the π_2^* resonance. The corresponding bands (both in the DEA and in vibrational excitation spectra) are approximately 2 eV wide. The width of the band is determined by two factors: (i) the autodetachment width Γ and (ii) the projection of the nuclear wave function on the resonant state (reflection principle). Such broad bands suggest that Γ itself is rather large, in agreement with the theoretical calculations which evaluated it to be 1.1 eV [16] or 0.76 eV [17]. From the uncertainty principle, a resonance width of 1 eV corresponds to a lifetime towards electron autodetachment of 0.3 femtoseconds. It is somewhat surprising that such a short-lived state gives rise to a rather high dissociative cross section. An alternative origin of the DEA yield would be a core-excited resonance: neutral HC_3N possesses electronically excited states ($^1\Delta_u$) lying between 5.5 and 6.2 eV [43]. Assuming a typical stabilization energy of 0.4 eV, the corresponding Feshbach resonance would be located exactly around the present DEA band. Such resonances are typically very narrow and are not visible in the vibrational excitation cross section [38]. They also typically lead to a rich fragmentation pattern [25,44]. The agreement in Fig. 6 thus might be coincidental. It is worth noting that a similar dispute, whether the dominant DEA band is caused by an accidentally overlapping shape π^* or a core-excited resonance, has appeared for diacetylene C_4H_2 [45,46].

Only the C_3N^- fragment, created by the hydrogen abstraction, is observed at lower energies with a peak at 1.7 eV. It was shown by calculating the threshold energies [12] that other channels are energetically closed in this energy range. The threshold for the C_3N^- production is 1.37 ± 0.2 eV which causes a sharp onset of the present cross section in Fig. 9. Two effects can in principle contribute to the origin of this band.

(i) As assigned previously [12], it can originate from a high-energy shoulder of the π_1^* resonance (the center of the resonance lies considerably below the threshold energy). This seemed very reasonable, since this resonance is rather narrow so it would lead to a high survival factor. However, as can be seen in Fig. 4, all the cross sections for the vibrational excitation are diminishing above 1.3 eV, so the DEA band seems to have almost no overlap with the π_1^* resonance.

(ii) The second option is that the DEA proceeds via formation of the σ^* resonance, whose lower tail overlaps with the DEA band as can be seen in the C−H stretch vibrational excitation in Fig. 3. Judging from a large width of such resonance alone, it should lead to negligible DEA cross section, since all electrons would autodetach. However, it is now well established that in molecules with large dipole moments (or even nonpolar molecules with high polarizabilities), the dissociative cross section of σ^* resonances can reach very high values. The interaction of dipole-bound (or virtual) states with the pure σ^* states suppresses the autodetachment channel. The cyanoacetylene's dipole moment of 3.72 D opens this possibility. It should be however noted that such dipole-supported σ^* resonances often lead to sharp structures in the DEA cross section. These structures—downward steps or even oscillations—appear at the opening of the new vibrational excitation channels in the direction of the dissociating bond, in this case the C−H vibration. Taking into account the anharmonic vibrational levels [47], the $0 \rightarrow 4$ transition in the C−H stretch vibration is open at 1.56 eV and the $0 \rightarrow 5$ transition at 1.94 eV. No such structures are visible in Fig. 9. It should be noted that the DEA spectra of molecules like hydrogen halides [48–50] or formic acid [26] do show discernible structures at electron beam resolution comparable to the present one (approximately 100 meV).

There seems to be no unambiguous evidence for any of the two mechanisms to be prevalent in the dehydrogenation DEA around 1.7 eV. Our recent results for the HNCO molecule [51] even suggest that often there is even no sharp distinction between these possible: upon any out-of-line geometry distortion the π^* and σ^* states mix and the actual dissociation mechanism is given by the interplay of them.

IV. CONCLUSIONS

In conclusion, we have probed the resonances in cyanoacetylene by measuring cross sections for elastic electron scattering, vibrational excitation, and dissociative electron attachment. Data from these three scattering channels are mutually consistent and provide information about both the nondissociative and dissociative nuclear dynamics on the transient anion potential surfaces.

Several effects influence the probed electron-induced processes. One is the strong dipole moment of HC_3N which is manifested as the low-energy peak in the elastic scattering and as the threshold peaks in all the vibrational excitation channels. The second dominating effect is the formation of four resonances. The lower π_1* resonance is the narrowest and its long lifetime leads to pronounced boomerang oscillatory structures in the vibrational excitation cross sections. At higher electron energies, the formation of the broad σ_1^* and σ_2^* resonances is reflected in the vibrational excitation cross sections of the C−H stretch and C≡N stretch modes, while the CCH bending mode excitation is probably exclusively mediated by the formation of the π_2^* resonance. This resonance also dominates the DEA spectrum and it leads to production of four anionic fragments. The existence of the bound HC_3N^- anion and the crossing of its potential energy curve with that of the neutral molecule (boundary between the resonant and the bound state) is manifested by the threshold signal in the two-dimensional energy loss spectrum. Here the electrons are emitted with close-to-zero residual energies independently of the incident energy, which is caused by the randomization of the vibrational motion on the bound-anion surface.

ACKNOWLEDGMENTS

This work is part of Project No. 17-04844S of the Czech Science Foundation (CSF). L.B. acknowledges support from FWF Project No. DK-ALM:W1259-N27; M.P. and J.Ž. acknowledge partial support from CSF Project No. 17-14200S. We wish to thank Roman Čurík, Prague, for numerous discussions of resonances and of this manuscript.

[1] B. E. Turner, Astrophys. J. **163**, L35 (1971).
[2] J. H. Bieging and M. Tafalla, Astron. J. **105**, 576 (1993).
[3] W. M. Irvine *et al.*, Icarus **60**, 215 (1984).
[4] V. G. Kunde, A. C. Aikin, R. A. Hanel, D. E. Jennings, W. C. Maguire, and R. E. Samuelson, Nature (London) **292**, 686 (1981).
[5] A. J. Coates, F. J. Crary, G. R. Lewis, D. T. Young, J. H. Waite, and E. C. Sittler, Geophys. Res. Lett. **34**, L22103 (2007).
[6] S. Brunken, H. Gupta, C. A. Gottlieb, M. C. McCarthy, and P. Thaddeus, Astrophys. J. **664**, L43 (2007).
[7] J. Cernicharo, M. Guelin, M. Agundez, K. Kawaguchi, M. C. McCarthy, and P. Thaddeus, Astron. Astrophys. **467**, L37 (2007).
[8] P. Thaddeus, C. A. Gottlieb, H. Gupta, J. Cernicharo, S. Brunken, M. C. McCarthy, M. Agundez, M. Guelin, and J. Cernicharo, Astrophys. J. **677**, 1132 (2008).
[9] V. Vuitton, P. Lavvas, R. V. Yelle, M. Galand, A. Wellbrock, G. R. Lewis, A. J. Coates, and J.-E. Wahlund, Planet. Space Sci. **57**, 1558 (2009).
[10] O. May, J. Fedor, and M. Allan, Phys. Rev. A **80**, 012706 (2009).
[11] O. May, J. Fedor, B. C. Ibănescu, and M. Allan, Phys. Rev. A **77**, 040701(R) (2008).
[12] K. Graupner, T. L. Merrigan, T. A. Field, T. G. A. Youngs, and P. C. Marr, New J. Phys. **8**, 117 (2006).
[13] V. H. Dibeler, R. M. Reese, and J. L. Franklin, J. Am. Chem. Soc. **83**, 1813 (1961).
[14] P. W. Harland, Int. J. Mass Spectrom. **70**, 231 (1986).
[15] T. D. Gilmore and T. A. Field, J. Phys. B: At. Mol. Phys. **48**, 035201 (2015).
[16] T. Sommerfeld and S. Knecht, Eur. Phys. J. D **35**, 207 (2005).
[17] F. Sebastianelli and F. Gianturco, Eur. Phys. J. D **66**, 41 (2012).

[18] J. Kaur, N. Mason, and B. Antony, J. Phys. B: At. Mol. Phys. **49**, 225202 (2016).
[19] S. T. Chourou and A. E. Orel, J. Phys.: Conf. Ser. **300**, 012014 (2011).
[20] M. Allan, J. Phys. B: At. Mol. Phys. **25**, 1559 (1992).
[21] M. Allan, J. Phys. B: At. Mol. Phys. **38**, 3655 (2005).
[22] M. Allan, J. Phys. B: At. Mol. Phys. **40**, 3531 (2007).
[23] M. Stepanović, Y. Pariat, and M. Allan, J. Chem. Phys. **110**, 11376 (1999).
[24] J. Langer, M. Zawadzki, M. Fárník, J. Pinkas, J. Fedor, and J. Kočišek, Eur. Phys. J. D **72**, 112 (2018).
[25] M. Zawadzki, M. Ranković, J. Kočišek, and J. Fedor, Phys. Chem. Chem. Phys. **20**, 6838 (2018).
[26] R. Janečková, D. Kubala, O. May, J. Fedor, and M. Allan, Phys. Rev. Lett. **111**, 213201 (2013).
[27] K. Graupner, S. A. Haughey, T. A. Field, C. A. Mayhew, T. H. Hoffmann, O. May, J. Fedor, M. Allan, I. I. Fabrikant, E. Illenberger *et al.*, J. Phys. Chem. A **114**, 1474 (2010).
[28] F. A. Miller and D. H. Lemmon, Spectrochim. Acta, Part A **23**, 1415 (1967).
[29] D. Chen and G. A. Gallup, J. Chem. Phys. **93**, 8893 (1990).
[30] T. J. Millar, C. Walsh, and T. A. Field, Chem. Rev. **117**, 1765 (2017).
[31] I. I. Fabrikant, S. Eden, N. J. Mason, and J. Fedor, Adv. At. Mol. Opt. Phys. **66**, 545 (2017).
[32] D. E. Lide, *CRC Handbook of Chemistry and Physics*, 87th ed. (Taylor and Francis, Boca Raton, FL, 2007).
[33] I. I. Fabrikant, J. Phys. B: At. Mol. Opt. Phys. **49**, 222005 (2016).
[34] S. Leach, G. A. Garci, A. Mahjoub, Y. Bénilan, N. Fray, M.-C. Gazeau, F. Gaie-Levrel, N. Champion, and M. Schwell, J. Chem. Phys. **140**, 174305 (2014).
[35] K. Rohr and F. Linder, J. Phys. B: At. Mol. Phys. **9**, 2521 (1976).
[36] D. T. Birstwistle and A. Herzenberg, J. Phys. B: At. Mol. Phys. **4**, 53 (1971).
[37] K. Regeta and M. Allan, Phys. Rev. Lett. **110**, 203201 (2013).
[38] M. Allan, J. Electron Spectrosc. Relat. Phenom. **48**, 219 (1989).
[39] M. Allan, Phys. Rev. Lett. **98**, 123201 (2007).
[40] M. Allan, M. Lacko, P. Papp, Š. Matejčík, M. Zlatar, I. I. Fabrikant, J. Kočišek, and J. Fedor, Phys. Chem. Chem. Phys. **20**, 11692 (2018).
[41] J. Lengyel, P. Papp, Š. Matejčík, J. Kočišek, M. Fárník, and J. Fedor, Beilstein J. Nanotechnol. **8**, 2200 (2017).
[42] J. Lengyel, M. Ončák, J. Fedor, J. Kočišek, A. Pysanenko, M. K. Beyer, and M. Fárník, Phys. Chem. Chem. Phys. **19**, 11753 (2017).
[43] T. Ferradaz, Y. Benilan, N. Fray, A. Jolly, M.Schwell, M. C. Gazeau, and H.-W. Jochims, Planet. Space Sci. **57**, 10 (2009).
[44] R. Janečková, O. May, A. R. Milosavljević, and J. Fedor, Int. J. Mass Spectrom. **365-366**, 163 (2014).
[45] M. Allan, O. May, J. Fedor, B. C. Ibănescu, and L. Andric, Phys. Rev. A **83**, 052701 (2011).
[46] R. Čurík, I. Paidarová, M. Allan, and P. Čársky, J. Phys. Chem. A **118**, 9734 (2014).
[47] P. D. Mallinson and A. Fayt, Mol. Phys. **32**, 473 (1976).
[48] J. Fedor, M. Cingel, J. D. Skalný, P. Scheier, T. D. Märk, M. Čížek, P. Kolorenč, and J. Horáček, Phys. Rev. A **75**, 022703 (2007).
[49] J. Fedor, O. May, and M. Allan, Phys. Rev. A **78**, 032701 (2008).
[50] J. Fedor, C. Winstead, V. McKoy, M. Čížek, K. Houfek, P. Kolorenč, and J. Horáček, Phys. Rev. A **81**, 042702 (2010).
[51] M. Zawadzki, M. Čížek, K. Houfek, R. Čurík, M. Ferus, S. Civiš, J. Kočišek, and J. Fedor, Phys. Rev. Lett. **121**, 143402 (2018).

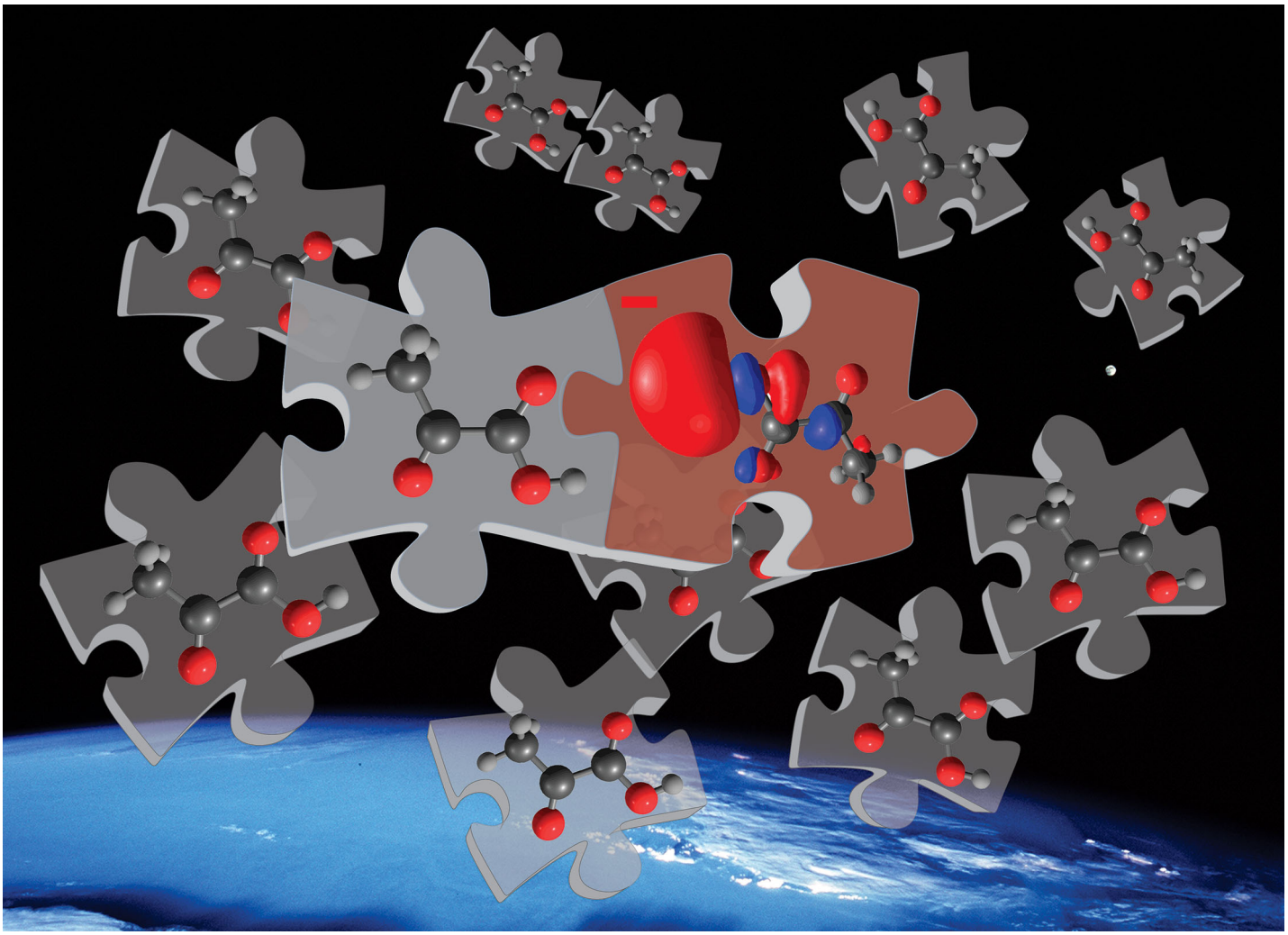

Showcasing research from Dr Juraj Fedor and his group at J. Heyrovský Institute of Physical Chemistry, Czech Academy of Sciences, in Prague, Czech Republic.

Dissociative electron attachment and anion-induced dimerization in pyruvic acid

The anions created in collisions of free electrons with pyruvic acid molecules trigger its dimerization with unusually high effectiveness. This process dramatically changes the outcome of the electron-induced chemistry: the fragmentation pattern for the molecule in the environment is very different from the isolated molecule. For pyruvic acid, this is happening already at very low gas-phase number densities. An example of such a low-density electron-rich environment is the Earth's limb.

As featured in:

See M. Zawadzki, J. Fedor *et al.*, *Phys. Chem. Chem. Phys.*, 2018, **20**, 6838.

ROYAL SOCIETY OF CHEMISTRY

rsc.li/pccp

Registered charity number: 207890

PCCP

PAPER

Cite this: *Phys. Chem. Chem. Phys.*, 2018, **20**, 6838

Dissociative electron attachment and anion-induced dimerization in pyruvic acid

M. Zawadzki,*† M. Ranković, J. Kočišek and J. Fedor *

Received 5th November 2017,
Accepted 2nd January 2018

DOI: 10.1039/c7cp07472g

rsc.li/pccp

We report partial cross sections for the dissociative electron attachment to pyruvic acid. A rich fragmentation dynamics is observed. Electronic structure calculations facilitate the identification of complex rearrangement reactions that occur during the dissociation. Furthermore, a number of fragment anions produced at electron energies close to 0 eV are observed, that cannot originate from single electron–molecule collisions. We ascribe their production to secondary reactions of the transient anions with neutral molecules. Such reactions turn out to be unusually efficient; the most probable reason for this is that they proceed *via* the formation of a double-hydrogen-bonded complex followed by an ultrafast proton transfer between the reaction partners.

1 Introduction

Pyruvic acid (CH_3–CO–COOH), the simplest α-keto acid, is an important molecule in atmospheric chemistry, biochemistry and astrochemistry. In the first area, it primarily originates from the photo-oxidation of both biogenic and anthropogenic precursors, mainly of the isoprene emitted from trees.[1] As such, it is also an important component of the in-cloud secondary organic aerosol and its decomposition processes thus attract a lot of attention.[2] In biochemistry, pyruvic acid is a product of glycolysis in living cells and serves as a precursor of several key species in the Krebs cycle. Its dehydrogenated anion, pyruvate (CH_3–CO–COO^-, throughout this paper designated as $(M - H)^-$), is directly an intermediate compound in the metabolism of carbohydrates, proteins, and fats. From the astrochemical point of view it is interesting to note that pyruvic acid has been suggested as a prebiotically plausible molecule.[3] It can be synthesized directly from CO_2 and H_2O at high temperatures and pressures[4] and it has been detected in carbonaceous meteorites.[5]

Under certain conditions, all of these environments – atmosphere, biological tissues, and outer space – can bear evidence for a significant amount of free electrons. In the atmosphere, this is mainly the case in high altitudes (stratosphere), where free electrons originate from, *e.g.*, photoionization, solar particles or cosmic rays and the corresponding secondary ionization processes. In biological tissues, a large amount of secondary electrons are created always when high-energy radiation passes through the cell. These electrons are rapidly thermalized in multiple collisions and their typical energy distribution peaks below 10 eV.[6] The role of such secondary electrons in radiation damage has been intensively studied over the past 15 years and it is well established that the interaction of low-energy electrons leads to efficient fragmentation of many biomolecules.[6,7] Such fragmentation is primarily caused by dissociative electron attachment (DEA), a process, where upon a collision of low-energy electron with a target molecule M, a temporary negative ion (resonance) $M^{\#-}$ is formed, which then dissociates.

The atmospheric and astrochemical importance of pyruvic acid has motivated intensive interest in its photochemical decomposition pathways.[2] UV-induced processes are interesting from the point of view of sunlight-driven photochemical synthesis: they provide an initial step for producing reactive species that then react further to create more complex molecules. Low-energy electrons represent an alternative triggering mechanism for molecular fragmentation and subsequent reactions. This has been shown on numerous examples, both in atmospheric chemistry[8] and astrochemically relevant electron-induced synthesis.[9,10] It is therefore interesting to probe the fragmentation channels in pyruvic acid induced by low-energy electrons.

In this paper we present absolute cross sections for individual DEA channels in pyruvic acid. The measurements are supported by DFT calculations of the asymptotic energetics, mainly the threshold energies. It turns out that the anions formed in the electron–pyruvic acid collisions are extremely reactive. Even at very low local pressures they initiate the dimerization reactions that lead to the synthesis of more complex anionic species.

2 Methods

Two experimental setups, recently transferred to Prague from the University of Fribourg, were used for the present studies.

J. Heyrovský Institute of Physical Chemistry, Czech Academy of Sciences, Dolejškova 3, 18223 Prague 8, Czech Republic. E-mail: mateusz.zawadzki@jh-inst.cas.cz, juraj.fedor@jh-inst.cas.cz

† Current address: Atomic Physics Division, Department of Atomic, Molecular and Optical Physics, Faculty of Applied Physics and Mathematics, Gdańsk University of Technology, ul. Gabriela Narutowicza 11/12, 80-233 Gdańsk, Poland.

The first setup, TEM-QMS, is a quadrupole mass spectrometer with a trochoidal electron monochromator.[11] The setup consists of a TEM that provides an electron beam of well defined incident energy; a target chamber where electrons collide with the target gas molecules; and a quadrupole filter for analyzing ions created in the dissociative attachment process. The whole system is situated in two vacuum chambers with differential pumping. In the main chamber, where the monochromator and an ion extraction lens are placed, the background pressure (measured using a Penning gauge) without the sample was typically 10^{-7} mbar. The pressure of the molecules in the collision chamber was kept typically in the 1×10^{-4}–1×10^{-3} mbar range. In this experiment the electron beam current was typically 20–40 nA and the resolution was below 100 meV.

The second setup, DEA-TOF, is a quantitative DEA spectrometer with a TOF analyzer.[12,13] It provides absolute DEA cross sections, *via* calibration to the 4.4 eV resonance in the O^- production from CO_2. The whole experiment is pulsed at 50 kHz. A 200 ns long electron beam passes through the chamber while it is field-free and after another 200 ns delay a −300 V pulse is applied to an extractor to extract the created anions from the collision chamber. Partly due to pulsing, the typical electron energy resolution of the second setup is worse, around 300 meV. We thus show the ion yield curves measured with the TEM-QMS setup calibrated to the absolute cross sections measured on the DEA-TOF setup, using an invariance of the energy-integrated cross section.[14] In both setups, the calibration of the energy scale was against the 4.4 eV band of O^- production from CO_2. The presence of low-energy electrons is verified by measuring the SF_6^- signal from SF_6 which has very high attachment cross section close to 0 eV.

The sample of pyruvic acid was obtained from Sigma Aldrich and has a declared purity of 97%. In addition, we have performed a range of measurements with fully deuterated pyruvic acid (CD_3–CO–COOD, obtained from Sigma Aldrich), in order to identify the chemical composition of anions, which could not be assigned unambiguously from the mass to charge ratio.

The experiments are supported by quantum chemical calculations of the bound electronic states (asymptotic energetics) at the B3LYP/aug-cc-pVTZ level. It has been shown[15,16] that this approach provides reliable values of threshold energies for the DEA reactions in organic molecules. Pyruvic acid itself has four conformers that lay relatively close in energy.[17–19] The optimized structures of the two lowest ones and the neutral pyruvic acid dimer are shown in Fig. 1. The lowest-energy conformer has an OH bond oriented towards the C=O group (top left panel of Fig. 1). However, all the energy thresholds given throughout the paper are with respect to the conformer that has the same structure as the dimerized units. This facilitates various comparisons. The energy difference between the two conformers is in the order of 0.1 eV.[17–19]

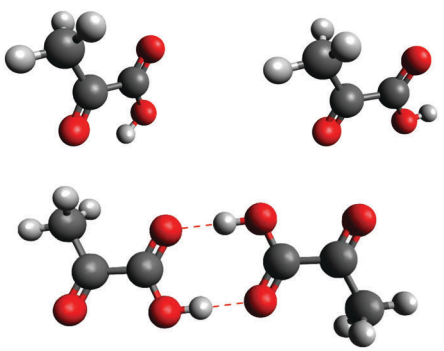

Fig. 1 Molecular structures of two monomeric conformers of pyruvic acid and the hydrogen-bonded dimer.

3 Results and discussion

3.1 DEA channels

Fig. 2 shows the cross sections for the production of anionic fragments upon electron attachment to pyruvic acid. A rich fragmentation dynamics was observed with a large number of anionic channels. The fragments are produced at five different energy regions (bands), centered around 1.3, 3.5, 6, 7.8 and 9.2 eV, and they clearly correspond to various states of transient anions (resonances). Each particular resonance dissociates only into certain fragments, which demonstrates that the dissociation is to a large degree driven kinematically, *i.e.*, the fragmentation pattern is determined by the direction of a resonant potential energy surface at the vertical attachment geometry; rather than driven statistically (*via* the redistribution of energy among the internal degrees of freedom).

Table 1 summarizes the calculated threshold energies for individual dissociation channels. These values are also marked in Fig. 2. The thresholds are obtained from the sums of electronic and zero-point energies. For several fragments, surprisingly complex rearrangement reactions are required in order that the calculated threshold is below the onset of the experimental signal.

The strongest DEA channel is

$$e^- + \underbrace{CH_3COCOOH}_{M} \xrightarrow{M^{\#-}} CH_3COCO + OH^-. \qquad (1)$$

Its cross section peaks at rather high electron energies, around 6 eV. The DEA in other carboxylic acids (formic acid[14,20] and acetic acid[21]) and a number of amino acids, such as glycine or alanine,[22] leads to a very efficient cleavage of the carboxylic OH bond, leading to a dehydrogenated anion $(M - H)^-$

$$e^- + \underbrace{CH_3COCOOH}_{M} \xrightarrow{M^{\#-}} (M - H)^- + H. \qquad (2)$$

Such a dehydrogenation channel has attracted a lot of attention in general, since it represents the most effective DEA bond-cleavage process in a range of biomolecules, including nucleobases.[7,23] Perhaps the most striking present result is that in pyruvic acid this channel is rather weak in comparison to other channels: its energy-integrated cross section is approximately 12 times smaller than that for the production of OH^-.

The 1.3 eV band in the $(M - H)^-$ cross section has a sharp onset at its energetic threshold. This is typical in all molecules

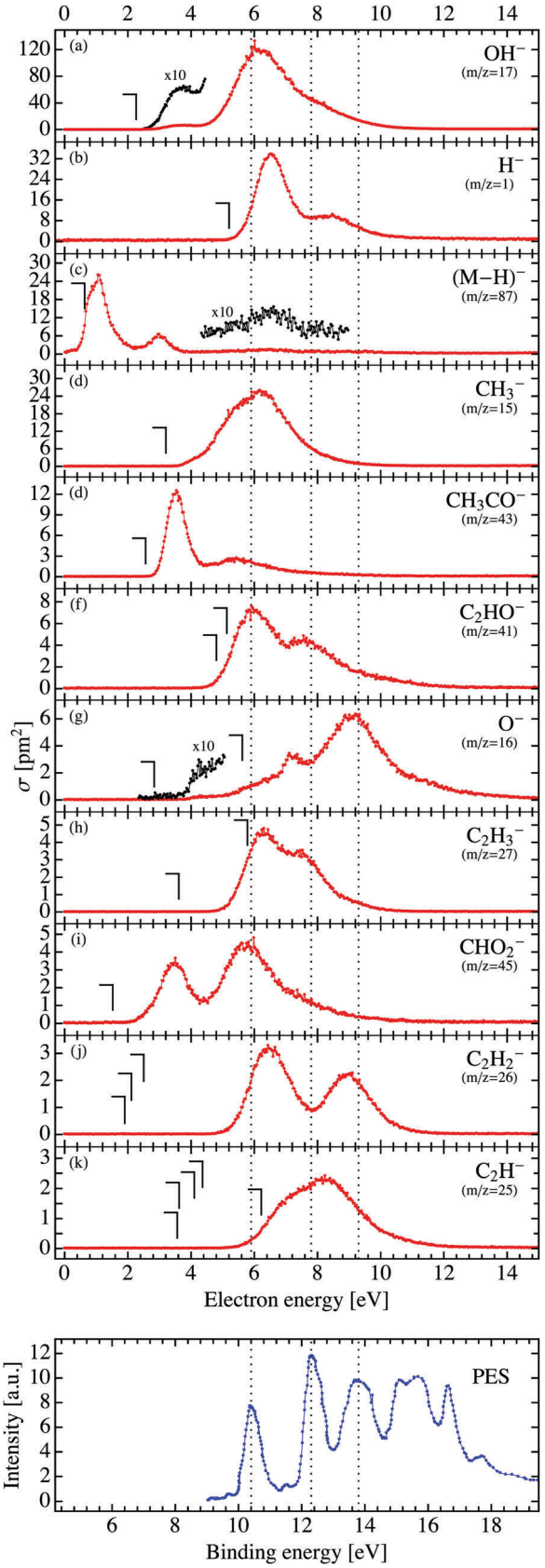

Fig. 2 Cross sections for individual DEA fragments of pyruvic acid. Last panel: photoelectron spectrum of McGlynn and Meeks.[29]

Table 1 B3LYP/aug-cc-pVTZ threshold energies for individual DEA fragmentation channels

Products		*m/z*	E_{th} (eV)
OH^-	+ CH_3COCO	17	2.26
H^-	+ M–H	1	3.76
$(M-H)^-$	+ H	87	0.63
CH_3^-	+ COCOOH	15	3.20
CH_3CO^-	+ COOH	43	2.56
C_2OH^-	+ H_2 + COOH	41	4.80
C_2OH^-	+ H + HCOOH	41	5.13
O^-	+ $CH_2CHCOOH$	16	2.83
O^-	+ CH_3CCOOH	16	5.62
CH_2CH^-	+ CO_2 + OH	27	3.61
CH_3C^-	+ CO_2 + OH	27	5.78
$COOH^-$	+ CH_3 + CO	45	1.52
$HCCH^-$	+ CH_2O_3	26	1.90
$C_2H_2^-$	+ H_2O + CO_2	26	2.11
$C_2H_2^-$	+ CH_2O_3	26	2.50
C_2H^-	+ H_2O + COOH	25	3.56
C_2H^-	+ H + H_2O + CO_2	25	3.62
C_2H^-	+ H + CH_2O_3	25	4.01
C_2H^-	+ OH + HCOOH	25	4.36
C_2H^-	+ CH_3O_3	25	6.23
$C_2O_3^-$	+ CH_3 + H	72	0.12
$C_2O_3^-$	+ CH_4	72	−0.93

mentioned above, where the dehydrogenation occurs.[23] In formic acid, which can serve as a prototype for this type of fragmentation, the origin of such a band sparks a significant amount of discussion. Two completely different DEA mechanisms were theoretically suggested to play a role. One was the formation of a π resonance with a subsequent symmetry lowering of the dissociating anion.[24] Another model suggested a dipole-supported σ* resonance which allows direct cleavage of the O–H bond.[25] For formic acid it has been shown experimentally[14] that the contribution from the second process dominates the DEA signal. The 1.3 eV $(M - H)^-$ band in pyruvic acid can in principle originate from both of these processes. The energy-integrated cross section of this band (24.4 eV pm^2) is lower than that in formic acid (98.4 eV pm^2). In the view of the extreme sensitivity of the DEA cross section to the position and width of the involved resonance, this is not a large drop. Nonetheless, we find it still somewhat surprising: the dipole moment of pyruvic acid[26] (2.3 Debye) is larger than that of formic acid[27] (1.4 Debye). The DEA cross section should increase with the strength of the long-range electron–molecule interactions.[28] Also, the threshold energy in pyruvic acid is lower than that in the DEA for formic acid, which should again lead to an increase of the DEA cross section. A theoretical model for DEA in pyruvic acid would be necessary to explain the relatively low cross section of the 1.3 eV band in the dehydrogenation channel.

At intermediate electron energies (between the threshold and the region of core-excited resonances above 5 eV), cross sections for several fragments (OH^-, $(M - H)^-$, CH_3CO^- and CHO_2^-) show a common band that peaks around 3.5 eV. Pyruvic acid has low-lying π* orbitals associated with the C=O double bonds and these can give rise to π* resonances. Such a resonance is the most probable origin of the band in this energy region. Individual fragments peak at slightly different electron energies (between 3.5 and 3.8 eV). This can be attributed to complex dissociation dynamics, with the profile of the DEA band mostly driven by the competition of dissociation and electron autodetachment (different survival factors in different dissociative directions of the resonant potential energy surface).

The DEA bands at electron energies above 5 eV are usually attributed to core-excited (Feshbach) resonances. Here the incoming electron excites the neutral target molecule and forms a Rydberg pair with the excited electron. The assignment of such bands is typically facilitated by the comparison with a photoelectron spectrum (PES). The PES carries information about the grandparent cation states. The resonance (anion state) can then be imagined as a Rydberg electron pair around this cation core. Due to a weak interaction of the diffuse pair with the core, the energy difference between the PES and the Feshbach resonances is usually around 4.5 eV (this assumption is based on a usual term energy of 4 eV and stabilization energy of the s^2 pair of 0.5 eV) and differs only weakly for different target molecules[15] (with several exceptions[30,31] where the assumption about the weak interaction is invalid). The last panel of Fig. 2 shows the PES of pyruvic acid[29] with the energy scale shifted by 4.5 eV. The molecular orbital notation of McGlynn and coworkers[32] is used to denote the bands. The first three PES bands overlap nicely with the DEA peaks of various fragments. On the basis of PES assignment we can identify the 6 eV DEA peak as the excitation from the lone-pair n_+ molecular orbital and formation of the Rydberg pair $(n_+^{-1}s^2)$. This resonance state leads to fragmentation producing OH^- (the single most dominant band in the whole DES spectrum) and several other anionic fragments. The DEA bands at around 7.8 eV originate from the Feshbach resonance with a configuration $(\pi_+^{-1}s^2)$ and the bands at 9.2 eV to the configuration $(\pi_-^{-1}s^2)$.

3.2 Anion-induced dimerization

The anions listed in the previous sections clearly originate from a single collision of an electron with a pyruvic acid monomer. Fig. 3 shows the ion-yield curves for a number of other fragments, for which this cannot be the case. This is clear for the ions with molecular masses higher than the monomer: the deprotonated dimer $(2M - H)^-$, and an anion with $m/z = 112$. In the experiments with deuterated pyruvic acid, the latter ion appeared at both masses 112 and 116; it thus corresponds to both $C_4O_4^-$ and $C_5O_3H_4^-$ ions. The $C_2O_3^-$ anion (m/z = 72) could in principle originate from the DEA to monomer – the threshold energy upon methane formation is −0.93 eV. However, this fragment has not been detected at all in the DEA-TOF setup, which strongly suggests that it originates from the same process as the dimeric anions (see below for the discussion of the difference between the two setups). The parent anion M^- could also in principle originate from a single-collision process if the heat capacity of pyruvic acid were high enough to sustain the electron affinity for the detection time window of several microseconds. However, it will be shown below that this is not the case (based on the pressure dependence). As shown in Fig. 4, at higher pressures in the collision chamber, the low-energy feature ion-yield for the $(M - H)^-$ anion appears as well

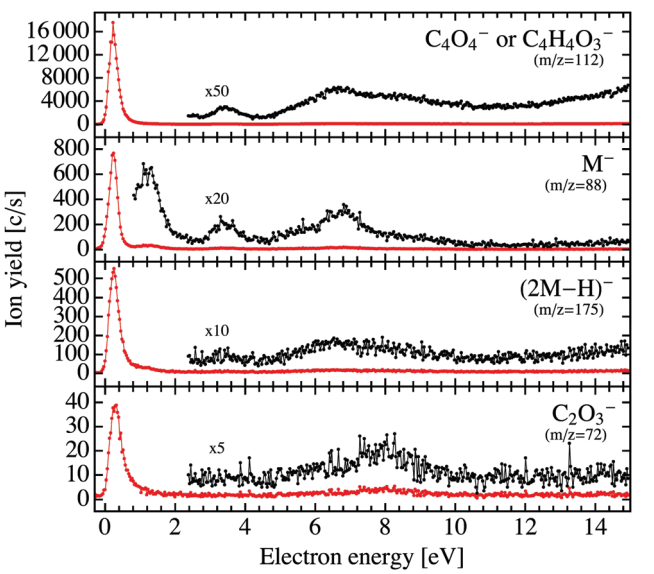

Fig. 3 Ion yield curves for the anions observed in a TEM-QMS setup that do not originate from the DEA to the pyruvic acid monomer.

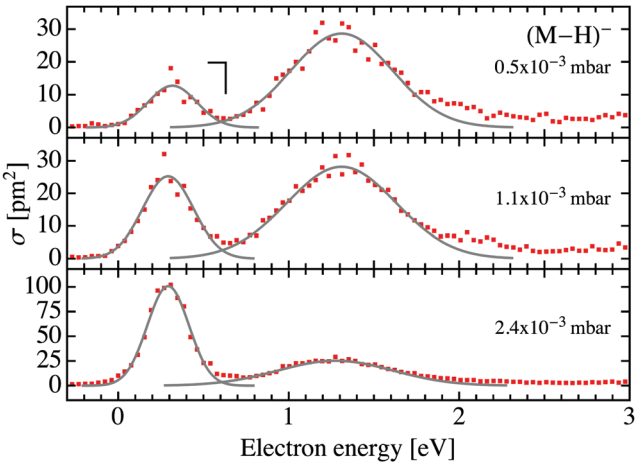

Fig. 4 Ion yield curves for the $(M - H)^-$ channel recorded at various sample pressures in the TEM-QMS collision chamber. The mark on the top panel denotes the threshold energy for DEA to the pyruvic acid monomer.

(and quickly becomes dominant). Again, since this signal appears below the energetical threshold for process (2), it cannot originate from the single-collision process.

A priori, there are several options for the possible origin of such species. One is that they originate from the dissociative electron attachment to pyruvic acid dimers. Carboxylic acids are known to efficiently form double hydrogen-bonded dimers (shown in Fig. 1) and already under normal conditions, the vapor from the liquid contains a considerable amount of such dimers. All the anions in Fig. 3 could in principle originate from the electron attachment to the neutral dimer. The resonances can be expected at lower electron energies,[33] and with increasing pressure in the collision chamber, the local density of the neutral dimers will increase due to the shift in the chemical equilibrium of the dimerization $M_2 \leftrightarrow M + M$. Nonetheless, we believe that the contribution from the DEA to neutral dimers is negligible. First, the complexation energy of the pyruvic acid dimer is 0.58 eV (present B3LYP/aug-cc-pVTZ value). We have calculated this value also at the MP2/aug-cc-PVTZ level which yielded 0.63 eV. This is very similar to the formic acid dimer (0.65 eV). Even though the equilibrium constants for dimerization will differ due to statistical factors, the concentration of the dimers in the formic acid vapor should be similar to that in the pyruvic acid vapor at comparable local pressures. We have performed additional DEA experiments on formic acid at the highest achievable local pressures in the collision chamber and we did not see any signal that would correspond to the presence of formic acid dimers.[33]

Much more probable origins of anions in Fig. 3 are the anion–molecule reactions. The transient anions of pyruvic acid $M^{\#-}$ can be formed at electron energies close to 0 eV. Their formation can be very efficient due to the considerable dipole moment of pyruvic acid but they are of course not visible in the DEA spectra in Fig. 2, since this energy range is lower than all the dissociative thresholds. The 0 eV transient anions will thus decay *via* electron autodetachment. The lifetime towards the autodetachment can range from femtoseconds to microseconds (in the case of an efficient intramolecular vibrational redistribution). Anions in Fig. 3 can be created by the collision of these transient anions with another pyruvic acid molecule in the collision chamber:

$$M^{\#-} + M \rightarrow (2M - H)^- + H \quad (3)$$

$$\rightarrow M^- + M \quad (4)$$

$$\rightarrow (M - H)^- + M + H \quad (5)$$

$$\rightarrow C_2O_3^- + M + \text{rest} \quad (6)$$

$$\rightarrow C_4O_4^- + \text{rest} \quad (7)$$

$$\rightarrow C_5O_3H_4^- + \text{rest} \quad (8)$$

Few remarks should be added at this point. First, the ion yield curves shown in Fig. 3 were measured on the TEM-QMS instrument. Out of the channels above, only the parent anion M^- was detected on the DEA-TOF instrument. Fig. 5 shows the log–log plot of the pressure dependence of the signal for individual ions. One can clearly see a quadratic dependence of the M^- signal, in contrast to a linear dependence of other DEA fragments, which shows that M^- is indeed created by a two-step process. The DEA-TOF instrument is operated at such pressures that the single electron–molecule collision conditions are ensured – typical drop in the electron current due to scattering by the gas molecules in the collision chamber is less than 5% in a length of 6 cm. Its operation at higher pressures is also hindered by the use of a multichannel plate located in the same vacuum chamber as the collision cell. In the TEM-QMS instruments, much higher local pressures in the collision chamber can be used (the quadrupole and channeltron are located in a differentially pumped chamber). The difference in local pressures used in the two instruments is the most probable cause of the fact that all of the reactions (3)–(8) are observed in TEM-QMS while only channel 4 is observed in DEA-TOF. It should also be mentioned that this dimerization cannot contribute to the surprisingly low cross section in the

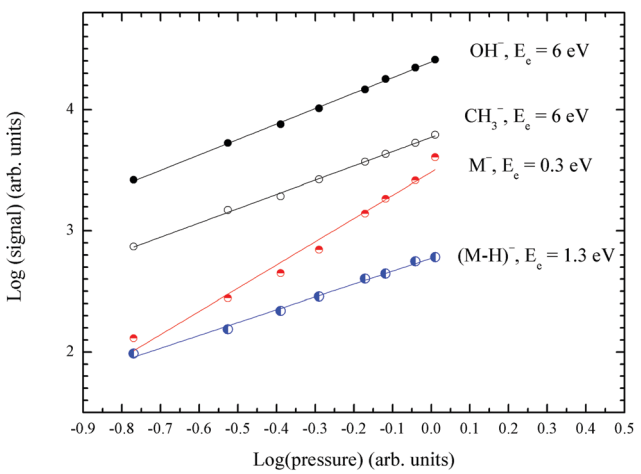

Fig. 5 A Log–log plot of the pressure dependence of several fragment anions, recorded on DEA/TOF (absolute setup). The slopes of the straight lines as determined from the least squares fitting are: 1.27 for OH^-, 1.17 for or CH_3^-, 1.96 for M^- and 1.08 for $(M - H)^-$.

$(M - H)^-$ dehydrogenation channel at 1.3 eV, since at this energy its pressure dependence is linear (Fig. 5).

While the occurrence of anion–molecule reactions in the TEM-QMS instrument is rather common,[34] pyruvic acid is the first molecule that shows such an effect in DEA-TOF (since the construction of the spectrometer in 2009). This suggests an unusually high cross section for the $M^{\#-}$ + M collisions. Few factors can contribute to this.

• First, the long-range interactions between $M^{\#-}$ and M lead to high cross section for their collision.[35] This can be quantitatively estimated to be a capture cross section in a classical collision of these two partners. For a central potential of the form $V(r) = -a/r^4$ this is $\sigma_{capt} = \pi\sqrt{8\frac{a}{\mu v^2}}$ (*e.g.*, ref. 36), where μ is the reduced mass of the collision partners and v is their relative velocity. The ion induced dipole interaction potential is readily given as $V_{induced}(r) = -\frac{1}{4\pi\varepsilon_0}\frac{\alpha e^2}{r^4}$, with α being the polarizability volume of pyruvic acid (7.3 Å^3). For the (dominant) contribution of the ion–permanent dipole interaction to the capture cross section, one should in principle use the average-dipole orientation theory[37] or one of its modifications.[38] However, for a rough estimate we will use the fact that the orientation-averaged ion–dipole interaction potential at gas temperature T is[39] $V_{dip}(r) = -\frac{1}{6k_BT}\left(\frac{ed}{4\pi\varepsilon_0}\right)^2\frac{1}{r^4}$ and the same expression for the capture cross section can be used. Here d is the dipole moment of pyruvic acid (2.3 Debye) and k_B is the Boltzmann constant. Using the mean thermal relative velocity $v = \sqrt{\frac{8kT}{\pi\mu}}$, we arrive at the capture cross section σ_{capt} = 702 Å^2. At a pressure of 5×10^{-4} mbar, this corresponds to a mean collision time of 31 μs.

In DEA-TOF, the anions exit the collision chamber approximately 1 μs after their creation. Based on the outlined rough estimate, a small fraction of the transient anions, in particular at the low-energy part of the Maxwell–Boltzmann distribution (higher σ_{capt}), will undergo collisional complex formation with neutral pyruvic acid. However, a wide range of organic molecules with similar molecular parameters (which lead to similar σ_{capt} values) do not show such an efficient dimerization, and the long-range interaction itself thus cannot be its single cause.

• Another effect contributing to the high cross section for the collisional complex formation is that $M^{\#-}$, the transient anion formed at very low electron energies, may have a form similar to dipole-bound anion states. These have a diffuse excess electron with large spatial extent[40] which leads to the large geometrical cross section of the anion.

• Finally, strong short-range interactions can contribute to an efficient energy transfer in reactions (3)–(8): the collision of a pyruvic acid anion with its neutral counterpart will probably lead to the formation of the double hydrogen bond, such as drawn in Fig. 1. It has been suggested theoretically[41,42] for a number of hydrogen bonded systems – and shown experimentally for the formic acid dimer[43] – that such situation induces ultrafast (barrierless) proton transfer along such bonds. The negatively charged partner attracts a proton from the neutral partner, yielding an anion–radical pair.

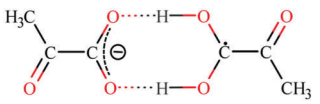

The resulting complex will be vibrationally hot due to the energy released by the proton transfer. The observed channels (3)–(8) bring useful insight into the subsequent dissociation of such a complex. The intact dimer anion is not observed, and the heat capacity does not allow its survival on the detection scale of the present experiments. Instead, it fragments *via* releasing an H-atom (forming $(2M - H)^-$) or *via* decaying into smaller fragments: intact monomer anion M^-, dehydrogenated monomer anion $(M - H)^-$, which can further release a methyl group and form $C_2O_3^-$. Both the fragments corresponding to m/z = 112 (channels (7) and (8)) require a rather complex rearrangement of the collisional complex.

Interestingly, all of these anions in Fig. 3 show weak bands at the energies of Feshbach resonances described in the previous section. The corresponding transient anions clearly induce similar anion–molecule reactions, albeit with lower probability than the transient anion formed close to 0 eV.

4 Conclusions

We have measured the dissociative electron attachment cross section in pyruvic acid. A rich fragmentation pattern has been revealed, with the strongest dissociation channel being the cleavage of a carbon-hydroxyl bond producing OH^- at electron energies around 6 eV. The cleavage of the hydroxyl bond that leads to the production of the $(M - H)^-$ anion – the channel normally dominant in a range of biologically relevant molecules[7] – has a lower cross section approximately by a factor of 12. All the observed DEA bands can be assigned to dipole-supported σ* resonances, π* resonances or Feshbach resonances.

We have observed several fragments that clearly cannot originate from the DEA to single pyruvic acid molecules; all of them are visible at electron energies close to 0 eV. The pressure dependence shows that their origin is in secondary reactions of the transient $M^{\#-}$ with other pyruvic acid molecules. Such reactions most probably proceed *via* a fast proton transfer from neutral pyruvic acid to the anion that forms a vibrationally hot dimer complex and induces the fragmentation.

The observed behavior has a consequence on our understanding of the electron-triggered processes in denser environments. Much effort has been dedicated to understanding the bond-breaking processes in individual molecular components of, for example, biological tissues of the upper atmosphere.[7,23] Several approaches have been developed to study the effect of the environment (*e.g.*, hydrogen bonding) on such bond-breaking, for example, by probing electron-induced chemistry in solid layers[10] or in hydrogen-bonded clusters.[44,45] In such cases, the target molecules are part of a molecular network

prior to the electron interaction. The present work untangles a slightly different mechanism: the primary electron first reacts with an isolated molecule that subsequently reacts with its environment. We show that such a reaction in pyruvic acid is surprisingly efficient (is operative even at pressure on the order of 0.5×10^{-3} Torr) and leads to a completely different fragmentation behavior. Importantly, it also shifts the range of relevant electron energies from relatively high ones (around 6 eV) to thermal energies close to 0 eV.

Conflicts of interest

There are no conflicts to declare.

Acknowledgements

The work was supported by the Czech Science Foundation projects no. 17-04844S and 16-10995Y.

References

1 R. W. Talbot, M. O. Andreae, H. Berresheim, D. J. Jacob and K. M. Beecher, *J. Geophys. Res.*, 1990, **95**, 16799.
2 R. J. Rapf and V. Vaida, *Phys. Chem. Chem. Phys.*, 2016, **18**, 20067–20084.
3 E. C. Griffith, R. K. Shoemaker and V. Vaida, *Origins Life Evol. Biospheres*, 2013, **43**, 341–352.
4 M. I. Guzman and S. T. Martin, *Astrobiology*, 2009, **9**, 833–842.
5 G. Cooper, C. Reed, D. Nguyen, M. Carter and Y. Wang, *Proc. Natl. Acad. Sci. U. S. A.*, 2011, **108**, 14015–14020.
6 G. G. Gomez-Tejedor and M. C. Fuss, *Radiation Damage in Biomolecular Systems*, Springer, Netherlands, 2012.
7 I. Baccarelli, I. Bald, F. A. Gianturco, E. Illenberger and J. Kopyra, *Phys. Rep.*, 2011, **508**, 1–44.
8 J. Lengyel, M. Ončák, J. Fedor, J. Kočišek, A. Pysanenko, M. K. Beyer and M. Fárnk, *Phys. Chem. Chem. Phys.*, 2017, **19**, 11713–12560.
9 M. C. Boyer, N. Rivas, A. A. Tran, C. A. Verish and C. R. Arumainayagam, *Surf. Sci.*, 2016, **652**, 26–32.
10 J. H. Bredehoft, E. Bohler, F. Schmidt, T. Borrmann and P. Swiderek, *ACS Earth Space Chem.*, 2017, **1**, 50–59.
11 M. Stepanović, Y. Pariat and M. Allan, *J. Chem. Phys.*, 1999, **110**, 11376.
12 O. May, J. Fedor, B. C. Ibanescu and M. Allan, *Phys. Rev. A: At., Mol., Opt. Phys.*, 2008, **77**, 040701(R).
13 O. May, J. Fedor and M. Allan, *Phys. Rev. A: At., Mol., Opt. Phys.*, 2009, **80**, 012706.
14 R. Janečková, D. Kubala, O. May, J. Fedor and M. Allan, *Phys. Rev. Lett.*, 2013, **111**, 203201.
15 B. C. Ibanescu, O. May, A. Monney and M. Allan, *Phys. Chem. Chem. Phys.*, 2007, **9**, 3163.
16 R. Janečková, O. May and J. Fedor, *Phys. Rev. A: At., Mol., Opt. Phys.*, 2012, **86**, 052702.
17 E. G. Schnitzler, N. A. Seifert, S. Ghosh, J. Thomas, Y. Xu and W. Jäger, *Phys. Chem. Chem. Phys.*, 2017, **19**, 4440–4446.
18 I. D. Reva, S. G. Stepanian, L. Adamowicz and R. Fausto, *J. Phys. Chem. A*, 2001, **105**, 4773–4780.
19 G. Silva, *J. Phys. Chem. A*, 2016, **120**, 276–283.
20 V. S. Prabhudesai, D. Nandi, A. H. Kelkar, R. Parajuli and E. Krishnakumar, *Chem. Phys. Lett.*, 2005, **405**, 172–176.
21 W. Sailer, A. Pelc, M. Probst, J. Limtrakul, P. Scheier, E. Illenberger and T. D. Märk, *Chem. Phys. Lett.*, 2003, **378**, 250–256.
22 R. Abouaf, *Chem. Phys. Lett.*, 2008, **451**, 25–30.
23 I. I. Fabrikant, S. Eden, N. J. Mason and J. Fedor, *Adv. At., Mol., Opt. Phys.*, 2017, **66**, 546–657.
24 T. N. Rescigno, C. S. Trevisan and A. E. Orel, *Phys. Rev. Lett.*, 2006, **96**, 213201.
25 G. A. Gallup, P. D. Burrow and I. I. Fabrikant, *Phys. Rev. A: At., Mol., Opt. Phys.*, 2009, **79**, 042701.
26 K. M. Marstokk and H. Mollendal, *J. Mol. Struct.*, 1974, **20**, 257–267.
27 H. Kim, R. Keller and W. D. Gwinn, *J. Chem. Phys.*, 1962, **37**, 2748.
28 I. I. Fabrikant, *J. Phys. B: At. Mol. Phys.*, 2016, **49**, 222005 (1–20).
29 S. P. McGlynn and J. L. Meeks, *J. Electron Spectrosc. Relat. Phenom.*, 1975, **6**, 269–279.
30 D. Kubala, K. Regeta, R. Janecková, J. Fedor, S. Grimme, A. Hansen, P. Nesvadba and M. Allan, *Mol. Phys.*, 2013, **111**, 2033–2040.
31 R. Janečková, O. May, A. R. Milosavljević and J. Fedor, *Int. J. Mass Spectrom.*, 2014, **365–366**, 163.
32 J. L. Meeks, H. J. Maria, P. Brint and S. P. McGlynn, *Chem. Rev.*, 1974, **75**, 603–610.
33 F. Gianturco, R. Lucchese, J. Langer, I. Martin, M. Stano, G. Karwasz and E. Illenberger, *Eur. Phys. J. D*, 2005, **35**, 417–428.
34 B. C. Ibanescu, PhD thesis, University of Fribourg, 2009.
35 A. Chachereau, J. Fedor, R. Janečková, J. Kočišek, M. Rabie and C. M. Franck, *J. Phys. D: Appl. Phys.*, 2016, **49**, 375201.
36 L. D. Landau and E. M. Lifshitz, *Mechanics*, Butterworth-Heinenann, 1981.
37 T. Su and M. T. Bowers, *Int. J. Mass Spectrom.*, 1975, **17**, 211–212.
38 E. T.-Y. Hsieh and A. W. Castleman, *Int. J. Mass Spectrom.*, 1981, **40**, 295–329.
39 J. O. Hirschfelder, *Intermolecular Forces*, Interscience (Wiley), New York, 1967.
40 M. Gutowski, K. D. Jordan and P. Skurski, *J. Phys. Chem. A*, 1998, **102**, 2624–2633.
41 R. A. Bachorz, M. Harańczyk, I. Dąbkowska, J. Rak and M. Gutowski, *J. Chem. Phys.*, 2005, **122**, 204304 (1–7).
42 Z. G. Keolopile, M. Gutowski, A. Buonaugurio, E. Collins, X. Zhang, J. Erb, T. Lectka, K. H. Bowen and M. Allan, *J. Am. Chem. Soc.*, 2015, **137**, 14329–14340.
43 M. Allan, *Phys. Rev. Lett.*, 2007, **98**, 123201 (1–4).
44 J. Kočišek, A. Pysanenko, M. Fárnk and J. Fedor, *J. Phys. Chem. Lett.*, 2016, **7**, 3401–3405.
45 J. Lengyel, J. Kočišek, M. Fárnk and J. Fedor, *J. Phys. Chem. C*, 2016, **120**, 7397–7402.

THE JOURNAL OF PHYSICAL CHEMISTRY Letters

Addition/Correction

Cite This: J. Phys. Chem. Lett. 2019, 10, 7397−7397

pubs.acs.org/JPCL

Correction to "K-Shell Excitation and Ionization of a Gas-Phase Protein: Interplay between Electronic Structure and Protein Folding"

Aleksandar R. Milosavljević,* Christophe Nicolas, Miloš Lj. Ranković, Francis Canon, Catalin Miron, and Alexandre Giuliani

J. Phys. Chem. Lett. **2015**, *6*, 16, 3132−3138. DOI: 10.1021/acs.jpclett.5b01288

In Figure 3 of our original Letter,[1] the valence shell ionization energies (IEs) taken from an earlier paper[2] to compare with our inner-shell IEs represent by mistake IEs of the cytochrome C instead of the ubiquitin protein. We report here the corrected Figure 3 from ref 1 with the valence shell ionization energies of ubiquitin previously published in ref 2. The figure still illustrates a good correlation between inner-shell and valence shell IE charge-state dependence. Therefore, despite the mistake in reporting previously published data, all the conclusions given in our original Letter remain valid.

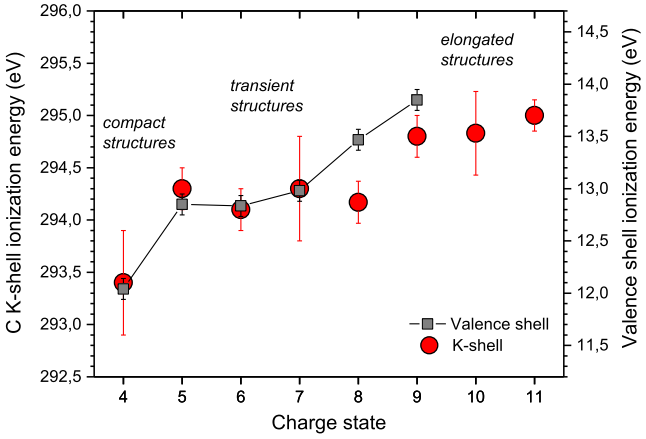

Figure 3. K-shell (circles) and valence-shell (squares)[7] ionization energies of protonated ubiquitin precursor as a function of the charge state.

REFERENCES

(1) Milosavljević, A. R.; Nicolas, C.; Ranković, M. Lj.; Canon, F.; Miron, C.; Giuliani, A. K-Shell Excitation and Ionization of a Gas-Phase Protein: Interplay Between Electronic Structure and Protein Folding. *J. Phys. Chem. Lett.* **2015**, *6*, 3132−3138.

(2) Giuliani, A.; Milosavljević, A. R.; Hinsen, K.; Canon, F.; Nicolas, C.; Réfrégiers, M.; Nahon, L. Structure and Charge-State Dependence of the Gas-Phase Ionization Energy of Proteins. *Angew. Chem., Int. Ed.* **2012**, *51*, 9552−9556.

Published: November 19, 2019

DOI: 10.1021/acs.jpclett.9b03345
J. Phys. Chem. Lett. 2019, 10, 7397−7397

PCCP

PAPER

View Article Online
View Journal

Cite this: DOI: 10.1039/c9cp02188d

Dissociative ionization dynamics of dielectric gas C_3F_7CN†

M. Ranković, [a] J. Chalabala,[b] M. Zawadzki, [ac] J. Kočišek, [a] P. Slavíček [ab]* and J. Fedor [a]*

Received 18th April 2019,
Accepted 2nd July 2019

DOI: 10.1039/c9cp02188d

rsc.li/pccp

Fluoronitrile C_3F_7CN is a promising candidate for the replacement of SF_6 dielectric gas in high-voltage insulation. We present a combined experimental and theoretical study on its ionization dynamics probed in the 0–100 eV energy range. We exploited the total ion collection technique to determine the absolute ionization cross section, mass spectrometry to determine the fragment branching ratios and *ab initio* nonadiabatic molecular dynamics to simulate the ionization process. The latter two approaches showed the dominating presence of the CF_3^+ cation over the whole electron energy range. The Binary-Encounter-Bethe (BEB) approximation reproduces experimental cross sections very well and reveals that the ionization from a surprisingly large number of orbitals contributes almost equally to the processes. We show that the initially populated cation excited states undergo an ultrafast internal conversion to the ground state where the dissociation into a single decay channel takes place. Implications for the use of C_3F_7CN as an insulating material are discussed.

1 Introduction

Heptafluoroisobutyronitrile (C_3F_7CN) is one of the most promising alternatives to SF_6. SF_6 is widely used as an insulator in high-voltage circuits and switchgear, however, it has an extremely high global warming potential (GWP) of 23 500. C_3F_7CN has also a high dielectric strength[1] and is environmentally much friendlier. The 100 year GWP of the pure gas is estimated between 1490 and 3650.[2,3] Moreover, due to the vapor pressure constraints, it is not used pure, but in mixtures with a buffer gas, which further reduces the GWP.[4] Depending on the mixing ratio, it can drop down to 230.[1] Several companies (*e.g.*, Alstom or GE Grid) already offer switchgear with fillings based on C_3F_7CN and several pilot installations are in operation around the world.[5]

In high-voltage electrical circuits, the electron collisions are the elementary mechanism driving the physics and chemistry of the discharges inception and extinction during the high-voltage switching. Due to the novelty of the C_3F_7CN as the insulation medium, little data is available on these elementary processes. The ionization cross section has been calculated by Xiong *et al.*[6] using a modified Deutsch–Märk formalism and the electron attachment rate constants have been reported by Chachereau *et al.*[1] Apart from these works, there is one experimental[7] and a number of recent theoretical[8–11] studies probing the macroscopic discharges containing C_3F_7CN.

In the present paper, we report the experimental absolute partial cross sections and electron impact ionization mass spectra of C_3F_7CN. We also did theoretical calculations of the bonding characters and potential energy surfaces (PES) of ionized and neutral C_3F_7CN, and the non-adiabatic molecular dynamics simulations triggered by the ionization. We show that the ionization leads almost exclusively to the molecular decomposition, creating reactive radicals, which may influence the long-term stability of the insulating medium.

2 Methods

2.1 Experiment

Two setups were used for the present study.

The absolute total ionization cross section was measured on a total ion collection setup. It was originally constructed for quantitative dissociative electron attachment experiments[12–14] and recently adapted to measure also positive ionization cross section.[15] A magnetically collimated beam of electrons with a well defined energy is produced by a trochoidal electron monochromator and passes through the collision cell filled with the target gas. The analogue positive ion current is recorded on an U-shaped ion collector, surrounding the electron beam path.

[a] *J. Heyrovský Institute of Physical Chemistry, Czech Academy of Sciences, Dolejškova 3, 18223 Prague, Czech Republic. E-mail: juraj.fedor@jh-inst.cas.cz*
[b] *Department of Physical Chemistry, University of Chemistry and Technology, Technická 5, 16628 Prague, Czech Republic. E-mail: petr.slavicek@vscht.cz*
[c] *Department of Atomic, Molecular, and Optical Physics, Faculty of Applied Physics and Mathematics, Gdańsk University of Technology, ul. G. Narutowicza 11/12, 80233 Gdańsk, Poland*

† Electronic supplementary information (ESI) available. See DOI: 10.1039/c9cp02188d

The local pressure in the collision cell is monitored by a capacitance manometer and kept in the range of 3–6 $\times$ 10^{-4} mbar, in order to ensure the single-collision conditions. The electron current is monitored in a Faraday cup placed after the collision cell. The cross section calibration procedure has been described recently in detail in ref. 15. The uncertainly of the absolute values is $\pm$20%.

The mass spectra at individual electron energies were measured using a reflectron time-of-flight (RTOF) setup.[16,17] Here, the electron beam is produced by a three-element lens and the whole setup is pulsed at 10 kHz repetition frequency: a 1 μs electron pulse passes the interaction region and after the electrons leave, the extraction pulse sends the cations towards the RTOF analyzer. A small amount of target gas is introduced into the background of the vacuum chamber and mass spectra are recorded as a function of the electron energy as two-dimensional data files. The individual ion yields are then normalized to the data from the total-ion collection setup and partial cross sections are determined. In contrary to the total ion collection setup, the ion extraction in this pulsed setup may suffer from the discrimination towards very fast ions. We have addressed this issue by comparing the sum of individual RTOF ion yields (corrected by the value of the weakly energy-dependent electron current) with the shape of the total cross section from the first setup. The agreement between the two data sets (within 10%) suggests almost full angular and kinetic energy acceptance of the RTOF setup in the probed electron energy range.

2.2 *Ab initio* modelling

2.2.1 Electronic structure. First, we optimized the geometries of ground neutral and ionized states of C_3F_7CN with Becke half and half density functional (BHandHLYP)[18] and 6-31G* basis set. For both optimized geometries, we analyzed character of the bonds with the Mayer bond order approach.[19] Dissociation energies were calculated using density-fitted, explicitly correlated, second-order Møller–Plesset perturbation theory within the spin-restricted, open-shell formalism (denoted further as MP2-F12)[20] with aug-cc-pVTZ basis set. The ionization energies of the neutral molecule were probed using the equation of motion ionization potential with the coupled clusters singles, doubles and perturbative triples method (EOM-IP-CCSD(dT)),[21,22] with the aug-cc-pVTZ basis set.

The ionization dynamics of C_3F_7CN was investigated by semiclassical nonadiabatic molecular simulations based on Tully's fewest switches surface hopping[23] (SH) scheme. As an electronic structure method, we chose the floating occupation molecular orbital complete active space configuration interaction (FOMO-CASCI)[24] approach which is an efficient and stable alternative to the complete active space self consistent field method (CASSCF).[25–27] The FOMO-CASCI nuclear gradients[28] and nonadiabatic couplings (NAC)[29] have been recently implemented in the TeraChem code[30,31] which is tailored for calculations on the graphics processing units (GPUs). The FOMO-CASCI method was shown to be suitable for nonadiabatic dynamics of excited and ionized states.[25,26] The active space comprised 13 electrons in the 7 highest occupied molecular orbitals and one virtual orbital (further noted as 13,8). This active space included C–C and C–F bonding orbitals necessary to describe dissociation processes. Larger active spaces were tested; however, these showed to be computationally too expensive and unstable during the dynamical simulations. All dynamical calculations were performed with the 6-31G* basis set. Details on the SH algorithm and its implementation in our in-house code ABIN[32] coupled with TeraChem was described in our previous study.[26]

In total, simulations for 6 lowest ionized states were performed with 100 independent trajectories per each state. The simulation time step was set to 10 a.u. and overall simulation time was 500 fs. Initial position were equidistantly extracted from 45 ps long path-integral molecular dynamics of neutral system that run again in the ABIN code. The dynamics was accelerated with the generalized Langevin equation (scheme known as PI-GLE[33,34]) at 300 K. Forces and energies required during the PI-GLE dynamics were calculated at the B3LYP[35,36]/6-31+G* level in the TeraChem code. The resulting data of the time-dependent populations and product channels were smoothed by the seventh-order, 33 point Savitzky–Golay filter. The populations were assigned standard errors based on binomial distribution with 95% confidence interval.

The BHandHLYP geometry calculations were performed in the Gaussian 09 program,[37] the bond order analysis in the Multiwfn code,[38] the MP2-F12 energies in the Molpro2015 code,[39,40] the EOM-IP-CCSD(dT) energies in the Q-Chem 5.0 code.[41]

We have also analyzed ionization cross section as this quantity is accessible by both theory and experiments. A straightforward approach is to use Binary-Encounter-Bethe (BEB) approximation which is a quantitative model for the ionization cross section.[42] The total cross section is given as a sum of the contributions from the ionization of individual occupied molecular orbitals (MOs) of the target molecule

$$\sigma_{\mathrm{BEB}} = \sum_{i}^{\mathrm{MOs}} \sigma_i. \tag{1}$$

The contribution from an orbital with a binding energy B_i is given by

$$\sigma_i = \frac{S_i}{t_i + u_i + 1}\left[\frac{\ln t_i}{2}\left(1 - \frac{1}{t_i^2}\right) + 1 - \frac{1}{t_i} - \frac{\ln t_i}{t_i + 1}\right]. \tag{2}$$

Here $t_i = T/B_i$ and $u = U_i/B_i$ are the normalized incident (T) and orbital kinetic (U_i) energies and $S_i = 4\pi a_0^2 N(R/B_i)^2$. In these expressions a_0 = 0.529 Å is the Bohr radius, N = 2 is the orbital occupation number, and R = 13.6 eV is the Rydberg energy. The expression 2 is valid only if the orbital binding energy B_i is smaller than the electron incident energy T, otherwise the contribution of the orbital i is zero.

We have used this model with the Hartree–Fock molecular orbitals obtained with the aug-cc-pVTZ basis. Maximum 47 molecular orbitals were taken into account in the summation (1).

3 Results and discussion

3.1 Ionization cross section

The positive ionization mass spectrum of C_3F_7CN recorded at 70 eV (Fig. 1) is dominated by the CF_3^+ fragment. The next

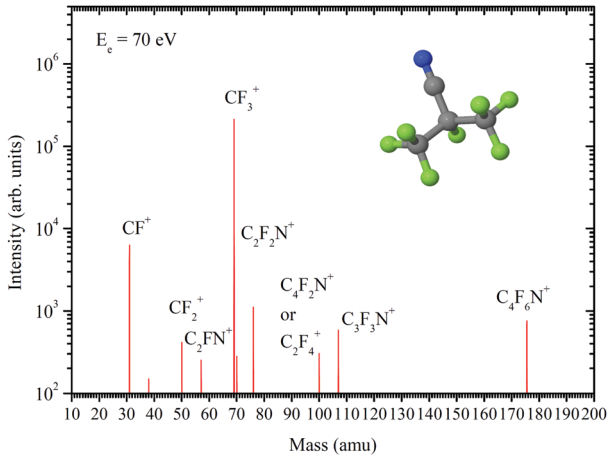

Fig. 1 Positive ionization mass spectrum of C_3F_7CN recorded at 70 eV electron energy.

fragment, CF^+, is more than 30 times weaker. The simplest fragmentation channel, removal of the fluorine atom, is few hundred times weaker. No signal of the parent ion $C_3F_7CN^+$ was detected. The ionization thus results in a complete fragmentation.

The measured total ionization cross section is shown in Fig. 2. The present BEB calculation agrees very well with the experimental values. This level of agreement might be fortuitous to some degree, taking into account the error bar of the absolute calibration and the fact, that the BEB method has been recently shown to overestimate the cross sections of fluorinated compounds by up to 30%.[43,44] Fig. 2 also shows the cross section calculated by Xiong *et al.*[6] using a modified Deutsch–Märk (DM) formalism. The DM calculation underestimates the cross section in the intermediate energy region (up to 50 eV), but the agreement is much better at higher energies. Typically, the ionization cross sections in small molecules reach values in the range of 0.5–10 Å^2 at around 100 eV electron energy.[45] The ionization of C_3F_7CN is therefore very efficient with the maximum cross section approaching 12 Å^2.

The bottom panel of Fig. 2 shows the partial cross sections obtained from the RTOF energy-dependent mass spectra, scaled to absolute values from the total ion collection setup. Here, the CF_3^+ fragment dominates over the whole energy region. The intense fragmentation is thus not limited only to high electron energies, but occurs already at the ionization threshold.

Table 1 (left column) shows the orbital energies entering into the BEB formula. Comparison with the EOM-IP-CCSD(dT) ionization energies shows that they are not fully accurate. The agreement is good for the HOMO electron, but soon they start to deviate.

Analysis of the BEB calculation shows that the contribution σ_i of the individual molecular orbitals at two incident electron energies T (see Fig. 3) appears to be similar for the full range of orbitals, though the HOMO and HOMO−1 are slightly more important. Clearly, the ionization from a wide range of orbitals contributes to the resulting cross section.

This means that the vertical ionization leads to population of a high number of ionized states, each with a hole in the corresponding orbital. Since these orbitals (see Fig. 3) have bonding or antibonding character along different bonds, one

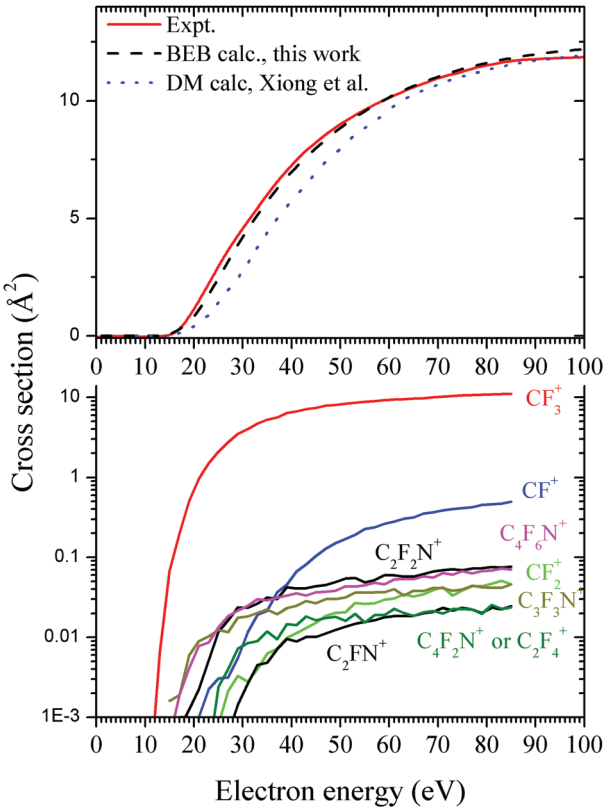

Fig. 2 (a) Total ionization cross section of C_3F_7CN. Full red line shows out experimental data obtained by total ion collection method. dashed black line calculated cross section using BEB formalism, dotted blue line calculated by Xiong *et al.*[6] using DM formalism. (b) Partial cross sections obtained by scaling the energy-dependent mass spectra.

Table 1 EOM-IP-CCSD(dT)/aug-cc-pVTZ ionization energies and Hartree–Fock orbital energies of neutral C_3F_7CN

HF Koopmans/eV	EOM-IP-CCSD(dT)/eV
14.26	13.85
14.48	14.37
16.52	14.42
16.60	15.08
17.80	15.66
18.86	16.24
19.02	16.44
19.16	16.63
19.27	16.79
19.54	17.11

would expect that dissociating directions along the cation PES of a electronic state after a vertical ionization will be different. It may seem thus somewhat surprising that almost all of these initial cation states finally lead to the same dissociation channel, the cleavage of the carbon–trifluoromethyl bond and production of ionic CF_3^+. We pay attention to this seeming puzzle in the next two sections.

3.2 Mapping the potential energy surface

Bonding characteristics of the C_3F_7CN molecule in the neutral state follows the formal chemical formula (Fig. 4), *i.e.* the molecule is

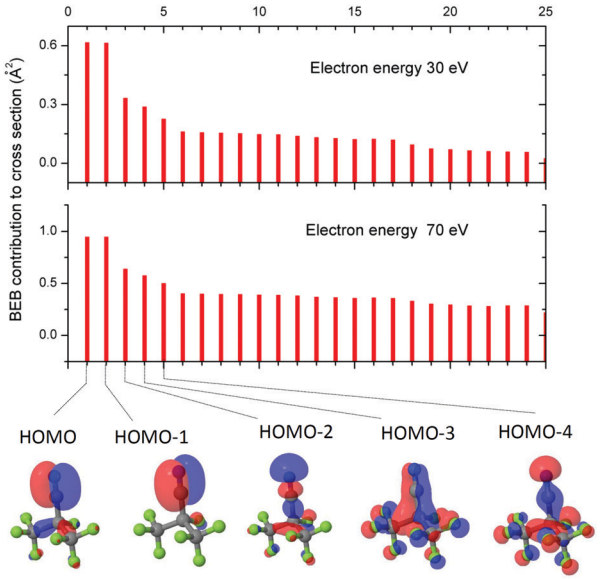

Fig. 3 BEB contributions to ionization cross section from individual molecular orbitals at two different incident electron energies. Number 1 stands for HOMO, the increasing index labels occupied orbitals with decreasing energy. The lower panel shows isosurfaces of the five highest occupied orbitals.

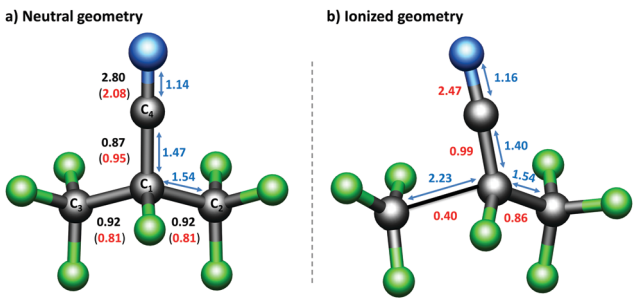

Fig. 4 Bond lengths (blue) and Mayer bond order indices of ground (a) neutral (black) and (b) ionized (red) states C_3F_7CN. Calculated at the BHandHLYP/6-31G* level, bond lengths in Å.

characterized by a triple C≡N bond and all others by a single bond. The highest occupied molecular orbital (HOMO) has a composite character, spanning the π orbitals of the CN bond and σ orbitals of the C–CF_3 bonds. Immediately upon the ionization of the HOMO electron, the bond order decreases both in the CN and C–CF_3 parts. We can therefore expect geometry relaxation leading either to CN bond prolongation or C–CF_3 bond(s) prolongation. The geometry optimization in the ground ionized state (Fig. 4b) shows that the molecule prefers relaxation *via* the C–CF_3 bond stretching. Note that this is just a local minimum calculated at the BHandHLYP/6-31G* level – it is however useful for the discussion. The CF_3 fragment is energetically almost unbound, the calculated bond order is only 0.4 and the equilibrium bond distance is 2.23 Å. As the relaxation energy at this point amounts to approximately 1 eV, the ion should fragment. This observation explains why no mother ion is observed in the experiment.

PES scan along the two C–CF_3 bonds for the geometry, with the remaining degrees of freedom fixed to the values in the neutral molecule (Fig. 5a) shows a relatively high dissociation barrier for the CF_3 group. Much lower barrier is observed for the 2D scan with the geometry parameters of BHandHLYP/6-31G* ionic minimum (Fig. 5b) and it diminishes in a fully relaxed scan (Fig. 5c). These figures indicate that the ionization dynamics of ground cation state should start by a relaxation which is then followed by a dissociation.

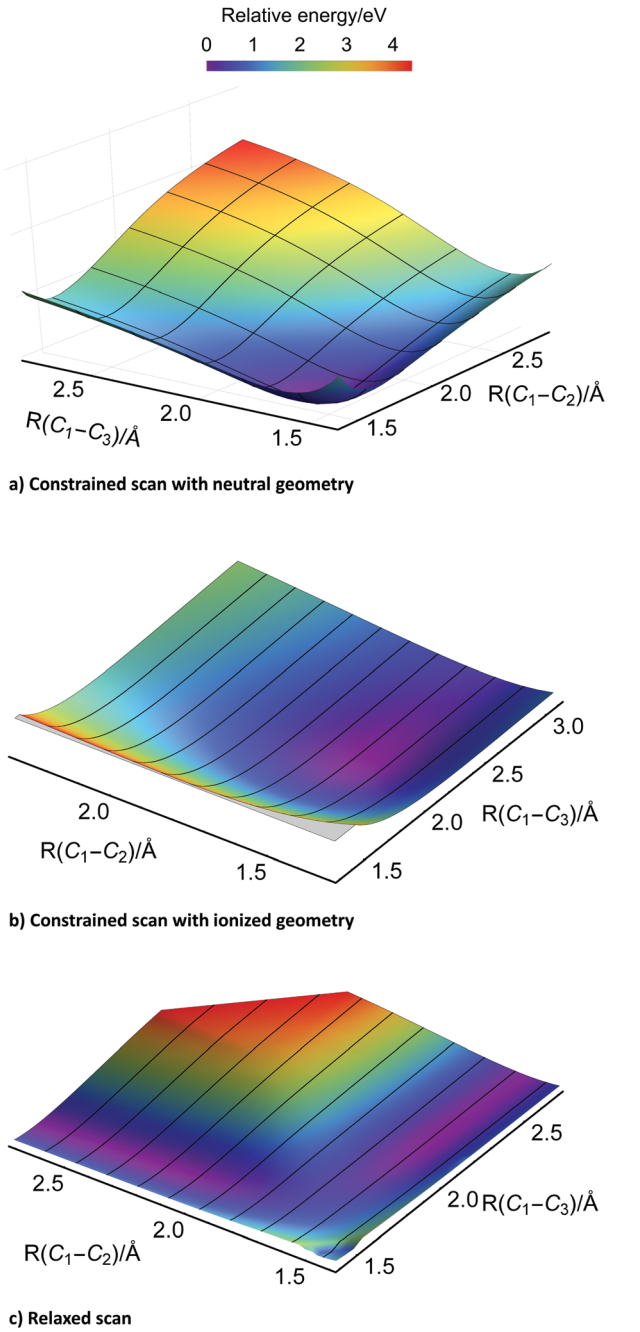

Fig. 5 Potential energy surfaces of ground state (D_0) of $C_3F_7CN^+$ along the two C–CF_3 bonds calculated at the BHandHLYP/6-31G* level. Constrained scans used fixed geometries of (a) neutral, (b) ionized molecule and (c) shows the fully relaxed PES at the BHandHLYP/6-31* level along two bond stretch.

In the ESI,† we also present potential energy surfaces at the FOMO-CASCI level for higher electronic states of the ionized molecule. The inspection of the potential energy surfaces provides only a limited insight into the dynamics, but it shows qualitative agreement with the BHandHLYP PESs. Fig. S3 (ESI†) also demonstrates the conical intersections, allowing for funneling of the electronic population to the ground state.

Let us now ask what are other possible products which might be open at higher ionization energies. The threshold energies for the dissociation into individual ionic fragments shown in Table 2 were obtained as the difference between total energies of the products and the neutral molecule.

The results show only little correspondence between the observed products and the asymptotic threshold energies. For example, the carbon–trifluoromethyl bond cleavage with an opposite charge distribution yielding $C_3F_4N^+$ + CF_3 has a relatively low threshold of 14.0 eV, however, it is not observed at all in the experiment. The CF^+ fragment has relatively high threshold energy of 17.48 eV. This is visible also in the partial cross sections in Fig. 2b, where this fragment has a high onset, however, with the increasing electron energy it becomes the second most abundant fragment. The energetically most accessible channel (E_{th} = 11.61 eV) is the one leading to the production of $C_3F_3N^+$ with the tetraflouromethane CF_4 as the neutral product. However, this reaction requires rather complex rearrangement (fluorine atom transferred between the two trifluoromethyl groups) which may be a reason for its low probability.

Table 2 MP2-F12/aug-cc-pVTZ dissociation energies of fragmentation channels of $C_3F_7CN^+$. Zero point energy corrections are not included (the values calculated at the BHandHLYP/6-31g* level are shown in parentheses). The inset pictures show molecules or fragments where the structure is not obvious from the summation formula

Products			m/z	E_{th} (eV)
CF_3^+	+	C_3F_4N 	69	12.74(−0.08)
CF^+	+	C_3F_4N+F_2	31	20.88(−0.31)
CF^+	+	C_3F_5N+F 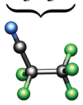	31	17.71(−0.23)
$C_3F_4N^+$ 	+	CF_3	126	14.11(−0.11)
$C_4F_6N^+$ 	+	F	176	15.00(−0.09)
$C_4F_6N^+$ 	+	F	176	15.88(−0.13)
$C_3F_3N^+$ 	+	CF_4	107	11.68(−0.07)
$C_3F_3N^+$ 	+	CF_4	107	14.36(−0.16)
$C_3F_7^+$ 	+	CN	107	15.30(−0.13)

3.3 Non-adiabatic dynamics

Mapping the potential energy surfaces provides only a limited access to the real dynamics as we inevitably rely on the proper selection of the reaction coordinates. This is a difficult task when we explore the dynamics in polyatomic molecules. The ultrafast dynamics is conveniently revealed by techniques of non-adiabatic dynamics. Within the *ab initio* context, we typically use trajectory-based approaches such as surface hopping or *ab initio* multiple spawning approach.[46,47] While the field of non-adiabatic simulations gradually reaches maturity, relatively small attention was paid to the dynamics upon the ionization.[25,48–53]

It is often assumed that the ionization is followed by a rapid internal conversion process $D_n \rightarrow D_{n-1} \rightarrow \rightarrow D_0$ followed by the dynamics on the hot ground ionized state D_0. The dynamical simulations are then typically performed within the Born–Oppenheimer molecular dynamics.[53–55] However, such an approach is not always justified, especially when the molecule decomposes very fast.[50,51] Here we therefore consider explicitly the coupling between electronic and nuclear dynamics.

The first question to address is whether the dissociation takes place (i) directly on the upper electronic state or (ii) *via* rapid internal conversion to the ground state and the subsequent statistical fragmentation. To answer this question, we plot the time development of the electronic population following the ionization in Fig. 6. We consider ionization into different initial states, corresponding to electron removal from different molecular orbitals. We observe no significant electron population transfer during the dynamics in the cationic ground state. When the HOMO−1 electron is ejected, there is a very fast, sub-100 fs population transfer into the ground electronic state. The population dynamics is somewhat slower in the higher electronic states yet still significant fraction of the electronic population reaches the ground electronic states within the simulation time of 500 fs. We also observe that higher electronic states are temporarily populated. Overall, we can conclude that internal conversion is very fast in the $C_3F_7CN^+$ ion and major part of the dynamics proceeds according to the scenario (ii). The dominance of a single product channel is in agreement with this finding.

Next, we ask what are the products and what is the timescale of their formation. The results are shown in Fig. 7. Given the

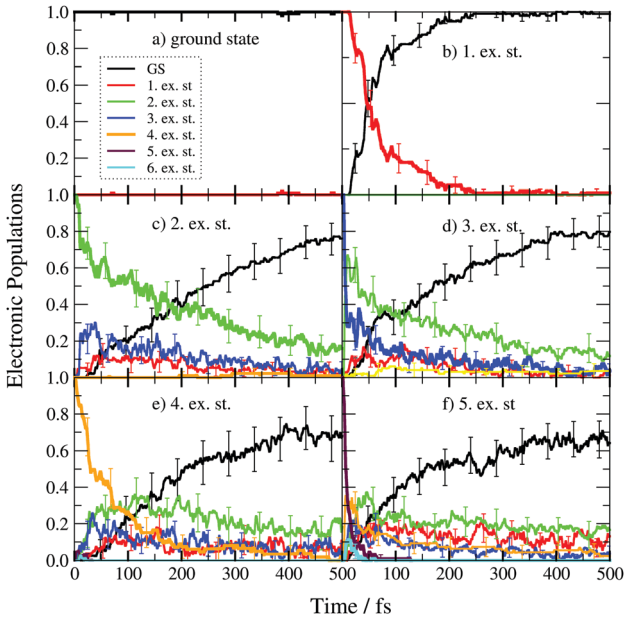

Fig. 6 Time evolution of the electronic state populations upon the ionization into the (a) ground (D_0) and (b–f) excited electronic states (D_1, D_2, D_3, *etc.*) of the $C_3F_7CN^+$ ion. Dynamics calculated at the FOMO-CASCI(13,8)/6-31g* level. Each curve denotes a normalized average electronic state number occupation over a set of 100 trajectories, *e.g.* graph (b) shows the dynamics of electronic states of a set of trajectories representing a wavepacket promoted initially into the D_1 first excited state.

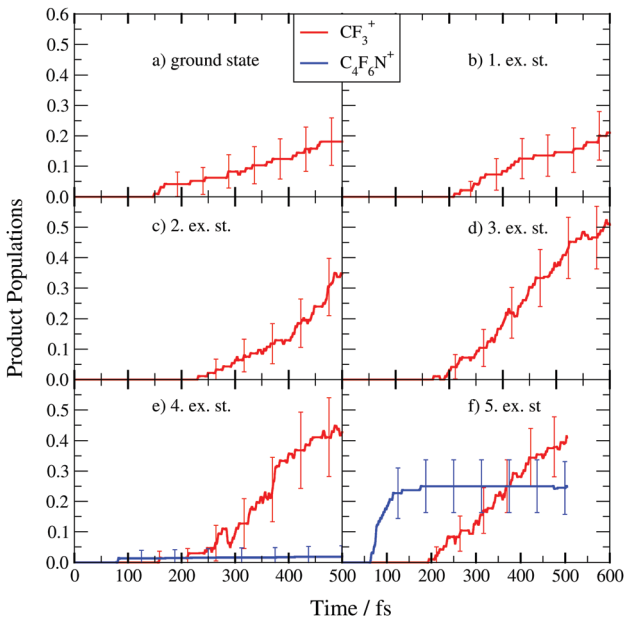

Fig. 7 Time evolution of reaction product populations of the ionized $C_3F_7CN^+$ radical cation upon ionization into the (a) ground (D_0) and (b–f) excited states (D_1, D_2, D_3, *etc.*). Dynamics calculated at the FOMO-CASCI(13,8)/6-31g* level. In all panels, the red curves correspond to the CF_3^+ radical which dissociates from the complex, blue curve correspond to the neutral F radical atom.

very fast internal conversion process discussed above, it is not surprising that the dominant fragment is the formation of the CF_3^+ fragment. This corresponds well to the barrierless pathway observed on the cation ground state potential energy scans (Fig. 5). However, the dissociation, while spontaneous, is by no means instantaneous. The process takes hundreds of femtoseconds even in the ground electronic state. This is again in accord with the shape of the PES 2D scans (Fig. 5), the molecule needs first to adjust its geometry before the dissociation is allowed. The timescale for the fragment formation is slightly shifted towards longer times for higher states as the system needs more time to relax to the lower electronic states.

In the 5th excited state, the fluorine radicals are produced, however in rather small quantities, which is in accord with the experimental data. No other products were observed in our simulations and we therefore conclude that the observed pathways represent the primary decomposition channels. We should keep in mind, however, that products of very different internal energies are formed upon the ionization of different electrons. For example, when fluorine atom departs, hot ionic fragment is left behind. This fragment can then further decompose on timescales longer than present simulations. Providing that the theory faithfully describes the ultrafast dynamics, the other ions observed in the experiment are likely the secondary products of the ionization process.

4 Conclusions

In conclusion, we have measured the ionization cross section of fluoronitrile C_3F_7CN in the range of 0 to 100 eV. The cross section reaches relatively high values. The ionization is completely dissociative, by far the most abundant fragment anion is CF_3^+.

Computational treatment of the ionization process showed that a broad range of cation states is initially formed, corresponding to holes in various molecular orbitals. The subsequent non-adiabatic dynamics is characterized by a fast internal conversion of these states into the ground cation electronic state and the subsequent dissociation into the CF_3^+ asymptotic limit. However, we observe also products which do not result from the dynamics on the hot ground electronic states, particularly the abstraction of the fluorine atom. The remaining ionic products are then probably fragments resulting from a dissociation of the two primary reaction channels. This picture is in a full agreement with the experimental observations.

Let us turn to the implications of the present findings to the use of C_3F_7CN in high-voltage insulation. The electric breakdown, or any gas discharge, is always accompanied by an electron avalanche from the ionization processes. As we show, almost each ionization event destroys the molecule and leads to the production of radicals, mainly the C_3F_4N shown in the second line of Table 2. This does not necessarily lead to the deterioration of the insulating medium: a good example is sulfur hexafluoride itself, where the ionization is also completely fragmentative.[56] In bulk SF_6 gas, the majority of created radicals recombines and reacts to form SF_6 again. Still, a small fraction of these leads to the creation of toxic decomposition products.[57]

The radical chemistry in C_3F_7CN is not known at the moment and ionization products may react to form different species than the original gas. We conclude, that it is important to pay attention to this issue in the future and suggest that the macroscopic discharge chemistry in C_3F_7CN is carefully probed. The first experiments with discharges[7,58,59] indeed indicate a rich plasma chemistry of this gas.

Conflicts of interest

There are no conflicts to declare.

Acknowledgements

This work is part of the project No. TH03020063 of the Technological Agency of the Czech Republic.

References

1 A. Chachereau, A. Hoessl and C. M. Franck, *J. Phys. D: Appl. Phys.*, 2018, **51**, 495201.
2 M. P. S. Andersen, M. Kyte, S. T. Andersen, C. J. Nielsen and O. J. Nielsen, *Environ. Sci. Technol.*, 2017, **51**, 1321–1329.
3 S. Blazquez, M. Antiolo, O. J. Nielsen, J. Albaladejo and E. Jimnez, *Chem. Phys. Lett.*, 2017, **687**, 297–302.
4 Y. Kieffel, *2016 IEEE International Conference on Dielectrics (ICD)*, 2016.
5 E. Laruelle, A. Ficheux, Y. Kieffel and M. Waldron, *Cigre Science and Engineering*, 2017, 102–108.
6 J. Xiong, X. Li, J. Wu, X. Guo and H. Zhao, *J. Phys. D: Appl. Phys.*, 2017, **50**, 445206.
7 Y. Li, X. Zhang, S. Xiao, Q. Chen, J. Tang, D. Chen and D. Wang, *Ind. Eng. Chem. Res.*, 2018, **57**, 5173–5182.
8 X. Zhang, Y. Li, D. Chen, S. Xiao, S. Tian, J. Tang and R. Zhuo, *RSC Adv.*, 2017, **7**, 50663.
9 X. Zhang, Y. Li, S. Xiao, S. Tian, Z. Deng and J. Tang, *J. Phys. D: Appl. Phys.*, 2017, **50**, 325201.
10 Y. Wu, C. Wang, H. Sun, A. B. Murphy, M. Rong1, F. Yang, Z. Chen, C. Niu and X. Wang, *J. Phys. D: Appl. Phys.*, 2018, **51**, 155206.
11 Y. Li, X. Zhang, S. Xiao, Q. Chen, C. Liu and Y. Shi, *J. Flourine Chem.*, 2018, **213**, 24–30.
12 J. Fedor, O. May and M. Allan, *Phys. Rev. A: At., Mol., Opt. Phys.*, 2008, **78**, 032701.
13 O. May, J. Fedor and M. Allan, *Phys. Rev. A: At., Mol., Opt. Phys.*, 2009, **80**, 012706.
14 O. May, J. Fedor, B. C. Ibănescu and M. Allan, *Phys. Rev. A: At., Mol., Opt. Phys.*, 2008, **77**, 040701(R).
15 M. Zawadzki, *Eur. Phys. J. D*, 2018, **72**, 12.
16 J. Kočišek, J. Lengyel and M. Fárník, *J. Chem. Phys.*, 2013, **138**, 124306.
17 J. Langer, M. Zawadzki, M. Fárník, J. Pinkas, J. Fedor and J. Kočišek, *Eur. Phys. J. D*, 2018, **72**, 112.
18 A. D. Becke, *J. Chem. Phys.*, 1993, **98**, 1372–1377.
19 I. Mayer, *Chem. Phys. Lett.*, 1983, **97**, 270–274.
20 G. Knizia and H.-J. Werner, *J. Chem. Phys.*, 2008, **128**, 154103.
21 P. A. Pieniazek, S. E. Bradforth and A. I. Krylov, *J. Chem. Phys.*, 2008, **129**, 074104.
22 A. I. Krylov, *Annu. Rev. Phys. Chem.*, 2008, **59**, 433–462.
23 J. C. Tully, *J. Chem. Phys.*, 1990, **93**, 1061–1071.
24 P. Slavíček and T. J. Martínez, *J. Chem. Phys.*, 2010, **132**, 234102.
25 J. Chalabala, O. Dvořák and P. Slavíček, *Chem. Phys.*, 2018, **515**, 221–230.
26 D. Hollas, L. Šištík, E. G. Hohenstein, T. J. Martínez and P. Slavíček, *J. Chem. Theory Comput.*, 2018, **14**, 339–350.
27 E. G. Hohenstein, *J. Am. Chem. Soc.*, 2016, **138**, 1868–1876.
28 E. G. Hohenstein, M. E. F. Bouduban, C. Song, N. Luehr, I. S. Ufimtsev and T. J. Martínez, *J. Chem. Phys.*, 2015, **143**, 014111.
29 E. G. Hohenstein, *J. Chem. Phys.*, 2016, **145**, 174110.
30 I. S. Ufimtsev and T. J. Martínez, *J. Chem. Theory Comput.*, 2009, **5**, 2619–2628.
31 A. V. Titov, I. S. Ufimtsev, N. Luehr and T. J. Martínez, *J. Chem. Theory Comput.*, 2013, **9**, 213–221.
32 D. Hollas, O. Svoboda, J. Suchan, M. Ončák and P. Slavíček, *ABIN*, 2018, DOI: 10.5281/zenodo.1228462.
33 M. Ceriotti, G. Bussi and M. Parrinello, *J. Chem. Theory Comput.*, 2010, **6**, 1170–1180.
34 M. Ceriotti, D. E. Manolopoulos and M. Parrinello, *J. Chem. Phys.*, 2011, **134**, 084104.
35 C. Lee, W. Yang and R. G. Parr, *Phys. Rev. B: Condens. Matter Mater. Phys.*, 1988, **37**, 785–789.
36 A. D. Becke, *J. Chem. Phys.*, 1993, **98**, 5648–5652.
37 M. J. Frisch, G. W. Trucks, H. B. Schlegel, G. E. Scuseria, M. A. Robb, J. R. Cheeseman, G. Scalmani, V. Barone, G. A. Petersson, H. Nakatsuji, X. Li, M. Caricato, A. V. Marenich, J. Bloino, B. G. Janesko, R. Gomperts, B. Mennucci, H. P. Hratchian, J. V. Ortiz, A. F. Izmaylov, J. L. Sonnenberg, D. Williams-Young, F. Ding, F. Lipparini, F. Egidi, J. Goings, B. Peng, A. Petrone, T. Henderson, D. Ranasinghe, V. G. Zakrzewski, J. Gao, N. Rega, G. Zheng, W. Liang, M. Hada, M. Ehara, K. Toyota, R. Fukuda, J. Hasegawa, M. Ishida, T. Nakajima, Y. Honda, O. Kitao, H. Nakai, T. Vreven, K. Throssell, J. A. Montgomery, Jr., J. E. Peralta, F. Ogliaro, M. J. Bearpark, J. J. Heyd, E. N. Brothers, K. N. Kudin, V. N. Staroverov, T. A. Keith, R. Kobayashi, J. Normand, K. Raghavachari, A. P. Rendell, J. C. Burant, S. S. Iyengar, J. Tomasi, M. Cossi, J. M. Millam, M. Klene, C. Adamo, R. Cammi, J. W. Ochterski, R. L. Martin, K. Morokuma, O. Farkas, J. B. Foresman and D. J. Fox, *Gaussian 09 Revision D.01*, Gaussian Inc., Wallingford CT, 2009.
38 T. Lu and F. Chen, *J. Comput. Chem.*, 2012, **33**, 580–592.
39 H.-J. Werner, P. J. Knowles, G. Knizia, F. R. Manby and M. Schütz, *WIREs Comput. Mol. Sci.*, 2012, **2**, 242–253.
40 H.-J. Werner, P. J. Knowles, G. Knizia, F. R. Manby, M. Schütz, P. Celani, W. Györffy, D. Kats, T. Korona, R. Lindh, A. Mitrushenkov, G. Rauhut, K. R. Shamasundar, T. B. Adler, R. D. Amos, A. Bernhardsson, A. Berning,

D. L. Cooper, M. J. O. Deegan, A. J. Dobbyn, F. Eckert, E. Goll, C. Hampel, A. Hesselmann, G. Hetzer, T. Hrenar, G. Jansen, C. Köppl, Y. Liu, A. W. Lloyd, R. A. Mata, A. J. May, S. J. McNicholas, W. Meyer, M. E. Mura, A. Nicklass, D. P. O'Neill, P. Palmieri, D. Peng, K. Pflüger, R. Pitzer, M. Reiher, T. Shiozaki, H. Stoll, A. J. Stone, R. Tarroni, T. Thorsteinsson and M. Wang, *MOLPRO version 2015.1, a package of Ab Initio Programs*, 2015.

41 Y. Shao, Z. Gan, E. Epifanovsky, A. T. Gilbert, M. Wormit, J. Kussmann, A. W. Lange, A. Behn, J. Deng, X. Feng, D. Ghosh, M. Goldey, P. R. Horn, L. D. Jacobson, I. Kaliman, R. Z. Khaliullin, T. Kuz, A. Landau, J. Liu, E. I. Proynov, Y. M. Rhee, R. M. Richard, M. A. Rohrdanz, R. P. Steele, E. J. Sundstrom, H. L. Woodcock III, P. M. Zimmerman, D. Zuev, B. Albrecht, E. Alguire, B. Austin, G. J. O. Beran, Y. A. Bernard, E. Berquist, K. Brandhorst, K. B. Bravaya, S. T. Brown, D. Casanova, C.-M. Chang, Y. Chen, S. H. Chien, K. D. Closser, D. L. Crittenden, M. Diedenhofen, R. A. DiStasio Jr., H. Do, A. D. Dutoi, R. G. Edgar, S. Fatehi, L. Fusti-Molnar, A. Ghysels, A. Golubeva-Zadorozhnaya, J. Gomes, M. W. Hanson-Heine, P. H. Harbach, A. W. Hauser, E. G. Hohenstein, Z. C. Holden, T.-C. Jagau, H. Ji, B. Kaduk, K. Khistyaev, J. Kim, J. Kim, R. A. King, P. Klunzinger, D. Kosenkov, T. Kowalczyk, C. M. Krauter, K. U. Lao, A. D. Laurent, K. V. Lawler, S. V. Levchenko, C. Y. Lin, F. Liu, E. Livshits, R. C. Lochan, A. Luenser, P. Manohar, S. F. Manzer, S.-P. Mao, N. Mardirossian, A. V. Marenich, S. A. Maurer, N. J. Mayhall, E. Neuscamman, C. M. Oana, R. Olivares-Amaya, D. P. ONeill, J. A. Parkhill, T. M. Perrine, R. Peverati, A. Prociuk, D. R. Rehn, E. Rosta, N. J. Russ, S. M. Sharada, S. Sharma, D. W. Small, A. Sodt, T. Stein, D. StÄĆÄ¡ck, Y.-C. Su, A. J. Thom, T. Tsuchimochi, V. Vanovschi, L. Vogt, O. Vydrov, T. Wang, M. A. Watson, J. Wenzel, A. White, C. F. Williams, J. Yang, S. Yeganeh, S. R. Yost, Z.-Q. You, I. Y. Zhang, X. Zhang, Y. Zhao, B. R. Brooks, G. K. Chan, D. M. Chipman, C. J. Cramer, W. A. Goddard III, M. S. Gordon, W. J. Hehre, A. Klamt, H. F. Schaefer III, M. W. Schmidt, C. D. Sherrill, D. G. Truhlar, A. Warshel, X. Xu, A. Aspuru-Guzik, R. Baer, A. T. Bell, N. A. Besley, J.-D. Chai, A. Dreuw, B. D. Dunietz, T. R. Furlani, S. R. Gwaltney, C.-P. Hsu, Y. Jung, J. Kong, D. S. Lambrecht, W. Liang, C. Ochsenfeld, V. A. Rassolov, L. V. Slipchenko, J. E. Subotnik, T. V. Voorhis, J. M. Herbert, A. I. Krylov, P. M. Gill and M. Head-Gordon, *Mol. Phys.*, 2015, **113**, 184–215.

42 W. Hwang, Y.-K. Kim and M. E. Rudd, *J. Chem. Phys.*, 1996, **104**, 2956.

43 J. Bull, M. Bart, C. Vallance and P. Harland, *Phys. Rev. A: At., Mol., Opt. Phys.*, 2013, **88**, 062710.

44 D. Gupta, H. Choi, M.-Y. Song, G. P. Karwasz and J.-S. Yoon, *Eur. Phys. J. D*, 2017, **71**, 88.

45 Electron–Molecule Interactions and Their Applications, 1984.

46 B. F. E. Curchod and T. J. Martínez, *Chem. Rev.*, 2018, **118**, 3305–3336.

47 M. Barbatti, *WIREs Comput. Mol. Sci.*, 2011, **1**, 620–633.

48 J. Chalabala, F. Uhlig and P. Slavíček, *J. Phys. Chem. A*, 2018, **122**, 3227–3237.

49 J. Chalabala and P. Slavíček, *Phys. Chem. Chem. Phys.*, 2016, **18**, 20422–20432.

50 O. Svoboda, D. Hollas, M. Ončák and P. Slavíček, *Phys. Chem. Chem. Phys.*, 2013, **15**, 11531–11542.

51 D. Hollas, O. Svoboda and P. Slavíček, *Chem. Phys. Lett.*, 2015, **622**, 80–85.

52 V. Ásgeirsson, C. A. Bauer and S. Grimme, *Chem. Sci.*, 2017, **8**, 4879–4895.

53 S. Grimme, *Angew. Chem., Int. Ed.*, 2013, **52**, 6306–6312.

54 H. Tachikawa, *Phys. Chem. Chem. Phys.*, 2011, **13**, 11206–11212.

55 E. Livshits, R. S. Granot and R. Baer, *J. Phys. Chem. A*, 2011, **115**, 5735–5744.

56 L. G. Christophorou and J. K. Olthoff, *J. Phys. Chem. Ref. Data*, 2000, **29**, 267–330.

57 C. T. Dervos and P. Vassiliou, *J. Air Waste Manage. Assoc.*, 2000, **50**, 137–141.

58 Y. Kieffel, F. Biquez, D. Vigouroux, P. Ponchon, A. Schlernitzauer, R. Magous, G. Cros and J. G. Owens, *CIRED, Open Access Proc. J.*, 2017, 1–4.

59 A. Hösl, A. Chachereau, J. Pachin and C. M. Franck, *J. Phys. D: Appl. Phys.*, 2019, **52**, 235201.

Mode-Specific Vibrational Autodetachment Following Excitation of Electronic Resonances by Electrons and Photons

Cate S. Anstöter,[1] Golda Mensa-Bonsu,[1] Pamir Nag,[2] Miloš Ranković,[2] Ragesh Kumar T. P.,[2] Anton N. Boichenko,[3] Anastasia V. Bochenkova,[3,*] Juraj Fedor,[2,†] and Jan R. R. Verlet[1,‡]

[1]*Department of Chemistry, Durham University, Durham DH1 3LE, United Kingdom*

[2]*J. Heyrovský Institute of Physical Chemistry, Czech Academy of Sciences, Dolejškova 3, 18223 Prague 8, Czech Republic*

[3]*Department of Chemistry, Lomonosov Moscow State University, 119991 Moscow, Russia*

(Received 9 March 2020; accepted 1 May 2020; published 19 May 2020)

Electronic resonances commonly decay via internal conversion to vibrationally hot anions and subsequent statistical electron emission. We observed vibrational structure in such an emission from the nitrobenzene anion, in both the 2D electron energy loss and 2D photoelectron spectroscopy of the neutral and anion, respectively. The emission peaks could be correlated with calculated nonadiabatic coupling elements for vibrational modes to the electronic continuum from a nonvalence dipole-bound state. This autodetachment mechanism via a dipole-bound state is likely to be a common feature in both electron and photoelectron spectroscopies.

DOI: 10.1103/PhysRevLett.124.203401

Processes involving the formation of electronic resonances are of fundamental importance in many fields of science and technology, ranging from astrophysics to biology and from electrical power distribution to semiconductor fabrication [1]. For many decades, transient electron capture and detachment have been studied by electron energy loss (EEL) spectroscopy [2], where the resonance is formed by an electron, with initial energy ε_i, colliding with a molecule M:

$$M + e^-(\varepsilon_i) \rightarrow M^{-*} \rightarrow M(\varepsilon_v) + e^-(\varepsilon_f).$$

Upon M^{-*} resonance formation, two types of vibrational excitation are generally identified [2]. The first is the excitation of specific vibrational modes, where the electron loses the energy corresponding to a given vibrational quantum, leading to a final energy ε_f that is lower than ε_i by this specific energy loss ε_v. The second mechanism is an unspecific vibrational excitation, where energy is randomized over the nuclear degrees of freedom and the electrons are emitted statistically with a thermal distribution (thermionic emission) [3]. With the recent introduction of two-dimensional (2D) EEL [4–6], a third type of emission has been observed in several molecules, in which electrons are emitted with low (but finite) constant ε_f over a range of ε_i and the spectra show vibrational structure [4,7]. Such detachment is inconsistent with either of the two excitation types, and no explanation has been provided so far.

More recently, 2D anion photoelectron (PE) spectroscopy has been used to provide complementary information to 2D EEL spectroscopy [8,9]:

$$M^- + h\nu \rightarrow M^{-*} \rightarrow M(\varepsilon_v) + e^-(\varepsilon_f).$$

Although the initial geometry of the resonance M^{-*} is different than in electron attachment, the same two types of excitation or emission are usually considered. A structured PE signal with low and constant ε_f has also been seen over a range of $h\nu$ in a number of targets, and this structure has been related to autodetachment from nonvalence states [10–12]. Here, we probe the electron detachment from electronic resonances in nitrobenzene (NB) using both 2D EEL and 2D PE spectroscopy in an attempt to gain insight into this structured low-energy electron emission channel. We show that signals are observed using both methods over a wide range of ε_i, despite the difference in geometric and electronic structure of the initial species. We suggest a mechanism for this emission which involves the nonvalence dipole-bound state (DBS) of the NB anion.

The 2D EEL spectroscopy was performed on an electrostatic spectrometer [13,14], where the incident electron beam is produced in a hemispherical electron monochromator and crosses the effusive beam of the neutral NB molecules at a temperature of 330 K. The scattered electrons are analyzed by a second hemispherical analyzer. The scattering angle has been fixed at 135°, and the electron energy resolution was 17 meV. The 2D EEL spectrum was constructed from individual EEL spectra taken at ε_i with 10 meV increments.

The 2D PE spectroscopy was carried out in an anion PE spectrometer that has been detailed previously [15]. Mass-selected NB^- was produced in a molecular beam source and irradiated with light from a tunable nanosecond Nd:YAG pumped optical parametric oscillator providing ≈5 ns

pulses. Photodetached electrons were collected using a velocity-map imaging PE spectrometer with a spectral resolution <3% of ε_f. The 2D PE spectrum was constructed by taking PE spectra over $1.2 \leq h\nu \leq 3.0$ eV with 25 meV intervals.

We additionally performed electronic structure calculations using extended multiconfiguration quasidegenerate perturbation theory [16,17] with an active space including the π orbitals and also an active space including the relevant n orbitals (see Fig. S1 [18]). Vertical excitation energy (VEE) calculations from either the neutral or anion geometry were performed to estimate energies of valence excited states. The calculations used the (aug)-cc-pVTZ basis set, where the augmented functions were affixed only to the oxygen atoms. The vertical detachment energy was determined by adding a p-type function with a 10^{-10} exponent to the active space in order to mimic electron detachment. The position of a nonvalence dipole-bound state with respect to the detachment threshold, its equilibrium geometry, and nonadiabatic couplings with discretized continuum states were computed using an active space additionally augmented with a subset of diffuse orbitals of A_1 symmetry. Full details and computational results are provided in Supplemental Material [18].

The 2D EEL and 2D PE spectra for NB are shown in Figs. 1(a) and 1(b), respectively. To aid the comparison, we made two modifications to standard ways of plotting these spectra. First, the horizontal axis of the 2D EEL spectra is ε_f and not the electron energy loss ($\varepsilon_i - \varepsilon_f$), as usually presented [4,25]. Second, the vertical axis of 2D PE spectra is not $h\nu$ but has been converted to $\varepsilon_i = h\nu - \mathrm{AEA}$ [8]. $\mathrm{AEA} = 0.95 \pm 0.03$ eV is the adiabatic electron affinity determined from the PE spectra, in good agreement with a previous PE spectrum [26]. Note also that the PE spectra have been normalized to total integrated signal levels to emphasize spectral changes as a function of the excitation energy.

The diagonal features in Fig. 1 have $\varepsilon_f = \varepsilon_i$ and $\varepsilon_f = \varepsilon_i - \varepsilon_v$, where ε_v is a constant energy left in the neutral. These correspond to specific vibrational excitation. In the 2D PE spectrum, diagonal features indicates direct detachment, whereby the intensity profile of specific ε_v levels in the neutral are determined by Franck-Condon factors between the anion and neutral ground state [27]. In the 2D EEL spectrum, the $\varepsilon_f = \varepsilon_i$ diagonal is the elastic scattering ridge, with parallel features corresponding to vibrational excitation of ε_v quanta in the neutral. In both spectroscopies, the formation of resonances can be identified by changes in the behavior of the diagonal signals. In the 2D PE spectrum, this can be seen clearly at $\varepsilon_i \geq 1.3$ eV. In 2D EEL, two resonances can be seen, centered around ~0.5 eV and ~1.5 eV (see Fig. S4 [18]), in agreement with positions seen in electron transmission spectroscopy (0.55 and 1.36 eV) [28,29] and in electron attachment spectroscopy (0.4 and 1.25 eV) [28,30].

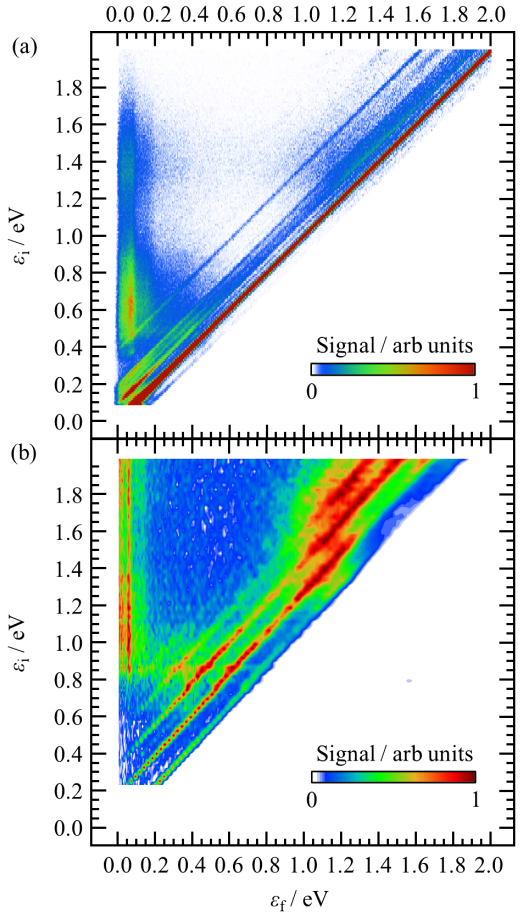

FIG. 1. (a) 2D electron energy loss spectrum of the nitrobenzene molecule and (b) 2D photoelectron spectrum of the nitrobenzene anion. The elastic ridge has been saturated for clarity and is shown in more detail in Fig. S4 [18].

In addition to the expected features, Fig. 1 also shows the electron signal with constant $\varepsilon_f < 0.2$ eV over a broad range of ε_i. Figure 2(a) shows the EEL spectrum, separately recorded at $\varepsilon_i = 0.8$ eV to attain high signal to noise, highlighting this spectral region. Figure 2(b) shows the average of PE spectra over the range $0.8 < \varepsilon_i < 2.0$ eV. Individual spectra at low energy are the same, and the average simply offers better signal to noise. Both spectra are broadly similar with a sharp peak at $\varepsilon_f = 60$ meV and a broad peak with a rough maximum at $\varepsilon_f \sim 130$ meV. The difference between the EEL and photoelectron spectrum at very low energies is most probably due to the different electron analyzers used; the hemispherical analyzer in the EEL experiment has a low transmission at very low ε_f.

Low ε_f emission is common in polyatomic molecules due to ultrafast conversion of resonances to the vibrationally hot anion ground state, which then emits electrons statistically. Because of the statistical nature, such emission should not display vibrational structure [31–33] and is inconsistent with the signal in Fig. 2. Nevertheless, the observation of this signal in both PE and EEL spectra

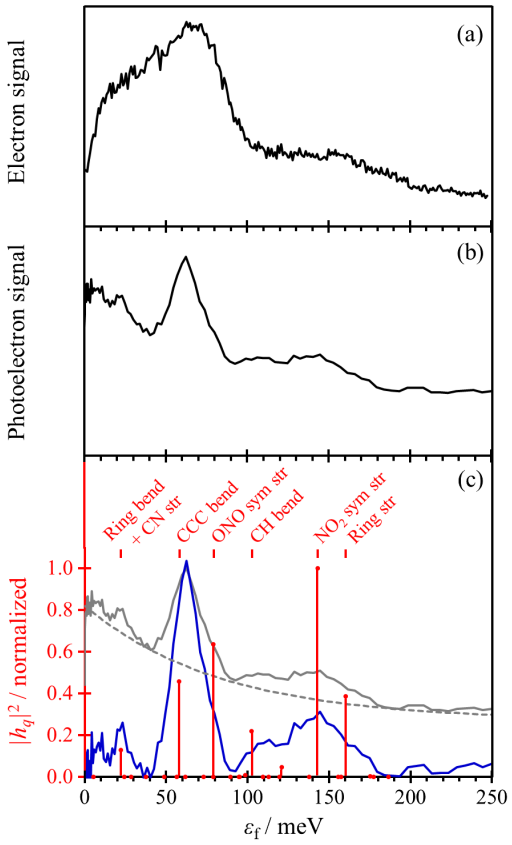

FIG. 2. (a) Low ε_f part of the EEL spectrum at $\varepsilon_i = 0.8$ eV. (b) Low ε_f part of the PE spectra averaged over the range $0.8 < \varepsilon_i < 2.0$ eV. (c) Comparison of data in (b) (gray solid line) to the norm-squares of the nonadiabatic coupling elements of h_q (red bars), with harmonic frequencies displaced by $E_{\mathrm{DBS}} = -27$ meV. The blue line is the PE signal with smoothly varying background (gray dashed line) subtracted. Dominant vibrational modes are labeled (nomenclature sym = symmetric; str = stretch), and all modes are in the molecular plane.

across a range of ε_i suggests that it arises from a single emission channel. To address the origin of these well-defined low ε_f peaks, we first consider the electronic structure and resonances involved (for details, see Fig. S2 [18]).

Modelli and Venuti [28] identified the resonances at 0.55 and 1.36 eV using electron transmission spectroscopy (ETS) as the two π^* shape resonances $^2A_2$ and $^2B_1$, respectively (NB has C_{2v} symmetry in both anion and neutral ground states). These energies are in reasonable agreement with our VEE calculations from the neutral (0.28 and 1.50 eV, respectively). The signal at low and constant ε_f in the 2D EEL spectrum is seen for $\varepsilon_i > 0.4$ eV, which coincides with the onset of the $^2A_2$ resonance, indicating that this is likely to be the lowest energy entrance channel. In the 2D PE spectrum, the analogous signal appears only at $\varepsilon_i > 0.8$ eV. The $^2A_2$ resonance is optically dark with a very weak oscillator strength for the transition from the ground state and is therefore not seen in Fig. 1(b). Our calculations instead show that the onset of the low and constant ε_f in the 2D PE spectrum can be correlated with excitation to the $^2B_2$ Feshbach resonance located at 0.75 eV, which has a very broad Franck-Condon window. The optical electronic transition to this state is symmetry forbidden, but B_1 and B_2 vibrational modes make it vibronically allowed. Feshbach resonances are typically not manifested in EEL excitation curves of specific vibrational modes (diagonals), but here the $^2B_2$ state may reveal itself indirectly and could serve as an entrance channel for the signal at low and constant ε_f across a wide range of ε_i between 0.4 and 1 eV in the 2D EEL spectrum. The higher-lying $^2B_1$ shape resonance is optically bright and seen in both experiments. It also leads to the low and constant ε_f signal. Surprisingly, we conclude that essentially any entrance channel, be it photon or electron excited, leads to a common exit channel that produces the structured signal at low ε_f.

We have already excluded purely statistical emission as the origin of the structure at low ε_f. In principle, it could also originate from the autodetachment from a low-lying resonance. Our calculations suggest that emission from the $^2A_2$ resonance may be consistent with the observed vibrational structure, as its potential energy surface along the CN bond length is similar to the neutral ground state with a total reorganization energy of ~0.2 eV. This resonance is calculated to be at ~0.3 eV vertically above the neutral ground state, and, hence, the adiabatic energy gap between them does not exceed 0.1 eV. Therefore, autodetachment from the $^2A_2$ could be consistent with the most prominent low-energy peak observed at 60 meV. However, the EEL and ETS experiments [28] suggest that the $^2A_2$ resonance is located higher in energy by ~0.2 eV.

An alternative source of the low-energy electrons is vibrational autodetachment from a nonvalence state. The best-known example of a nonvalence state is a dipole-bound state (DBS), in which the excess electron is loosely bound in a diffuse s-type orbital, located off the positive side of the permanent dipole moment of the neutral molecule, $\boldsymbol{\mu}$ [34]. Because of the weak interaction between the dipole-bound electron and the valence electrons of the neutral core, the potential energy surface associated with the DBS is very similar to that of the neutral molecule. For neutral NB, $|\boldsymbol{\mu}| = 4.2$ D, which is in excess of the $|\boldsymbol{\mu}| \approx 2.5$ D required to observe such states experimentally. Indeed, Rydberg electron transfer experiments by Desfrançois *et al.* verified that NB^- has a DBS with an estimated binding energy of 28 meV [26]. Hence, the DBS of NB^- may be a candidate for the source of the observed structure. But why should this lead to structured emission, and which modes facilitate the emission?

As the DBS is bound by $\boldsymbol{\mu}$ of the neutral core, intuition suggests that the vibrational modes that modulate $\boldsymbol{\mu}$ lead to electron emission. These are the infrared (IR) active modes. More specifically, it is the nonadiabatic coupling between

the DBS state and the electronic continuum that drives the autodetachment [35]. Because the DBS is totally symmetric, nonzero couplings arise for vibrational modes of A_1 symmetry, and the change in $\boldsymbol{\mu}$ should be parallel to $\boldsymbol{\mu}$ (the molecular axis of NB). Based on this analysis, only one IR-active mode, $v_8(A_1)$, which is the C-NO_2 symmetric stretch, modulates the DBS binding energy. We have calculated the nonadiabatic coupling matrix elements h_q between state-averaged complete active space self-consistent field wave functions that describe the DBS (ψ_{N+1}) and the discretized continuum state ($\psi_{N,\varepsilon}$) near the detachment threshold at the DBS equilibrium geometry [35]:

$$h_q = \langle \psi_{N,\varepsilon} | \nabla_q | \psi_{N+1} \rangle_r,$$

where ∇_q is the nuclear momentum operator along the q normal mode and r are the electronic coordinates. In a simplified picture where two nondisplaced harmonic potentials describe the DBS and the neutral ground state along all normal modes (see Fig. 3), and assuming that h_q is independent of nuclear coordinates, the vibrational prefactor is the same for all modes and nonzero only if the final state has one less vibrational quantum. This gives the propensity rule associated with vibrational autodetachment from the DBS, which is to lose one quantum of vibrational energy, $\Delta v = -1$ [35,36].

The norm-squares of h_q are shown in Fig. 2(c) together with the spectrum from Fig. 2(b). The experimental spectrum also appears to have an unstructured thermal spectral component, and we have crudely subtracted an exponentially decaying function to represent this thermionic component, leaving the vibrational autodetachment spectrum. In order to make a correlation between $|h_q|^2$ and the emission spectrum, the positions of all the calculated harmonic frequencies must be displaced by approximately −27 meV. Given the $\Delta v = -1$ propensity, electron emission energies correspond to $\varepsilon_f = h\nu_e - E_{\mathrm{DBS}}$, where the $h\nu_e$ is the vibrational frequency of a given mode and E_{DBS} is the binding energy of the DBS (see Fig. 3). Hence, the

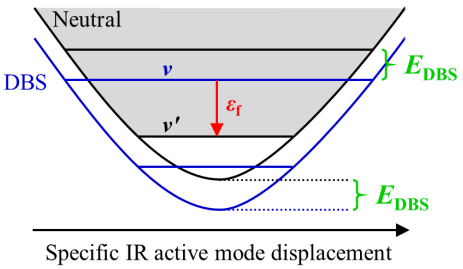

FIG. 3. Schematic of mode-facilitated electron loss from the DBS of the anion. Electron emission ε_f occurs from an IR-active vibrational mode of the DBS, v, by losing one quantum of vibrational energy to the neutral (black), $v' = v - 1$. The DBS (blue) and neutral (black) surfaces are offset by the DBS binding energy E_{DBS}.

displacement arises from the binding energy of the DBS, and we determine that $E_{\mathrm{DBS}} \sim 27$ meV, in excellent agreement with the previous estimate by Desfrançois *et al.* of 28 meV [26]. Figure 2(c) confirms that the IR-active C-NO_2 symmetric stretch mode $v_8(A_1)$ leads to the largest nonadiabatic coupling between the DBS state and the electronic continuum.

There is a very good overall correlation between most peaks observed in the emission spectrum and the calculated $|h_q|^2$. However, the relative intensities do not agree as well. We note that a direct comparison might be misleading. First, the subtraction of the unstructured thermal spectral component, which contributes more toward lower frequency, may skew the overall intensities. Second, while the experimental peak at ∼130 meV is not the peak with the highest amplitude, its integrated signal (assuming the feature is a single peak) is, in fact, similar to that at 60 meV. Finally, the mode with the largest h_q may be manifested not only as the most prominent peak but also as the spectrally broadest peak, as the coupling to the continuum implies a more rapid decay. Taking all these observations together, we conclude that the most likely exit channel leading to the structured signal at low ε_f is vibrational autodetachment from the DBS of NB^-.

It is also tempting to simply compare an offset IR spectrum of NB to the vibrational autodetachment spectrum in Fig. 2. Such a comparison is shown in Fig. S3 [18]. As above, a good overall correlation between peak positions can be attained when a shift of −27 meV is applied to the IR spectrum. Although such a comparison has very different intensities, in line with the differing physical origins of the spectra, it provides a useful experimental tool and first indicator of the modes that are important and of the binding energy of the DBS.

There are two mechanisms by which the DBS can be populated. The first is by internal conversion through a conical intersection from a valence resonance [10–12]. For the second, a fraction of the population of the resonance internally converts to reform the vibrationally hot ground state of the anion, which could then populate the DBS. For example, the statistical sampling of all vibrational levels could lead to the transient formation of the DBS, which then undergoes rapid vibrational autodetachment. This second mechanism is supported by the smoothly decreasing background of the spectra in Fig. 2, which points to a thermionic contribution to the mode-specific autodetachment.

The electron emission mechanism described here can be compared with several processes involving the coupling of molecular vibrations with electrons in continuum. (i) In low-energy electron collisions with polar molecules, the IR-active modes are efficiently excited at the threshold via direct dipole excitation [37]. The autodetachment process described here can be, in principle, viewed as a reverse mechanism: The electron leaving the hot molecule via a nonvalence state deexcites specific modes.

(ii) Mode-specific vibrational autodetachment has been observed from nonvalence states populated by internal conversion from resonances; however, this emission occurs on a picosecond timescale and applies to resonances excited near the threshold [10–12]. (iii) Signatures of IR modes have also been seen in the direct photodetachment from nonvalence states. For example, Bailey *et al.* observed weak features in the PE spectrum of the dipole-bound anion CH_3CN^- that were redshifted by the IR modes of CH_3CN [38]. Similar features have been observed in the nonvalence correlation-bound state of $C_6F_6^-$, where both IR and Raman modes can contribute [39]. However, while this process similarly is based on nonadiabatic coupling between the nonvalence orbital and specific vibrations, the mechanism presented here fundamentally differs, as it is an autodetachment rather than photodetachment process. (iv) Lunt *et al.* observed a minimum in the total scattering cross section of electrons from NB around 0.1 eV [40], which they tentatively assigned to interference between a dipole-bound resonance and the direct scattering channel. While our results are not sensitive to such interference (the signal at $\varepsilon_f < 0.2$ eV cannot interfere with the direct channel), it does demonstrate that vibrational levels of the DBS serve as emission channels.

In conclusion, we have presented an interpretation of the origin of structure in low-energy electron loss channels observed in both electron energy loss and photoelectron spectroscopy. The structure observed in nitrobenzene arises from vibrational mode-specific electron loss from a nonvalence state of the anion and can be correlated with the IR-active modes of the neutral with A_1 symmetry, offset by the binding of a DBS. Our results provide a framework from which structured low-energy electron emission can be interpreted and highlight the ubiquity of nonvalence states in the dynamics of anions.

This work is supported by the Royal Society (IEC\R2 \181068), the European Research Council (306536), the EPSRC (EP/M507854/1), the Czech Science Foundation (20-11460S), the European Regional Development Fund [OP RDE (CZ.02.2.69/0.0/0.0/16_027/0008355)], and the Russian Foundation for Basic Research (19-53-10003 KO_a). A. N. B. and A. V. B. also acknowledge support from the Lomonosov Moscow State University Program of Development. The research is carried out using the equipment of the shared research facilities of HPC computing resources at Lomonosov Moscow State University.

*bochenkova@phys.chem.msu.ru
†juraj.fedor@jh-inst.cas.cz
‡j.r.r.verlet@durham.ac.uk

[1] I. I. Fabrikant, S. Eden, N. J. Mason, and J. Fedor, in *Advances In Atomic, Molecular, and Optical Physics*, edited by E. Arimondo, C. C. Lin, and S. F. Yelin (Academic, New York, 2017), pp. 545–657.
[2] M. Allan, J. Electron Spectrosc. Relat. Phenom. **48**, 219 (1989).
[3] J. N. Bull, C. W. West, and J. R. R. Verlet, Chem. Sci. **6**, 1578 (2015).
[4] K. Regeta and M. Allan, Phys. Rev. Lett. **110**, 203201 (2013).
[5] F. Currell and J. Comer, Phys. Rev. Lett. **74**, 1319 (1995).
[6] T. Reddish, F. Currell, and J. Comer, J. Phys. E **21**, 203 (1988).
[7] M. Allan, M. Lacko, P. Papp, Š. Matejčík, M. Zlatar, I. I. Fabrikant, J. Kočišek, and J. Fedor, Phys. Chem. Chem. Phys. **20**, 11692 (2018).
[8] C. W. West, J. N. Bull, E. Antonkov, and J. R. R. Verlet, J. Phys. Chem. A **118**, 11346 (2014).
[9] C. S. Anstöter, J. N. Bull, and J. R. R. Verlet, Int. Rev. Phys. Chem. **35**, 509 (2016).
[10] J. N. Bull and J. R. R. Verlet, Sci. Adv. **3**, e1603106 (2017).
[11] J. N. Bull, C. W. West, and J. R. R. Verlet, Chem. Sci. **7**, 5352 (2016).
[12] J. N. Bull, C. S. Anstöter, and J. R. R. Verlet, Nat. Commun. **10**, 5820 (2019).
[13] M. Allan, J. Phys. B **25**, 1559 (1992).
[14] M. Allan, J. Phys. B **38**, 3655 (2005).
[15] J. P. Rogers, C. S. Anstöter, J. N. Bull, B. F. E. Curchod, and J. R. R. Verlet, J. Phys. Chem. A **123**, 1602 (2019).
[16] A. A. Granovsky, J. Chem. Phys. **134**, 214113 (2011).
[17] A. A. Granovsky, Firefly version 8.2.0, http://classic.chem.msu.su/gran/firefly/index.html.
[18] See Supplemental Material at http://link.aps.org/supplemental/10.1103/PhysRevLett.124.203401, which includes Refs. [19–24], for: computational details and results; a comparison of electron spectra with IR spectrum; and the full 2D EEL spectrum.
[19] M. J. Frisch *et al.*, *Gaussian 16, Revision A.03* (Gaussian, Inc., Wallingford, CT, 2016).
[20] J. Schiedt and R. Weinkauf, J. Chem. Phys. **110**, 304 (1999).
[21] A. A. Kunitsa and K. B. Bravaya, J. Phys. Chem. Lett. **6**, 1053 (2015).
[22] A. A. Kunitsa, A. A. Granovsky, and K. B. Bravaya, J. Chem. Phys. **146**, 184107 (2017).
[23] A. Giussani and G. A. Worth, J. Chem. Theory Comput. **13**, 2777 (2017).
[24] M. W. Schmidt, K. K. Baldridge, J. A. Boatz, S. T. Elbert, M. S. Gordon, J. H. Jensen *et al.*, J. Comput. Chem. **14**, 1347 (1993).
[25] M. Ranković, P. Nag, M. Zawadzki, L. Ballauf, J. Žabka, M. Polášek, J. Kočišek, and J. Fedor, Phys. Rev. A **98**, 052708 (2018).
[26] C. Desfrançois, V. Périquet, S. A. Lyapustina, T. P. Lippa, D. W. Robinson, K. H. Bowen, H. Nonaka, and R. N. Compton, J. Chem. Phys. **111**, 4569 (1999).
[27] R. R. Corderman and W. C. Lineberger, Annu. Rev. Phys. Chem. **30**, 347 (1979).
[28] A. Modelli and M. Venuti, Int. J. Mass Spectrom. **205**, 7 (2001).
[29] N. L. Asfandiarov, S. A. Pshenichnyuk, V. G. Lukin, I. A. Pshenichnyuk, A. Modelli, and Š. Matejčik, Int. J. Mass Spectrom. **264**, 22 (2007).
[30] A. Pelc, P. Scheier, and T. D. Märk, Vacuum **81**, 1180 (2007).

[31] E. E. B. Campbell and R. D. Levine, Annu. Rev. Phys. Chem. **51**, 65 (2000).
[32] J. U. Andersen, E. Bonderup, and K. Hansen, J. Phys. B **35**, R1 (2002).
[33] C. L. Adams, K. Hansen, and J. M. Weber, J. Phys. Chem. A **123**, 8562 (2019).
[34] K. D. Jordan and F. Wang, Annu. Rev. Phys. Chem. **54**, 367 (2003).
[35] J. Simons, J. Am. Chem. Soc. **103**, 3971 (1981).
[36] G.-Z. Zhu and L.-S. Wang, Chem. Sci. **10**, 9409 (2019).
[37] Y. Itikawa, Int. Rev. Phys. Chem. **16**, 155 (1997).
[38] C. G. Bailey, C. E. H. Dessent, M. A. Johnson, and K. H. Bowen, J. Chem. Phys. **104**, 6976 (1996).
[39] J. P. Rogers, C. S. Anstöter, and J. R. R. Verlet, Nat. Chem. **10**, 341 (2018).
[40] S. L. Lunt, D. Field, J.-P. Ziesel, N. C. Jones, and R. J. Gulleye, Int. J. Mass Spectrom. **205**, 197 (2001).

Electron-impact vibrational excitation of isocyanic acid HNCO

Ragesh Kumar T. P.[1] P. Nag[1] M. Ranković[1] R. Čurík,[1,*] A. Knížek[1] S. Civiš[1] M. Ferus,[1] J. Trnka[2] K. Houfek[2] M. Čížek,[2,†] and J. Fedor[1,‡]

[1]*J. Heyrovský Institute of Physical Chemistry, Czech Academy of Sciences, Dolejškova 3, 18223 Prague, Czech Republic*

[2]*Institute of Theoretical Physics, Faculty of Mathematics and Physics, Charles University, Holešovičkách 2, 180 00 Prague, Czech Republic*

(Received 29 October 2020; accepted 8 December 2020; published 24 December 2020)

In a combined experimental and theoretical study, we probe the vibrational excitation of isocyanic acid induced by electron impact in the energy range up to 5 eV. Experimentally, we report differential elastic and vibrationally inelastic cross sections at the scattering angle of 135°. Theoretically, we characterize the involved resonant states using a regularized analytical continuation method. We also apply a nonlocal resonance model to calculate cross sections for vibrational mode that involves the N-H stretching motion. The model reproduces all the features observed in the experiment: efficient excitation at threshold, sharp cusps in the excitation functions, and the formation of an A' shape resonance. There is a second (A'') resonance visible in the spectra; however, it excites only selected vibrational modes. The origins of this selectivity are discussed.

DOI: 10.1103/PhysRevA.102.062822

I. INTRODUCTION

HNCO is the simplest molecule containing all four basic chemical elements that are constituents of a broad range of organic molecules and biomolecules. As such, it has been attracting attention as a possible important precursor in prebiotic chemistry [1,2]. This interest is intensified by the fact that it is an abundant interstellar molecule: It was among the very early molecules to be detected in space, in the Galactic center clouds [3]. It is also abundant in dark clouds, such as TMC-1 [4], and translucent clouds [5]. In a survey of 81 molecular clouds, its detection rate was 70% [6]. It was also detected in hot cores [7], high-mass young stellar objects [8], molecular outflows [9], and comets [10].

It is believed that in the interstellar space with low particle density, the decomposition reactions are to a large degree initiated by ultraviolet light, x rays, and cosmic rays (most of which are high-energy protons). When such high-energy radiation interacts with interstellar icy grains that probably serve as reservoirs for chemical reactions, it produces an avalanche of secondary electrons. One high-energy proton may release 10^4 secondary electrons in its passage through a single ice-covered dust grain [11]. These secondary electrons have mean kinetic energies in the region of units and tens of electronvolts [11]. In this paper, we address the question of how such low-energy electrons excite HNCO vibrationally. Previous works on other astrophysically relevant unsaturated molecules such as C_4H_2 [12], HC_3N [13], and NCCN [14] have shown that electrons can be very efficient in mediating the vibrational excitation, although various normal modes can be excited selectively.

HNCO is an interesting target for electron scattering experiments also from a purely fundamental point of view. First, due to the two double bonds, the molecule has low-lying unoccupied π^* orbitals. These are expected to give rise to π^* shape resonances. Due to the nonlinear structure of the molecule (CNH angle is 124°), the lower of these resonances (A' symmetry) has a mixed π^*/σ^* character from the point of view of the N-H bond. Second, HNCO is a polar molecule with the dipole moment of 1.6 Debye [15]. We have recently shown [16] that the combination of these properties leads to the dissociative electron attachment (DEA) cross section which is rich in fine features. There, we presented a one-dimensional nonlocal resonance model which reproduced the experimental DEA cross section very well. With a simplified description, such electron-induced dissociation can be viewed as a multistep process: The electron is attached, change in the electronic configuration induces motion of the nuclei, and the bond is cleaved, producing stable anionic fragment and a neutral radical (in this case, $NCO^- + H$). If, however, the electron detaches during this process, the configuration of nuclei is different than the neutral ground-state minimum and as a result, the molecule is left vibrationally excited. Probing the vibrational excitation channels thus provides information about earlier stage of the nuclear motion than the DEA. It thus represents an independent test of the theoretical model. Additionally, the ability to follow the different normal modes brings the information about the direction of the induced motion upon the resonance formation.

II. EXPERIMENTAL SETUP

The electron scattering experiments were performed on the electrostatic spectrometer with the hemispherical electron monochromator and analyzer [17,18]. Electrons scattered on the effusive beam of pure sample gas were analyzed at a fixed scattering angle. The energy of the incident beam was

*roman.curik@jh-inst.cas.cz
†cizek@mbox.troja.mff.cuni.cz
‡juraj.fedor@jh-inst.cas.cz

calibrated on the 19.365-eV 2^2S resonance in helium. Combined electron-energy resolution was 17 meV. The absolute elastic scattering cross section was calibrated against the one of helium using a relative flow method.

The present data were taken by operating the spectrometer in two different measurement modes. In the first one, the electron energy-loss spectrum of HNCO was measured at a constant incident energy. Here the electron monochromator was set to pass the electrons with the fixed incident energy and the analyzer was scanned for residual energy of scattered electrons. The signal is typically plotted as a function of the difference between the incident and residual energy, which is the energy loss of the electron. In the second mode of the measurement, the excitation functions of the given energy losses were recorded. Here, both monochromator and analyzer were scanned for the entire range of electron energies, with their difference kept constant.

All the present data were taken at a fixed scattering angle of 135°. This is the highest angle which is mechanically achievable due to constraints given by the physical space occupied by the monochromator and analyzer. The preference for high scattering angle in this work was driven by the interest in the resonant processes. It is well established that the cross section for direct dipole scattering is forward peaked [19,20], and the resonant processes are thus best visible at high scattering angles.

The HNCO sample was synthesized by a pyrolysis of cyanouric acid [21]. During the measurements, the sample was kept at the temperature of solid CO_2 (−78.5 °C), only slightly above the HNCO melting temperature of (−86 °C). The low temperature contributes to the purity of sample vapor since it keeps partial pressures of possible volatile impurities low.

III. THEORY

A. RAC analysis of the shape resonances

The shape resonances were analyzed by using the regularized analytic continuation (RAC) method [22,23]. In this method, an additional perturbation field V is applied to the molecular Hamiltonian H, $H \to H + \lambda V$. The attractive one-electron operator λV makes the quasibound resonant state truly bound, and therefore it can be described by the standard quantum chemistry software. Several forms of the perturbation potential (e.g., Coulomb, Gaussian, and their product [24–26]) do not require any software modifications of the quantum chemistry programs. In the present study, the nuclear potential of the molecule was utilized as the perturbation field, i.e.,

$$V = \sum_{A=1}^{4} \sum_{i} \frac{Z_A}{|\vec{r}_i - \vec{R}_A|}, \tag{1}$$

where $\vec{r}_i$ are the electronic coordinates, vectors $\vec{R}_A$ denote positions of the H, N, C, and O atoms, and Z_A are their corresponding nuclear charges. The chosen form of the perturbation potential has provided reasonably accurate A' resonance parameters in our previous DEA study on this molecular system [16]. The electron affinities $\Delta E(\lambda) = \kappa^2(\lambda)$ in the presence of the perturbation potential were computed by the coupled clusters (CCSD-T) method [27,28] as implemented in MOLPRO 2010 package of quantum chemistry programs [29] with the Dunning's augmented correlation-consistent basis set [30] (aug-cc-pVTZ).

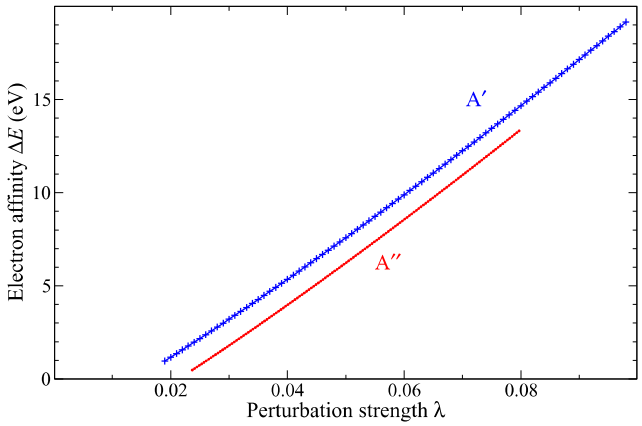

FIG. 1. Computed vertical electron affinities $\Delta E(\lambda)$ for the two π^* resonances at the equilibrium geometry. The data points for the in-plane A′ resonance are shown as crosses, while the data points for the out-of-plane resonance A″ are displayed by small circles (overlapping into a line).

The data points used in the present study are shown in Fig. 1 for the two π^* resonances examined. The RAC method continues the real-valued affinity momenta $\kappa(\lambda) = \sqrt{\Delta E(\lambda)}$ to the complex plane by applying the Padé approximation on the inverse function $\lambda(\kappa)$. We utilized the RAC [3/1] Padé approximation [23],

$$\lambda^{[3/1]}(\kappa) = \lambda_0 \frac{(\kappa^2 + 2\alpha^2\kappa + \alpha^4 + \beta^2)(1 + \delta^2\kappa)}{\alpha^4 + \beta^2 + \kappa[2\alpha^2 + \delta^2(\alpha^4 + \beta^2)]}, \tag{2}$$

where $\lambda_0, \alpha, \beta, \delta$ are the fitting parameters that provide the resonance energy $E_r = \beta^2 - \alpha^4$ and the resonance width $\Gamma = 4\alpha^2|\beta|$.

At the equilibrium geometry of the neutral HNCO, the A' and A'' resonances were calculated at 2.49 eV ($\Gamma = 0.48$ eV) and 4.10 eV ($\Gamma = 0.80$ eV), respectively.

B. Nonlocal model for the N-H stretch vibration

For energies above 1.16 eV, the electron scattering process competes with dissociative electron attachment in which NCO^- anion is created. In our previous work, we have developed a nonlocal resonance model to treat this process [16]. The same model can be used to describe the vibrational excitation of NH stretch mode by the electron impact. The ability of this model to describe the current vibrational excitation data is an independent check of the model and the underlying assumptions and validates also our understanding of the dissociative electron attachment process.

The nonlocal resonance model for the excitation of HNCO along NH-stretch coordinate and its construction is described in detail in Ref. [16]. Here we summarize briefly the key information and show the potential energy curves in Fig. 2. The model is based on the Fano model of discrete-state interaction with continuum that can be used to parametrize the interaction of incoming electron with the molecule [31]

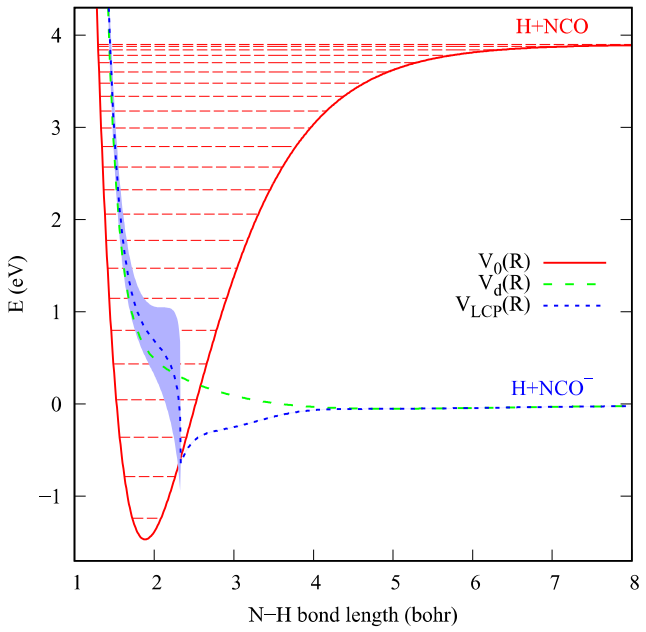

FIG. 2. Potential energy curves $V_0(R)$, $V_d(R)$, and $V_{LCP}(R)$ for the model describing N–H stretch dynamics. Vibrational energies are included with dash-dotted lines and the width of the fixed-nuclei resonance (± imaginary part of V_{LCP}) is marked by extent of the blue-shaded area.

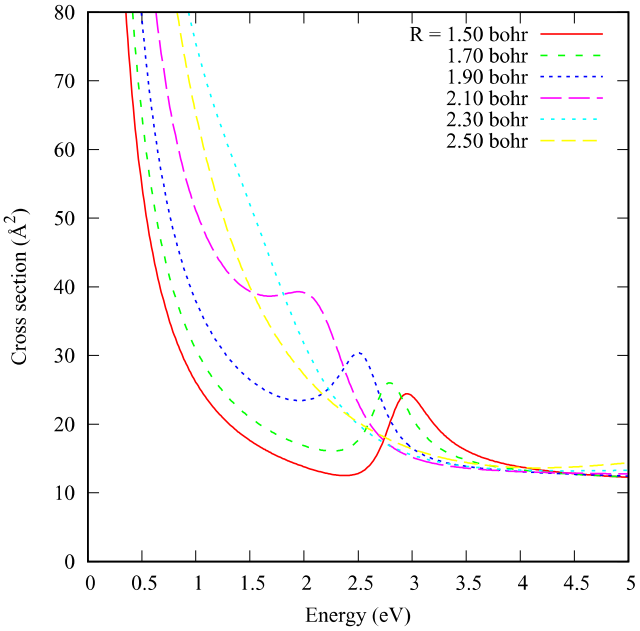

FIG. 3. Fixed-nuclei scattering cross sections for the A' symmetry determined from the R-matrix data used in Ref. [16] to construct the model for the N–H stretch dynamic for several NH-bond lengths R. Equilibrium bond length is approximately $R = 1.9$ bohr.

for each fixed position of nuclei. In our case, the discrete state describes the narrow resonance at the equilibrium geometry of HNCO which changes its character with stretching NH distance until it becomes a bound electronic state corresponding to the NCO^- ion and the H atom for large NH separations. The model is fully described by potential energy curves (cuts of the full surfaces along the NH bond) of the neutral molecule and the anion discrete state and also by the discrete-state-continuum coupling, which is closely related to the width of the anion resonance. The potential energy curves for electronically bound states were calculated in Ref. [16] using the coupled-clusters approach, CCSD-T/aug-cc-pVTZ [27,28,30], and the resonance parameters were extracted using regularized analytic continuation (RAC) method [22,32]. To fully characterize the electron-molecule interaction in the model and to fix the discrete-state-continuum coupling, we performed the fixed-nuclei R-matrix scattering calculations. The resulting cross sections for the A' symmetry are shown in Fig. 3 for several N–H distances around the equilibrium geometry, showing resonances in the range 1.5–3.5 eV corresponding to the 2.5-eV resonance in the experimental cross sections. To justify the one-dimensional approach, we also verified that the energy of the discrete state depends only weakly on the CNH-bending angle. We thus finally constructed in Ref. [16] the nonlocal resonance model that is fully based on *ab initio* calculations. The only additional tuning in the model was the shift of the dissociative attachment threshold caused by relaxation of the geometry of the NCO^- fragment. This relaxation cannot be described by a one-dimensional model. Here we use this final model to calculate the vibrational excitation cross sections of the NH-stretch mode. Numerical treatment follows the procedure developed for the nonlocal resonance theory in our earlier works [33–35]. To check the sensitivity of the resulting vibrational excitation cross sections on the fitting procedure in the construction of the nonlocal model, we constructed two additional models with slightly changed assumptions on the analytic form of the model functions. We found that the results are quite robust with respect to these changes, with overall shape of the excitation curves unchanged and the absolute magnitude of the cross sections remaining within 30% of the original data.

IV. RESULTS AND DISCUSSION

Figure 4 shows the electron energy-loss spectrum of HNCO recorded at the constant incident energy of 2.2 eV and at the scattering angle of 135°. The peak at 0 eV (no energy loss) corresponds to the elastic scattering and the higher lying peaks to the excitation of individual vibrational modes. The assignment of the peaks has been done based on the optical infrared (IR) spectra of HNCO [36]; the mode numbering follows Ref. [36]. HNCO has six normal modes. All of them are excited by the electron impact. Apart from these, there are weak peaks visible in the spectra which are overtones and/or combination bands. Of these, the strongest is the first overtone of the NH stretch mode. The low-lying closely spaced bending modes υ_4 to υ_6 are not fully resolved by the spectrometer.

Figures 5 and 6 show the excitation curves of the individual vibrations. They are divided into these two figures depending on whether the one-dimensional nonlocal resonance model provides the theoretical prediction of the corresponding cross

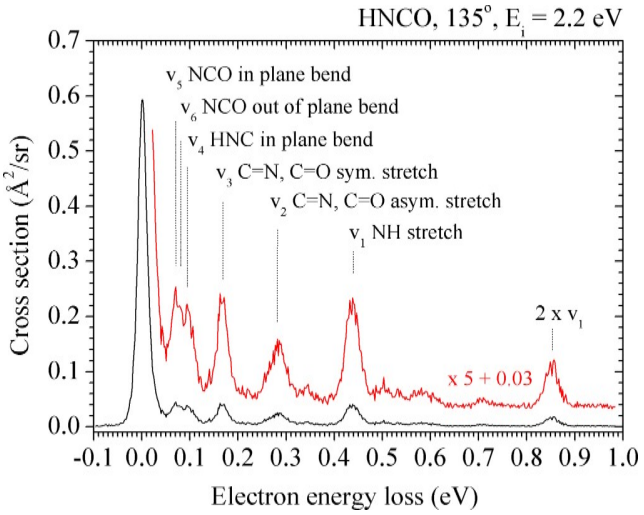

FIG. 4. Electron energy-loss spectrum of HNCO recorded at the constant incident energy of 2.2 eV and at the scattering angle of 135°.

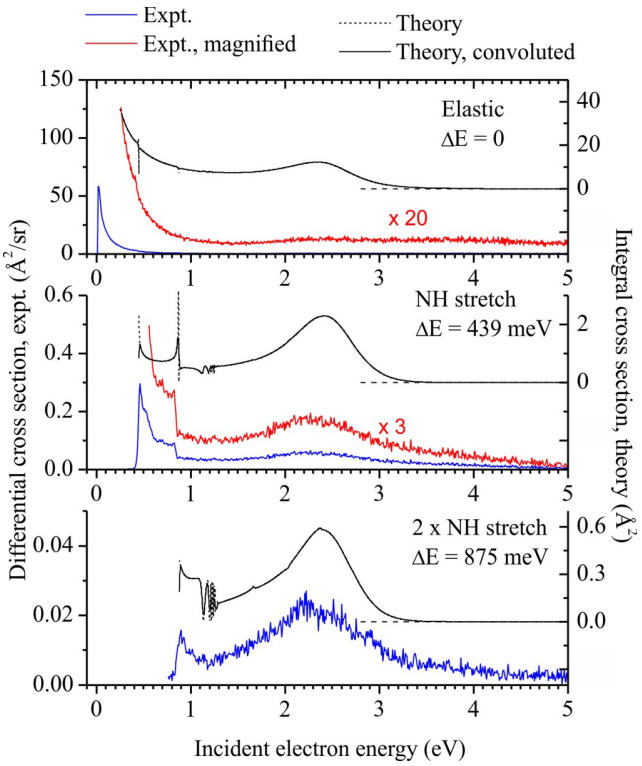

FIG. 5. Excitation curves for elastic scattering ($0 \rightarrow 0$), the NH stretch vibration ($0 \rightarrow 1$), and its first overtone ($0 \rightarrow 2$). The experimental data (noisy lines, left axis) are the differential cross sections at the 135° scattering angle, and the theoretical data (smooth lines, right axis) are the calculated integral cross section. For the sake of clarity, the experimental and theoretical curves are vertically offset. The full theoretical line is the calculated cross section convoluted with a Gaussian of 17-meV FWHM.

sections. We first discuss Fig. 5, i.e., the elastic scattering and the N-H stretch containing vibrations.

There is a very good qualitative correspondence between the experimental and calculated data. The excitation curves for all three channels show a threshold peak of varying intensity. This is typical for dipolar systems [37,38]: The slow incoming electron interacts with the molecule via the long-range potential, which leads to bond deformation, and as it departs, the molecule is left vibrationally excited. The threshold peak for the NH stretch overtone ($0 \rightarrow 2$) transition is very weak. This is expected—the cross section for vibrational excitation in the Born approximation is proportional to IR intensity of the given transition [38]. This is, in the harmonic approximation, zero for the first overtone. In the current model, the threshold peak in the $0 \rightarrow 1$ curve is much weaker than in experiment, but this may well be consequence of reduced dimensionality of the model. The second dominant feature in the cross sections is the broad resonance centered between 2 and 3 eV. This is the $^2A'$ resonance, predicted by the RAC method at 2.49 eV. In the experimental elastic cross section, it is barely visible, but in the $0 \rightarrow 1$ and $0 \rightarrow 2$ NH stretch transitions, it is very clear. The $0 \rightarrow 2$ excitation curve seems to have the maximum shifted to lower energies; actually it rather looks as a small "side" maximum at the left flank of the broad peak. However, this is most likely the effect of a nitrogen impurity in the sample. The frequency of the $N_2(0 \rightarrow 3)$ transition (876 meV) accidentally overlaps with the NH($0 \rightarrow 2$) transition. The excitation function of $N_2(0 \rightarrow 3)$ is known to have very strong oscillatory structure with the maximum at 2.2 eV. Even the trace amount of the residual nitrogen can be responsible for the observed difference in the shape of the NH($0 \rightarrow 1$) and NH($0 \rightarrow 2$) resonance bands.

Additionally, the excitation cross sections show a number of sharp features. These are similar to those observed in low-energy electron scattering from hydrogen halides. From the theoretical point of view, this is not surprising, since the shape of the current model functions is qualitatively similar to those used for treatment of hydrogen halides [39,40]. The different channels are strongly coupled, which results in the presence of the Wigner cusps at opening of higher channels. These cusps in the elastic and $0 \rightarrow 1$ cross sections below 1.1 eV are combined with peaks and dips due to vibrational Feshbach resonances known from scattering of electrons [41] and positrons [42] from molecules. The most prominent cusp is visible in the $0 \rightarrow 1$ cross section at the $0 \rightarrow 2$ threshold energy 0.86 eV; its shape agrees very well in theory and experiment. Theory also predicts a very narrow cusp in the elastic cross section at the $0 \rightarrow 1$ threshold energy 0.44 eV, which is smoother when convoluted according to experimental resolution. Still, there is a hint of a structure in the experimental elastic cross section at this energy. The predicted cusps in the $0 \rightarrow 2$ cross sections above 1.3 eV are unfortunately too weak to be resolved in the experiment. The same is true about the boomerang oscillations [43] visible in the theoretical data below the dissociative attachment threshold at 1.1–1.2 eV. This is a pity because we also do not know if extension of the theoretical model by accounting for other vibrational modes will not suppress these structures. This problem will be subject of future theoretical study.

Figure 6 shows the excitation curves for other HNCO normal modes. It should be remembered that the bending modes

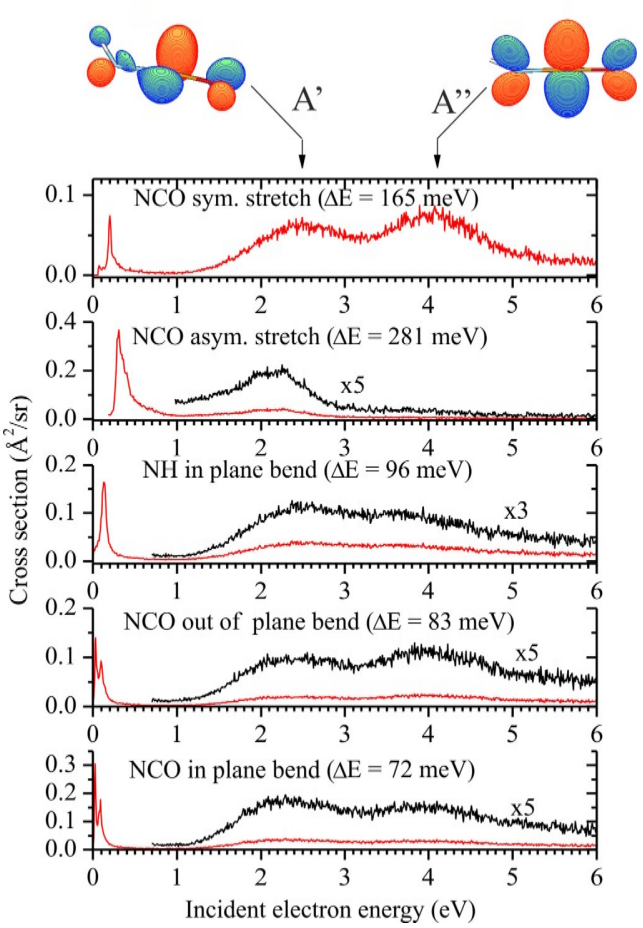

FIG. 6. Excitation curves for the normal modes, which involve multidimensional motion, measured at the 135° scattering angle. The two arrows on top mark the RAC-calculated positions of the A' and A'' shape resonances. The isosurfaces are the singly occupied $HNCO^-$ orbitals in the reference determinant used in the CCSD-T calculations.

are not fully resolved and the individual excitation functions contain contributions of the neighboring mode. This is manifested, for example, in the seemingly doubled threshold peaks in the lowest two panels of Fig. 6; it is an artifact explained in detail in Ref. [44]. Anyhow, apart from the threshold peaks (their intensities again reflect the IR activities of the modes), the spectra are dominated by two resonances. These are the A' resonance, already discussed above, and the A'' resonance. Experimentally, the A'' band is centered around 4 eV, which is in an excellent agreement with the RAC calculated value of 4.10 eV.

The individual modes are excited selectively by the formation of resonances, and especially the A'' is visible only in the NCO symmetric stretch and in the bending modes. As seen from the orbital isosurface in Fig. 6, this is an out-of-plane π^* resonance. The first type of modes which it is expected to excite are thus those that break the planar symmetry. Indeed, it is strong in the NCO out-of-plane bend. In the two in-plane bends, it is visible as much weaker and this is probably again an effect of instrumental resolution. Additionally, the resonance will be visible in modes involving a stretching along the N–C and C–O bonds that are weakened by the presence of the resonant electron. Hence, it is strong in the NCO symmetric stretch mode and invisible in the HN stretch mode in Fig. 5.

In light of this, the absence of the A'' resonance in the NCO asymmetric stretch excitation curve may be surprising. However, this phenomena can be explained by a high similarity between the present out-of-plane π^* resonance and the well-known Π_u shape resonance of CO_2 situated around 3.6 eV [45]. HNCO is isoelectronic with CO_2 and is only slightly bent with respect to the carbon atom. Frequency of the CO_2 symmetric stretch is only different by 7 meV than the one in HNCO and of the asymmetric stretch by 10 meV [46]. Furthermore, the top panel of Fig. 6 shows that the A'' resonance is quite symmetric with respect to interchange of the nitrogen and oxygen atoms. These observations set up conditions for the A'' resonant curve having even symmetry along the asymmetric stretch coordinate ν_2, as occurs in the case of CO_2 [47]. The resulting vibrational excitation cross section is then strongly suppressed for the initial and final vibrational states of different symmetry along the asymmetric stretch coordinate, as was observed in CO_2 both experimentally [45] and theoretically [47]. From the same reason, the A'' resonance is not manifested in the $\nu_2(0 \rightarrow 1)$ asymmetric stretch transition of HNCO.

V. CONCLUSIONS

In conclusion, we probed the vibrational excitation of isocyanic acid by low-energy electron impact. Experimentally, we observe the excitation of all six normal modes. Their excitation curves are rich on various features: They exhibit threshold peaks of varying intensities and two resonances which excite the vibrations selectively. Additionally, the N-H stretch vibration shows a pronounced sharp cusp at the opening of the next vibrational level.

The RAC calculation predicts positions of the two shape resonances in an excellent agreement with the experiment. The properties of their wave functions provide reasoning behind the mode selectivity of the vibrational excitation. The nonlocal resonance model, which was originally constructed to describe the N-H bond cleavage via dissociative electron attachment [16], was used here to calculate the elastic scattering cross section and the cross sections for the $0 \rightarrow 1$ and $0 \rightarrow 2$ excitations of the N-H stretch mode. The model reproduces all the experimentally observed effects and additionally predicts finer features which are hidden in the experiment due to insufficient signal to noise ratio. We would like to stress that even though the model is one dimensional, the qualitative agreement with the present experiment confirms that it describes the N-H stretch motion very well. Still, the considerable excitation of all the other normal modes observed experimentally shows that the dynamics is inherently multidimensional. The addition of other vibrational modes into the nonlocal model would be desirable in the future in order to describe the low-energy electron interaction with HNCO fully.

ACKNOWLEDGMENTS

This work was supported by Projects No. 20-11460S (J.F.), No. 19-20524S (M.Č., K.H., and J.T.), No. 19-03314S

(M.F.), and No. 18-02098S (R.Č.) of the Czech Science Foundation. M.F. also acknowledges ERDF/ESF "Centre of Advanced Applied Sciences" (No. CZ.02.1.01/0.0/0.0/16_-019/0000778).

[1] G. Fedoseev, S. Ioppolo, D. Zhao, T. Lamberts, and H. Linnartz, MNRAS **446**, 439 (2015).
[2] L. Song and J. Kastner, Phys. Chem. Chem. Phys. **18**, 29278 (2016).
[3] L. S. D. Buhl, Astrophys. J. **177**, 619 (1972).
[4] R. L. Brown, Astrophys. J. **248**, L119 (1981).
[5] B. E. Turner, R. Terzieva, and E. Herbst, Astrophys. J. **518**, 699 (1999).
[6] I. Zinchenko, C. Henkel, and R. Q. Mao, Astron. Astrophys. **361**, 1079 (2000).
[7] F. P. Helmich and E. F. van Dishoeck, Astron. Astrophys. Suppl. Ser. **124**, 205 (1997).
[8] S. E. Bisschop, J. K. Jorgensen, E. F. van Dishoeck, and E. B. M. de Wachter, Astron. Astrophys. **465**, 913 (2007).
[9] N. J. Rodriguez-Fernandez, M. Tafalla, F. Gueth, and R. Bachiller, Astron. Astrophys. **516**, A98 (2010).
[10] D. C. Lis, J. Keene, K. Young, T. G. Phillips, D. Bockelée-Morvan, J. Crovisier, P. Schilke, P. F. Goldsmith, and E. A. Bergine,Icarus **130**, 355 (1997).
[11] S. Pimblott and J. la Verne, Radiat. Phys. Chem. **76**, 1244 (2007).
[12] M. Allan, O. May, J. Fedor, B. C. Ibănescu, and L. Andric, Phys. Rev. A **83**, 052701 (2011).
[13] M. Ranković, P. Nag, M. Zawadzki, L. Ballauf, J. Žabka, M. Polášek, J. Kočišek, and J. Fedor, Phys. Rev. A **98**, 052708 (2018).
[14] P. Nag, R. Čurík, M. Tarana, M. Polášek, M. Ehara, T. Sommerfeld, and J. Fedor, Phys. Chem. Chem. Phys. **22**, 23141 (2020).
[15] J. N. Shoolery, R. G. Shulman, and D. M. Yost, J. Chem. Phys. **19**, 250 (1951).
[16] M. Zawadzki, M. Čížek, K. Houfek, R. Čurík, M. Ferus, S. Civiš, J. Kočišek, and J. Fedor, Phys. Rev. Lett. **121**, 143402 (2018).
[17] M. Allan, J. Phys. B: Atom. Molec. Phys. **25**, 1559 (1992).
[18] M. Allan, J. Phys. B: Atom. Molec. Phys. **38**, 3655 (2005).
[19] M. Allan, J. Electr. Spectr. Rel. Phenomena **48**, 219 (1989).
[20] M. Allan, M. Lacko, P. Papp, Š. Matejčík, M. Zlatar, I. I. Fabrikant, J. Kočišek, and J. Fedor, Phys. Chem. Chem. Phys. **20**, 11692 (2018).
[21] G. Fischer, J. Geith, T. M. Klapotke, and B. Krumm, Z. Naturforsch. **57**, 19 (2002).
[22] J. Horáček, I. Paidarová, and R. Čurík, J. Chem. Phys. **143**, 184102 (2015).
[23] R. Čurík, I. Paidarová, and J. Horáček, Europ. Phys. J. D **70**, 146 (2016).
[24] A. F. White, M. Head-Gordon, and C. W. McCurdy, J. Chem. Phys. **146**, 044112 (2017).
[25] T. Sommerfeld, J. B. Melugin, P. Hamal, and M. Ehara, J. Chem. Theory Comput. **13**, 2550 (2017).
[26] R. Čurík, I. Paidarová, and J. Horáček, Phys. Rev. A **97**, 052704 (2018).
[27] P. J. Knowles, C. Hampel, and H. Werner, J. Chem. Phys. **99**, 5219 (1993).
[28] M. J. Deegan and P. J. Knowles, Chem. Phys. Lett. **227**, 321 (1994).
[29] H. J. Werner, P. J. Knowles, R. Lindh, F. R. Knizia, F. R. Manby, M. Schütz *et al.*, MOLPRO, version 2010.1, a package of *ab initio* programs.
[30] T. H. Dunning, J. Chem. Phys. **90**, 1007 (1989).
[31] W. Domcke, Phys. Rep. **208**, 97 (1991).
[32] J. Horáček, I. Paidarová, and R. Čurík, J. Phys. Chem. A **118**, 6536 (2014).
[33] P. Čársky and R. Čurík (eds.), *Low-Energy Electron Scattering from Molecules, Biomolecules, and Surfaces* (CRC Press, Boca Raton, FL, 2012).
[34] M. Čížek, J. Horáček, A.-C. Sergenton, D. B. Popović, M. Allan, W. Domcke, T. Leininger, and F. X. Gadea, Phys. Rev. A **63**, 062710 (2001).
[35] J. Fedor, C. Winstead, V. McKoy, M. Čížek, K. Houfek, P. Kolorenc, and J. Horáček, Phys. Rev. A **81**, 042702 (2010).
[36] M. Lowenthal, R. Khanna, and M. H. Moore, Spectrochim. Acta A **58**, 73 (2002).
[37] I. I. Fabrikant, J. Phys. B: Atom. Molec. Phys. **49**, 222005 (2016).
[38] Y. Itikawa, Int. Rev. Phys. Chem. **16**, 155 (1997).
[39] M. Čížek, J. Horáček, M. Allan, and W. Domcke, Czech. J. Phys. **52**, 1057 (2002).
[40] K. Houfek, Nucl. Instr. Meth. Phys. Res. B **279**, 71 (2012).
[41] H. Hotop, M. Ruf, M. Allan, and I. I. Fabrikant, Adv. At. Mol. Opt. Phys. **49**, 85 (2003).
[42] G. Gribakin, Nucl. Instr. Meth. Phys. Res. B **192**, 26 (2002).
[43] M. Allan, M. Čížek, J. Horáček, and W. Domcke, J. Phys. B **33**, L209 (2000).
[44] T. P. R. Kumar, J. Kočišek, K. Bravaya, and J. Fedor, Phys. Chem. Chem. Phys. **22**, 518 (2020).
[45] M. Allan, J. Phys. B: Atom. Molec. Phys. **35**, L387 (2002).
[46] G. Herzberg, *Molecular Spectra and Molecular Structure I: Spectra of Diatomic Molecules* (Van Nostrand, Princeton, New Jersey, 1950).
[47] V. Laporta, J. Tennyson, and R. Celiberto, Plasma Sources Sci. Technol. **25**, 06LT02 (2016).

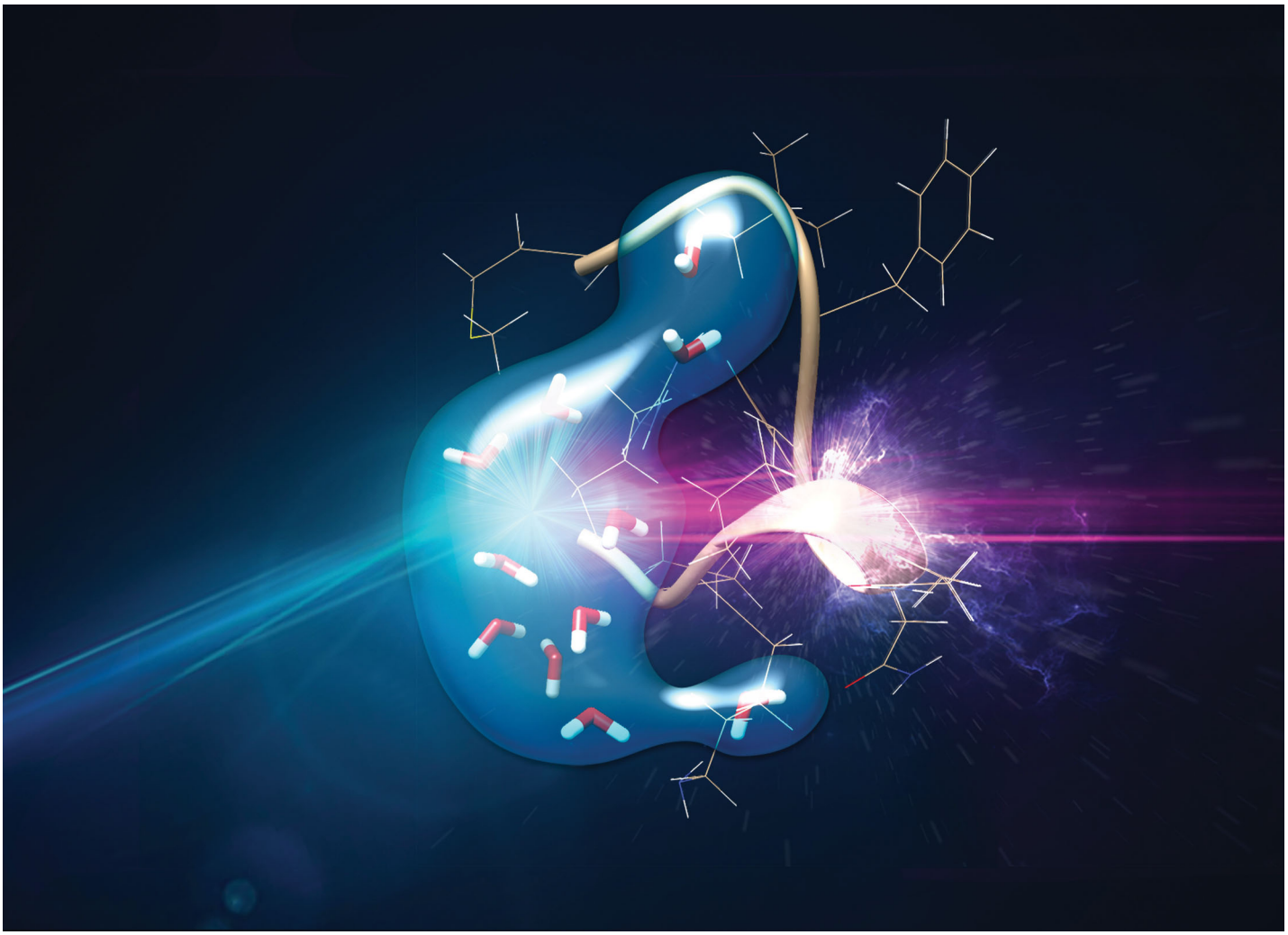

Showcasing research from Dr Aleksandar Milosavljević, Dr Alexandre Giuliani and coauthors performed at SOLEIL synchrotron, France.

Oxygen K-shell spectroscopy of isolated progressively solvated peptide

This work investigates decomposition of an isolated progressively solvated neuropeptide, substance P, upon oxygen core-level resonant excitation by soft X-rays. Oxygen atoms in different chemical environments were probed selectively by fine-tuning the photon energy to be resonant with oxygen atoms in the peptide or the water cluster. Ionic fragmentation of the solvated complexes, observed with a linear ion trap mass spectrometer coupled to the beamline, showed how the excitation of the first water solvation shell influences the fragmentation of the peptide on a molecular level.

As featured in:

See Aleksandar R. Milosavljević, Alexandre Giuliani *et al.*, *Phys. Chem. Chem. Phys.*, 2020, **22**, 12909.

ROYAL SOCIETY OF CHEMISTRY

rsc.li/pccp

Registered charity number: 207890

PCCP

ROYAL SOCIETY OF CHEMISTRY

PAPER

View Article Online
View Journal | View Issue

Cite this: *Phys. Chem. Chem. Phys.*, 2020, **22**, 12909

Oxygen K-shell spectroscopy of isolated progressively solvated peptide†

Aleksandar R. Milosavljević, *[a] Kari Jänkälä, [b] Miloš Lj. Ranković,‡[c] Francis Canon,[d] John Bozek,[a] Christophe Nicolas[a] and Alexandre Giuliani*[ae]

Received 21st February 2020,
Accepted 22nd April 2020

DOI: 10.1039/d0cp00994f

rsc.li/pccp

Gas-phase near-edge X-ray-absorption fine structure (NEXAFS) action spectroscopy around the oxygen K-edge and mass spectrometry were employed to probe isolated substance P (SP) molecular ions, both bare and progressively solvated with 4 and 11 water molecules. Detailed mass spectra of bare and hydrated precursors are presented for the resonant photon energy of 532 eV that corresponds to O1s → $\pi_{(amide)}$* core excitation, triggering resonant Auger decay and fragmentation from the ionized radical molecular system. The fragmentation pattern of doubly protonated SP hydrated with 4 water molecules clearly shows a series of abundant doubly charged backbone fragments, as well as triply charged precursor with small neutral losses, all preserving full water cluster. This is drastically different from the collisional induced dissociation of the hydrated peptide where the water loss is a dominant relaxation process. Moreover, the action NEXAFS obtained from several resolved small backbone fragments revealed increased fragmentation of hydrated SP relative to the bare one, due to a resonant O1s excitation of the attached water molecules. Such unexpected result inspires further experimental developments to investigate possible nonlocal energy transfer from the solvent to the biomolecules within the first solvation shell. The experiment is supported by molecular dynamics and DFT calculations to estimate the intensity of the resonant X-ray absorption of bare and hydrated SP around peptide and water O1s excitation region.

Introduction

There has been a constant effort to study the impact of solvation of biomolecules on an atomic level.[1] Water is ubiquitous in biology and is directly involved in numerous biomolecular processes, such as reactivity, molecular recognition[2–4] and the outcome of vibrational or electronic excitation. In the latter case, solvating water is perceived as a sink able to dissipate the excess energy absorbed by a biochemical system. Upon exposure to ionizing radiation, such as X-rays, the solvating water is a potential source of secondary radiation damage to dissolved molecules through the formation of reactive products upon radiolysis.[5,6] Moreover, previous studies[6,7] indicate that the first solvation shell (structural water) can also induce so-called "quasi direct" damage by a mechanism such as charge transfer. However, in spite of the technical and therapeutic applications of X-rays in imaging and crystallography[8] or radiation therapy,[9] molecular processes in hydrated biomolecules and the effect of the surrounding water molecules are not well understood.[10] Such processes are difficult to study in solution due to the dynamic nature of solvation and the inhomogeneity of the interaction, therefore an experimental approach providing a controllable level of solvation is needed.[10]

Controllably hydrated mass and charge selected biomolecular clusters have been previously characterized through a combination of mass spectrometry, ion mobility and spectroscopic techniques in the infrared or ultraviolet domains.[10,11] These spectral ranges lack the atomic specificity inherent to X-rays, which allows specific atoms within the system to be excited or ionized. Soft X-rays have been used to study smaller systems, such as amino acids or small peptides, in solution or in liquid microjet experiments.[12] In such studies, microsolvation cannot be controlled in a precise way, however, and the spectra obtained reflect only the average local environment. Although both approaches are of great value, there is a pressing need to

[a] *SOLEIL, l'Orme des Merisiers, St Aubin, BP48, 91192 Gif sur Yvette Cedex, France. E-mail: milosavljevic@synchrotron-soleil.fr*
[b] *Nano and Molecular Systems Research Unit, University of Oulu, P.O. Box 3000, 90014 Oulu, Finland*
[c] *Institute of Physics Belgrade, University of Belgrade, Pregrevica 118, 11080 Belgrade, Serbia*
[d] *Centre des Sciences du Goût et de l'Alimentation, CNRS, INRAE, Université de Bourgogne Franche-Comté, F-21000 Dijon, France*
[e] *INRAE, UAR1008, Transform Department, Rue de la Géraudière, BP 71627, 44316 Nantes, France. E-mail: giuliani@synchrotron-soleil.fr*

† Electronic supplementary information (ESI) available. See DOI: 10.1039/d0cp00994f

‡ Present address: Institute of Physical Chemistry J. Heyrovsky, CAS, Dolejškova 3, 18223 Prague 8, Czech Republic.

combine the two methodologies in order to address larger peptides hydrated in a controlled manner with the atomic sensitivity provided by soft X-rays.

In the following we present the first spectroscopic study at the oxygen K-shell edge of a neuropeptide, substance P (SP), and upon addition of 4 and 11 water molecules in a gas phase microsolvation cluster. Doubly protonated ions of SP, bare and hydrated by 4 and 11 water molecules were formed from an aqueous solution of the peptide using electrospray ionization. The clusters of interest were mass and charge selected, stored in a linear ion trap and then irradiated using synchrotron radiation in the 530–539 eV range.[13] In this photon range, we dominantly probe resonant absorption at discrete energies by the oxygen atoms in different chemical environments.

Experimental and theoretical methods

Action spectroscopy

The experimental setup is based on a commercial linear quadrupole ion trap mass spectrometer, which was coupled to the soft X-ray beamline PLEIADES at the synchrotron radiation facility SOLEIL (France), as described previously.[13,14] The photon irradiation time of 500 ms was controlled by a mechanical shutter activated by a signal sent from the spectrometer through a pulse generator (DG645, Stanford 150 Research Systems, Sunnyvale, CA, USA) that ensures a short delay (50 ms) of ion recording in order to reduce background contributions. The doubly protonated substance P molecules were generated by a nano-electrospray (NSI) from a pure water solution at 100 μM. The NSI potentials were adjusted to preserve the hydrated species, and the temperature of the transfer tube was kept at 50–70 °C. The X-ray beam was introduced from the back side of the trap connected to the beamline *via* a dedicated differential pumping stage. For each precursor, the tandem mass spectra were recorded during 10–15 min, as a function of the photon energy scanned in small steps of 0.2/0.25 eV from 529 to 540 eV, resulting in a total scanning time of 8–13 hours per initial species. For each NEXAFS scan, under the same beamline parameters, the corresponding energy dependence of the photon flux was measured either before or after the scan, by using a photodiode (AXUV-100, IRD) placed in a differentially pumped vacuum chamber upstream to the ion trap. The final NEXAFS spectra were normalized to this photon flux and the total ion current (or precursor intensity) measured by the LTQ.

The transfer of protonated SP from solution to the gas phase has been investigated in details previously[15,16] by using cryogenic ion mobility-mass spectrometry.[17] The studies have shown that upon electrospray ionization, the doubly protonated SP dehydrated conformers observed in the gas phase originate from stepwise evaporation of extensively hydrated clusters, so they are produced by the charge residue model (CRM).[15] Moreover, the authors[15] argued that the population of so produced conformers resembles the native one in the solution. However, since our ion trap mass spectrometer operates at the room temperature, the density of hydrated precursors strongly decreases with the increase of the number of attached water molecules.[15]

Collision induced dissociation (CID) experiments were conducted on the hydrated precursor ions to make sure these ions were actually containing water. Indeed, under CID activation conditions, the hydrated peptide ions lose several water molecules. The nature of the fragment ion was assessed by the comparison of the m/z with theoretical values and also by checking the isotopic ratio of the ions, from which the charge could be determined.

Samples

Substance P acetate salt hydrate has been provided by Sigma Aldrich, with a stated purity ~95%, and has been dissolved in pure Milli-Q water solution at 100 μM. The photon energy calibration was performed with molecular CO_2 gas from Air Liquide, with a stated purity of 99.998%, respectively.

PLEIADES beamline

A permanent magnet APPLE II type undulator, with a period of 80 mm, was used as synchrotron radiation source, with a circular polarization providing high photon flux in the O K-edge region (520–550 eV). A high-flux, 600 l mm^{-1} grating was used to monochromatize the synchrotron radiation produced by the undulator. The exit slit of the modified Pertersen plane grating monochromator was set to 200 μm and 800 μm, to reach an average resolution of 0.6 eV and 2.6 eV, for bare and hydrated SP, respectively. The photon energy was calibrated according to O1s → π* transition in CO_2 reported at 535.4 eV.[18] The calibration gas was introduced to the calibration chamber (upstream of the ion trap) by an effusive jet crossing at right angles the SR beam, the created ions were extracted by a continuous electric field and detected using two polarizable grids which attract the cations, a multichannel plates chevron stacks, and a 50 Ω-adapted full-metal anode. The calibration was performed several times during the experiment, before or after the NEXAFS scans, and for some spectra of bare SP, even in parallel to the scan. The overall accuracy of the photon energy calibration (bare and hydrated precursors) was estimated to be 100 meV, not including the error of the literature value for CO_2.[18]

Calculations

The theoretical oxygen K-shell absorption spectra were obtained by combining molecular dynamics (MD) simulations with quantum mechanical time-dependent density functional theory (TD-DFT).[19] Due to the size, type and internal temperature of the studied target, the observed absorption spectra are composed of averages of spectra from a multitude of different geometrical orientations. This was accounted by running MD simulations where the system consisting of bare protonated substance P or protonated substance P with 11 water molecules was first annealed for 3 ns and then run for 3 ns in stable conditions. From the final 2 ns of the MD runs 10 random snapshots were selected for further TD-DFT calculations providing the averaged K-shell absorption spectra. MD simulations

were done by using GROMACS[20] with CHARMM27 force field with TIP3P model for water.[21] The TD-DFT calculations were carried out using ORCA[22] package with cc-pVDZ basis set[23] and B3LYP[24] exchange–correlation functional together with RIJ-COSX approximation for the Coulomb integrals.[25] The B3LYP calculation typically underestimates the core excitation energies (about 14 eV in the present case), therefore, the energy was calibrated to a water spectrum (see below). Initial conformation for the bare protonated substance P was obtained by first optimizing the structure using Avogadro program[26] and refining it using ORCA with the same basis set and functional that is used in the TD-DFT calculations.

Results and discussion

Promotion of oxygen core electrons to unoccupied molecular orbitals produces highly unstable core-excited states that will decay primarily through the emission of an Auger electron. In this process, a valence electron fills the core vacancy and another valence electron is emitted into the continuum.[27] Ultimately, such resonant Auger decay leads to the formation of radical cations or fragment ions, both of which may be observed by mass spectrometry.

A theoretical photoabsorption curve of an isolated doubly protonated bare SP peptide ion, obtained by molecular dynamics (MD) and density functional theory (DFT) calculations (see Fig. SI.1 for example structures, ESI†), is presented in Fig. 1 (blue curve). The theoretical curve is broadened according to the experimental resolution and compares very well to the experimental total ion yield (TIY) curve, obtained as a sum of dominant well-resolved singly, doubly and triply charged fragments (see Fig. 2a and further discussion below). As expected, the spectra reveal dominant O1s → $\pi_{(amide)}^*$ resonance, indicating strong fragmentation of the molecule upon resonant Auger decay, as shown previously for a protein.[13] The theoretical energy scale has been independently calibrated according to the first water resonance (Fig. 1, orange curve, transition $1a_1$ to the mixed $4a_1/3sa_1$ state[28]), and matches perfectly the position of the measured peptide resonance. The present experimentally determined resonant energy of 532.15 ± 0.10 eV is close to the previously reported O1s → $\pi_{(amide)}^*$ (O═CNH) for small gaseous dipeptide molecules: 532.2 eV[29] and 531.85 eV.[30]

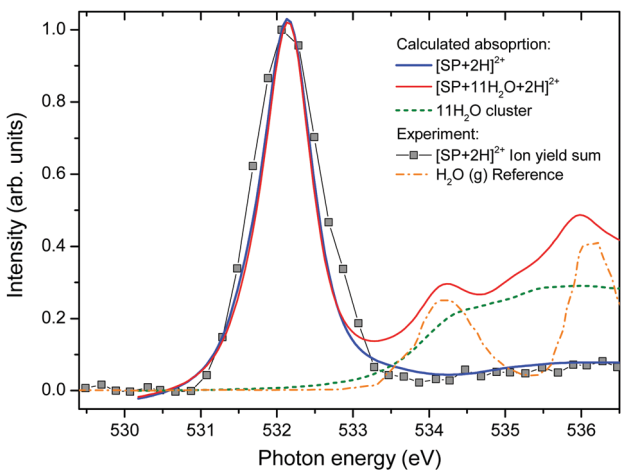

Fig. 1 Theoretical absorption intensity of bare substance P (blue curve), substance P hydrated with 11 water molecules (red curve) and the water cluster isolated from the peptide (dotted green curve). The experimental total ion yield obtained as a sum over all resolved fragments in the *m*/*z* 200–650 range (see Fig. 2) for bare substance P is presented by gray square symbols. The previously published total ion yield of gaseous water[46] is also shown (orange dash-dotted line).

The SP used in the present experiment is the substance P acetate salt hydrate (as provided by Sigma-Aldrich), therefore it should not have OH and COOH groups, excluding thus O1s excitation to the associated high-energy lying (>535 eV) σ_{OH}^* and σ_{C-OH}^* molecular orbitals, as reported from gas phase NEXAFS spectroscopy of small dipeptides.[29,30] On the other hand, the amide σ_{OCNH}^* resonance was previously reported at 534 eV.[29] Therefore, somewhat increased fragmentation of bare SP at higher photon energies can be due to O1s – Rydberg transitions,[31,32] and/or the opening of direct ionization channel, above the O K-shell ionization potential (IP), which we estimate to be above 538 eV. Since the acetylated form of SP does not possess any OH groups, photoabsorption by the hydrated targets in the 534–538 eV range can be ascribed mainly to the oxygen belonging to the water molecules,[33] whereas in the 530–534 eV region primarily oxygen atoms from the peptide moiety are photoexcited, as shown by the calculations in Fig. 1. Hence, resonant Auger excitation enables specific oxygen atoms of the clusters, from the peptide chain or the water molecules to be selected, as already proposed by Gokhberg *et al.*[27]

Fig. 2 shows the tandem mass spectra upon irradiation of the different precursor ions at the resonant photon energy that corresponds to the most intensive O1s → $\pi_{(amide)}^*$ excitation found at about 532 eV (see Fig. 1). In recent years, SP has become a model peptide system that has been investigated by a number of activation methods.[34–41] There has been no studies, however, on soft X-ray induced dissociation of SP by resonant photon absorption at the oxygen K-edge. Fig. 2a shows a rich fragmentation pattern dominated by a, b and c backbone fragments, corresponding to C–C, C–N and N–C bond cleavage, respectively, with charge residing on the N-terminal, following the Biemann's nomenclature.[42] This indicates, as expected,[15] that the protonation sites of the protonated SP precursor are localized near the N-terminus. The strongest channels correspond to small singly charged and large doubly charged a and b fragments, as well as triply charged ions of ionized precursor $[SP + 2H]^{3+}$ with associated neutral losses. The recorded fragmentation pattern of doubly protonated SP (Fig. 2a) appears to be similar to previously reported electron ionization dissociation (EID) spectrum.[38] In the present case, the O1s electron excitation to an unoccupied molecular orbital produces a core hole, resulting in a highly energetic excited state which quickly relaxes (on a femtosecond time scale) by a spectator resonant Auger decay,[43] resulting in single or multiple ionization of the doubly protonated precursor. Therefore, as in the case of EID,[38] the precursor dissociation probably occurs from a highly

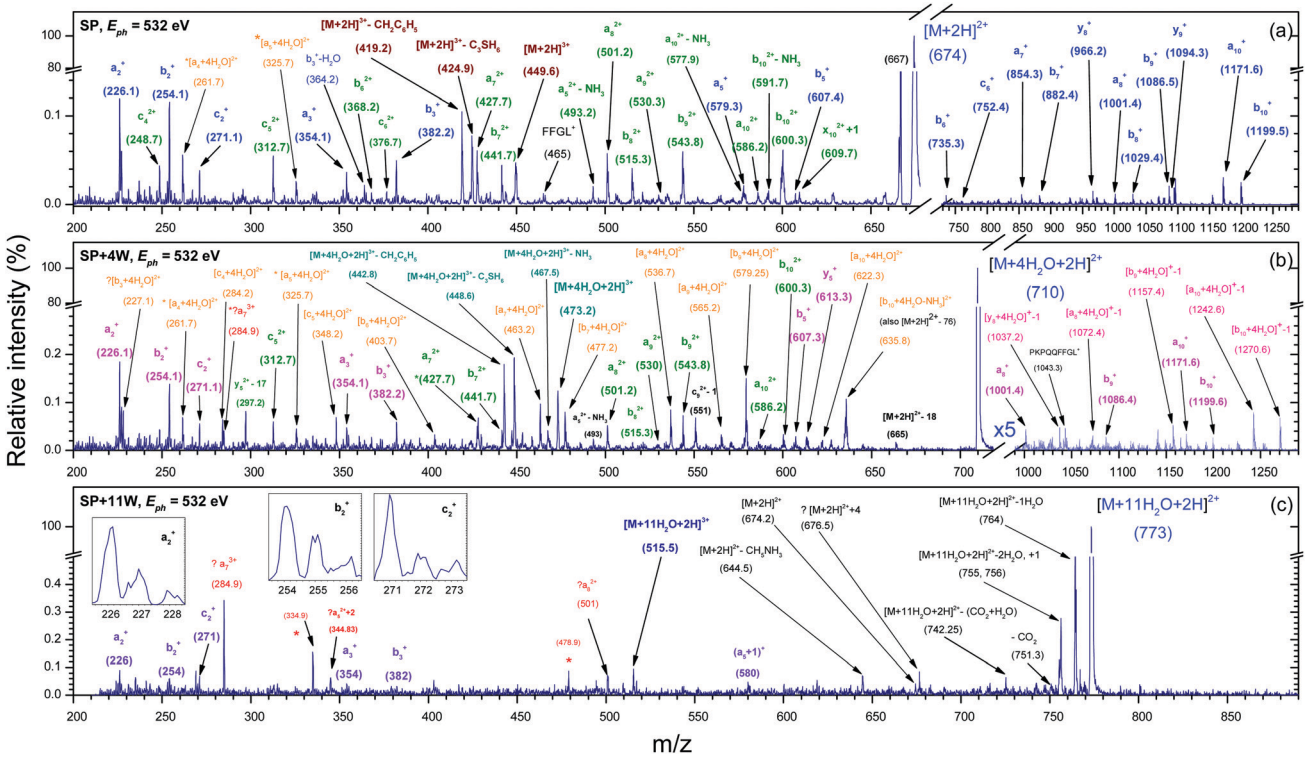

Fig. 2 Tandem mass spectra (MS^2) of bare and hydrated substance P. MS^2 of (a) $[SP + 2H]^{2+}$ (*m/z* 674), (b) $[SP + 4H_2O + 2H]^{2+}$ (*m/z* 710) and (c) $[SP + 11H_2O + 2H]^{2+}$ (*m/z* 773), recorded after 500 ms irradiation at the photon energy of 532 eV. The insets in (c) show a zoom-in of the selected *m/z* regions. The assignment of the fragments is given in the figure (different colors correspond to different charge states and precursors).

excited ionized radical. Still, a significantly higher energy stored in the system and possibility to produce multiply ionized radicals, provides even richer fragmentation pattern.

Fig. 2b presents fragmentation of doubly protonated SP, hydrated with 4 water molecules $[SP + 4H_2O + 2H]^{2+}$ at 532 eV. There are immediately several striking observations when comparing the fragmentation pattern of hydrated SP to the bare one (Fig. 2a). Both the ionized hydrated precursor $[SP + 4H_2O + 2H]^{3+}$ and all associated triply charged species formed by neutral losses preserve the whole water cluster. Furthermore, all doubly charged backbone fragments dominantly preserve the water cluster, allowing for the resolving a whole series of fully hydrated a, b and c backbone fragments. Note that the ionic species match both the expected *m/z* position and the isotopic mass distribution. Another striking observation is that the inner-shell excitation of the $[SP + 4H_2O + 2H]^{2+}$ precursor does not induce a significant water loss, which is barely seen in the mass spectrum. This is in strong contrast to the CID (Fig. SI.2, ESI†), where a detachment of 1 or 2 water molecules represents the dominant relaxation channel. Therefore, even though a large amount of energy is stored in the hydrated precursor through the peptide O1s core excitation, the weak hydrogen bonds linking the molecules in a water cluster attached at the protonation site of the peptide stay unaffected. On the other hand, interestingly the small singly charged backbone fragments are dominantly formed without attached water. Thus, they seem to be produced by a severe destruction of the precursors and, as in the case of SP, represent one of the dominant fragmentation channels. It should be noted that fragments with *m/z* smaller than about 200 could not be detected in our experiment.

By increasing the number of attached water molecules to 11, the tandem mass spectrum becomes more difficult to analyze (Fig. 2c). Since the $[SP + 11H_2O + 2H]^{2+}$ precursor was of very low abundance, this is also the case with the peptide fragments; additionally, the precursor *m/z* isolation window always contained a non-negligible amount of background pollutants. It is also important to note that $[SP + 11H_2O + 2H]^{2+}$ precursor significantly loses water molecules (''evaporates'') just by being preserved in the ion trap during the irradiation time of 500 ms, even without photon irradiation (see Fig. SI.3, ESI†). Therefore, as in the case of $[SP + 4H_2O + 2H]^{2+}$, the apparent photon-induced water loss is rather weak. This suggests that the hydration of SP does not protect the peptide from X-ray induced fragmentation. Such effect has been previously reported in the case of collision-induced fragmentation of isolated adenosine monophosphate ions, which appeared strongly suppressed by increasing the number of attached water molecules above 13, due to evaporative cooling of the system.[44] Likewise, it is difficult to clearly conclude if the apparent lack of any hydrated peptide fragments for $[SP + 11H_2O + 2H]^{2+}$ precursor is due to the fact that the larger attached water cluster is less stable and is preferably destroyed upon fragmentation (taking also into account that large precursor encounters more collisions due to a big cross section, leading to higher internal energy), or simply the hydrated fragments are below the detection limit and could

not be resolved from the background. For the present study, it is important that at least several specific peptide fragments, as well as the triply charged hydrated peptide $[SP + 11H_2O + 2H]^{3+}$ (the ionized precursor), could be well-resolved in the mass spectrum. This allows studying the photon energy deposition in the micro-solvated precursor over the oxygen K-edge by the action NEXAFS spectroscopy.

The present experimental method provides means of analyzing each separate fragment ion yield for a selected precursor. A detailed study of the energy dependence of different peptide fragmentation channels would be, however, out of limit of the present paper. The O K-edge action NEXAFS spectra of SP, which represent partial ion yields summed over specified singly, doubly and triply charged fragments (see Fig. 2), are shown in Fig. 3. A significant fragmentation of the peptide also exists below the O1s excitation threshold, due to C and N K-shell, as well as direct outer-shell ionization, producing a flat background in the action NEXAFS spectra (insets in Fig. 2a and b). The interesting finding is that the yield of small singly charged backbone fragments (Fig. 3a) increases markedly stronger with the photon energy above the O1s $\rightarrow \pi_{(amide)}^*$ resonance, than that of larger doubly and triply charged ions (Fig. 3b and c). The large doubly and triply charged backbone fragments apparently cannot survive higher energy load into the peptide system. It should be noted that a similar effect has been reported previously in a study of near C-edge X-ray absorption mass spectrometry of a smaller protonated leucine encephalin peptide isolated in the gas phase.[45] The authors observed that the large fragments mainly resulted from C1s excitation and not from ionization. In the present study, with increasing the size of the singly charged fragments the associated ion yields become less dependent on the photon energy.

Fig. 4a and c compare the sum over the selected fragment ion yields (a_2, a_3, b_2, b_3, and c_2, which can be clearly resolved for all three target precursors) for the solvated peptide to those of the bare peptide. Fig. 4b and d present the yields of the bare protonated peptide $[SP + 2H]^{2+}$ corresponding to the loss of all water molecules. The maximum fragmentation yields for all product ions in Fig. 4 are observed for the peptide O1s $\rightarrow \pi_{(amide)}^*$ resonance at around 532 eV. While the product ion yields for bare SP remain lower between 534 eV and 538 eV, Fig. 4a and c highlight that hydration of SP results in an enhanced fragmentation efficiency in that energy range. As mentioned above, this spectral region involves the well-known transitions from the water O1s levels to the $4a_1$, $2b_2$ and $2b_1$ orbitals (see Fig. 1).[46]

Absorption of a photon by the non-covalently bonded water molecules surprisingly leads to considerably enhanced fragmentation of the peptide backbone (Fig. 4a and c), rather than just a loss of water molecules (Fig. 4b and d). This is intuitively unexpected, since one would presume that a core excitation of the water cluster triggers an ultra-fast local resonant Auger decay that promptly destroys the weakly bound water network. The observed effect cannot be clearly explained by any of the expected indirect radiation damage mechanisms. Following oxygen K-shell photoexcitation, the resonant Auger decay of water will produce radicals, ions and energetic electrons.

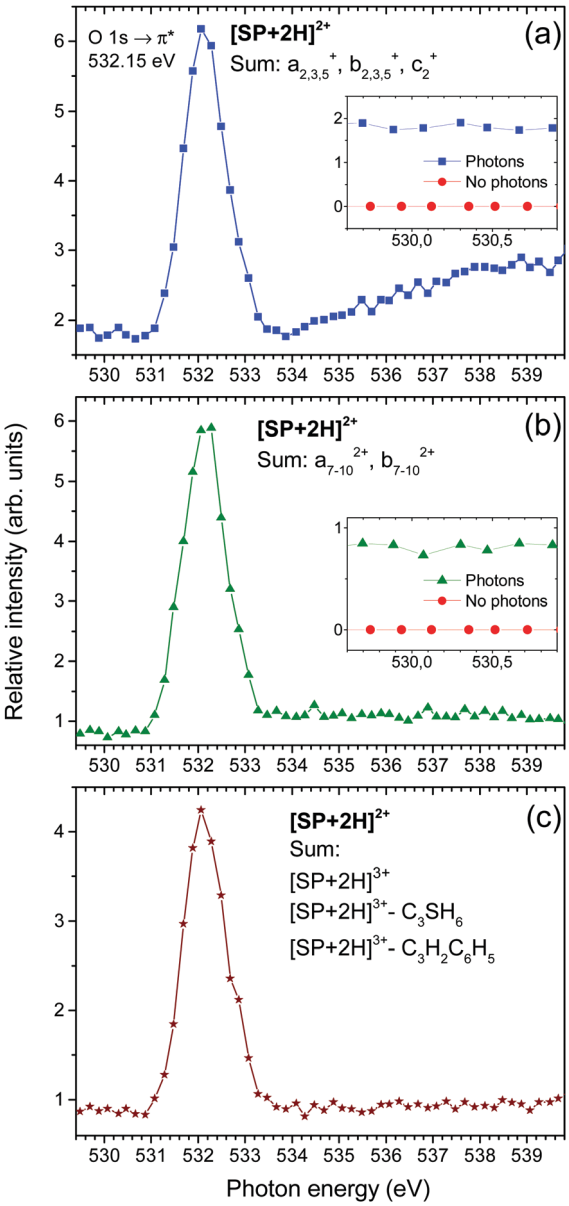

Fig. 3 Normalized photodissociation ion yields from doubly protonated bare substance P $[SP + 2H]^{2+}$ precursor. The yields are obtained by summing up fragmentation intensity of resolved singly charged backbone fragments (a), doubly charged backbone fragments (b), and triply charged precursor and associated small neutral losses (c). The integrated mass ranges include the isotopic distribution of the corresponding peaks. The insets in (a) and (b) show the signal intensity along the base line with and without the photon irradiation. The colors correspond to the color scheme used in Fig. 2.

The effect of protons, O^+ or OH^+ cations can be disregarded as overcoming the Coulomb barrier generated by the two protonated sites on the peptide would require high kinetic energy. The reaction with OH radical should have led to the observation of oxidation products of the protonated molecule corresponding to mass increase of 16 or 14 Da,[47] along with the backbone fragments. High flux of H atoms is necessary to interact with the peptide ions, the main product of the reaction being the attachment and abstraction of H atoms from the

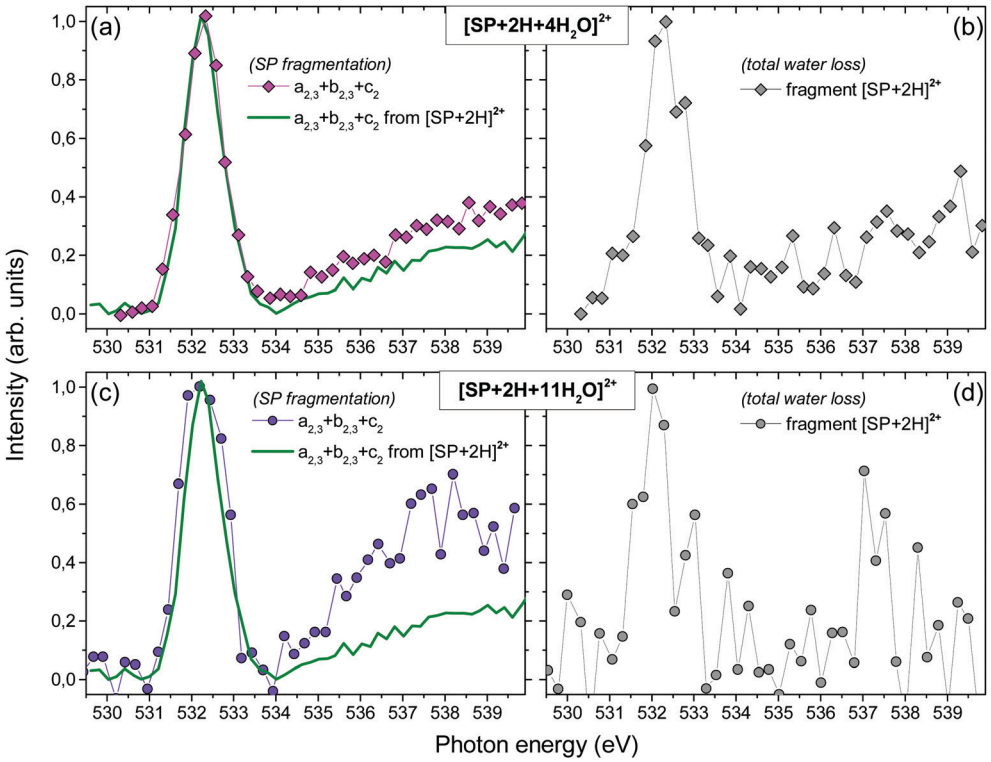

Fig. 4 Experimental product ion yields for substance P hydrated with 4 (a and b) and 11 (c and d) water molecules, respectively $[SP + 2H + 4H_2O]^{2+}$ and $[SP + 2H + 11H_2O]^{2+}$ precursors. Left panels present the sum of yields of a_2, a_3, b_2, b_3 and c_2 ions, linked to fragmentation of the peptide backbone. The corresponding ion yields for the bare substance P precursor $[SP + 2H]^{2+}$ are compared to the hydrated ones in panels (a) and (b) (green curves). A net increase in the product ion yields is observed above 535 eV on the hydrated ions. The right panels present the fragmentation channel corresponding to the total loss of attached water molecules from hydrated substance P ion precursors, resulting in $[SP + 2H]^{2+}$ ion yields. The intensity of the $[SP + 2H]^{2+}$ yield relative to the precursor above 535 eV is about 50 (b) and 5 (d) times lower than the intensity of the corresponding backbone fragment a_2.

precursor ion, thereby affecting its isotopic distribution pattern groups.[48] We do not observe any such modifications under our conditions. Reactions of electrons with kinetic energies of hundreds of eV, such as would result from Auger decay in water, with isolated peptide ions have been reported previously.[49,50] The main outcome of such interactions is the formation of the ionized radical precursor, along with a lower abundance of fragment ions. Hence, Auger electrons emitted by water molecules would ionize the doubly protonated peptide precursor ion into a triply charged radical. The corresponding peptide triply charged yield curve (Fig. SI.4, ESI†) would exhibit an increase in the vicinity of water absorption (534–538 eV), which is not the case. Note that all ionized precursors are sufficiently stable to be detected as clearly seen at the peptide resonance of 532 eV in Fig. SI.4 (ESI†). Finally, the conversion of Coulomb energy into internal excitation energy was reported for long distance interaction with highly charged ions (Xe^{20+}),[51,52] which is very different from the present case, where the absorbing water molecules are in close proximity with the target and would gain 2 or 3 charges upon Auger decay.

Previous macroscopic studies with ''dry'' plasmid DNA have shown that X-ray absorption by the primary hydration shell resulted in ''quasi direct'' damage to DNA.[6,7] This effect was tentatively ascribed to the charge transfer (see ref. 7 and references therein). The present work, therefore, may represent an experimental demonstration at the molecular level of such quasi-direct radiation damage. Our experimental method, however, cannot determine which mechanism exactly is involved in the process that results in the fragmentation of a biomolecule due to a core–shell excitation of closely situated structural water molecules. One possibility is, for example, a non-local energy transfer such as intermolecular coulombic decay (ICD),[27,53–56] which represents a very efficient relaxation mechanism in weakly bound systems through the transfer of the excess of energy from the absorbing center to the neighbors. These processes have been studied in prototypical systems, such as in water clusters,[53,57] liquid jets of pure water[54] and solvated organic ions,[55] suggesting its importance on radiation damage to real biological systems. Recently, Gokhberg *et al.*[27] have shown that such processes could take place following resonant Auger decay. Note that from the radial distribution functions for the water–peptide and water–water distances calculated for three molecular dynamic simulations (Fig. SI.5, ESI†), it appears that the water molecules are more likely to be closer to the peptide than to the other members of the water cluster; a nonlocal energy transfer process has therefore higher probability to involve the peptide than another water molecule, and thus should be operative for the first solvation shells around the biomolecule. Still, an unambiguous proof requires further, more complex experiments, in which, for example, the electrons

emitted from hydrated biomolecules would be collected and measured.

Conclusions

In conclusion, we have performed an oxygen K-shell action X-ray spectroscopy and mass spectrometry to study a progressively micro-solvated peptide ion isolated in an ion trap at room temperature. The action NEXAFS spectra of both bare and hydrated targets show strong photon absorption and increased peptide fragmentation at the resonant energy of about 532 eV corresponding to O1s $\rightarrow \pi_{(amide)}^*$ transition, in agreement with previously reported values for small peptides. The X-ray photon induced fragmentation of SP is triggered by the resonant Auger decay process and strongly differs to the CID. This is also the case for the hydrated SP targets, with the notable exception of $(SP + 4H_2O + 2H)$ precursor where doubly ionized precursor and doubly charged backbone fragments retaining all the water molecules are also very abundant.

Finally, the present experiment also shows that increased hydration of SP results in an enhanced fragmentation of the peptide backbone upon X-ray absorption by water molecules. The later results may represent the first observation of the radiation damage of a biomolecule caused by closely situated structural water, on the molecular level. The present method offers great potential to further investigate such processes in specific microhydrated bio-systems and allows for better understanding of possible nonlocal relaxation mechanisms that could play a substantial role in radiation damage in aqueous environments.

Conflicts of interest

There are no conflicts to declare.

Acknowledgements

SOLEIL support is acknowledged under projects no. 20160335 and 20161170. We also thank the technical staff of SOLEIL for smooth and efficient running of the facility. This work was partially supported by the Agence Nationale de la Recherche Scientifique, France, under Project Number ANR-08-BLAN-0065. M. R. acknowledges support from the Ministry of education, science and technological development of Republic of Serbia under the grant OI 171020.

Notes and references

1 O. Dopfer and M. Fujii, Probing Solvation Dynamics around Aromatic and Biological Molecules at the Single-Molecular Level, *Chem. Rev.*, 2016, **116**, 5432–5463.
2 P. Ball, Water as an active constituent in cell biology, *Chem. Rev.*, 2008, **108**, 74–108.
3 S. K. Pal and A. H. Zewail, Dynamics of Water in Biological Recognition, *Chem. Rev.*, 2004, **104**, 2099–2124.
4 H. Fujisaki and J. E. Straub, Vibrational energy relaxation in proteins, *Proc. Natl. Acad. Sci. U. S. A.*, 2005, **102**, 6726–6731.
5 B. Boudaïffa, P. Cloutier, D. Hunting, M. A. Huels and L. Sanche, Resonant Formation of DNA Strand Breaks by Low-Energy (3 to 20 eV) Electrons, *Science*, 2000, **287**, 1658–1660.
6 D. Becker and M. D. Sevilla, The Chemical Consequences of Radiation Damage to DNA, *Adv. Radiat. Biol.*, 1993, **17**, 121–180.
7 A. Eschenbrenner, M. A. H. Du Penhoat, A. Boissiere, G. Eot-Houllier, F. Abel, M. F. Politis, A. Touati, E. Sage and A. Chetioui, Strand breaks induced in plasmid DNA by ultrasoft X-rays: Influence of hydration and packing, *Int. J. Radiat. Biol.*, 2007, **83**, 687–697.
8 O. Carugo and K. D. Carugo, When X-rays modify the protein structure: Radiation damage at work, *Trends Biochem. Sci.*, 2005, **30**, 213–219.
9 D. De Ruysscher, G. Niedermann, N. G. Burnet, S. Siva, A. W. M. Lee and F. Hegi-Johnson, Radiotherapy toxicity, *Nat. Rev. Dis. Prim.*, 2019, **5**, 13.
10 N. S. Nagornova, T. R. Rizzo and O. V. Boyarkin, Interplay of Intra- and Intermolecular H-Bonding in a Progressively Solvated Macrocyclic Peptide, *Science*, 2012, **336**, 320–323.
11 A. R. Milosavljević, V. Z. Cerovski, F. Canon, L. Nahon and A. Giuliani, Nanosolvation-Induced Stabilization of a Protonated Peptide Dimer Isolated in the Gas Phase, *Angew. Chem., Int. Ed.*, 2013, **52**, 7286–7290.
12 J. W. Smith and R. J. Saykally, Soft X-ray Absorption Spectroscopy of Liquids and Solutions, *Chem. Rev.*, 2017, **117**, 13909–13934.
13 A. R. Milosavljević, F. Canon, C. Nicolas, C. Miron, L. Nahon and A. Giuliani, Gas-phase protein inner-shell spectroscopy by coupling an ion trap with a soft X-ray beamline, *J. Phys. Chem. Lett.*, 2012, **3**, 1191–1196.
14 A. R. Milosavljević, C. Nicolas, J. F. Gil, F. Canon, M. Réfrégiers, L. Nahon and A. Giuliani, VUV synchrotron radiation: A new activation technique for tandem mass spectrometry, *J. Synchrotron Radiat.*, 2012, **19**, 174–178.
15 J. A. Silveira, K. L. Fort, D. Kim, K. A. Servage, N. A. Pierson, D. E. Clemmer and D. H. Russell, From Solution to the Gas Phase: Stepwise Dehydration and Kinetic Trapping of Substance P Reveals the Origin of Peptide Conformations, *J. Am. Chem. Soc.*, 2013, **135**, 19147.
16 K. A. Servage, J. A. Silveira, K. L. Fort and D. H. Russell, From Solution to Gas Phase: The Implications of Intramolecular Interactions on the Evaporative Dynamics of Substance P during Electrospray Ionization, *J. Phys. Chem. B*, 2015, **119**, 4693–4698.
17 K. A. Servage, J. A. Silveira, K. L. Fort and D. H. Russell, Cryogenic Ion Mobility-Mass Spectrometry: Tracking Ion Structure from Solution to the Gas Phase, *Acc. Chem. Res.*, 2016, **49**, 1421–1428.
18 M. N. Piancastelli, A. Kivimäki, B. Kempgens, M. Neeb, K. Maier and A. M. Bradshaw, High-resolution study of resonant decay following the O1s $\rightarrow \pi^*$ excitation(s) in CO_2: evidence for an overlapping Rydberg transition, *Chem. Phys. Lett.*, 1997, **274**, 13–17.

19 E. Runge and E. K. U. Gross, Density-Functional Theory for Time-Dependent Systems, *Phys. Rev. Lett.*, 1984, **52**, 997–1000.
20 B. Hess, C. Kutzner, D. Van Der Spoel and E. Lindahl, GRGMACS 4: Algorithms for highly efficient, load-balanced, and scalable molecular simulation, *J. Chem. Theory Comput.*, 2008, **4**, 435–447.
21 W. L. Jorgensen, J. Chandrasekhar, J. D. Madura, R. W. Impey and M. L. Klein, Comparison of simple potential functions for simulating liquid water, *J. Chem. Phys.*, 1983, **79**, 926–935.
22 F. Neese, The ORCA program system, *Wiley Interdiscip. Rev.: Comput. Mol. Sci.*, 2012, **2**, 73–78.
23 T. H. Dunning, Gaussian basis sets for use in correlated molecular calculations. I. The atoms boron through neon and hydrogen, *J. Chem. Phys.*, 1989, **90**, 1007–1023.
24 C. Lee, W. Yang and R. G. Parr, Development of the Colle-Salvetti correlation-energy formula into a functional of the electron density, *Phys. Rev. B: Condens. Matter Mater. Phys.*, 1988, **37**, 785–789.
25 F. Neese, F. Wennmohs, A. Hansen and U. Becker, Efficient, approximate and parallel Hartree–Fock and hybrid DFT calculations. A 'chain-of-spheres' algorithm for the Hartree–Fock exchange, *Chem. Phys.*, 2009, **356**, 98–109.
26 M. D. Hanwell, D. E. Curtis, D. C. Lonie, T. Vandermeersch, E. Zurek and G. R. Hutchison, Avogadro: an advanced semantic chemical editor, visualization, and analysis platform, *J. Cheminf.*, 2012, **4**, 17.
27 K. Gokhberg, P. Kolorenč, A. I. Kuleff and L. S. Cederbaum, Site and energy-selective slow-electron production through intermolecular coulombic decay, *Nature*, 2014, **505**, 661–663.
28 K. R. Wilson, B. S. Rude, T. Catalano, R. D. Schaller, J. G. Tobin, D. T. Co and R. J. Saykally, X-ray Spectroscopy of Liquid Water Microjets, *J. Phys. Chem. B*, 2001, **105**(17), 3346–3349, DOI: 10.1021/JP010132U.
29 M. L. Gordon, G. Cooper, C. Morin, T. Araki, C. C. Turci, K. Kaznatcheev and A. P. Hitchcock, Inner-shell excitation spectroscopy of the peptide bond: Comparison of the C1s, N1s, and O1s spectra of glycine, glycyl–glycine, and glycyl–glycyl–glycine, *J. Phys. Chem. A*, 2003, **107**, 6144–6159.
30 V. Fever, O. Plekan, R. Richtery, M. Coreno, K. C. Prince and V. Carravetta, Photoemission and photoabsorption spectroscopy of glycyl–glycine in the gas phase, *J. Phys. Chem. A*, 2009, **113**, 10726–10733.
31 C. C. Tsai, J. L. Chen, W. P. Hu, Y. S. Lin, H. R. Lin, T. Y. Lee, Y. T. Lee, C. K. Ni and C. L. Liu, Selectivity of peptide bond dissociation on excitation of a core electron: Effects of a phenyl group, *Chem. Phys. Lett.*, 2016, **660**, 60–68.
32 C. Li, P. Salén, V. Yatsyna, L. Schio, R. Feifel, R. Squibb, M. Kamińska, M. Larsson, R. Richter, M. Alagia, S. Stranges, S. Monti, V. Carravetta and V. Zhaunerchyk, Experimental and theoretical XPS and NEXAFS studies of N-methylacetamide and N-methyltrifluoroacetamide, *Phys. Chem. Chem. Phys.*, 2016, **18**, 2210–2218.
33 M. Montenegro, S. N. Nahar, A. K. Pradhan, K. Huang and Y. Yu, Monte carlo simulations and atomic calculations for auger processes in biomedical nanotheranostics, *J. Phys. Chem. A*, 2009, **113**, 12364–12369.
34 J. Axelsson, M. Palmblad, K. Håkansson and P. Håkansson, Electron capture dissociation of substance P using a commercially available Fourier transform ion cyclotron resonance mass spectrometer, *Rapid Commun. Mass Spectrom.*, 1999, **13**, 474–477.
35 A. S. Misharin, O. A. Silivra, F. Kjeldsen and R. A. Zubarev, Dissociation of peptide ions by fast atom bombardment in a quadrupole ion trap, *Rapid Commun. Mass Spectrom.*, 2005, **19**, 2163–2171.
36 W. Cui, M. S. Thompson and J. P. Reilly, Pathways of peptide ion fragmentation induced by vacuum ultraviolet light, *J. Am. Soc. Mass Spectrom.*, 2005, **16**, 1384–1398.
37 M. S. Thompson, W. Cui and J. P. Reilly, Factors That Impact the Vacuum Ultraviolet Photofragmentation of Peptide Ions, *J. Am. Soc. Mass Spectrom.*, 2007, **18**, 1439–1452.
38 Y. M. E. Fung, C. M. Adams and R. A. Zubarev, Electron ionization dissociation of singly and multiply charged peptides, *J. Am. Chem. Soc.*, 2009, **131**, 9977–9985.
39 V. Larraillet, A. Vorobyev, C. Brunet, J. Lemoine, Y. O. Tsybin, R. Antoine and P. Dugourd, Comparative dissociation of peptide polyanions by electron impact and photo-induced electron detachment, *J. Am. Soc. Mass Spectrom.*, 2010, **21**, 670–680.
40 S. Bari, R. Hoekstra and T. Schlathölter, Fast side-chain losses in keV ion-induced dissociation of protonated peptides, *Int. J. Mass Spectrom.*, 2011, **299**, 64–70.
41 F. Canon, A. R. Milosavljević, L. Nahon and A. Giuliani, Action spectroscopy of a protonated peptide in the ultraviolet range, *Phys. Chem. Chem. Phys.*, 2015, **17**, 25725–25733.
42 K. Biemann, Sequencing of peptides by tandem mass spectrometry and high-energy collision-induced dissociation, *Methods Enzymol.*, 1990, **193**, 455–479.
43 A. R. Milosavljević, C. Nicolas, M. L. Ranković, F. Canon, C. Miron and A. Giuliani, K-Shell Excitation and Ionization of a Gas-Phase Protein: Interplay between Electronic Structure and Protein Folding, *J. Phys. Chem. Lett.*, 2015, **6**, 3132–3138.
44 B. Liu, S. Brøndsted Nielsen, P. Hvelplund, H. Zettergren, H. Cederquist, B. Manil and B. A. Huber, Collision-induced dissociation of hydrated adenosine monophosphate nucleotide ions: protection of the ion in water nanoclusters, *Phys. Rev. Lett.*, 2006, **97**, 133401.
45 O. González-Magaña, G. Reitsma, M. Tiemens, L. Boschman, R. Hoekstra and T. Schlathölter, Near-edge X-ray absorption mass spectrometry of a gas-phase peptide, *J. Phys. Chem. A*, 2012, **116**, 10745–10751.
46 K. R. Wilson, B. S. Rude, T. Catalano, R. D. Schaller, J. G. Tobin, D. T. Co, R. J. Saykally, V. Uni and L. Berkeley, X-ray Spectroscopy of Liquid Water Microjets, *J. Phys. Chem. B*, 2001, **105**, 3346–3349.
47 G. Xu and M. R. Chance, Hydroxyl Radical-Mediated Modification of Proteins as Probes for Structural Proteomics, *Chem. Rev.*, 2007, **107**, 3514–3543.
48 H. Takahashi, S. Sekiya, T. Nishikaze, K. Kodera, S. Iwamoto, M. Wada and K. Tanaka, Hydrogen Attachment/Abstraction Dissociation (HAD) of Gas-Phase Peptide Ions for Tandem Mass Spectrometry, *Anal. Chem.*, 2016, **88**, 3810–3816.

49 R. A. Zubarev and H. Yang, Multiple soft ionization of gas-phase proteins and swift backbone dissociation in collisions with $\leq$99 eV electrons, *Angew. Chem., Int. Ed.*, 2010, **49**, 1439–1441.

50 S. Bari, D. Egorov, T. L. C. Jansen, R. Boll, R. Hoekstra, S. Techert, V. Zamudio-Bayer, C. Bülow, R. Lindblad, G. Leistner, A. Ławicki, K. Hirsch, P. S. Miedema, B. von Issendorff, J. T. Lau and T. Schlathölter, Soft X-ray Spectroscopy as a Probe for Gas-Phase Protein Structure: Electron Impact Ionization from Within, *Chem. – Eur. J.*, 2018, **24**, 7631–7636.

51 H. Zettergren, H. T. Schmidt, P. Reinhed, H. Cederquist, J. Jensen, P. Hvelplund, S. Tomita, B. Manil, J. Rangama and B. A. Huber, Stabilities of multiply charged dimers and clusters of fullerenes, *J. Chem. Phys.*, 2007, **126**(22), 224303, DOI: 10.1063/1.2743433.

52 A. I. S. Holm, H. Zettergren, H. A. B. Johansson, F. Seitz, S. Rosén, H. T. Schmidt, A. Ławicki, J. Rangama, P. Rousseau, M. Capron, R. Maisonny, L. Adoui, A. Méry, B. Manil, B. A. Huber and H. Cederquist, Ions colliding with cold polycyclic aromatic hydrocarbon clusters, *Phys. Rev. Lett.*, 2010, **105**, 1–4.

53 T. Jahnke, H. Sann, T. Havermeier, K. Kreidi, C. Stuck, M. Meckel, M. Schöffler, N. Neumann, R. Wallauer, S. Voss, A. Czasch, O. Jagutzki, A. Malakzadeh, F. Afaneh, T. Weber, H. Schmidt-Böcking and R. Dörner, Ultrafast energy transfer between water molecules, *Nat. Phys.*, 2010, **6**, 139–142.

54 S. Thürmer, M. Ončák, N. Ottosson, R. Seidel, U. Hergenhahn, S. E. Bradforth, P. Slavíček and B. Winter, On the nature and origin of dicationic, charge-separated species formed in liquid water on X-ray irradiation, *Nat. Chem.*, 2013, **5**, 590–596.

55 E. F. Aziz, N. Ottosson, M. Faubel, I. V. Hertel and B. Winter, Interaction between liquid water and hydroxide revealed by core-hole de-excitation, *Nature*, 2008, **455**, 89–91.

56 Y. Morishita, X. J. Liu, N. Saito, T. Lischke, M. Kato, G. Prümper, M. Oura, H. Yamaoka, Y. Tamenori, I. H. Suzuki and K. Ueda, Experimental evidence of interatomic coulombic decay from the Auger final states in argon dimers, *Phys. Rev. Lett.*, 2006, **96**, 1–4.

57 M. Mucke, M. Braune, S. Barth, M. Förstel, T. Lischke, V. Ulrich, T. Arion, U. Becker, A. Bradshaw and U. Hergenhahn, A hitherto unrecognized source of low-energy electrons in water, *Nat. Phys.*, 2010, **6**, 143–146.

The Journal of Chemical Physics

Temporary anions of the dielectric gas C_3F_7CN and their decay channels

Cite as: J. Chem. Phys. **152**, 244304 (2020); https://doi.org/10.1063/5.0008897
Submitted: 27 March 2020 . Accepted: 02 June 2020 . Published Online: 22 June 2020

M. Ranković, Ragesh Kumar T P, P. Nag, J. Kočišek, and J. Fedor

The Journal of Chemical Physics ARTICLE scitation.org/journal/jcp

Temporary anions of the dielectric gas C_3F_7CN and their decay channels

Cite as: J. Chem. Phys. 152, 244304 (2020); doi: 10.1063/5.0008897
Submitted: 27 March 2020 • Accepted: 2 June 2020 •
Published Online: 22 June 2020

M. Ranković, Ragesh Kumar T P, P. Nag, J. Kočišek, and J. Fedor[a)]

AFFILIATIONS

J. Heyrovský Institute of Physical Chemistry, Czech Academy of Sciences, Dolejškova 3, 18223 Prague, Czech Republic

[a)]Author to whom correspondence should be addressed: juraj.fedor@jh-inst.cas.cz

ABSTRACT

We probe the transient anion states (resonances) in the dielectric gas C_4F_7N by the electron energy loss spectroscopy and the dissociative electron attachment spectroscopy. The vibrationally inelastic electron scattering leads to two excitation types. The first is the excitation of specific vibrational modes that are assigned with the help of an infrared spectrum of this molecule and quantum chemistry calculations. In the second type of vibrational excitation, the excess energy is randomized via internal vibrational redistribution in the temporary anion, and the electrons are emitted statistically. The electron attachment proceeds in three different regimes. The first is the formation of the parent $C_4F_7N^-$ anion at energies close to 0 eV. The second is a statistical evaporation of the F-atom, leading to the defluorinated anion $C_4F_6N^-$. Finally, the third is dissociative electron attachment proceeding via the formation of several resonances and leading to a number of fragments. The present data explain the puzzling recent results of the pulsed-Townsend experiments with this gas.

I. INTRODUCTION

The interest in electron collisions with C_3F_7CN (heptafluoroisobutyronitrile, marketed under the name Novec 4710) is motivated by its potential use in high-voltage switchgear and insulation. SF_6, which has been used for this purpose for decades, has an extremely high global warming potential of 23 500 (GWP is a measure of how much heat a gas traps in the atmosphere relative to the same mass of CO_2). In this respect, the global warming potential of C_3F_7CN, estimated[1,2] to be between 1490 and 3650, would be a big improvement. When used in mixtures with buffer gas, the GWP drops even more down to 230.[3,4] This fact, together with the high dielectric strength of its mixtures,[4,5] makes C_3F_7CN one of the most promising candidates for SF_6 replacement.

The physical nature of the electric breakdown in gases determines the crucial role of the electron-molecule collisions. Very little data are available for this gas. Positive ionization, which leads to the electron multiplication during breakdown, has been treated theoretically,[6] and we have recently reported details of the dissociative ionization dynamics.[7] Equally important is the electron attachment, which leads to electron scavenging. It has been probed so far only in a pulsed-Townsend experiment,[4,5] where a pulse of electrons is sent through the gas at intermediate pressures and attachment properties are derived from the shape of the pulse. These recent experiments revealed puzzling results, which could not be explained based on the simple (associative) electron attachment events. There were footprints on the strong electron detachment following the anion formation. The data also suggested the presence of three types of anions: a stable one (non-detaching), a slowly detaching one, and finally, a short-lived anion responsible for the fast electron detachment. These effects strongly influence the critical breakdown field.

In this paper, we focus on the temporary anions of C_3F_7CN formed under the single collision conditions, when one electron is interacting with maximum one target molecule. In three experimental setups, we monitor either the scattered electrons, thus obtaining information about the detachment channel, or the formed stable anions, thus obtaining information about the final attachment products. The experiments reveal several phenomena occurring in electron collisions with this gas. A number of resonances are formed in the scattering, which lead to vibrational excitation of the target molecule. At low incident energies, there is a strong emission of slow electrons with a statistical kinetic energy distribution, which corresponds to the thermionic emission from the hot

transient anion. At these energies, a strong signal of the non-dissociated anion is observed. At higher electron energies, the dissociative electron attachment sets on, which leads to a number of stable anionic fragments.

II. EXPERIMENT

Three electron collision setups were used for the present study.

The vibrationally inelastic electron scattering was probed on an electron energy loss spectrometer with a hemispherical monochromator and analyzer.[8,9] All the present experiments were performed at the fixed scattering angle of 135°. The energy scale was calibrated using the 19.365 eV 2^2S resonance in the elastic scattering on helium. The electron energy resolution (combined resolution of the monochromator and the analyzer) was around 18 meV. The lowest energy of electrons present in the beam was around 20 meV. The analyzer of the instrument is equipped with a Wien filter that serves to separate electrons from anions. For certain measurements, the Wien filter was set to pass anions, thus enabling high-resolution measurements of the electron attachment spectra.

The mass resolved electron attachment was probed using two setups. The anion yield as a function of the incident electron energy was recorded on the setup equipped with a trochoidal electron monochromator and a quadrupole mass filter.[10,11] The velocity map images of fragment ions were recorded on the setup that combines a trochoidal monochromator with velocity map imaging spectrometer.[12] It is equipped with a delay-line detector, which records the arrival time and position of every ion. These were used to reconstruct the Newton half-sphere for each fragment. The kinetic energy distributions were obtained from these half-spheres. In both attachment instruments, the energy scale was calibrated using the O^- yield from CO_2.

Additionally, we recorded the infrared spectrum of C_3F_7CN using a commercially available Bruker IFS 125 HR spectrometer (Bruker Optics, Germany).

III. RESULTS AND DISCUSSION

A. Vibrational spectrum of C_3F_7CN

In order to ease the interpretation of the electron-impact vibrational excitation, we have first recorded the optical infrared spectrum of C_3F_7CN. We are not aware of any previous publication of such data. Figure 1 shows the IR spectrum in the transmittance scale, together with the spectrum calculated at the B3LYP/aug-cc-pVDZ level of theory. The primary purpose of the calculation was to assign the observed IR lines. The top panel of Fig. 1 shows an electron energy loss spectrum, recorded at the constant residual energy $E_r = 0.05$ eV. This means that the incident energy E_i is being scanned and the electron analyzer is kept at a constant potential so that only the electrons with the given E_r are detected. The signal intensity is plotted as a function of the energy loss $\Delta E = E_i - E_r$. The emission of near-threshold electrons, thus, maps the vibrational modes, which are excited at threshold, as soon as the incident electron has enough energy to do so. These are typically IR-active modes.[13,14] Indeed, the intensity profile of the energy loss spectrum corresponds to the IR spectrum. The dominant vibrational group, closely spaced CC and

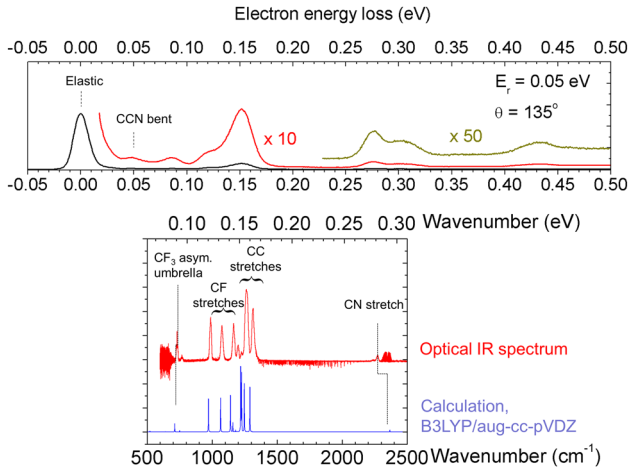

FIG. 1. Top panel: electron energy loss spectrum of C_3F_7CN, recorded at a constant residual energy (E_r) of 50 meV. Bottom panel: infrared spectrum, red: experimental, blue: calculated at the B3LYP/aug-cc-pVDZ level of theory.

CF vibrations, is smeared out by the resolution of the electron spectrometer into one band peaking at 0.155 eV. This group also shows overtones peaking at 0.30 eV and 0.44 eV. Apart from the vibrations visible in the IR spectrum, the electron energy loss spectrum shows also the soft CCN bend vibration at 0.05 eV, which is out of the range of the FTIR spectrometer.

B. Specific vibrational excitation by electron impact

Figure 2 shows the electron energy loss spectra of C_3F_7CN recorded at various constant incident electron energies. These spectra reflect which modes get excited upon the electron impact. The strong peak at 0 eV is the elastic scattering (no energy loss). At all energies, the dominant inelastic process is the excitation of the C-C and C-F stretch modes. This excitation has a prominent overtone progression. Apart from these, all modes discussed in Sec. III A are visible in the energy loss spectra. The spectrum at $E_i = 1.1$ eV shows a strong rising continuous signal near the complete energy loss ($\Delta E = E_i$). These are statistically emitted electrons discussed in Sec. III C. Perhaps, the strongest difference among the different incident energies is in the intensity of the C≡N stretch vibration at 279 meV, which is very high at $E_i = 1.1$ eV and gets much weaker at higher incident energies.

Such intensity variation is best monitored by recording the excitation curves of the given vibration as a function of the incident energy. These are shown in Fig. 3. All three vibrations shown are strongly excited at the threshold, which is a common effect in polar molecules, as discussed in Sec. III A. The second effect, strongly enhancing the effectivity of vibrational excitation, is the formation of resonances, temporary anion states. To predict at which energies the resonances will occur is a very challenging task, which requires special theoretical approaches, since the electron wave function is embedded in continuum. For data interpretation, we can, however, use a simplified approach of correlating the shape resonances to temporal occupation of virtual molecular orbitals of

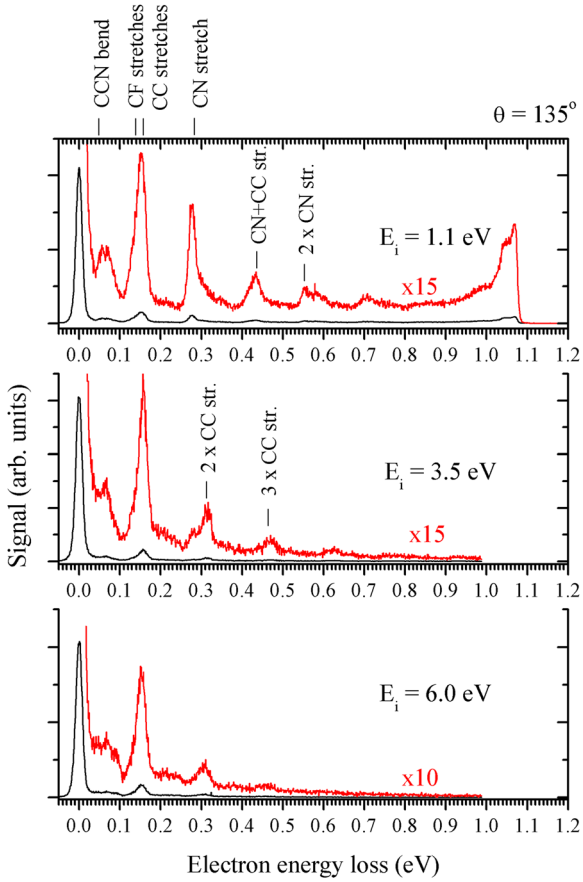

FIG. 2. Electron energy loss spectra recorded at three different incident electron energies.

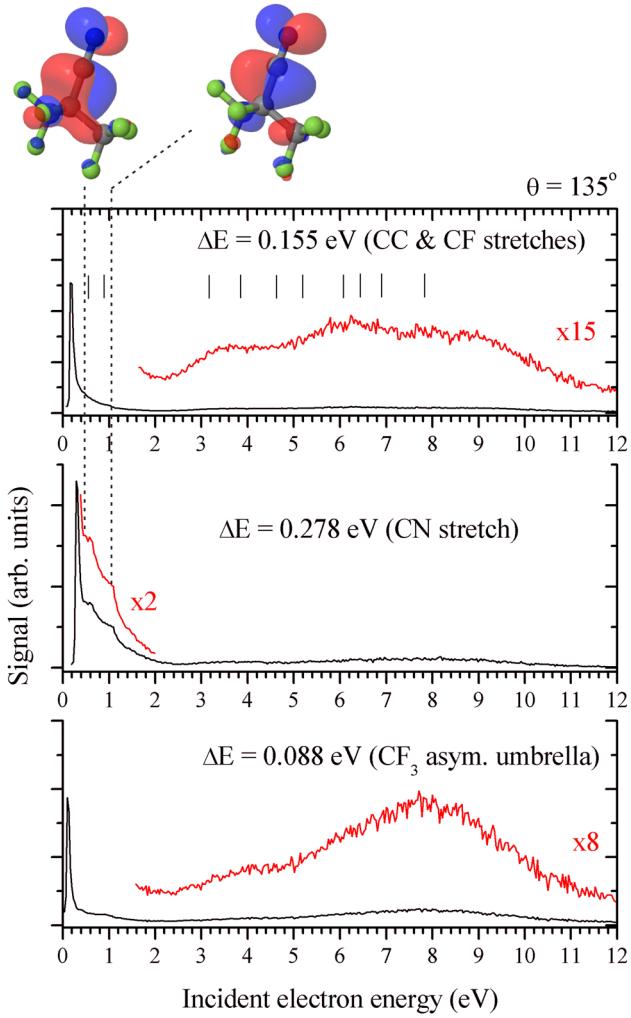

FIG. 3. Excitation curves of three different energy losses, recorded at the scattering angle of 135°.

the neutral molecule. A number of scaling formulas have been developed to connect the virtual orbital energies with the resonance energies.[15–17] In order to keep the consistency with our previous work, we use the scaling of Chen and Gallup,[15] which operates with Hartree–Fock orbitals and sets the resonance energy to [E_{res} = (E_{MO} − 2.33 eV)/1.31]. The resonant energies obtained from this scaling are shown as vertical bars in Fig. 3. The bars, thus, correspond to the occupation of LUMO and LUMO + 1, in the order of increasing energy. The closely spaced states above 3 eV correspond to various orbitals with a dominant C-C or C-F σ^* character. These cause the nearly continuous broad bands in vibrational excitation between 3 eV and 11 eV. They are visible in all three modes without a clear specificity, and only the CF_3 asymmetric umbrella vibration is primarily excited around 7.8 eV.

In addition to this "σ^* mountain," there are two resonances predicted at lower energies. In Fig. 3, we show the virtual orbitals to which these two resonances correspond. The excitation curve of the CN stretch (second panel), indeed, shows clear structures at energies of 0.58 eV and 1.12 eV, superimposed on the threshold peak. Since the virtual orbitals of the two low-lying resonances have nodal planes along the C≡N bond, it is reasonable to assume that they will primarily excite the CN vibration; we, thus, assign the sharp structures to the formation of these two shape resonances. It should be, however, noted that another effect (independent from the presence of shape resonances) could contribute to the structures in the CN excitation curve, namely, the formation of vibrational Feshbach resonances (VFRs). Here, the electron is trapped in the long-range potential of the molecule, and the vibrational energy of the temporary anion is slightly lower than the energy of the neutral. This typically leads to cusps at the opening of higher vibrational excitation channels. The positions of the observed structures coincide with the openings of the $2v_{CN}$ and $4v_{CN}$ vibrations.

C. Unspecific vibrational excitation by electron impact: Thermal electron emission

The dynamics of temporary anions is, perhaps, best revealed by a two-dimensional electron-energy loss spectrum.[18] Figure 4 shows

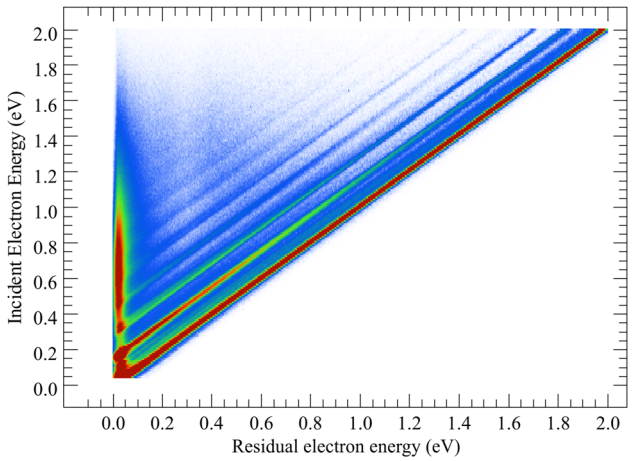

FIG. 4. Two dimensional electron energy loss spectrum of C_3F_7CN. Diagonal features correspond to specific vibrational excitation, the vertical feature at low residual energies to delayed statistical emission of electrons from a vibrationally hot anion.

such a spectrum for C_3F_7CN. Here, the residual and incident energies are plotted on the *x*- axis and *y*- axis, respectively, and the intensity is color-coded. When the data are plotted in this way (which is different than in our previous studies,[19,20] where the *x*-axis corresponded to energy loss), the strong saturated diagonal line ($E_i = E_r$) is the elastically scattered electrons. The parallel diagonals are lines with a constant energy loss ($E_i = E_r + \Delta E$) and correspond to the excitation of specific vibrational modes discussed in Sec. III B. The visually apparent series of diagonals are the overtone progressions and combination bands.

An interesting feature is the strong vertical trace at low residual energies. It corresponds to the emission of slow electrons at a broad range of incident energies; they appear at E_i roughly from 0.3 eV to 1.4 eV. The origin of this signal is thermal electron emission. After the temporary anion is formed, the internal energy randomizes among the vibrational degrees of freedom via a fast intramolecular vibrational redistribution (IVR). The electron is then emitted statistically. Even though such unspecific excitation is common in large molecules,[19–21] in the present case, the intensity of this channel is unusually high: at E_i = 0.7 eV, the ratio of the elastic to thermal signal (peak values) is 3.5:1. For comparison, in formic acid dimer, where the double hydrogen bond strongly enhances the electron thermalization, this ratio is approximately 30:1.[22] This points to a high capacity of C_4F_7N to thermalize the electrons.

D. Dissociative electron attachment

Figure 5 shows the ion yields of the negative ions resulting from the electron collisions with C_4F_7N. The strongest channel is the formation of the parent anion $C_4F_7N^-$ close to 0 eV. At higher incident energies, anionic fragments appear, namely, the defluorinated anion $C_4F_6N^-$, the cyano anion CN^-, the de-fluoromethylated anion $C_3F_4N^-$, and the fluorine anion F^-. The last three fragments peak between 1.2 eV and 1.4 eV, and the fluorine anion additionally shows two higher-energy bands at 4 eV and 7.3 eV.

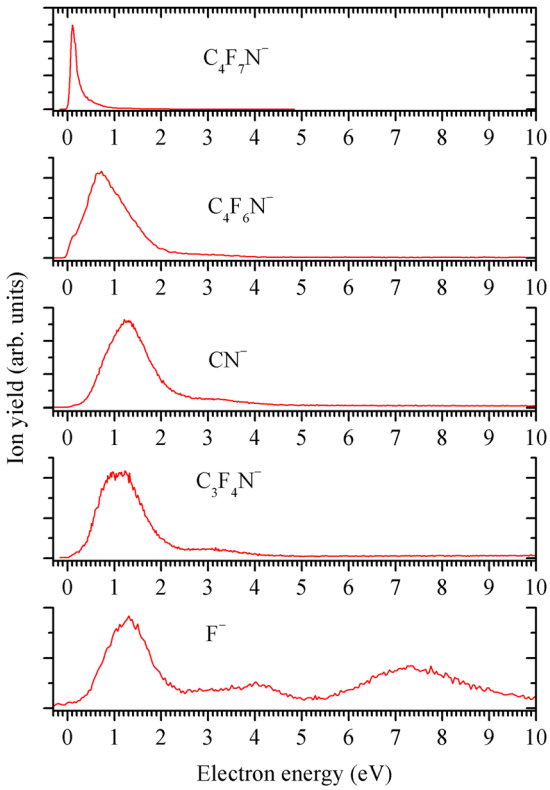

FIG. 5. Ion yield of individual dissociative electron attachment fragments as a function of electron energy.

Table I shows computed threshold energies for the individual anionic channels. The threshold energy for the formation of the parent anion is, by definition, negative of the adiabatic electron affinity (AEA). C_3F_4N, thus, has a positive AEA = 1.74 eV, which explains the formation of a parent anion close to 0 eV. Formation of all fragment anions is slightly endothermic. For the $C_4F_6N^-$ and F^- channels, where the neutral or anionic fluorine can be abstracted either from the central carbon or from the fluoromethyl group, the former

TABLE I. Computed B3LYP/aug-cc-pVDZ threshold energies for formation of anionic fragments. The thresholds are obtained as a difference between the total energies of the products and neutral molecule (taking into account zero point energies). The E_{th} value for the parent anion is the negative of the adiabatic electron affinity.

Product(s)	E_{th} (eV)
$C_4F_7N^-$	-1.74
$C_4F_6N^-$ + F (from C_1)	0.12
$C_4F_6N^-$ + F (from CF_3)	2.50
CN^- + C_3F_7	0.39
$C_3F_4N^-$ + CF_3	0.18
F^- + C_4F_6N (from C_1)	0.24
F^- + C_4F_6N (from CF_3)	1.40

is clearly the case, since the signal onset is much below the latter threshold.

We have also recorded the total anion yield on the spectrometer with a hemispherical analyzer by setting the Wien filter to pass anions instead of electrons. This is shown in Fig. 6(a). The residual energy was kept fixed at 0.016 eV since the major ions are all expected to have very low kinetic energies. Note that the y-axis is in the logarithmic scale. The rough Wien filter does not distinguish the masses of anions; however, the comparison with the data from a trochoidal instrument tells us that the narrow low-energy peak corresponds to the parent anion $C_4F_7N^-$ and the higher energy band around 1.2 eV corresponds to fragment anions.

The parent anion formed in a binary collision with a free electron cannot be stable over an infinite time, since the total energy of the system suffices for the electron detachment. However, as seen in Sec. III C, the excess energy is dissipated among the vibrational degrees of freedom, which, together with a high heat capacity of the molecule, results in a long lifetime of the parent anion. The current detection times are approximately 120 μs in the trochoidal spectrometer and 60 μs in the spectrometer with hemispherical analyzers. The parent anion lifetime is clearly higher than these.

Other panels of Fig. 6 elucidate the parent anion decay dynamics. Figure 6(b) shows the yield of E_r = 0.05 eV electrons as a function of the incident energy. Such a spectrum corresponds to the intensity profile across the 2D spectrum (Fig. 4) along a vertical line

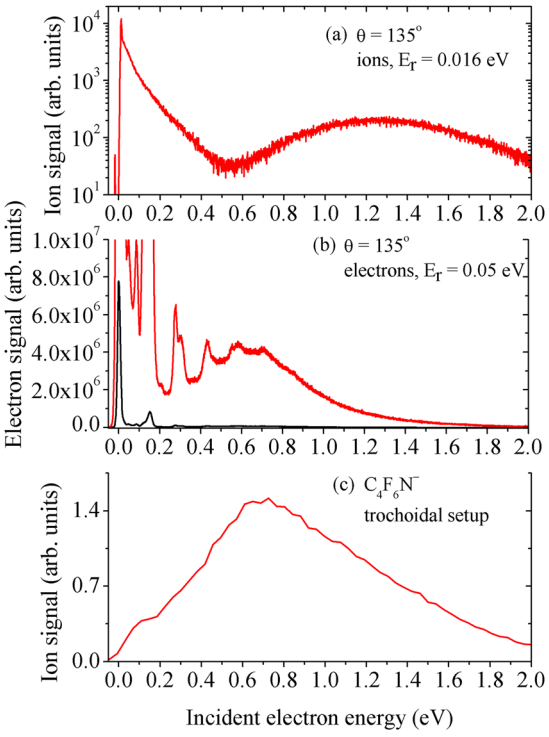

FIG. 6. (a) Total anion yield as recorded on the spectrometer with hemispherical analyzers. (b) Yield of threshold electrons (with a residual energy of 50 meV) recorded on the same spectrometer. (c) Yield of the defluorinated anion recorded on the trochoidal spectrometer.

at this residual energy. The broad background peak centered around 0.7 eV reflects the abundance of thermal electrons. Their emission clearly sets on at incident energies where the signal of parent anions steeply decreases. The same is true for the ion yield of the defluorinated fragment anion $C_4F_6N^-$, shown in Fig. 6(c). This is given by the metastable nature of the parent anion. Its energy content is determined by the electron affinity of the target molecule and by the incident electron energy. When the latter is close to zero, the parent anion does not decay within the detection time and $C_4F_7N^-$ is detected. As the incident electron energy increases, the higher internal energy leads to the decay of the parent anion, either by the emission of the thermal electron [Fig. 6(b)] or by the evaporation of the neutral F atom [Fig. 6(c)].

Finally, we address the question of energy partitioning in the DEA. Figure 7 shows the velocity map images [(a) and (b)] and the corresponding kinetic energy distributions (c) of the two lightest fragment ions, CN^- and F^-. The other fragments have very low kinetic energies since they are much heavier than their neutral counterparts. The vertical lines in Fig. 7 show hypothetical maximum kinetic energies of the two fragments. These were obtained by assuming that (i) the excess energy is equal to the difference of the electron incident energy and the calculated threshold (Table I), (ii) all the excess energies go into the kinetic energy of the fragments, and (iii) it is shared between the anionic and neutral fragments based on momentum conservation. Clearly, only a small part of the available energy actually goes into the fragment kinetic energy, which shows that the fragments are created vibrationally and rotationally hot. In order to verify the operation of the (relatively new) velocity map imaging spectrometer, we recorded the kinetic energies of all ions on the electrostatic instrument. This is performed by scanning the residual energy with the incident energy kept constant and with the Wien filter set to ion transmission. The resulting spectrum is shown in Fig. 7(d) together with the weighted sum of individual fragment distributions from the VMI spectrometer. The distributions are in a very good agreement, and the latter is broader, which can be ascribed to an instrumental effect (worse resolution both in the incident electron energy and in the fragment kinetic energy).

The F^- fragment is the only one that shows also resonances at higher electron energies. The VMI images of these energies and the corresponding kinetic energy distributions are shown in Fig. 8. Apart from higher kinetic energies of the fragments, the general character of the distribution does not change. The images are isotropic, and the distributions have a statistical character.

E. Relation to breakdown and electron transport properties

Due to its promising use as an insulating medium, a lot of attention has been paid recently to the dielectric properties of C_3F_7CN.[4,5,23] A surprisingly large scatter of the data has been pointed out in Ref. 5. There, a careful study of the electron transport through this gas was conducted by a pulsed-Townsend experiment. In such experiments, a well defined pulse of electrons is sent through the gas at intermediate pressures, and the electron-interaction properties are deconvoluted from the shape of the resulting electron pulse. Hösl *et al.*[5] constructed a complex kinetic model that reproduced their data, including a strong pressure and electrode-distance

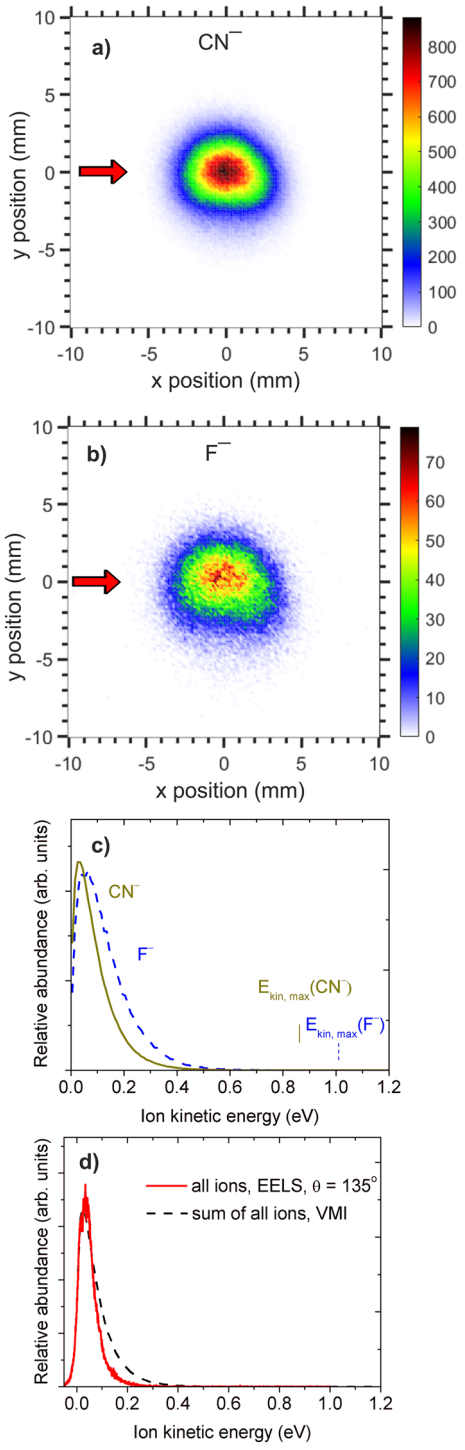

FIG. 7. [(a) and (b)] Velocity map images of two dissociative electron attachment fragments recorded at an incident electron energy 1.4 eV. The red arrow indicates the direction of the electron beam. (c) Corresponding kinetic energy distributions. (d) Kinetic energy distribution of all ions, obtained as the sum of velocity map imaging data (dashed line) and measured on the spectrometer with hemispherical analyzers (full line).

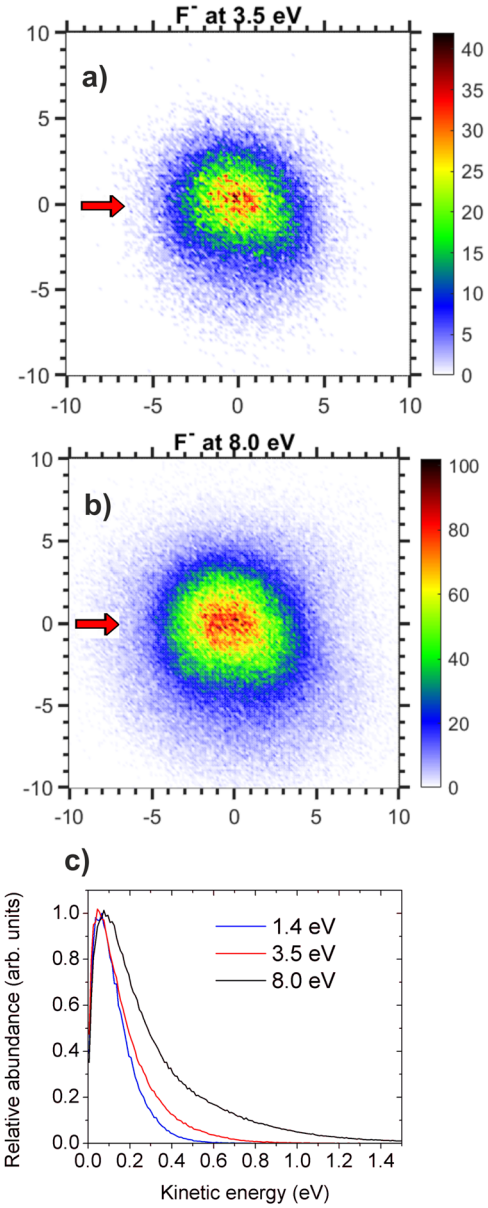

FIG. 8. Velocity map images of the F^- fragment at two higher incident energies, 3.5 eV and 8.0 eV, and the corresponding kinetic energy distributions.

dependence. An important conclusion was that the data cannot be explained on the basis of a simple ionization/attachment/scattering picture, but that there is a strong electron detachment channel. The detachment suppresses the removal of free electrons during the breakdown and, therefore, influences the dielectric strength of the compound.

Hösl *et al.*[5] postulated existence of three types of negative ions. Two of these were long-lived with distinctly different ion mobilities, denoted as M_1^- and M_2^-. The M_1^- showed a slow electron detachment. The third anion M_3^- was short-lived, characterized by a fast electron

detachment. Present results bring further insight into this problem. The M_2^- can be any (or all) of the stable dissociative attachment products formed around the energy of 1.2 eV. The M_3^- is clearly the parent anion $C_4F_7N^-$, where we also directly observe the detachment channel. The slowly detaching M_1^- is somewhat puzzling, since according to Hösl *et al.*, it seems to be formed at higher electron energies than M_2^-. A possible explanation, also mentioned in Ref. 5, is that M_1^- is a stable anion (DEA product or a collisionally stabilized parent anion[24,25]) and the slow detachment from it is due to the collisions with other gas molecules. Another option is that it is the defluorinated $C_4F_6N^-$, which has not been cooled down sufficiently by the evaporation of one fluorine atom and has still enough internal energy to detach the electron statistically.

IV. CONCLUSIONS

In conclusion, we probed the dynamics of temporary anions of the promising dielectric gas C_4F_7N. The vibrational electron energy loss spectra revealed that a number of vibrational modes are excited upon the electron impact. Most prominently, the group of C-C and C-F vibrations is excited up to high overtones. The vibrational excitation is enhanced both at the threshold, due to a direct-dipole excitation, and at the energies where resonances are formed. These are, on one hand, two low-lying resonances at 0.58 eV and 1.12 eV and a broad band of overlapping σ^* resonances at higher energies. Apart from the direct vibrational excitation, we observe an unspecific vibrational excitation, where the electron is emitted statistically after an internal vibrational distribution on the anion surface. This thermal process is manifested as the emission of slow electrons up to the incident energy of approximately 1.4 eV.

We also observed a number of anionic products resulting from electron collisions with this gas. At very low electron energies, the parent anion is formed. At the binary collision conditions, it has to be necessarily metastable. The statistical electron detachment is one of its decay channels, and another one is the evaporation of the neutral fluorine atom and the production of a stable $C_4F_6N^-$ anion. Other anionic fragments are detected at higher electron energies. The measurement of their kinetic energies, either by the velocity map imaging method or by using a hemispherical energy analyzer, reveals that only a small part of available excess energy goes into the kinetic energies of fragments.

The present results elucidate, in detail, the dynamics of both the transient and permanent electron attachment to C_4F_7N. These effects strongly influence the dielectric properties.[5] Our data provide a molecular explanation of effects observed in pulsed-Townsend experiments, especially on the strong role of the delayed electron detachment.

ACKNOWLEDGMENTS

Support from Eaton and Project No. TH03020063 of the Technological Agency of the Czech Republic is gratefully acknowledged.

DATA AVAILABILITY

The data that support the findings of this study are available from the corresponding author upon reasonable request.

REFERENCES

[1] M. P. S. Andersen, M. Kyte, S. T. Andersen, C. J. Nielsen, and O. J. Nielsen, Environ. Sci. Technol. **51**, 1321 (2017).
[2] S. Blázquez, M. Antiñolo, O. J. Nielsen, J. Albaladejo, and E. Jiménez, Chem. Phys. Lett. **687**, 297 (2017).
[3] Y. Kieffel, in *2016 IEEE International Conference on Dielectrics (ICD)* (IEEE, 2016).
[4] A. Chachereau, A. Hoessl, and C. M. Franck, J. Phys. D **51**, 495201 (2018).
[5] A. Hösl, A. Chachereau, J. Pachin, and C. M. Franck, J. Phys. D: Appl. Phys. **52**, 235201 (2019).
[6] J. Xiong, X. Li, J. Wu, X. Guo, and H. Zhao, J. Phys. D **50**, 445206 (2017).
[7] M. Ranković, J. Chalabala, M. Zawadzki, J. Kočišek, P. Slavíček, and J. Fedor, Phys. Chem. Chem. Phys. **22**, 16451 (2019).
[8] M. Allan, J. Phys. B: At., Mol. Opt. Phys. **25**, 1559 (1992).
[9] M. Allan, J. Phys. B: At. Mol. Phys. **38**, 3655 (2005).
[10] M. Stepanović, Y. Pariat, and M. Allan, J. Chem. Phys. **110**, 11376 (1999).
[11] J. Langer, M. Zawadzki, M. Fárník, J. Pinkas, J. Fedor, and J. Kočišek, Eur. Phys. J. D **72**, 112 (2018).
[12] P. Nag, M. Polášek, and J. Fedor, Phys. Rev. A **99**, 052705 (2019).
[13] I. I. Fabrikant, J. Phys. B: At., Mol. Opt. Phys. **49**, 222005(1) (2016).
[14] Y. Itikawa, Int. Rev. Phys. Chem. **16**, 155 (1997).
[15] D. Chen and G. A. Gallup, J. Chem. Phys. **93**, 8893 (1990).
[16] S. W. Staley and J. T. Strnad, J. Chem. Phys. **98**, 116 (1994).
[17] K. Graupner, T. L. Merrigan, T. A. Field, T. G. A. Youngs, and P. C. Marr, New J. Phys. **8**, 117 (2006).
[18] K. Regeta and M. Allan, Phys. Rev. Lett. **110**, 203201 (2013).
[19] M. Allan, M. Lacko, P. Papp, Š. Matejčík, M. Zlatar, I. I. Fabrikant, J. Kočišek, and J. Fedor, Phys. Chem. Chem. Phys. **20**, 11692 (2018).
[20] M. Ranković, P. Nag, M. Zawadzki, L. Ballauf, J. Žabka, M. Polášek, J. Kočišek, and J. Fedor, Phys. Rev. A **98**, 052708 (2018).
[21] M. Allan, J. Electron Spectrosc. Relat. Phenom. **48**, 219 (1989).
[22] M. Allan, Phys. Rev. Lett. **98**, 123201 (2007).
[23] H. E. Nechmi, A. Beroual, A. Girodet, and P. Vinson, IEEE Trans. Dielectr. Electr. Insul. **24**, 886–892 (2017).
[24] A. Chachereau, J. Fedor, R. Janečková, J. Kočišek, M. Rabie, and C. M. Franck, J. Phys. D **49**, 375201 (2016).
[25] M. Zawadzki, M. Ranković, J. Kočišek, and J. Fedor, Phys. Chem. Chem. Phys. **20**, 6838 (2018).